FINAL REPORT

Effects of Near-Term Sea-Level Rise on Coastal Infrastructure

SERDP Project RC-1700

MARCH 2013

Joseph F. Donoghue, Ph.D., P.G.
James B. Elsner, Ph.D.
Bill X. Hu, Ph.D.
Stephen A. Kish, Ph.D.
Alan W. Niedoroda, Ph.D., P.G.
Yang Wang, Ph.D.
Ming Ye, Ph.D.
Florida State University

This document has been cleared for public release

SERDP
DOD ▪ EPA ▪ DOE

This report was prepared under contract to the Department of Defense Strategic Environmental Research and Development Program (SERDP). The publication of this report does not indicate endorsement by the Department of Defense, nor should the contents be construed as reflecting the official policy or position of the Department of Defense. Reference herein to any specific commercial product, process, or service by trade name, trademark, manufacturer, or otherwise, does not necessarily constitute or imply its endorsement, recommendation, or favoring by the Department of Defense.

REPORT DOCUMENTATION PAGE

Form Approved
OMB No. 0704-0188

Public reporting burden for this collection of information is estimated to average 1 hour per response, including the time for reviewing instructions, searching existing data sources, gathering and maintaining the data needed, and completing and reviewing this collection of information. Send comments regarding this burden estimate or any other aspect of this collection of information, including suggestions for reducing this burden to Department of Defense, Washington Headquarters Services, Directorate for Information Operations and Reports (0704-0188), 1215 Jefferson Davis Highway, Suite 1204, Arlington, VA 22202-4302. Respondents should be aware that notwithstanding any other provision of law, no person shall be subject to any penalty for failing to comply with a collection of information if it does not display a currently valid OMB control number. **PLEASE DO NOT RETURN YOUR FORM TO THE ABOVE ADDRESS.**

1. REPORT DATE *(DD-MM-YYYY)*
11-16-2012

2. REPORT TYPE
Final Technical Report

3. DATES COVERED *(From - To)*
March 2009 – June 2012

4. TITLE AND SUBTITLE
Effects of Near-Term Sea-Level Rise on Coastal Infrastructure

5a. CONTRACT NUMBER
W912HQ-09-C-0010

5b. GRANT NUMBER

5c. PROGRAM ELEMENT NUMBER

6. AUTHOR(S)

Donoghue, Joseph F.; Elsner, James B.; Hu, Bill X.; Kish, Stephen A.; Niedoroda, Alan W.; Wang, Yang; Ye, Ming

5d. PROJECT NUMBER
RC-1700

5e. TASK NUMBER

5f. WORK UNIT NUMBER

7. PERFORMING ORGANIZATION NAME(S) AND ADDRESS(ES)

Florida State University; URS Corporation

8. PERFORMING ORGANIZATION REPORT NUMBER

9. SPONSORING / MONITORING AGENCY NAME(S) AND ADDRESS(ES)

Strategic Environmental Research and Development Program
4800 Mark Center Dr.,Suite 17D08
Alexandria, VA 22350-3605

10. SPONSOR/MONITOR'S ACRONYM(S)
SERDP

11. SPONSOR/MONITOR'S REPORT NUMBER(S)

12. DISTRIBUTION / AVAILABILITY STATEMENT

Approved for public release; distribution is unlimited.

13. SUPPLEMENTARY NOTES

14. ABSTRACT

The objective of this investigation was to develop new methods for comprehensive modeling of the effects and potential risk of projected sea-level rise, and increased storminess, on coastal environments and infrastructure over the next century. The project has focused on the Eglin Air Force Base (EAFB) region on the northwest Florida coast. The methods that have been developed in this work are applicable to military installations in similar coastal settings. The project had six major components: (1) analyzing historic coastal change and remote sensing data; (2) modeling future storms; (3) analyzing the paleostorm history in coastal sediments; (4) modeling coastal wetlands; (5) modeling coastal groundwater; (6) modeling morphologic change and analyzing uncertainty. The project has had several significant outcomes. We have developed one of the most comprehensive databases ever assembled on historic changes in shorelines and barrier island morphology. A regional storm history has been developed for use in the modeling effort, both for historic and prehistoric time. We have combined our field and archival data to develop a purpose-built numerical model of coastal morphology, incorporating morphological, sea-level, and storm climatology data to predict changes over the next century. The outcomes of this study can be used to evaluate how to make reliable predictions of the effects of future climate change on coastal infrastructure and natural coastal systems. The expected result will be to enable cost-effective mitigation and adaptation strategies to prepare for a warmer future.

15. SUBJECT TERMS
Sea-level rise, climate change, coastal modeling, coastal morphology, coastal systems, storm hazards, barrier island, remote sensing, coastal wetlands, groundwater modeling, coastal infrastructure, shoreline evolution, uncertainty assessment

16. SECURITY CLASSIFICATION OF:			17. LIMITATION OF ABSTRACT	18. NUMBER OF PAGES	19a. NAME OF RESPONSIBLE PERSON
					Dr. Joseph Donoghue
a. REPORT	b. ABSTRACT	c. THIS PAGE		xi + 172	19b. TELEPHONE NUMBER *(include area code)* 405-744-6375

Standard Form 298 (Rev. 8-98)
Prescribed by ANSI Std. Z39.18

Table of Contents

Abstract 1

1. Objectives 3
- **1.1 SERDP Statement of Need (SON)** 3
- **1.2 Overall Project Objectives** 5
- **1.3 Specific Project Objectives** 7
  - **1.3.1 Analyzing Historic Coastal Change and Remote Sensing Data** 7
  - **1.3.2 Modeling Future Storms** 7
  - **1.3.3 Analyzing Paleostorm History in Coastal Sediments** 8
  - **1.3.4 Modeling Coastal Wetlands** 8
  - **1.3.5 Modeling Coastal Groundwater** 8
  - **1.3.6 Modeling Morphologic Change** 8

2. Background 9
- **2.1 Environmental Issues Addressed** 9
- **2.2 Summary of Past Research** 9

3. Materials and Methods 15
- **3.1 Analyzing Historic Coastal Change and Remote Sensing Data** 15
- **3.2 Modeling Future Storms** 19
- **3.3 Analyzing Paleostorm History in Coastal Sediments** 21
  - **3.3.1 Historic Storm Record** 22
  - **3.3.2 Long-Term Geologic Record of Coastal Storms** 24
  - **3.3.3 Coastal Dune Lake Sediments** 24
  - **3.3.4 Core Preparation** 25
  - **3.3.5 Sediment Analyses** 25
  - **3.3.6 Micropaleontology** 25
  - **3.3.7 Geochronologic Analyses** 26
  - **3.3.8 Determining Storm Surge Heights Using SLOSH** 26
  - **3.3.9 Geochemical Analyses** 26
  - **3.3.10 Paleostorm Analytical Methods** 27
  - **3.3.11 Organic Geochemical Proxy (OGP) Methodology** 27
  - **3.3.12 Paleostorm Detection Model** 28

3.4 Modeling Coastal Wetlands 29
3.5 Modeling Coastal Groundwater 34
3.5.1 Model Conceptualization.....34
3.5.2 Numerical Modeling 37
3.5.3 Model Settings 38
3.5.4 Hydrostratigraphic Units 38
3.5.5 Sea-Level Rise Scenarios 40
3.6 Modeling Morphologic Change 41
3.6.1 The MoCCS Model 44
3.6.2 Overall Structure of the MoCCS Model 44
3.6.3 The MoCCS Chronic Regime 45
3.6.4 The MoCCS Acute Regime 55
3.6.5 Approach for Predicting Future Morphology.....58
3.6.6 Analyzing Uncertainty.....58

4. Results and Discussion.....63
4.1 Analyzing Historic Coastal Change and Remote Sensing Data.....63
4.1.1 Geomorphic Setting and Eglin Air Force Base Island Infrastructure.....63
4.1.2 Shoreline Change - Overview 65
4.1.3 Inlet Morphologic Change 70
4.1.4 Shoreline Change – DSAS Analysis.....75
4.2 Modeling Future Storms 78
4.2.1 Storm Losses versus Wind Speed 78
4.2.2 Effect of Sea Surface Temperature on Storms.....81
4.2.3 Modeling Hurricane Intensity Changes.....86
4.2.4 Modeling Future Wind and Surge Damage Losses 88
4.3 Analyzing Paleostorm History in Coastal Sediments 92
4.3.1 Lake Data.....92
4.3.2 Core Description 93
4.3.3 Sedimentologic and Isotopic Data 94
4.3.4 Micropaleontological Data 95
4.3.5 Geochronology.....96
4.3.6 Storm Surge Heights from SLOSH.....98
4.3.7 Storm Model Results.....98
4.4 Modeling Coastal Wetlands 101
4.4.1 SLAMM Modeling.....101
4.4.2 Results – Yellow River.....103
4.4.3 Results – Choctawhatchee Bay 106
4.4.4 Results – Eglin AFB – Santa Rosa Island.....108
4.4.5 Shoreline Orientation and Erosion 109
4.5 Modeling Coastal Groundwater 111
4.5.1 Impacts of Sea-Level Rise on Unconfirmed Aquifers.....111
4.5.2 Impacts of Sea-Level Rise on Confirmed Aquifers.....112
4.5.3 Groundwater simulation Results for 2100.....118
4.6 Modeling Morphologic Change 122
4.6.1 Project Shoreline Change.....122
4.6.2 Projecting Island Morphology Change.....130

4.6.3 Projected Inlet Zone Changes.....136
4.6.4 Discussion of Results.....136

5. Conclusions and Implications for Future Research and Implementation.....141
5.1 Analyzing Historic Coastal Change and Remote Sensing Data.....141
5.2 Modeling Future Storms 142
5.3 Analyzing Paleostorm History in Coastal Sediments 143
5.4 Modeling Coastal Wetlands 145
5.5 Modeling Coastal Groundwater 146
5.6 Modeling Morphologic Change 147

6. Literature Cited 149

List of Tables

Table 2.2.1: Project model features....12
Table 2.2.2: Explanation for project model selection....13
Table 3.1.1: Inventory of mapping, aerial imaging, and Lidar data used for DSAS analysis of the foreshore of Santa Rosa Island, Florida....16
Table 3.1.2: List of tide gauge measurements used to calculate mean high water elevation....18
Table 3.3.1: Storm parameters for major storms passing within 140-km radius of the study area at the eastern margin of Eglin AFB during historic time, 1851-present....22
Table 3.4.1: Principal input parameters for SLAMM for the Yellow River – Blackwater Bay and Catfish Basin, western perimeter of Eglin Air Force Base....33
Table 3.6.1: The time-averaged net shoreline change against storm intensity....54
Table 4.1.1: Major geomorphic units and land cover for the eastern half of Santa Rosa Island (from Navarre Beach to East Pass)....64
Table 4.2.1: Statistics from the quantile regressions. Values in parentheses are the 95% confidence intervals....80
Table 4.2.2: Census tract number and total area (acres) of the tracts used on our wind loss model....89
Table 4.3.1: Radiocarbon data for Western Lake core....97
Table 4.4.1: Predicted change in wetland habitats associated with a one meter sea level rise (2000-2100 for Yellow River delta and adjacent Catfish Basin, Santa Rosa County, Florida....103
Table 4.4.2: Predicted change in wetland habitats associated with a 0.69 meter sea level rise (IPCC A-1B maximum scenario) for Yellow River delta and adjacent Catfish Basin, Santa Rosa County, Florida for the time period 2000-2100....104
Table 4.4.3: Predicted change in wetland habitats associated with a two meter sea level rise (2000-2100 for Yellow River delta and adjacent Catfish Basin, Santa Rosa County, Florida....106
Table 4.4.4: Predicted change in wetland habitats associated with a one meter sea level rise (2000-2100 for Choctawhatchee Bay, Walton County, Florida....107
Table 4.6.1: One example of storm series for a 100-yr simulation....123
Table 4.6.2: Predicted shoreline change at location A for four sea level rise scenarios simulated by one hundred realizations of the next 100 years....127
Table 4.6.3: Predicted shoreline change at Location B for four sea level rise scenarios simulated by one hundred realizations of the next 100 years....128
Table 4.6.4: Predicted shoreline change at Location C for four sea level rise scenarios simulated by one hundred realizations of the next 100 years....129

List of Figures

Figure 1.1.1: Digital elevation model of the Eglin Air Force Base region, NW Florida. Boundary of the Eglin facility is shown with solid black line 4

Figure 1.1.2: Air photo showing the location of some of the significant infrastructure on Eglin AFB, Florida....5

Figure 1.2.1: Projected sea-level rise scenarios over the next century as well as the equation for calculating sea-level rise 6

Figure 1.2.2: Flowchart illustrating how the project modeling efforts, archival data compilation and field research were combined to develop methodologies for assessing the effects of sea-level rise and increased storminess on coastal military installations. 7

Figure 3.1.1: Comparison of HWL-derived shorelines (2007) derived by air photo mapping versus MHW-Lidar positions (2006 and 2008) for Santa Rosa Island 19

Figure 3.1.2: Representative transect locations for foreshore DSAS analysis of Santa Rosa Island, Florida 20

Figure 3.3.1: Tracks of the 32 hurricanes (Cat. 1-5) which have passed within a 140-km radius of the study area at the eastern margin of Eglin AFB 22

Figure 3.3.2: Tracks of the 14 major storms (cat. 3-5) which have passed within a 140-km radius of the study area at the eastern margin of Eglin AFB....23

Figure 3.3.3: Map of Eglin AFB region with inset air photo showing one of the coastal dune lakes in the study area which provided sediment cores for paleostorm analysis....25

Figure 3.4.1: SLAMM inundation model showing the general elevation hierarchy of the wetlands and their boundaries....32

Figure 3.4.2: Scaling from IPCC scenario A1B to the 1 meter, 1.5 meter and 2 meter SLR scenarios 32

Figure 3.4.3: Coastal wetland areas (marsh) in the vicinity of Eglin Air Force Base....33

Figure 3.5.1: Comparison of three conceptual models used for visualizing the impacts of sea-level rise on a saltwater wedge....35

Figure 3.5.2: Freshwater movement and the morphology of freshwater lens on a barrier island under varying conditions....36

Figure 3.5.3: Location of transect used for 2D freshwater lens model on Santa Rosa Island 38

Figure 3.5.4: Typical hydrogeologic section within the study area depicting the hydrostratigraphic sequences in this study domain 39

Figure 3.5.5: Surficial drainage units and pumping well locations in the study area....40

Figure 3.6.1: Schematic of the Model of Complex Coastal Systems (MoCCS) Chronic Component Parts....46

Figure 3.6.2: East Pass Inlet with the areas of the inlet mouth (yellow), flood tide shoal (red) and ebb tide shoal (blue) outlined 52

Figure 3.6.3: Comparison of measured and modeled shoreline change during the period of mild storm activity 53
Figure 3.6.4: Beach shoreline changes during the period of major hurricane landfalls showing a trend line indicating periods of retreat followed by partial recovery 54
Figure 3.6.5: Definition sketch for a cross-section profile of a barrier island with a single dune 55
Figure 3.6.6: Representative oblique views from LIDAR image and equivalent MoCCS model 56
Figure 3.6.7: Partitioning mechanisms of eroded dune sediment deposits considering three possible processes 57
Figure 3.6.8: Generated storm numbers fitted with Poisson distribution 59
Figure 3.6.9: Uniform distribution is used to generate storm tracks 59
Figure 3.6.10: Maximum storm surge height values and probabilities for different storm sizes 60
Figure 4.1.1: Eglin AFB infrastructure on Santa Rosa Island. Sites showing the primary mission test facilities and ancillary facilities 63
Figure 4.1.2: Northward oriented, oblique aerial image of Santa Rosa Island near test site A-10 showing the major geomorphic subdivisions 64
Figure 4.1.3: Topography of Santa Rosa Island approximately 1 kilometer east of the Eglin Air Force Base OAHL tower 65
Figure 4.1.4: Long-term changes of the shoreline of Santa Rosa Island in the vicinity of Eglin Air Force Base test site A-13 67
Figure 4.1.5: Development of major overwash fans on a narrow section of Santa Rosa Island near test site A-6 68
Figure 4.1.6: Damage to Eglin Air Force Base test sites following hurricanes Ivan and Dennis 69
Figure 4.1.7: Major geomorphic change in the position of the eastern terminus of Santa Rosa Island 71
Figure 4.1.8: Long-term changes in the shoreline position of the western terminus of Santa Rosa Island and Pensacola Pass (1856-2007) 72
Figure 4.1.9: Cumulative dredging volume for Pensacola Pass at the western end of Santa Rosa Island 73
Figure 4.1.10: Net shoreline change along Santa Rosa Island for selected time periods 74
Figure 4.1.11: Net shoreline change along Santa Rosa Island for the time period 1934-1994 75
Figure 4.1.12: Detail of shoreline changes for two selected locations - western (Fort Pickens) and eastern (Eglin Air Force Base) portions of Santa Rosa Island 76
Figure 4.1.13: Detail of shoreline changes for two selected locations - western (Fort Pickens) and eastern (Eglin Air Force Base) portions of Santa Rosa Island for the period 1994-2010 77
Figure 4.2.1: Time series of normalized losses 79

Figure 4.2.2: Frequency distribution of wind speeds (right) and damage (left) of all U.S. hurricanes since 1900 79
Figure 4.2.3: Quantile fits of economic damage as a function of wind speed 80
Figure 4.2.4: Hurricane frequency and intensity over the period 1981-2010 82
Figure 4.2.5: Limiting intensities and model parameters over the western Caribbean Sea and Gulf of Mexico 83
Figure 4.2.6: Scatter plots of limiting intensity and model parameters versus SST for grids having SST values greater than 26^0C 84
Figure 4.2.7: Scatter plots of limiting intensity versus SST 85
Figure 4.2.8: Change in Gulf of Mexico tropical cyclone intensity from 1900–2009 86
Figure 4.2.9: Gulf of Mexico SST trend showing the change in SST over the past 110 years (1900–2009 87
Figure 4.2.10: Modeled wind loss curves and percentage increase in losses 91
Figure 4.2.11: Future hurricane Opal with stronger winds and higher sea level 92
Figure 4.3.1: Location map of Western Lake, on the NW Florida coast 93
Figure 4.3.2: LIDAR imagery of the Western Lake area, NW Florida 94
Figure 4.3.3: X-radiograph, and profiles of percent sand, δ^{13}C, and % N' for core 070910-03 95
Figure 4.3.4: Comparison of δ^{13}C and δ^{15}N values of organic matter in lake sediment within the study area 96
Figure 4.3.5: The time-depth curve derived from the radiocarbon dates from Core 070910-03 97
Figure 4.3.6: Results of the storm model applied to the Western Lake core data 100
Figure 4.3.7: Major storm history for the northwest Florida coast, based on the paleostorm model 101
Figure 4.4.1: Digital orthophoto mosaic of the Yellow River, Blackwater Bay and Catfish Basin salt marsh estuary system 102
Figure 4.4.2: Change in the area of wetland habitats for the Yellow River delta and adjacent Catfish Basin between 2000 and 2100 104
Figure 4.4.3: Change in wetland habitats for the Yellow River delta and adjacent Catfish Basin between the years 2000 and 2100 105
Figure 4.4.4: Change in the area of wetland habitats for the Choctawhatchee Bay, Walton County, Florida for the period 2004-2100 108
Figure 4.4.5: Limited fresh and tidal marsh located on the north side of Santa Rosa Island 109
Figure 4.4.6: Variation in shoreline erosion in the Catfish Basin, located along the southern edge of the Yellow River delta 110
Figure 4.5.1: Comparison of steady-state salt wedges in the unconfined aquifer before and after sea-level rise 111
Figure 4.5.2: Comparison of hydraulic head distributions in the barrier island before and after sea-level rise 112

Figure 4.5.3: Comparison of freshwater lens predicted before and after the sea-level rise on the barrier inland 112
Figure 4.5.4: Hydraulic head distribution of surface aquifer in pre-development condition 113
Figure 4.5.5: Hydraulic head distribution of upper Floridian aquifer in pre-development condition 113
Figure 4.5.6: Hydraulic head distribution of lower Floridian aquifer in pre-development condition 114
Figure 4.5.7: Pre-development salinity distribution in the upper Floridian Aquifer 115
Figure 4.5.8: Pre-development salinity distribution in the lower Floridian Aquifer 115
Figure 4.5.9: The hydraulic head distribution in upper Floridian Aquifer, 1998 116
Figure 4.5.10: Potentiometric surface of the Floridian Aquifer system, 1998 116
Figure 4.5.11: The hydraulic head distribution in lower Floridian Aquifer, 1998 117
Figure 4.5.12: The distribution of salinity difference between 1942 and 1998 in Upper Floridian Aquifer 117
Figure 4.5.13: The distribution of salinity difference between 1942 and 1998 in Lower Floridian Aquifer 118
Figure 4.5.14: Hydraulic head difference of surface aquifer from 1998 to 2010 119
Figure 4.5.15: Hydraulic head distributions in 1998 and in 2100 with +1m sea level rise in Upper Floridian Aquifer 119
Figure 4.5.16: Hydraulic head distributions in 1998 and in 2100 with +1m sea level rise in the Lower Floridian Aquifer 120
Figure 4.5.17: The salinity distributions in 1998 and in 2100 after +1m sea level rise in the Lower Floridian Aquifer 121
Figure 4.5.18: Salinity difference between 1998 and 2100 with +1m and + 2m level rise in the Upper Floridian Aquifer 121
Figure 4.5.19: Salinity difference between 1998 and 2100 with +1m and + 2m level rise in the Lower Floridian Aquifer 122
Figure 4.6.1: MoCCS model predictions of relative shoreline changes over the central portion of Santa Rosa Island for a future 100-year scenario for different rates of sea level rise 125
Figure 4.6.2: Locations of the results given in the next three figures 125
Figure 4.6.3: Projections of shoreline change at Location A (Section 90) 126
Figure 4.6.4: Projections of shoreline change at Location B (Section 140) 127
Figure 4.6.5: Projections of shoreline change at Location C (Section 260) 128
Figure 4.6.6: Projected shoreline changes near the Test Area 13B Tower for the scenario where the present rate of sea level rise continues 129
Figure 4.6.7: Projected mean values of the shoreline position change at the Test Area 13B Tower for the scenario where the present rate of sea level rise continues 130

Figure 4.6.8: Changes over three island cross-sections of dune height, bay shore and island platform freeboard for a 100-yr simulation containing six hurricane events 132
Figure 4.6.9: Comparison of the island response to five 100-yr sea level rise scenarios for the narrow (100 m) cross section 133
Figure 4.6.10: Temporal variation of mean and variance of bay-shore position under the five sea-level rise scenarios at Profile 3.....134
Figure 4.6.11: Probability density function (PDF) of bay-shore position at cross-section 60 at (a) 25 years, (b) 50 years, (c) 75 years, and (d) 100 years. 134
Figure 4.6.12: Scenario averaging of (a) mean and (b) variance of backshore position prediction at cross-section 60 using 126 scenario probability sets 135
Figure 4.6.13: PDFs of backshore position prediction at cross-section 60 on year (a) 25, (b) 50, (c) 75, and (d) 100 using scenario averaging. 136
Figure 4.6.14: Computed relative changes on the shoreline adjoining the East Pass Inlet for different rates of future sea level rise 137
Figure 5.2.1: Future hurricane Opal with stronger winds and higher sea level, showing roadway grid 144

List of Acronyms

DGH: Dupuit-Ghyben-Herzberg
DHT: Dune Height
EAFB: Eglin Air Force Base
FEMA: Federal Emergency Management Agency
HiRAM: The Geophysical Fluid Dynamics Institute (GFDI) High Resolution Atmospheric Model
IDW: Inverse-Distance Weighted
IMZ: intertidal mixing zone
IPCC: Intergovernmental Panel on Climate Change
IPCC-SRES: IPCC Special Report on Emissions Scenarios
MC: Monte Carlo
MLW: Mean Low Water
MoCCS: Model of Complex Coastal Systems
NAVD88: North American Vertical Datum of 1988
NED: National Elevation Dataset
netCDF: network Common Data Format
NOAA: National Oceanic and Atmospheric Administration
NRC: National Research Council
NW: Northwest
NWI: National Wetlands Inventory
OGP: Organic Geochemical Proxy
POT: Peaks Over Threshold
RMS: Root Mean Square
SERDP: Strategic Environmental Research and Development Program
SLAMM: Sea Level Affecting Marshes Model
SLOSH: Sea, Lake and Overland Surges from Hurricanes
SLR: Sea Level Rise
SON: Statement of Need
SST: Sea Surface Temperature
USACOE: U.S. Army Corps of Engineers
USFWS: U.S. Fish and Wildlife Service

Keywords

Sea-level rise, climate change, coastal modeling, coastal morphology, coastal systems, storm hazards, barrier island, remote sensing, coastal wetlands, groundwater modeling, coastal infrastructure, shoreline evolution, uncertainty assessment

Acknowledgements

This project was supported through a contract with the Strategic Environmental Research and Development Program (SERDP RC-1700) to Florida State University. Dr. John Hall served as SERDP program manager for the project. Field work was carried out with the cooperation of the Natural Resources Section, Eglin Air Force Base, Florida. We are grateful for the assistance of the following EAFB personnel: Michael Applegate, Ralph Armstrong, Chadwick Avery, Glen Barndollar, Robin Bjorklund, Bruce Hagedorn, Thomas Heffernan, John Hiers, Rip Kirby, Steve Laine, Joe Meyer, Bob Miller, William Pizzalato, and Brett Williams. The Choctawhatchee Basin Alliance and Dr. Jon Bryan, of the Department of Earth Sciences at Northwest Florida State College, provided essential help in field work. Kris Barrios and Ron Bartel, of the Northwest Florida Water Management District provided monitoring instruments which aided the field work. The assistance of Jennifer Coor, Heng Dai, Oindrila Das, Shawn Lewers, Jill Malmstadt (Trepanier), Ravi Sankar, Kelsey Scheitlin, Thomas Wallace, Xiaoying Zhang, and Brandon Adams in various aspects of this project is gratefully acknowledged. We also are grateful for the assistance of Rick Sanborn, URS Corporation, in assembling this report.

Final Technical Report

Effects of Near-Term Sea-Level Rise on Coastal Infrastructure (SERDP RC-1700)

Abstract

Objectives. The objective of this investigation was to develop new methods for comprehensive modeling of the effects and potential risk of projected sea-level rise, and increased storminess, on coastal environments and infrastructure. The project has focused on the Eglin Air Force Base (EAFB) region on the northwest Florida coast. The methods that have been developed in this work are applicable to military installations in similar coastal settings.

Technical Approach. The project had six major components: (1) analyzing historic coastal change and remote sensing data; (2) modeling future storms; (3) analyzing the paleostorm history in coastal sediments; (4) modeling coastal wetlands; (5) modeling coastal groundwater; (6) modeling morphologic change and analyzing uncertainty. The project's modeling efforts have employed various sea-level rise scenarios, ranging from 0.5 meters to 2.0 meters by the year 2100.

Results. The project has had several significant outcomes. We have developed one of the most comprehensive databases ever assembled on historic changes in shorelines and barrier island morphology. By combining remote sensing and survey data, we have created a unique time series of shorelines and barrier evolution. This robust data set has informed our model development and enabled the creation of a conceptual model for the evolution of the Santa Rosa Island barrier plus a purpose-built numerical model. Santa Rosa is important as the site of substantial EAFB infrastructure.

A regional storm history has been developed for use in the modeling effort, both for historic and prehistoric time. The historic database encompasses approximately 150 years. The prehistoric record, from coastal sediment cores, extends back over approximately four millennia. A storm model incorporates this history to create an ensemble of future storm tracks and potential storm effects for the region. Changes in future storm wind and storm surge damage from more common large hurricanes can thereby be assessed.

We have developed a purpose-built numerical model of coastal morphology, incorporating morphological, sea-level, and storm climatology data to predict changes over the next century. This Model of Complex Coastal Systems (MOCCS) includes representations of the shoreline position and coastal landform changes caused by periods of both ordinary weather and storm events. The system components include the beach and surf-zone, the adjoining shoreface and inner continental shelf, the tidal inlet and adjacent bay, along with the coastal dune system and the overwash deposits that affect the freeboard of the barrier island and the position of its bay shoreline. All components respond to variations in the major forcing parameters, which include the sediment supply, wave climate and changing sea level. The model represents the complex

non-linear interactions between these system components in response to the five different sea level rise scenarios. These are the four specified previously and one representing the continuation of the present sea level rise rate continued over the coming century. Uncertainty analyses are employed to characterize uncertainty sources and to quantify propagation of the uncertainty through numerical models. In particular, the scenario uncertainty of sea-level rise is quantified using a scenario averaging method. Results regarding barrier island shoreline and morphologic changes are stated probabilistically and are suitable for use by base planners and managers.

Benefits. The outcomes of this study can be used to evaluate how to make reliable predictions of the effects of future climate change on coastal infrastructure and natural coastal systems. The expected result will be to enable cost-effective mitigation and adaptation strategies to prepare for a warmer future.

1. Objectives

1.1. SERDP Statement of Need (SON)

This project was undertaken in response to the SERDP Statement of Need SISON-09-05, Assessment of the Impact of Sea-Level Rise on Military Infrastructure. The SON requirements include the following:

- Develop analysis methods to assess the impacts of local mean sea-level rise of 0.5 m, 1.0 m, 1.5 m, and 2.0 m, and utilize these methods to assess the impacts to a coastal military installation.

- Include an assessment of the potential impacts caused by an increase in the frequency and intensity of storms.

- Include an analysis of the impacts due to: (1) inundation of land; (2) increased storm and flood damage; (3) loss of wetlands; (4) changes in erosion patterns and rates; (5) salt water intrusion in surface and ground waters; (6) rising water tables; and (7) changes in tidal flows and currents.

- For the specific military installation selected, examine: (1) loss of or damage to mission essential infrastructure; (2) loss or degradation of mission capabilities; (3) loss of training and testing lands; (4) loss of transportation means, facilities and/or corridors; (5) increased risk of storm damage; and (6) increased potential for loss of life (not including disease or other indirect health impacts).

- Utilize routinely available data and existing models.

- Develop methodologies capable of implementation at any DoD installation worldwide that may be affected by a rise in sea level.

The Department of Defense has recognized climate change and sea-level rise as emerging issues with potential national security implications. This report summarizes our information-to-action approach in addressing how near future climate change and sea-level rise might affect a coastal military installation, using Eglin Air Force Base (EAFB) as a typical example. Our emphasis has been on how the base's infrastructure could be affected by sea-level rise and changes in the intensity of tropical cyclones over the next century. The regional location of EAFB on the northwest Florida coast is shown in Figure 1.1.1. Location of some of the significant base infrastructure is shown in Figure 1.1.2.

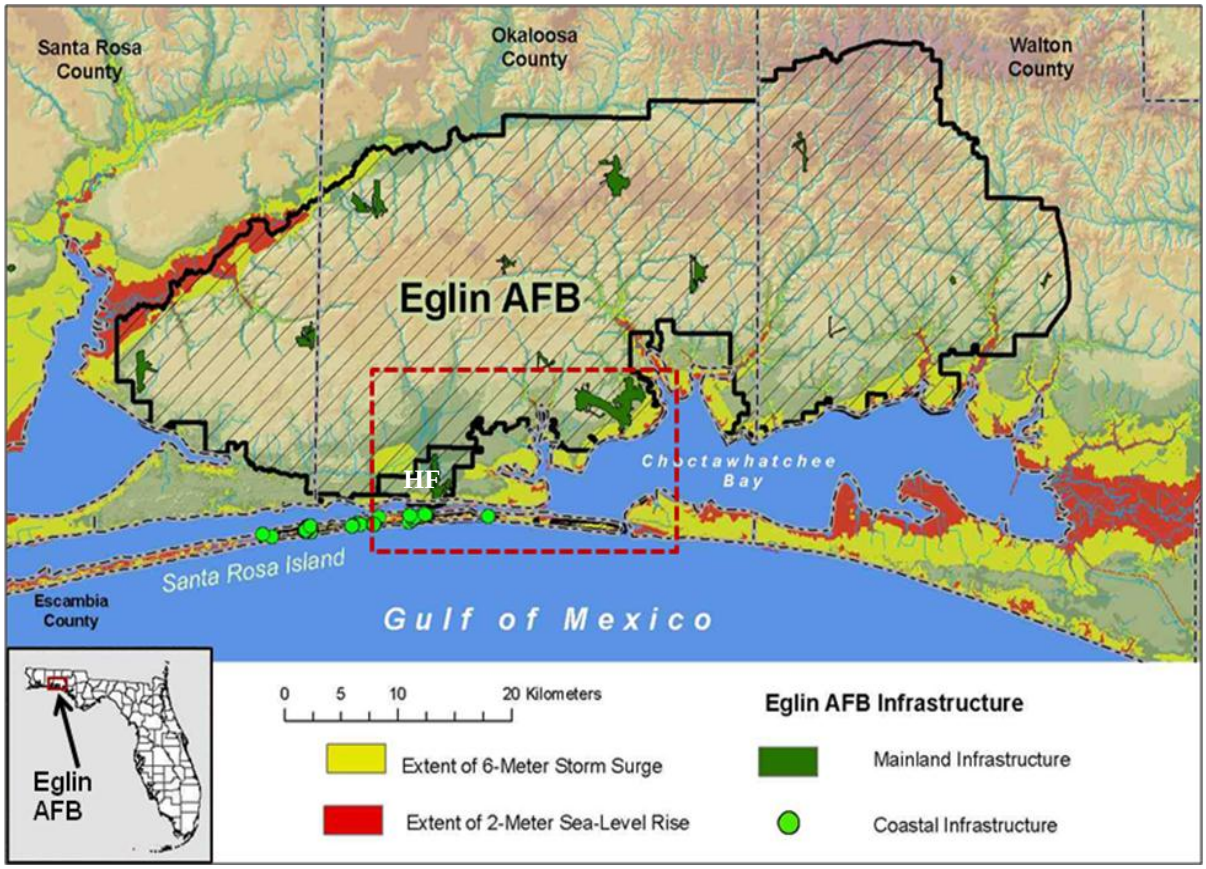

Figure 1.1.1. Digital elevation model of the Eglin Air Force Base region, NW Florida. Inset map shows regional location. Boundary of the Eglin facility is shown with solid black line. The border (HF) inside the overall base outline represents the location of Hurburt Field, a major infrastructure area on EAFB located landward from Santa Rosa Island. Hurlburt Field is separated from other developed areas of Eglin AFB by the city of Fort Walton Beach. The 6-meter elevation boundary represents the height of maximum storm surge from a major storm under current conditions. The red rectangle indicates the location of Figure 1.1.2.

Located on the panhandle coast of northwest Florida, EAFB is used by the U.S. military as a development and testing ground for air-delivered weaponry and training. The military has made considerable infrastructure investment on the base, ranging from roads and airfields to personnel housing and radar installations. Given its low elevation and proximity to the Gulf of Mexico, much of this built environment is exposed to hurricane winds and storm surge. Some of the most sensitive infrastructure has been constructed on a barrier island, Santa Rosa Island. In particular, military planners are concerned with the potential increasing risk of enhanced effects of storm surge and wind under future climate scenarios (Heffernan, 2011).

Our technical approach has been to develop frameworks for understanding the future risk to Eglin AFB infrastructure by combine preexisting and purpose-built numerical and statistical models in novel ways. This has resulted in innovative methodologies for projecting future impacts on coastal infrastructure and coastal environments. We have developed the methodology

for the EAFB, but the approach is general enough to be applied at other hurricane-vulnerable coastal military installations.

This report provides a detailed description of the principal activities that comprised the project. The order in which they appear in the following sections is: (1) Analyzing Historic Coastal Change and Remote Sensing Data; (2) Modeling Future Storms; (3) Analyzing Paleostorm History in Coastal Sediments; (4) Modeling Coastal Wetlands; (5) Modeling Coastal Groundwater; (6) Modeling Morphologic Change and Analyzing Uncertainty.

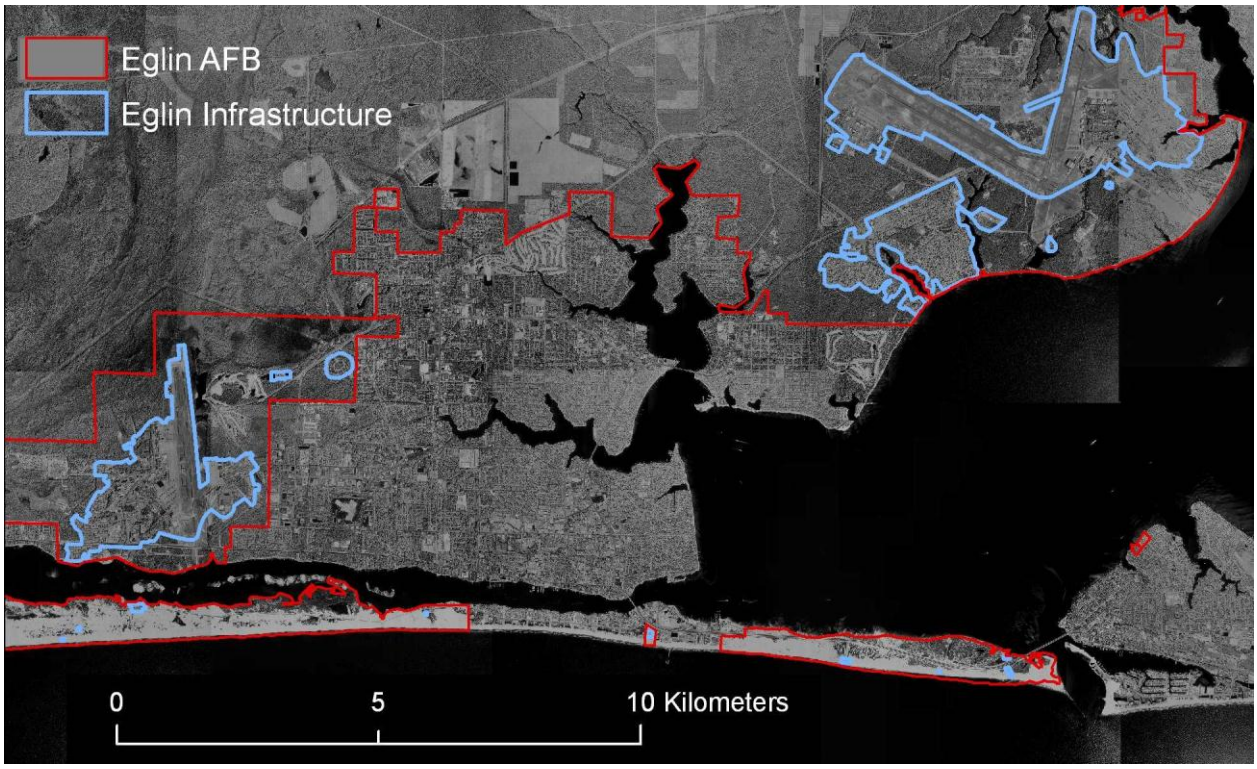

Figure 1.1.2. Air photo showing location of some of the significant infrastructure on Eglin AFB, Florida. Location of image is shown by red rectangle in Figure 1.1.1. Major base infrastructure include two major airfields, outlined in blue: Eglin Main Base (east side of figure) and Hurlburt Field (west side). Both locations support a large number of training facilities. Infrastructure facilities on Santa Rosa Island (Figure 1.1.1) include radar, optical and electronic tracking sites in support of the Eglin Gulf Test and Training Range. A major test structure, the one hundred meter high "open-air-hardware-in-the-loop" tower test facility (OAHL), is located in close proximity to the Gulf shoreline near the mid-point of the base portion of the island (Figure 4.1.6A).

1.2. Overall Project Objectives

The overall objective of the project has been to develop analysis methods to assess the impacts of a local mean sea level rise of 0.5 meters, 1.0 meters, 1.5 meters and 2.0 meters, and associated phenomena, including storm surge, on military infrastructure, and to assess the utility of these methods for predicting potential impacts to specific coastal military installations. A graphical depiction of the four sea-level rise scenarios, along with some recent model predictions, is shown in Figure 1.2.1. The research has been specifically directed at evaluating the impacts given in the SON, which include: (a) loss or damage to mission essential infrastructure, (b) degradation of

mission capabilities, (c) loss of training and testing lands, (d) loss of transportation means, facilities and/or corridors, (e) increase in storm damage and (f) increased potential for loss of life. The investigation has been responding to the SERDP SON by developing methods for quantifying the hazard risk to coastal facilities. Where possible, these methods are quantitative and generally rely on existing empirical, stochastic or deterministic numerical models or on purpose-built new ones. The models are designed to predict the extent of increased risk under near-future scenarios of sea-level change.

To meet the overall objective, the work was partitioned into several tasks, each with specific objectives, which are summarized below. A schematic showing how the various project components interacted with each other is shown in Figure 1.2.2.

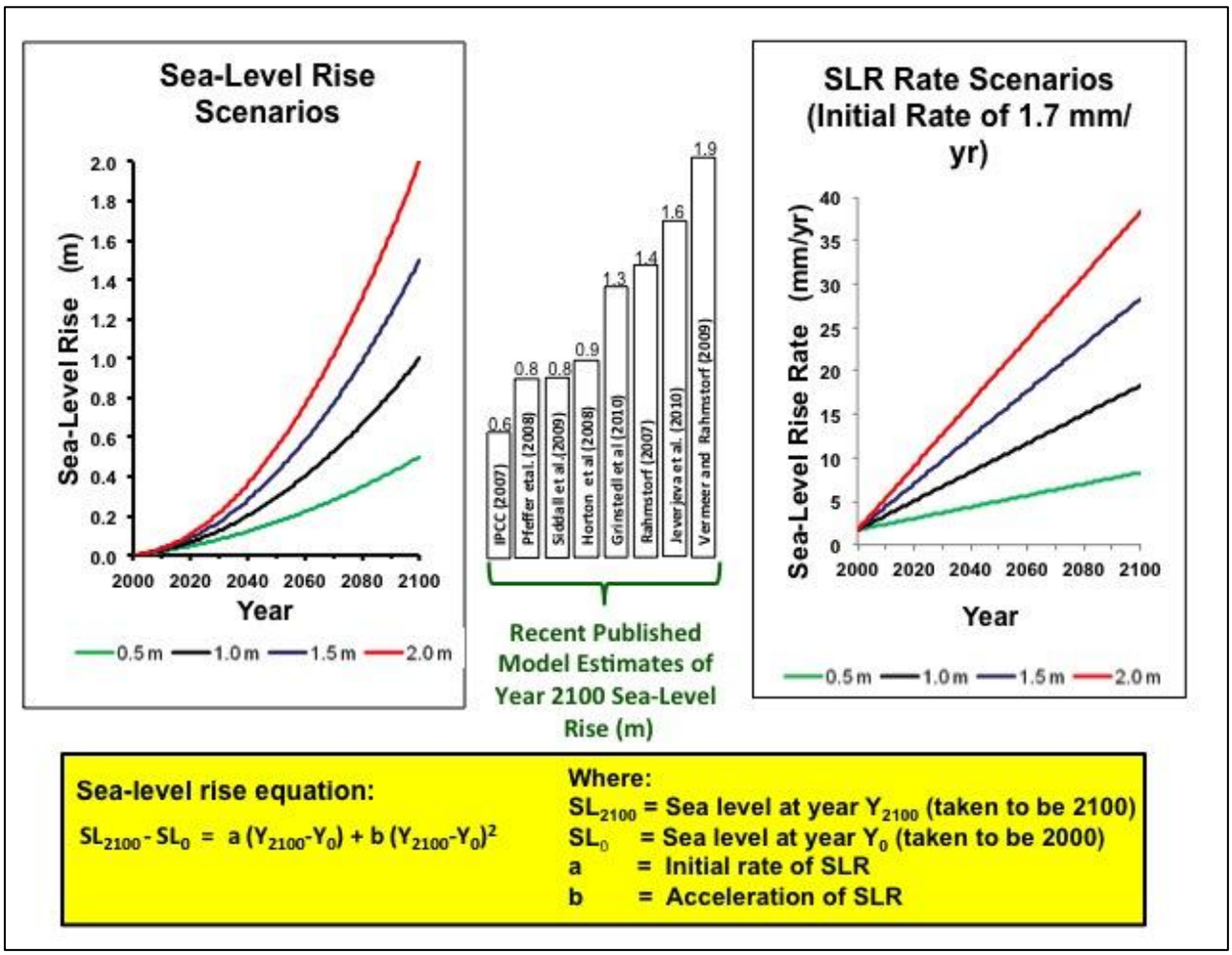

Figure 1.2.1. Sea-level rise scenarios used in this project are shown at left. Change in sea-level rise rates is depicted at right. Histograms of several recent model estimates of sea-level rise over the next century are shown in center for comparison. The equation for projecting sea-level rise is shown at the bottom. The initial rate of SLR (a) is taken to be 1.7 mm/yr, the global tide gage long-term average. The acceleration of sea-level rise (b) is taken from U.S. Army Corps of Engineers (2009) and National Research Council (1987).

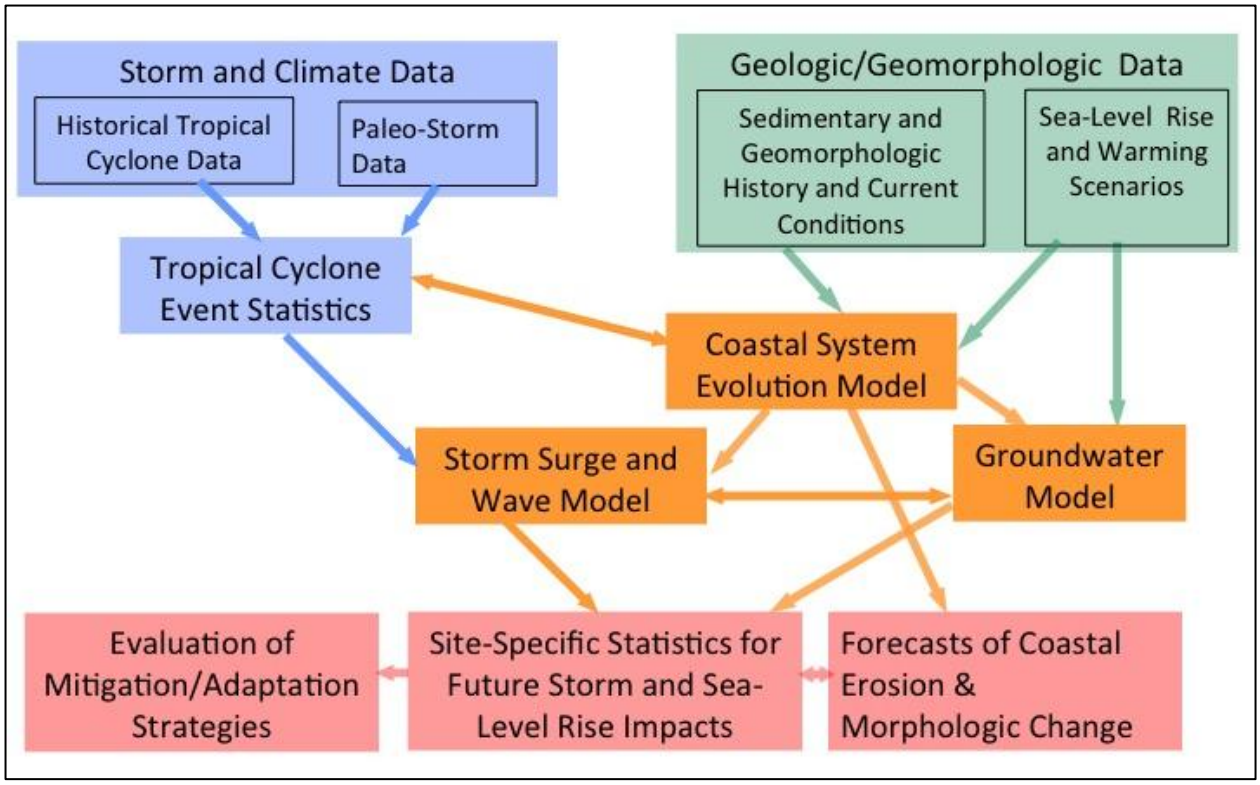

Figure 1.2.2. Flowchart illustrating how the project modeling efforts, archival data compilation and field research were combined to develop methodologies for assessing the effects of sea-level rise and increased storminess on coastal military installations.

1.3. Specific Project Objectives

1.3.1. Analyzing Historic Coastal Change and Remote Sensing Data. The objective of this component of the project has been to develop a comprehensive collection of data defining the morphological changes in the project area over as long a period as possible. These data include recent and historic maps, aerial photographs, LIDAR, and other remote sensing imagery. The data were employed to support an analysis of shoreline and barrier island change in relation to the storm climate, to provide the basis of a conceptual model, and to provide information needed to calibrate and verify a morphodynamic model being developed as part of another project task.

1.3.2. Modeling Future Storms. The objectives of this component of the project were to characterize the present storm climatology affecting the Eglin Air Force Base project area, to project future changes to this storm climatology over the coming century, and to use this information to estimate the potential change in base infrastructure damage for different scenarios of sea level change and storm climatology. The chief goal was to develop an understanding of the methods, models, and tools for conducting vulnerability and impact assessments related to future hurricane risk along the Gulf coast of the United States. Hurricanes cause an average of $10 billion in damage in the United States annually. In the stormy years of 2004 and 2005, the damage totaled $150 billion (Pielke et al., 2008). Approximately 85% of U.S. hurricane damage comes from major hurricanes (Category 3 or higher on the Saffir-Simpson hurricane scale), while they comprise only 24% of landfalling hurricanes (Pielke et al., 2008). In fact, the top 35 loss events (less than 16% of the total number of loss events) account for more than 81% of the

total loss amount (Jagger et al., 2011) with losses increasing exponentially with wind speed at landfall.

1.3.3. Analyzing Paleostorm History in Coastal Sediments. The objective of this component was to develop and apply a new geochemical and statistical approach to paleostorm analysis. The historic record of coastal storms is typically limited to 150 years or less. Longer proxy records, of several millennia, are available in the sediments of coastal lakes and wetlands. We have refined a new proxy method as part of this project and have obtained a more quantitative understanding of major storm occurrence as a result. The outcome enables greater confidence in future storm modeling. It also serves as a new technique that can be applied to other regions of the U.S. coast.

1.3.4. Modeling Coastal Wetlands. The objective of this task was to estimate the probable changes in coastal wetland systems in the project area on and surrounding Eglin Air Force Base. This objective was supported by the use of the Sea Level Affecting Marshes Model (SLAMM) and other similar numerical models with input data developed from our Sediment Elevation Table (SET) databases for this region. These predictions were carried out for five sea-level rise scenarios: continuation of the present rate and four other rates leading to century-long changes of 0.5, 1.0, 1.5 and 2.0 m.

1.3.5. Modeling Coastal Groundwater. The objectives of this study were to: (1) simulate the saltwater intrusion interface based on a synthetic model, using field data from nearby St. George Island; (2) determine the morphology of the freshwater lens and water table variation on Santa Rosa Island; (3) estimate the possible effects of surge on the freshwater lens and the island hydrological environment; and (4) evaluate the influence of sea level rise on the groundwater resources in the mainland Eglin Air Force Base area.

1.3.6. Modeling Morphologic Change. The goal of this component was to develop a comprehensive numerical modeling framework, designated the Model of Complex Coastal Systems (MoCCS), for providing quantitative predictions of changes in coastal morphology that need to be factored into planning, engineering and civil infrastructure maintenance efforts. To be comprehensive and capable of application in a range of actual settings where coastal military bases are located, the modeling framework represents the full set of components of a complex coastal system. This segment of the project also characterized uncertainties and quantified their propagation in the morphologic change modeling. Two categories of uncertainty were considered: uncertainty in modeling scenarios (e.g., sea-level rise) and uncertainty in coastal components, dynamic processes, and system properties, such as storm characteristics. The former is referred to scenario uncertainty and the latter to parametric uncertainty. Propagation of parametric uncertainty is first quantified using Monte Carlo method, followed by quantification of scenario uncertainty propagation using a scenario-averaging method Results of the uncertainty analysis are important for decision-making in coastal management. It is worth mentioning that the methods of uncertainty analysis are general and can be applied to other models developed in this project and other coastal systems.

2. Background

2.1. Environmental Issues Addressed

Hurricanes are complex dynamical systems covering a large range of spatial and temporal scales and a broad range of characteristics (intensity, track, forward speed, etc.). High resolution weather prediction models are capable of forecasting much of this complexity out several days or more with reproducible skill which exceeds that obtainable from empirical or statistical approaches. Improvements to the model physics and resolution will likely lead to even better forecasts.

On the climate scale, however, ranging from months to multiple decades, reliable projections of tropical cyclone activity remain a challenge and it is not yet apparent that global climate models (GCMs) are up to the task. GCMs do not yet have sufficient space and time resolutions to capture the inner eye-wall thermodynamics of real tropical cyclones. This is particularly germane to local assessments of future storminess. Collectively, intensity, frequency, location, and track define local hurricane activity. Of these, only intensity -- estimated by the maximum wind speed inside the hurricane -- is theoretically linked via potential intensity to anthropogenic climate change, on the basis of upward trends in ocean heat. The problem is complicated by environmental conditions that influence hurricane frequency and their paths, but there is yet no credible evidence that wind shear or other factors that might inhibit hurricanes will change in the future, at least not relative to increases in ocean warmth.

2.2. Summary of Past Research

A major effort in coastal science in recent years has involved the advancement of models to assess the enhanced risk associated with accelerated sea-level rise and increased storminess which may result from projected future warming. Modeling efforts have focused on better evaluating coastal storm surge risk (e.g., Westerink et al., 2008), infrastructure damage (e.g., Hamid et al., 2010), the potential for future storminess (e.g., Vecchi and Knutson, 2008; Landsea et al., 2010; Elsner et al., 2008), the long-term responses of natural coastal systems (e.g., Cowell et al., 2003a and 2003b; deVriend et al., 1993; Niedoroda et al., 2001 and 2003), and effects on tide ranges (e.g., van Goor et al., 2001), river systems (e.g., Fagherazzi et al., 2004a and 2004b) and salt marshes (e.g., Morris et al., 2002; Mudd et al., 2004).

These and other similar studies have produced process-oriented numerical models. There is a growing movement to harness such modeling advances within multi-disciplinary studies of natural systems (e.g., Capobianco et al., 1999; deVriend, 2001). An example is the Dynamic Interactive Vulnerability Assessment (DIVA) model, developed by the European DINAS-COAST Consortium, which operates on very large scales using old static coastal inundations (so called ‘bathtub flooding’), which has been used at national levels as a planning tool (Hinkel and Klien, 2003; Hinkle 2005). The aim of the current project has been to make maximum use of such developments in coastal modeling, at the local scale and over longer time scales, in order to produce a comprehensive localized analysis of the effects of sea-level rise on natural coastal systems and infrastructure.

Over the past several decades a number of geophysical numerical models have been developed and put into use. These represent various aspects meteorological, oceanographic and coastal

morphodynamic processes that are useful in wide range of engineering, emergency management, and planning applications. An extensive list containing many, of these models is provided in the Community Surface Modeling System collection which is maintained at the University of Colorado. Two of these existing models are of special interest because they are used to evaluate parameters that are used in MoCCS Model.

The NOAA SLOSH model is used by the National Hurricane Center (NHC) to estimate storm surge heights and winds resulting from historical, hypothetical, or predicted hurricanes by accounting for pressure, radius, forward speed, track, and winds. It is a two-dimensional, depth-integrated finite difference code. SLOSH utilizes a curvilinear grid system to allow high resolution in the area of forecast interest, computes surges over bays and estuaries, retains some non-linear terms in the equations of motion, and allows for the representation of sub-grid scale features such as channels, barriers, and flow of surge up rivers. The telescoping grid provides a large geographical area with detailed land topography. The smallest grid represents an area of about 0.1 square mile (sq mi). This grid size permits inclusion of topographic details such as highway and railroad embankments, causeways, and levees. The largest grid cell is approximately 11.6 sq mi. The model accounts for astronomical tides by specifying an initial tide level, but does not include rainfall amounts, riverflow, or wind-driven waves.

The SLOSH model has a mathematical representation of the moving wind and pressure field of tropical cyclones which is used to evaluate the surface wind stress and atmospheric pressure over the model domain during the transit of a model hurricane (see Jelesnianski et al. 1992). This forcing drives a coupled hydrodynamic model which produces a time-history of the spatially varying coastal storm surge. The model has a moving boundary with allows the storm surge to flood inland. The model was developed for use as a tool for real-time predictions of coastal storm surge heights and has been used for decades by the NHC to warn coastal communities. The inputs include a topo-bathy mesh representing the land elevations and water depths over the model domain. The mesh also contains representations of river and stream channels as well as small scale linear flow barriers such as dune line and embankments as sub-grid elements. These inputs also include specification of the storm track, central pressure deficit, radius to maximum winds and forward speed of the storm.

There are now many models of hurricane storm surge to choose between and these could be readily substituted for SLOSH for its use with MoCCS. The purpose of the surge model is to derive a set of maximum surge heights and their longshore spatial gradients that are associated with a limited number of hurricane storm conditions which represent the range of storm intensities within a project area as derived from historic records. Although the SLOSH model is considered to be an older member of currently available models it is still in very widespread use. It has been extensively tested by the NHC and various parameters such as wind drag and bottom friction coefficients are considered by NOAA and the general user community to be well calibrated. In most uses of the model the values of the model parameters are not changed.

The U.S. Army Corps of Engineers Coastal Modeling System has recently developed two linked models that are used to develop input parameters to MoCCS. These are the CMS-Flow and CMS-Wave models. CMS Flow is a coupled time-dependent 2D depth-averaged circulation, sediment transport and morphodynamic model. The model is based on the numerical solution of the depth-averaged mass and momentum equations on a Cartesian grid network. The model is supported by the USACE. The circulation model component supports wind, tide and wave

radiation stress forcing, and includes special features such as flooding and drying, wind-speed dependent (time-varying) wind-drag coefficient, variably-spaced bottom-friction coefficient, time-and space-varying wave-stress forcing, efficient grid storage in memory, and hot-start options. Sediment transport is forced by the circulation model derived currents and coupled wave models (CMS Wave). Various bedload and suspended load models such as Lund-CIRP and Van Rijn formulations are available via user options in the model. The sediment transport model is coupled to a morphodynamic module that calculates time-dependent changes in the bed elevation. The hydrodynamic grid is then updated to reflect the depth changes, which then completes the coupling. The CMS Flow model is supported with the SMS Stormwater Modeling Software package, which provides a GUI for model setup, running and post-processing. Details of the theory and numerical implementation are presented in the CMS-Flow technical report (Buttolph et al., 2006).

CMS-Wave can simulate important coastal wave processes including diffraction, refraction, reflection, wave breaking and dissipation mechanisms, wave-current interaction, and wave generation and growth. The wave diffraction process is calculated in the wave-action balance equation. Other features of CMS-Wave include the grid nesting capability, variable rectangle cells, wave overtopping, wave run-up on beach face, and assimilation for full-plane wave generation. Details of the theory and numerical implementation are presented in the CMS-Wave technical report (Lin et al., 2006).

This model pair is used to create long-term (e.g., one year) simulations of currents and waves over the same size model domain as represented in MoCCS. These models operate at time scales of seconds and are used to output conditions at 6-hour increments over the whole year for a large number of points distributed over the model domain. This is considered as a synthetic representation of the wind driven and tidal currents and locally generated waves from which time averaged values of the horizontal diffusion and entrained sediment concentration are derived. The CMS model pair are operated in an uncalibrated mode based on the reasoning that their outputs substitute for what could be a very expensive program of current and wave measurements or for the results from calibrated versions of these or other models. For the purposes of the MoCCS development reasonable inaccuracies in the representation of the long-term behavior of waves and currents in the model domain do not affect the operation of MoCCS. It would only be necessary to bear the considerable expense of an extensive field measurement program to calibrate the CMS model pair when the results of the MoCCS model are to be applied to a specific coastal base or facility.

The MoCCS model was developed to rely on SLOSH and CMS FLOW/WAVE for parameterized inputs. The structural limitations, model sensitivities, relationship between input and output uncertainties and how these have been verified, calibrated or validated are described in Table 2.2.1. This table also includes similar descriptions for other numerical models used in this project.

Table 2.2.1. Project Model Features.

Model	Structural Limitations	Model Sensitivities (decending order)	Input/Output Uncertainties	Verification, Calibration, Validation
MoCCS	Large time scales model uses parameterized/ schematized short time scale processes. Uses simplified topography and smoothed bathymetry. Assumes maintained tidal inlets.	Hydrodynamic/storm climate Sea level rise rate. Sediment supply rate Topo/bathy simplifications	Output uncertainties are nonlinearly proportional to input uncertainties.	Verified against more than 100-yrs of measured morphological changes
SLOSH	Fixed and inflexible inputs. Basic imbedded hurricane model Simplified topography. Relatively coarse grid No astronomical tide	Central pressure Radius to max. wind Forward speed Track azimuth Local topography	Operator-dependent results comparable with other models	Verified in many scores of NOAA predictions and FEMA studies.
CMS Flow/Wave	Requires extensive input data. Intended for engineering scale problems not 100-yr simulations. High computational loads. Long run times	Topo-bathy inputs Wind speed/direction Tide inputs Sediment grain sizes	Complex interactions	Verified by USACE in numerous projects although not for the Eglin project area
SLAMM	Fixed vegetation inputs No suspended sediment processes Region-dependent responses No storm erosion Output in terms of land use only, no infrastructure component	Sedimentation rate Erosion rate Growth curves Tide range Sea level rise rate Topography	Relationships are complex and undocumented	Parallel field study by Warren Pinnacle Consulting in Choctawhatch ee Bay
Modflow	Fixed domain boundary and cannot address dynamic shoreline Use Dupuit assumption that ignores seepage face from auifer to ocean Linearized source terms, e.g. rivers	Hydraulic conductivity Pumping rate Sea level River stage Storativity	Hydraulic conductivity is inherently uncertain. Output uncertainty if not quantified	Validation and verification done by developer, the U.S.Geological Survey
Seawat	Loosely coupled between seawater and groundwater Numerical error is not negligible Computational expensive and difficult to converge	Hydraulic conductivity Pumping rate Sea level rise Recharge	Hydraulic conductivity and dispersivity are inherently uncertain. Output uncertainty is not quantified	Validation and verification done by developer, the U.S. Geological Survey
HAZUS	Basic imbedded hurricane model with Holland B parameter Fixed infra-structure inventory. Not comprehensive for military. Generalized impact relationships	Central pressure Radius to max. wind Forward speed Track azimuth Local topography Structure inventory	Operator dependent results comparable with other models. .Percentiles of loss distributions	Used extensively by FEMA and insurance studies

HURISK	Historic storm climatology Model uncertainty (shear, etc.)	Ocean temperature Record length	Predictive distributions Input distributions	Used by the insurance industry. Peer reviewed literature

In the process of designing MoCCs a number of supporting models were considered. These are listed in Table 2.2.2 along with the equivalent that was selected. A brief explanation for the choice is also provided.

Table 2.2.2. Explanation for Project Model Selection.

Model Selected	Candidates Rejected	Explanation
SLOSH	FEMA Surge	Outmoded & too complex
	ADCIRC	Too demanding of computer resources, too detailed
	Mike 3	Too detailed, not public
CMS FLOW	Delft- 2/3 D	Too complex & detailed
	FV Com	Unfamiliar
	ADCIRC	Computational resource demands
	CH3D	Not well documented/supported
	Mike 21	Not public, documentation
CMS WAVE	SWAN	Not compatible with CMS Flow
	STWave	Superseded by CMS Wave
	WAM	Poor nearshore representations

Another recent focus in coastal modeling has involved the development of methods to better quantify the long-term record of major storms for a given coastal region. The long-term record, over geologic timescales, provides a longer baseline and a better understanding of the variability in climate behavior. Such records allow detection of long-term patterns of hurricane activity and can help constrain models that are used to predict future storm events. The most commonly-employed method for reconstructing long-term records of hurricane landfalls is to identify hurricane-induced overwash sand layers in sediment cores from coastal lakes or lagoons (Liu and Fearn, 1993, 2000a, b; Liu, 2004; Donnelly et al., 2007; Mann et al., 2009; Wallace and Anderson, 2010). This method has been applied to several sites along the Atlantic coasts and the northern Gulf Coast, and the results suggest significant temporal and spatial variations in major hurricane landfall history (Liu and Fearn, 1993; 2000a, b; Liu et al., 2008; Scileppi and Donnelly, 2007; Donnelly et al., 2001a, b; 2004; Donnelly and Woodruff, 2007; Woodruff et al., 2008; Mann et al., 2009; Lane et al., 2010, 2011). However, this method suffers from several important weaknesses (Otvos, 1999; 2002; Mertz et al., 2003; Mann et al., 2009) and underestimates the number of hurricanes impacting a site (Lambert et al., 2008; Lane et al., 2010, 2011).

An alternative method for identifying storm surge deposits is based on analysis of marine microfossils (Parson, 1998; Collins et al., 1999; Hippensteel and Martin, 1999, 2000; Scott et al.,

2003; Cochran et al., 2005). However, in some circumstances, microfossils can be rare or absent from sediments and are of limited use in these cases (e.g., Horton et al., 2009). A recent study (Lambert et al., 2008) suggested that organic geochemical proxies (i.e., $\delta^{13}C$, $\delta^{15}N$, C%, N% and C/N) in coastal lake sediments are a more sensitive indicator of severe storm events than overwash sand deposits and can detect storm surge events that did not deposit overwash sediment in coastal lakes. Despite its potential, this new method has not been applied to or further tested in other coastal lakes. One of our objectives in the current project was to test and further develop this method for reconstruction of paleo-storms. As discussed later in the report, our results confirm that overwash/seawater flooding events can be detected by examining the isotopic signatures of coastal lake sediments, and that the resulting paleo-storm history can be employed in modeling the long-term effects of storms on a coastal region.

3. Materials and Methods

3.1. Analyzing Historic Coastal Change and Remote Sensing Data

Digitized images derived from historical charts (NOAA), topographic maps (USGS), aerial imaging (USDA, USGS, NOAA, Florida Department of Transportation (FDOT), Florida Department of Environmental Protection (FDEP), and Lidar surveys (USACE, NOAA, FEMA) were obtained and adapted for this study. Approximately 20-25 data sets representing time intervals ranging from 30 years to multiple data sets per year were incorporated for analysis of shoreline change (Table 3.1.1). Data without coordinate system information was georegistered using ESRI ArcGIS© tools and Florida DOT orthophotography (2006-2007) as the registration base. Initially, digital images were assigned to the Florida State Plane Coordinate System (Zone North – NAD83). For final analysis, data were reprojected to UTM coordinates (Zone 16 North - NAD83). Pixel resolution for most images was approximately 0.3 – 1.0 meters. A limited number of images had resolutions of only 3 meters. The registration of images utilized a first order polynomial (affine) transformation. The root mean square (RMS) sum error for most images was 3-5 meters. A limited number of images did not have uniform scaling across the width of the image (possibly due to aircraft pitch or roll during image acquisition). Images with variable scaling were georegistered using a second order polynomial transformation, with an RMS sum error of the transformation of 3-5 meters.

Historical charts and published maps had estimated positional accuracy of approximately 10 meters (Stapor, 1975; Morton et al., 2004). For historical charts, shoreline position was defined as the mean high water line (MHW). For aerial images, shoreline position was defined as the "wet line" or the high water line (HWL). The HWL can be considered to be the last high tide position visible on the aerial image. Under optimal conditions the wet line will approximate MHW, but a significant uncertainty may be present due to variations in the daily tide level, wind generated wave run-up and actual misidentification of the "wet line." In addition, older aerial images often had poor contrast and the "wet line" position could not be established with a high degree of accuracy due to poor image quality. The MHW shoreline derived from Lidar mapping is based upon a MHW value of +0.257 meters (NAVD88) measured at Navarre Beach, Florida, which is within the project study area (Table 3.1.2). The Navarre Beach tide gauge is at an open water location, approximately midway between the two ends of the Santa Rosa barrier island.

Note also in Table 3.1.2 that the long-term rate of sea-level rise in the EAFB region, represented by the 1926-2006 record from the Pensacola tide gage, is 2.10 +/- 0.26 mm/yr. This is statistically equivalent to the long-term global (eustatic) rate of sea-level rise (IPCC, 2007). This is confirmation that there is little or no subsidence or uplift in the study area, and that this region represents a good proxy for stable coastal regions in general.

The vertical accuracy of Lidar measurements is approximately ± 15 cm. The position of the Lidar-defined MHW line was derived using a modified version of the method of Sallenger et al. 2003, in which a linear regression of elevations across the beach face was used to define the horizontal intersection of the MHW datum and the profile line. Morton et al. (2005) have provided an estimate of the maximum measurement error for Gulf of Mexico shorelines using the methodologies that have been described. Maximum uncertainties are estimated to be approximately 11 meters for traditional methods (land based mapping and aerial imaging) and up

to 19 meters for newly developed Lidar methods relative to HWL positions. Differences between HWL and MHW-lidar derived shorelines are minimized in the northern Gulf of Mexico due to limited high tide range (0.2 meters) and steep (0.05) slopes on the upper shore face. A comparison of HWL and MHW-lidar derived shoreline obtained during a 12-month interval for Santa Rosa Island yielded differences of 3 to 5 ± 7m for major sections of the shoreline (Figure 3.1.1).

Table 3.1.1. Inventory of mapping, aerial imaging, and LIDAR data used for DSAS analysis of the historic shorelines of the three counties encompassing Santa Rosa Island, Florida.

Year	Method	Source	Date Acquired	County Coverage		
				Escambia	Santa Rosa	Okaloosa
1856	T-Sheet	USC&GS	1856	P	ND	ND
1870	T-Sheet	USC&GS	1870	P	A	P
1871	T-Sheet	USC&GS	1871	ND	P	A
1920	T-Sheet	USC&GS	1920	P	ND	ND
1930	T-Sheet	USC&GS	1930	P	A	P
1934	T-Sheet	USC&GS	1934	A	A	A
1951	Aerial	USDA/APFO	03/21/1951	ND	P	A
1955	Aerial	USDA/APFO	04/15/1955	ND	P	A
1958	Aerial	USDA/APFO	01/04/1958	P	ND	ND
1965	Aerial	USGS	01/01/1965	A	ND	ND
1969	Aerial	USGS	11/15/1969	ND	A	A
1973a	Aerial	FDOT	01/20/1973	ND	A	A
1973b	Aerial	FDOT	05/04/1973	P	ND	ND
1978	Aerial	NOAA	03/01/1978	A	A	A
1981	Aerial	FDOT	02/02/1981	A	A	ND
1985	Aerial	FDOT	02/15/1985	ND	P	A
1988	Aerial	FDOT	01/30/1988	P	P	ND
1994	Aerial	USGS	01/09/1994	A	A	A
1995	Aerial	FDOT	10/12/1995	ND	P	A
1997	Aerial	FDOT	02/02/1994	A	P	P
1999	Aerial	USGS	01/09/1999	A	A	A
2004a	Aerial	NOAA-RSD	01/17/2004	P	ND	P
2004b	Aerial	USGS	03/01/2004	A	A	A
2005	Aerial	NOAA-RSD	07/12/2005	P	P	P
2006a	Aerial	FDOT	11/26/2006	ND	P	P
2006b	Aerial	NOAA	05/15/2006	P	A	A
2007a	Aerial	FDOT	01/09/2007	A	P	ND
2007a2	Aerial	FDOT	02/23/2007	ND	ND	P
2007b	Aerial	FDEP	07/10/2007	ND	ND	A
2008	Aerial	FDEP	04/04/2008	A	A	ND
2010	Aerial	FDOT	01/10/2010	A	A	A

Table 3.1.1. Inventory of mapping, aerial imaging, and LIDAR data used for DSAS analysis of the historic shorelines of the three counties encompassing Santa Rosa Island, Florida.

Year	Method	Source	Date Acquired	County Coverage		
				Escambia	Santa Rosa	Okaloosa
1998	Lidar	FDEP	01/15/1998	P	A	A
1998	Lidar	NOAA/NASA/USGS	11/01/1998	A	A	A
2001	Lidar	USGS/NASA	10/02/2001	A	A	A
2004	Lidar	FDEP	08/15/2004	P	A	A
2004	Lidar	USACE	12/01/2004	A	A	A
2005	Lidar	USACE	07/15/2005	P	A	A
2005	Lidar	USACE	11/01/2005	A	A	A
2006	Lidar	NOAA/NWFWMD	07/15/2006	A	A	P
2007	Lidar	NWFWMD	07/15/2007	ND	ND	A

Sources of Data:

USC&GS U. S. Coast and Geodetic Survey
USDA/APFO U.S. Department of Agriculture, Air Photo Field Office
USGS U.S. Geological Survey
USACE U.S. Army Corps of Engineers
NASA National Aeronautics and Space Administration
NOAA-RSD NOAA, Remote Sensing Division
FDOT Florida Department of Transportation
FDEP Florida Department of Environmental Protection, Beaches and Coastal Systems
NWFWMD Northwest Florida Water Management District

Acquisition Dates:

Acquisition dates for nautical charts are reported as the dates of survey publication. Some aerial imaging consists of multiple dates. An average of the dates is reported in the table. Lidar acquisition is reported to the middle of the month of data acquisition.

County Coverage:

A – complete coverage; P – partial coverage; ND – no data acquired.

Table 3.1.2. List of tide gauge measurements used to calculate mean high water elevation.

Location	**Navarre Beach**	**Shield Point†**	**Pensacola**
Station Number	*8729678*	*8729747*	*8729840*
Mean High Water (MHW)	0.257	0.309	0.276
Mean Sea Level (MSL)	0.057	0.096	0.089
Mean Low Water (MLW)	-0.128	-0.115	-0.090
Mean Tidal Range (MN)	0.385	0.424	0.365
Historical Sea Level Rise††			2.10±0.26 mm/yr

Values are reported in meters relative to the NAVD88 vertical datum
Tidal Epoch 1983-2001
Tidal datum analysis period: 01/01/1978-12/31/1987
† Shield Point data used for SLAMM modeling; Mean Tide Level (MTL) is 0.097 meters.
†† Sea level trend reported at the 95% confidence interval for the period 1923 to 2006.

Source: http://tidesandcurrents.noaa.gov/

Figure 3.1.1. Comparison of HWL-derived shorelines (2007) derived by air photo mapping versus MHW-Lidar positions (2006 and 2008) for the Escambia and Santa Rosa county portions of Santa Rosa Island. The gap between transects 370-500 represents locations where beach renourishment has modified the shoreline between the dates of Lidar and aerial image acquisition.

Shoreline positions obtained from mapping data were converted into vectorized ArcGIS shapefiles and analyzed using the USGS Digital Shoreline Mapping and Analysis Systems (DSAS) ArcGIS extension (Thieler et al., 2009). A transect spacing of 100 meters was used for the DSAS analysis of the approximately 70 kilometer length of the island. Representative locations of the transect positions are shown in Figure 3.1.2.

3.2. Modeling Future Hurricane Intensities

Our solution to the problem of estimating future storminess locally for this project has been to combine empirical evidence and statistical models with physical theory. The empirical evidence comes from the set of historical hurricanes that have affected the region. This set includes at least 100+ years of data on the speed, approach, and intensity of hurricanes. The attributes of each cyclone in the vicinity contribute to a catalogue of evidence about the past. A statistical model is then developed that relates the change in cyclone intensity to regional ocean heat content. The model includes a component that expresses this change in terms of different intensity levels.

The empirical evidence together with the statistical model is then used to project the intensities of future hurricanes given the expected (or modeled) increases in ocean temperature. Physical limitations related to the heat-engine theory are used to inform the projection. The assumption is

that the historical catalogue is a representative sample of the frequency and intensity of future hurricanes, but that the strongest hurricanes will be stronger due to the availability of additional surface ocean heat energy.

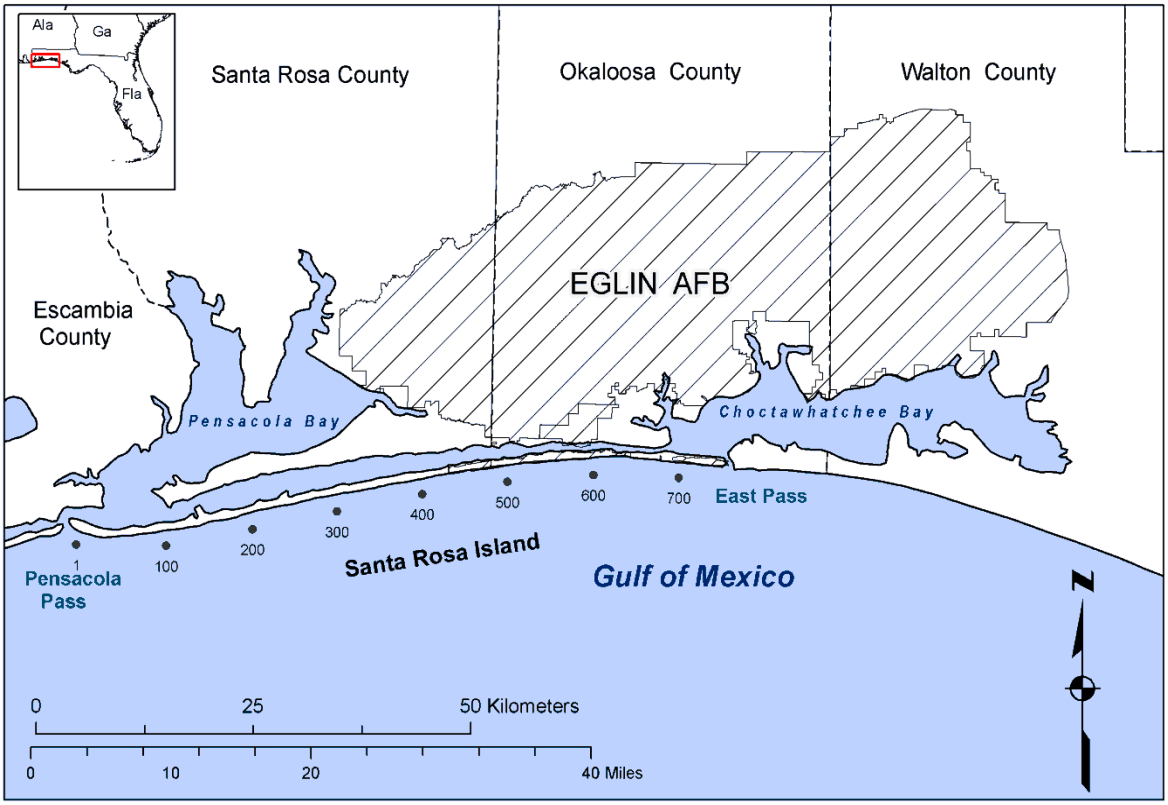

Figure 3.1.2. Representative transect locations and transect numbers for foreshore DSAS analysis of Santa Rosa Island, Florida. Individual transects are spaced at a 100 meter interval.

Additional hurricane attributes, including radius to maximum winds, a wind decay parameter, and minimum central pressure, needed to be added to the catalogue of cyclones to make them useful for storm surge and wind-field components, like those included in the U.S. Federal Emergency Management Agency (FEMA) HAZUS model. Lacking evidence that these vitals will change in the future, we use historical values for them. In this way we obtain a catalogue of hurricanes representing a view of the future, a view that is consistent with the current evidence and theory of hurricane intensity and which aligns with the consensus view on anthropogenic global warming.

Recent research involving theory, models, and data provide the background for estimating possible future damage losses from hurricanes. For example, the heat-engine theory of tropical cyclone intensity argues for an increase in the maximum potential intensity of hurricanes with increases in sea-surface temperature. Model projections from the IPCC (SRES A1B) indicate an increase in average tropical cyclone wind speed of 2 to 11% globally by the late 21st century with the increase in the strongest hurricanes possibly even higher. Data analysis and modeling using a set of homogeneous tropical cyclone winds show that the strongest hurricanes are getting stronger, particularly in the Gulf of Mexico and Caribbean Sea with increases as high as 20% per

degree C for the strongest hurricanes (Elsner and Jagger, 2010). Here we estimate future hurricane wind speeds and corresponding wind losses for EAFB. We begin by estimating the potential change in the strength of hurricanes over the Gulf of Mexico as Gulf water temperatures increase.

The first step is to estimate the potential influence of global warming on hurricane intensity. Knutson and Tuleya (2004) estimate an average 8% increase in hurricane intensity for every 1C rise of SST based on global tropical cyclone activity and for average hurricane intensity. Here we examine evidence for hurricane intensity increases over the Gulf of Mexico. We define the Gulf of Mexico as the region between 80 and 98W longitude and 19 and 32N latitude. We choose all storms entering or developing within this domain over the period 1900 through 2009. The choice results in 450 storms. We eliminate the four storms having only a single 1-hr position within the domain.

The SST data are NOAA's reconstructed sea-surface temperatures (SST v3) from the Earth System Research Laboratory Physical Science Division and available in netCDF format. NetCDF (network Common Data Form) is a set of software libraries and machine-independent data formats that support the creation, access, and sharing of array-oriented scientific data. We consider the July SST value averaged over the Gulf of Mexico region as an indicator of the heat content available for hurricanes during the peak season of August through October. Of the 39 hurricanes to affect EAFB, all occurred after July 1st and 32 occurred after August 1st. July SST is a reliable indicator of the amount of ocean heat available to hurricanes before the season begins.

We match the year of the July SST with the year of the per storm maximum tropical cyclone intensity so years with more than one tropical cyclone in the Gulf of Mexico will have the same July SST value. Using this data set, we model the trend in tropical cyclone intensity as a function of SST using quantile regression. Quantile regression, introduced by Koenker and Bassett (1978), extends the ordinary least squares regression model to conditional quantiles (e.g., 90th percentile) of the response variable. Quantiles are points taken at regular intervals from the cumulative distribution function of a random variable. The quantiles mark a set of ordered data into equal-sized data subsets.

For example, of the 446 maximum storm intensity values in our Gulf of Mexico data set, 25% of them are less than 22 m/s, while 50% are less than 31 m/s. Thus, there are an equal number of tropical cyclones with intensities between 22 and 31 m/s as there is between 31 and 44 m/s. When we state that the median maximum intensity is 31 m/s, we mean that half of all cyclones have intensities less than this value and half have intensities greater. Similarly, the quartiles (deciles) divide the sample of intensities into four (ten) groups with equal proportions of the sample in each group. The quantiles, or percentiles, refer to the general case.

3.3. Analyzing Paleostorm History in Coastal Sediments

For low- to moderate-energy coastal regions, such as that of the northern Gulf of Mexico, storms are the major agent of coastal change. Coastal storms, and especially major storms, cause retreat of the shoreline, loss of coastal wetlands, and damage to coastal infrastructure. Understanding and quantifying the potential damage from storms to coastal systems and infrastructure, and predicting their future occurrence, is in large part dependent on the available history of major

storms. The historic record of major storms is brief and not necessarily representative of the true characterization of hurricanes, especially the intense and damaging storms that are poorly represented in the relatively brief recorded history of storms. The record extends only to the mid-1800's for the northern Gulf of Mexico. A more robust history, encompassing several millennia, is available in the sediments of coastal water bodies and can be accessed in order to enhance future storm modeling.

3.3.1. Historic Storm Record. During historic time, 32 hurricanes (Cat. 1-5) have passed within 140 km of the study area at the eastern margin of Eglin Air Force Base (Lat. 30.3265 N, Lon. 86.1510 W) (NOAA, 2012a). The storm tracks are shown in Figure 3.3.1. The 140-km radius is a close approximation of the radius to hurricane-force winds for a major storm (categories 3-5), as determined by Keim et al., (2007). A total of 32 Category 1-5 storms passed within 140 km of one of the EAFB region coastal water bodies, Western Lake, during historic time. A total of 14 were major storms (Category 3-5) at some point during their track (Figure 3.3.2). Ten of these were major storms at their closest approach to the study area. Therefore, the return period over historic time for major storms directly impacting the region is approximately 16 years. Table 3.3.1 provides details on these storms.

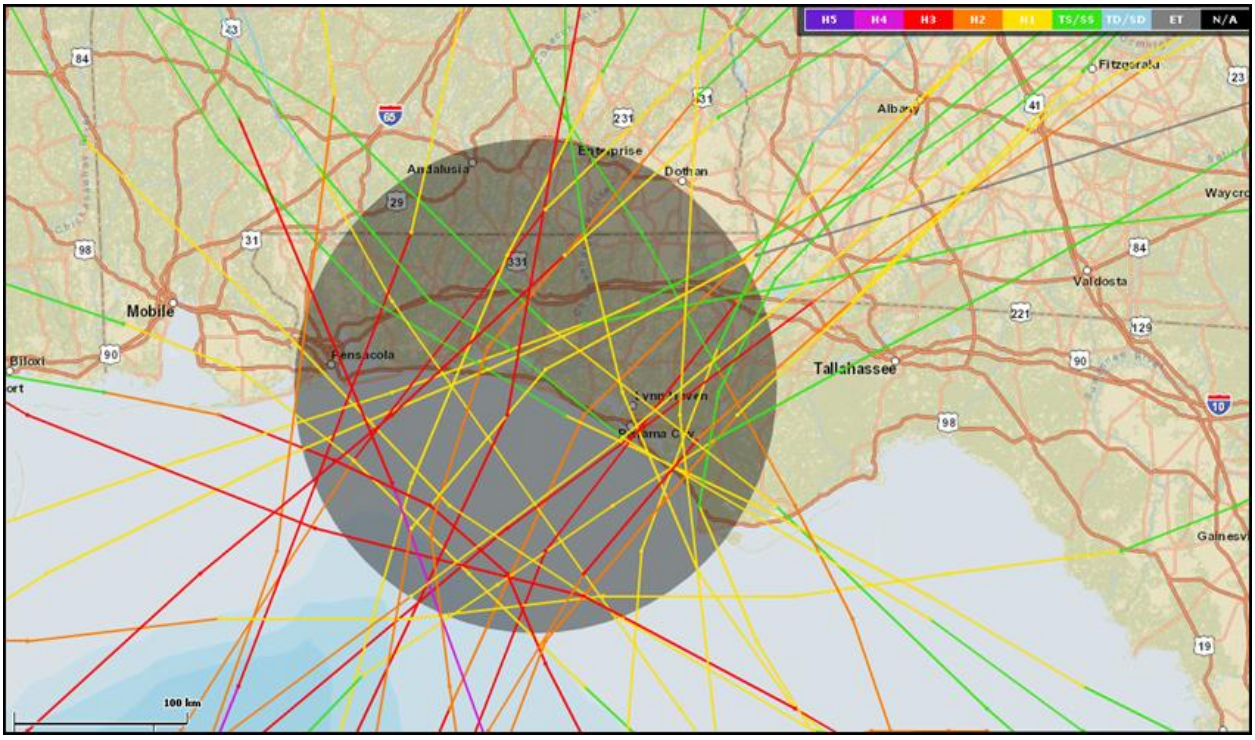

Figure 3.3.1. Tracks of the 32 hurricanes (Cat. 1-5) which have passed within a 140-km radius of the study area at the eastern margin of Eglin AFB (Lat. 30.3265 N, Lon. 86.1510 W), 1851-present. (Source: NOAA, 2012a).

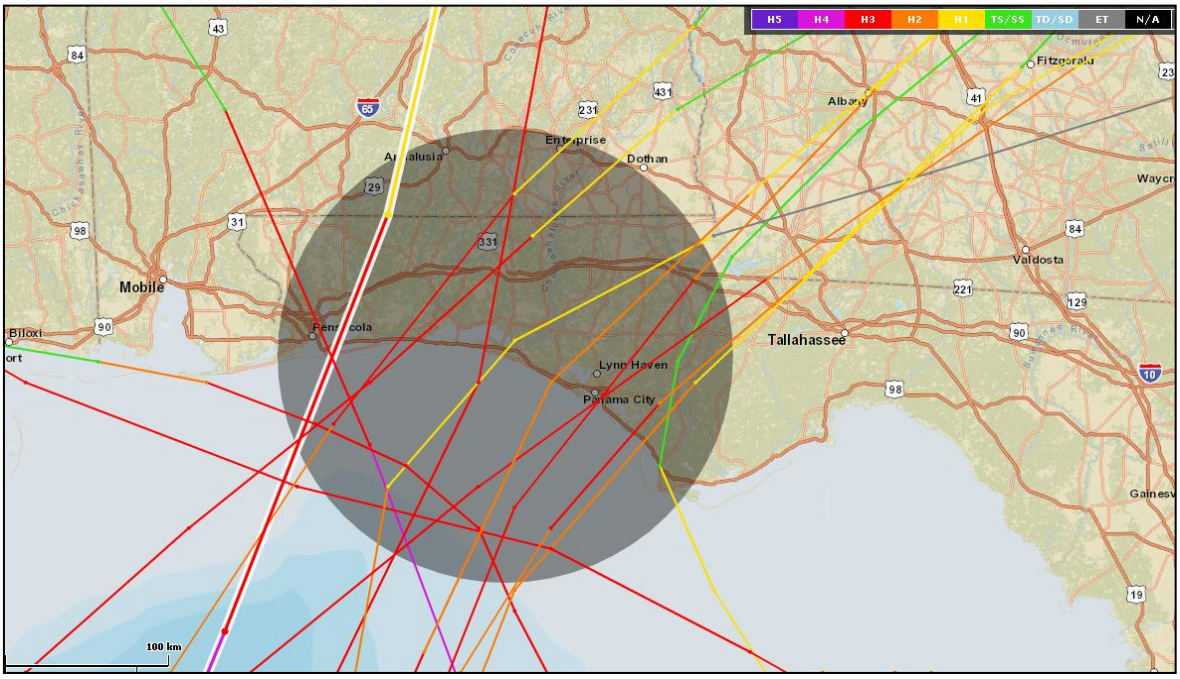

Figure 3.3.2. Tracks of the 14 major storms (cat. 3-5) which have passed within a 140-km radius of the study area at the eastern margin of Eglin AFB (Lat. 30.3265 N, Lon. 86.1510 W), 1851-present. (Source: NOAA, 2012a).

Table 3.3.1. Storm parameters for major storms passing within 140-km radius of the study area at the eastern margin of Eglin AFB during historic time, 1851-present.

Storm Name	Year	Landfall Location	Storm		ΔP^c	$R_{mw}{}^d$	Surge Height[e] (m)
			Category[a]	Category[b]	(mb)	(km)	
No Name	1851	Panama City, FL	3	3	57	40	0.3
No Name	1856	Panama City, FL	3	3	57	40	0.3
No Name	1877	Mexico Beach, FL	3	3	57	40	0.0
No Name	1882	Ft. Walton Beach, FL	3	3	57	40	1.6
No Name	1894	Panama City, FL	3	3	62	40	0.4
No Name	1917	Ft. Walton Beach, FL	3	4	72	61	1.6
No Name	1926	Dauphin Island, AL	2	4	67	35	1.0
No Name	1929	Indian Pass, FL	1	4	57	56	0.3
Florence	1953	Grayton Beach FL	1	3	72	30	0.7
Eloise	1975	Dune Allen Beach, FL	3	3	61	29	1.3
Elena	1985	Gulfport, MS	3	3	60	27	0.4
Kate	1985	Mexico Beach, FL	2	3	59	30	0.0
Opal	1995	Pensacola, FL	3	4	94	80	2.7
Dennis	2005	Pensacola, FL	3	4	83	13	1.9

Notes:
a. Saffir-Simpson category of storm at closest approach to study area (NOAA, 2012a)
b. Saffir-Simpson category of storm at maximum strength (NOAA, 2012a)
c. Maximum change in pressure, as determined from HURDAT database (NOAA, 2012b)
d. Radius to maximum winds (NOAA, 2012b)
e. Surge height estimate based on SLOSH model (Jelesnianski et al., 1992)

3.3.2. Long-Term Geologic Record of Coastal Storms. A better understanding of the true risk associated with major storms is essential in modeling and mitigating future risk. Storm models predict that a warmer world – and a warmer ocean – will enhance the intensity of the larger storms over the next 100 years (Elsner et al., 2008). As a result, EAFB and similarly situated coastal military facilities will likely experience significant changes to coastal environments and man-made infrastructure due to shoreline retreat, increased flooding and erosion, changes in groundwater flow, increased saltwater intrusion, and greater wind loads and storm surge. A more accurate knowledge of the frequency of the larger storms in the geologic past can greatly improve model projections of future storm effects.

A better estimate of the true long-term storm risk can be obtained from regional coastal sediments, which extend the storm history well beyond the historic record. Coastal sediments, if undisturbed, incorporate a signature of major storm impacts. Our objective in this component of the project has been to locate undisturbed sediment sequences in the EAFB region and extract a storm record from them, in order to determine and quantify the increasing storm-related risk of shoreline change and damage to coastal infrastructure in the EAFB region.

With this goal, we have investigated the sedimentology, geochemistry and geochronology of coastal lake sediments in the EAFB area. The objective has been to obtain a long-term estimate of the frequency of saltwater inundation by storm surge from major storms in the region over the past several millennia. With this objective in mind, cores were collected from coastal lakes in the EAFB region, with the aim of creating a proxy record of major storm occurrence.

3.3.3. Coastal Dune Lake Sediments. The Eglin AFB coastal region includes more than a dozen coastal dune lakes (Figure 3.3.3). The lakes are long-lived and permanent water bodies, though water levels may fluctuate substantially due to precipitation, groundwater seepage through the surrounding coastal sands, and storms. During major storm events the dunes may be breached, forming a temporary inlet, and the normally fresh to brackish lakes are inundated by marine water and sometimes overwash sediment.

Several of the major storms which have impacted the Eglin AFB coastal region during historic time are known to have overwashed the dunes separating the coastal lakes from the ocean and opened temporary inlets. When the dunes are open to the Gulf of Mexico, a short-term brackish transition zone is created between the ocean and the uplands, allowing saltwater and freshwater to mix (Florida Lakewatch, 2008). These periods of overwash and open outfalls can be expected to leave behind a sedimentary and geochemical record (Liu and Fearn, 1993; Liu and Fearn, 2000; Donnelly et al., 2001; Lambert et al., 2008).

Selected lakes were sampled using piston push cores, in order to prevent disturbance of the sediments. The sediment cores were subjected to high-resolution sedimentologic and stable isotope analysis, complemented by geochronology and micropaleontology, in order to refine a method for identifying and quantifying paleostorm impacts. This essential information was sought in order to make estimates, by use of multiple models, regarding the frequency and magnitude of prehistoric storms, and, by projection, the effect of future storms on coastal infrastructure and coastal environments.

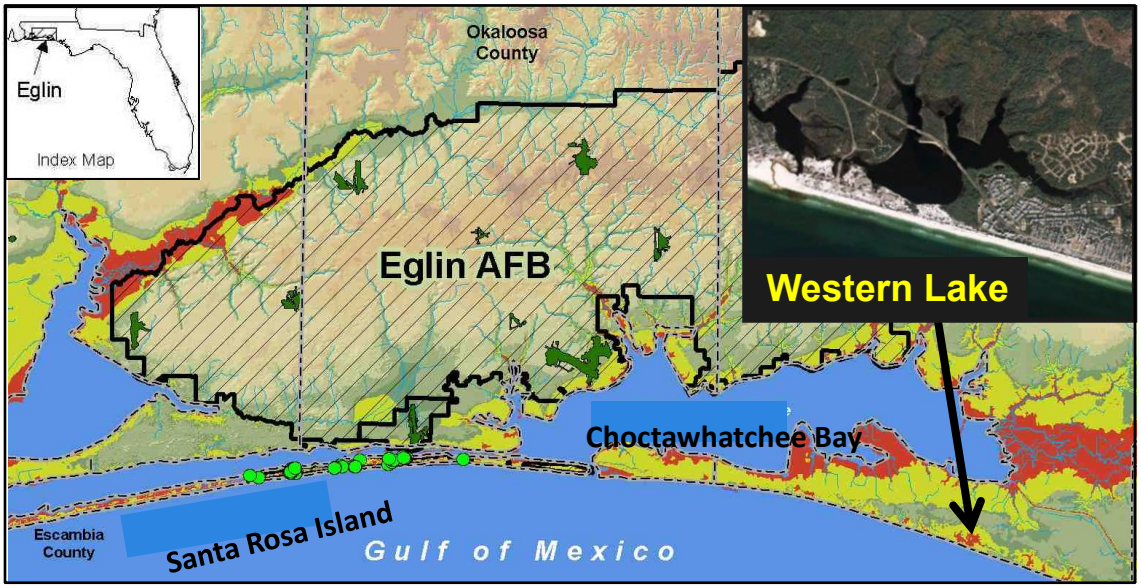

Figure 3.3.3. Eglin AFB region, on the NW Florida coast. Inset air photo shows one of the long-lived coastal dune lakes in the study area which provided sediment cores for paleostorm analysis.

3.3.4. Core Preparation. Prior to sediment analysis, the lake sediment cores were split and opened. One half of each core was used for analysis, and the archive half was stored at 2°C for preservation. Cores were imaged with a digital line scan camera. X-radiographs were obtained for the half cores using a Torrex 120D digital x-radiograph set at 2 mA and 75 kV. Following the scanning, samples of organic sediment for radiocarbon analysis were collected adjacent to sand layers, based on a review of the x-radiographs.

3.3.5. Sediment Analyses. The lake core that was selected for intensive sampling was sampled for sedimentologic analysis at 0.5 cm intervals throughout the core. Samples were placed in pre-weighed plastic dishes, weighed immediately after sampling, then placed overnight in a drying oven at 65°C, and weighed again after cooling to determine percent moisture. After drying, approximately 0.5 g of sample was taken from each sample and placed in a pre-weighed aluminum dish, weighed, and placed in a furnace for 2 hours at 550° C. Samples were cooled overnight and weighed again to determine percent combustible, a standard method of bulk organic analysis. The fraction not used for combustion analysis was weighed, wet-sieved, dried, and weighed again to determine percent sand and percent fines. The percent fine fraction was discarded, and grain size analysis was completed on the sand fraction using an automated settling tube and the GRANPLOT program (Balsillie et al., 2002). GRANPLOT calculates settling tube size fractions in quarter-phi intervals based on settling times and velocities and application of the Gibbs settling equation. The program produces standard grain-size statistics (mean grain size, standard deviation, skewness, kurtosis, and dispersion) along with frequency histograms and cumulative plots.

3.3.6. Micropaleontology. The coastal dune lakes historically are known to be fresh to brackish. When remains of marine organisms, such as shells of marine foraminifera, are found at

depth in the lake sediments, it can be inferred that they entered the lakes during a period of marine inundation. This would typically occur as a result of storm surge associated with tropical storms. Sediment samples were collected from the upper and lower 5 cm of each core, in addition to each visible sand layer, for identification of foraminifera that might provide information on the occurrence of brackish or marine conditions in the lake.

3.3.7. Geochronologic Analyses. Radiocarbon dating was utilized to establish a chronology in the core. Radiocarbon samples were collected at selected depths throughout the core, particularly near any visible sand layer. During sample collection, approximately 1 cm^3 of sediment was placed in a pre-weighed dish, weighed, dried in an oven overnight at 65°C, weighed after cooling, ground into a powder for homogeneity, and placed in a pre-weighed and labeled glass vial. Vials were sent to the National Ocean Sciences Accelerator Mass Spectrometry Facility (NOSAMS) at Woods Hole Oceanographic Institute for radiocarbon analysis.

3.3.8. Determining Storm Surge Heights Using SLOSH. Direct measurements of storm surge heights were not available for most of the storms which impacted the study area during historic time. As a result, surge heights for this investigation were calculated using the SLOSH (Sea, Lake, and Overland Surges from Hurricanes) model to estimate surge heights from known storms of the historic period. SLOSH, developed by the National Weather Service, is one of the most commonly used tools for estimating storm surge and wind resulting from historical or predicted storms (Jelesnianki et al., 1992). The model's input parameters include the storm's track, the radius to maximum winds (R_{MW}), and the pressure deficit (ΔP), or the deviation from one standard atmosphere noted every 6 hours during the track of the storm (Houston, et al., 1999; Lane et al., 2011, NOAA, 2012a).

Comparisons of SLOSH model calculations with observed storm surge heights have shown that 79% of the predictions are within 1 standard deviation of the mean error, 97% are within two standard deviations, and 99% are within three standard deviations (Jarvinen and Lawrence, 1985), though SLOSH is known to commonly underestimate observed storm surge heights (Houston et al., 1999). SLOSH's design allows for storm surge computations to be made with incomplete knowledge of a storm's structure and intensity (Houston et al., 1999). This makes the model ideal for forecasting, as well as for back-calculating storm surges, of storms early in the historic and prehistoric record. The modeled surge heights for the historic storms in the study area are shown in Table 3.3.2.

Forward modeling of surge heights using SLOSH is reliable under conditions of sea-level rise, as long as the shoreline morphology adjusts upward more or less in balance with the rise in sea level. One important goal of the model development which was part of this project was to determine if in fact such adjustment persists over the range of sea-level rise scenarios tested. This is discussed in Section 4.

3.3.9. Geochemical Analyses. The cores selected for geochemical analysis was sampled at approximately 3 mm intervals using thin, hollow plastic tubes similar to the method described by Lavoie (1996) and Lambert (2003). Samples were freeze-dried and ground with a mortar and pestle for homogeneity. Stable isotope analyses were carried out at the National High Magnetic Field Laboratory at Florida State University, on a Finnigan MAT delta PLUS XP stable isotope

ratio mass spectrometer (IRMS) connected to a Carlo Erba Elemental Analyzer (EA) through a Conflo III interface.

Sample analysis was initiated by weighing a given amount of sample (depending on %C and %N) into a silver cup, after which the sediment was moistened with deionized water and exposed to concentrated HCl vapor for 24 hours to remove carbonate material. Samples were then dried overnight in an oven at 70°C. After drying, samples were wrapped in a tin cup for isotope analysis. Two sets of five different standards including YWOMST-1 (cane sugar), YWOMST-2 (phenylalanine), YWOMST-3 (L-phenylalanine), YWOMST-5 (urea), and urea-2 were also weighed and wrapped in tin cups for isotope analysis. Samples were then loaded into the auto sampler of the EA connected to the IRMS for isotopic measurements. Each batch of samples was loaded into an autosampler, which held a total of 50 samples, including standards and blanks. Typically, ten samples in each batch were standards.

Results were reported in the standard delta (δ) notation in per mil (‰) relative to the international VPDB standard for $\delta^{13}C$, and air for $\delta^{15}N$ (Sharp, 2007). The precision of C and N isotope analyses was ± 0.2 ‰ or better based on repeated analyses of the lab standards.

3.3.10. Paleostorm Analytical Methods. The standard approach for characterizing paleostorm layers in lake sediments is to identify storm overwash sand deposits through proxies, based on sedimentologic, x-radiographic and visual analysis (Liu and Fearn, 1993; Donnelly et al., 2001; Nott, 2004; Scileppi and Donnelly, 2007). Sediment records based on overwash layers from coastal lakes have been used to obtain major storm recurrence intervals for selected regions of the northern Gulf of Mexico (Liu and Fearn 1993, Liu and Fearn, 2000).

We carried out such analyses on the lake sediment core from the Eglin AFB vicinity. In addition, we employed the identification of marine microfossils, as an additional indicator of storm surge in lake environments. Further, we have refined a potentially more sensitive indicator of marine storm surge inundation. The new method is based on organic geochemical proxies (OGP), such as %C, %N, $\delta^{13}C$ and $\delta^{15}N$, and can be used to identify instances of incursion of marine waters to coastal lakes. Coastal lakes are normally fresh to brackish. During major storm events the dunes are breached, commonly forming a temporary inlet, and the lakes are impacted by marine water and sometimes overwash sediment. The marine waters carry a geochemical signature that temporarily affects the lake biota and imparts a signal to the lake bottom sediments. Lambert et al., (2008) first used OGPs in coastal lake sediment cores to reconstruct millennia-long storm records. The OGP method is by its nature a more sensitive indicator than overwash sand deposits for severe storm events.

3.3.11. Organic Geochemical Proxy (OGP) Methodology. Organic geochemical proxies (OGPs) are important indicators in paleoenvironmental studies, as they record environmental conditions at the time of deposition (Castenada and Schouten, 2011). Using stable isotopes to identify prehistoric storm events has been shown to correlate with sediment-based paleostorm analyses, but has the additional ability to detect storm events that did not leave an overwash layer of sand in coastal sediments (Lambert, 2003).

Using the OGP method, organic-rich sediments are analyzed in order to create $\delta^{13}C$ and $\delta^{15}N$ core profiles. Marine environments are typically more enriched than terrestrial environments in the heavier ^{13}C isotope, versus the lighter and more common ^{12}C isotope. As a result, lacustrine

plants and plankton typically have more negative $\delta^{13}C$ values than their marine counterparts (Valero-Garces et al., 1997). In coastal freshwater or brackish environments, marine incursions can be detected in core profiles as shifts from more negative $\delta^{13}C$ values, indicating terrestrial C3 vegetation, (O'Leary, 1988; Cerling et al., 1997) to less negative $\delta^{13}C$ values, indicating a marine environment (Sackett, 1964; Shultz and Calder, 1976; Meyers, 1994; Thornton and McManus, 1994; Corbett et al., 2007; Lambert et al., 2008). Similarly, $\delta^{15}N$ values are generally more positive in marine settings, as they are also more enriched in the "heavy" ^{15}N isotope than in more terrestrial settings, as observed in coastal sediments dating from the Albemarle and Pamlico Sounds in North Carolina (Thornton and McManus, 1994; Middleburg and Nieuwenhuize, 1998; Corbett et al., 2007).

The technique of using organic geochemical proxies for studying storms has advanced the field of paleotempestology, as it no longer requires an overwash sand layer to record the occurrence of a storm event. The technique employs $\delta^{13}C$ and $\delta^{15}N$ values in organic sediments in coastal lakes (Lambert, 2003). Significant shifts in $\delta^{13}C$ and $\delta^{15}N$ values in sediment core profiles, followed by rapid returns to base values, are indicative of storm events, as ocean waters are more enriched in heavy isotopes, both ^{13}C and ^{15}N, than fresh or brackish lacustrine waters (Lambert et al., 2008). However some studies (Lambert, 2003; Lambert et al., 2008) have provided evidence of storm signals corresponding to a shift in $\delta^{13}C$ and $\delta^{15}N$ values both in the positive and negative directions. A negative shift from normal lake values might be expected in the case of a coastal storm event dominated by precipitation (excessive coastal flooding) rather than by wind (high storm surge). In recent years, this method has been employed in several investigations (Meyers, 1997; Lambert, 2003; Parker et al., 2006; Lambert et al., 2008; Page et al., 2009).

Our study of various carbon pools in two coastal lakes in north Florida confirm that an input of marine-derived OM (due to overwash or seawater flooding) is the only process that could cause concurrent positive shifts in $\delta^{13}C$ and $\delta^{15}N$ (Das et al., in press), and thus support the OGP-based method for identifying severe storm events as proposed by Lambert et al. (2008). In addition, we have recognized a few other patterns in our sediment geochemical data that could be interpreted as indicating changes in certain aspects of the lake environment (Das et al., in press). For example, storms that produce freshwater flooding (i.e., increased terrestrial runoff) would shift the $\delta^{13}C$, $\delta^{15}N$, and $\delta^{18}O$ signatures of the lake to lower values but the C/N to higher values, very different from the changes expected from seawater flooding. Thus, not only are catastrophic storms that produced overwash/seawater inundation recognizable in lake sediments, our data suggest that storms large enough to produce freshwater flooding could also be recognizable in coastal lake sediment cores by examining the patterns in multiple geochemical proxies (Das et al., in press).

3.3.12. Paleostorm Detection Model. A model was developed for identifying the signature of inundation events in the sedimentary record of coastal lakes (Coor et al., in review). The model employed a sediment core from a coastal pond with a high sedimentation rate, enabling individual storm events to be discerned in the sedimentary record. Lead-210 dating provided the chronology for identifying the horizons representing major storms of the past century. Storm magnitude and surge data were obtained from archival records. Stable isotope and sedimentologic analyses were carried out at high resolution throughout the core. A series of multiple regressions was carried out on the core data set in order to determine which of the sedimentologic and isotopic data variables were statistically significant and most influenced the data. The parameters examined through regression were: $\delta^{13}C$, $\delta^{15}N$, % C, % N, $\delta^{13}C'$, $\delta^{15}N'$, %

C′, % N′, % combustible, % sand, mean grain size, and standard deviation of grain size. The primed (′) variables represent a data smoothing process, employing the depth derivative of the variable (i.e., % N to % N′). Results of multiple linear regression analysis showed that $\delta^{13}C$, percent sand, and percent N′ were the most statistically significant variables, in other words, changes in these variables during a storm would be the most readily identifiable indicators of inundation events affecting the coast. These variables were then used as inputs to a generalized linear model, resulting in the logistic regression equation (Hilbe, 2009):

$$logit(\widehat{pi}) = -27.67971 - 1.51101\ \delta^{13}C - \ 0.09596\ \%Sand - 57.15150\ \%\ N' \qquad (3.3.1)$$

In the above equation, $logit(\widehat{pi})$ is a function that describes the log of the odds ratio of storm to non-storm events, as observed in the data. The results of the $logit(\widehat{pi})$ equation were then transformed, to generate a probability distribution of the *logit* expression from 0 to 1 (Hilbe, 2009):

$$Probability\ (storm) = \frac{e^{logit(\widehat{pi})}}{1+e^{logit(\widehat{pi})}} \qquad (3.3.2)$$

In the above equation, P(0) would indicate minimal probability of a storm having occurred and P(1) would indicate maximal probability of a storm. A storm event cutoff probability of 0.50 was chosen for the purposes of the model. This value maximized the number of events identified by the model, and minimized the number of false positives, based on the known history of storms.

3.4. Modeling Coastal Wetlands

Sea level rise associated with climate change can affect wetlands and destroy coastal habitats (Fujii and Raffaelli, 2008). As sea level rises, coastal areas and estuaries are inundated, eroded, or washed away. This can result in habitat loss. The long-term sustainability of wetlands ecosystems is dependent upon the dominant macrophytes that maintain the elevation of their respective habitats within a relatively narrow portion of the intertidal zone (Mander et al., 2007).

Salt marshes worldwide have generally maintained elevation in equilibrium with sea level for the past approximately 4000 years through the accumulation of mineral sediment and organic matter (Redfield, 1972). This is in large part due to the slow rate of sea-level rise that has pertained during the past several millennia. However, in apparent response to the recent increase in sea level rise rates and land-use related decreases in sediment delivery rates, wetlands in large portions of North America and Europe are deteriorating. Much of the modern wetland area has converted to open water or bare mudflats (Hartig et al., 2002). Recent work suggests that tidal marshes respond to SLR and sediment delivery changes in a particularly complex fashion, governed by three-way interactions between vegetation, hydrology, and sediment transport (Kirwan et al., 2008).

The Sea Level Affecting Marshes Model (SLAMM) simulates the dominant processes involved in wetland land use conversion and shoreline modification during long-term sea level rise. Clough (2006) applied the SLAMM model to nine sites in Florida and discussed land use changes relative to the year 2100. Chu-Agor et al., (2010) applied a generic evaluation framework consisting of a state-of-the-art screening and variance-based global sensitivity and uncertainty analyses to simulate changes in the wetlands and coastal habitats of the barrier island

environments in the EAFB region.

In the current study, the SLAMM model was applied to evaluate the vulnerability to sea level rise of the coastal wetland habitats on portions of Eglin Air Force Base, Florida. SLAMM-6 is the latest version of the SLAMM wetlands model, developed in 2010. It includes multiple upgrades from previous versions, as a result of feedbacks from other scientists working in the field (Kirwan and Guntenspergen, 2009). Model flexibility has been improved with respect to accretion feedback, integrated elevation analysis, and the salinity model. Technical documentation on the SLAMM Model can be found in Clough et al., (2010).

Within SLAMM, there are five primary processes that affect wetland fate under different scenarios of sea level rise: inundation, erosion, overwash, saturation and salinity. Each wetland site is divided into cells of equal area, and each land-cover class within a cell is simulated separately. SLAMM then uses a flexible and complex decision tree, incorporating geometric and qualitative relationships, to represent transfers in land use among coastal wetland classes.

The SLAMM-6 wetland hierarchy (Figure 3.4.1) depends on elevation, while maintaining the spatial structure (e.g., physiographic features, such as dunes, tidal flats, etc.) within each elevation range. SLAMM has traditionally been run using a fixed set of sea-level rise scenarios taken from the Intergovernmental Panel on Climate Change (IPCC). In SLAMM-6 a customized sea level rise is possible, and 1, 1½ and 2 meter scenarios are also included. The IPCC A1B scenario we use in this report is shown in Figure 3.4.2. The one-meter sea level rise scenario is shown in subsequent figures.

The SLAMM wetland model has certain limitations, including the following: (1) The model does not use predictive hydrodynamic modeling; (2) Only simple erosional parameters are incorporated in the model (major storm-related erosional events are not incorporated into the erosional parameters of the model); (3) Preferred erosion of marsh due to a variable geometry of the shoreline is not included in the model (see Figure 4.4.6); (4) Reworking of marsh sediments due to storms and bank sloughing is not included in the model; (5) Accretion rates are based upon empirical data. A mechanistic model of sediment supply is not utilized in the modeling; (6) The overwash component of the model is very simplified. It does not include long-term, developing factors such as the formation of foreshore dune systems that can act as barriers to overwash fan development.

Three significant wetlands areas (Figure 3.4.3) are present in the Eglin Air Force Base region. The Blackwater Bay – Catfish Basin region was selected for additional study. The Choctawhatchee River wetlands and minor marshes on the bayside of Santa Rosa Island have been recently modeled by Warren Pinnacle Consulting (2011a) and their results will be summarized in this report. The Yellow River Marsh Aquatic Preserve (Blackwater Bay and Catfish Basin) includes significant biological resources, and maintains these resources in an essentially natural condition. This pristine preserve is fringed by forested wetlands, marshes, and submerged grasses that provide food and habitat for numerous fish, reptiles, amphibians, birds, mammals and benthic invertebrates.

SLAMM model inputs included data from NOAA Digital Coast, National Elevation Dataset (NED), NOAA tidal data, and the USFWS National Wetlands Inventory (NWI). SLAMM, a cell-based model, was run at 10 m resolution based on NED characteristics within the study

region. Model simulations were based on the SERDP-mandated scenarios for SLR (0.5, 1.0, 1.5, and 2.0 m by 2100) with a time step of 25 years. A maximum sea level value of two meters is presented in the following tables. The parameters used in SLAMM modeling are modified from the values developed by Warren Pinnacle Consulting (2011a) for the Choctawhatchee River wetlands (Table 3.4.1). Modifications include different initial sea level trends, tidal parameters (Table 3.1.2) and erosion rates.

Accretion and erosion data were adapted from our long-term SET (Sediment Elevation Table) sites east of the study area, on the Apalachicola River coast of northwest Florida. SET data are the only reliable source of wetland accretion-erosion data. Such data have to be collected over a lengthy period in order to be reliable. No SET sites have ever been established in the EAFB region, and the project timetable did not allow sufficient time to establish reliable sites. The Apalachicola coast and wetlands are analogous to the EAFB coastal region. As a result, it was determined that the Apalachicola SET data would provide the best estimate for accretion-erosion data for the EAFB region SLAMM modeling. In testing the sensitivity of the SLAMM modeling parameters for different locations in the Gulf Coast region Warren Pinnacle Consulting (2011a, 2011b, 2011c) found that variations in marsh accretion rates may produce significant changes in model response. The Warren Pinnacle studies indicate the irregularly flooded marsh is the most sensitive environment controlled by variations in accreation rates. For the irregularly flooded marsh in the Choctawhatchee system their study indicates that increasing accretion rates by 15% resulted in a prediction of nearly 5% more irregularly-flooded marsh in the region (Warren Pinnacle Consulting, 2011a).

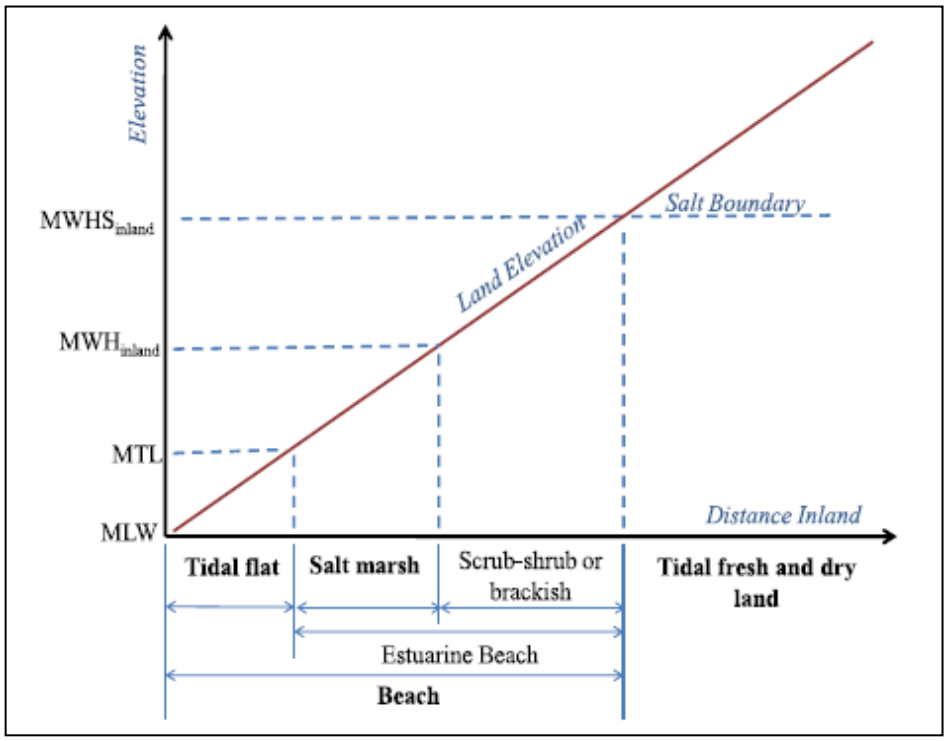

Figure 3.4.1. SLAMM inundation model showing the general elevation hierarchy of the wetlands and their boundaries. MLW is the mean low water heights observed; MTL is the datum located midway between the mean of high water and the mean of low water heights observed; MWH inland is the mean of inland high water heights relative to MTL; and MWHS inland is the mean of spring high water levels (after Clough, 2006).

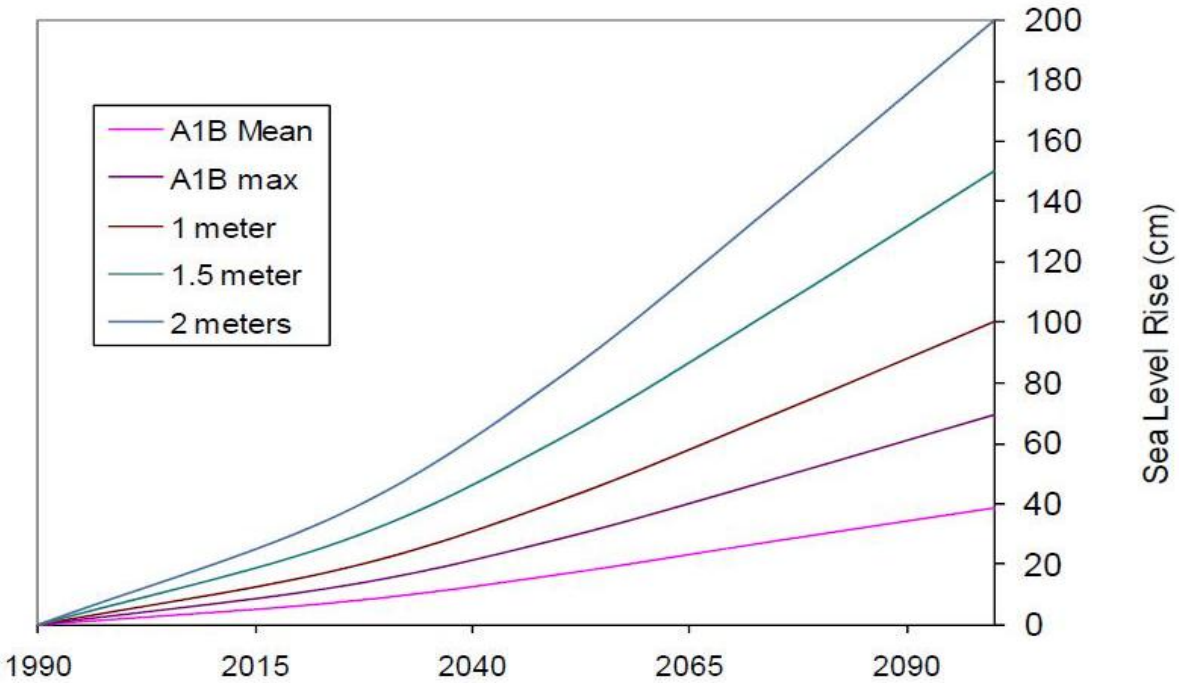

Figure 3.4.2. Scaling from IPCC scenario A1B to the 1 meter, 1.5 meter and 2 meter SLR scenarios.

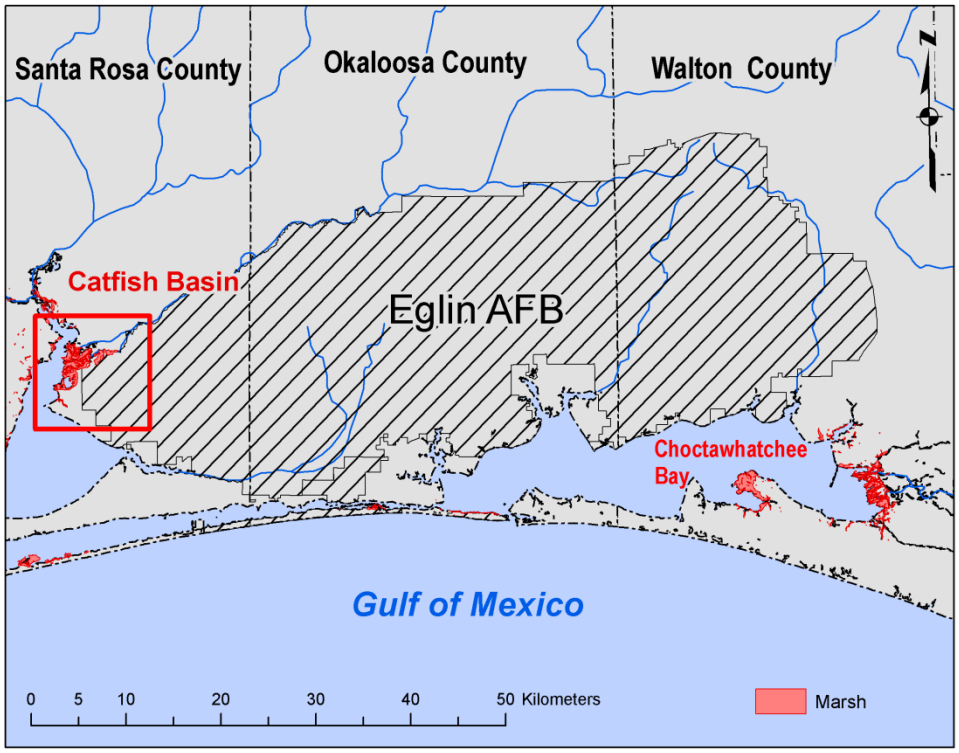

Figure 3.4.3. Coastal wetland areas (marsh) in the vicinity of Eglin Air Force Base.

Table 3.4.1. Principal input parameters for SLAMM for the Yellow River – Blackwater Bay and Catfish Basin, western perimeter of Eglin Air Force Base.

SLAMM Parameter	Value
Description	Blackwater Bay – Catfish Basin
NWI Photo Date	2000
DEM Date)	2006
Direction Offshore	West
Historic Trend (mm/yr)	2.1
MTL-NAVD88 (m)	0.096
GT Great Diurnal Tide Range (meters)	0.492
Salt Elevation (meters above MTL)	0.309
Marsh Erosion (horizontal meters /yr)[1]	0.5
Swamp Erosion (horizontal meters /yr)	0
Tidal Flat Erosion (horizontal meters /yr)[1]	0.5
Regularly Flooded Marsh Accretion (mm/yr)	2.35
Irregularly Flooded Marsh Accretion (mm/yr)	0
Tidal Fresh Marsh Accretion (mm/yr)	4
Beach Sedimentary Rate (mm/yr) [2]	6.41
Frequency Overwash (years) [2]	12
Use Elevation Pre-processor [True,False]	TRUE
Notes: 1 – Erosion rates are highly variable (0-1 meters/yr) 2 – Beach and overwash parameters are not applicable to Blackwater Bay.	

3.5. Modeling Coastal Groundwater

Groundwater is the source of potable water throughout Eglin Air Force Base and the surrounding region. Although there is minor use of water derived from the near surface aquifers, by far the major sources of potable water are the two confined layers of the Floridan Aquifer. The surface of the upper layer of the Floridan Aquifer is generally located 30 to 500 m below the land surface. It ranges in thickness between 35 and 45 m. It is separated from the lower layer by the Bucatunna Clay confining unit which is generally on the order of 30 m in thickness. In the EAFB region the lower layer of the Floridan Aquifer is approximately 300 m thick. There have been a number of studies of this groundwater resource (NWFWMD, 2000; Pratt et al., 1996; 2001) and these clearly establish that there is a relatively high flow rate and that there is a persistent issue related to a significant drawdown of the potentiometric surface due to groundwater pumping near the coast.

An initial review of these groundwater conditions suggested that the scale of the confined aquifers, the relatively high freshwater discharge rates and the location of the major drawdown could be expected to significantly limit the impact of future sea-level rise. In order to provide a more comprehensive analysis of the effects of future sea-level rise scenarios, it was decided to extend the analysis to include their effects on both the confined aquifers which are the major consumptive freshwater resource, and the unconfined surficial aquifers of Santa Rosa Island. Although there is relatively little consumptive use of water from the surficial aquifers on the island, these aquifers have important roles in island ecology.

3.5.1. Model Conceptualization. Groundwater in coastal aquifers generally flows towards the sea. Seawater has higher density than groundwater and has the tendency to intrude inland, creating a wedge of saltwater in the lower portion of the aquifers. To study saltwater intrusion, density-dependent flow dynamics are needed to simulate flow in the transition zone between freshwater and saltwater. The groundwater flow is affected by the density variation due to changes in salinity. Thus, groundwater flow needs to couple with salt transport to describe the saltwater intrusion.

3.5.1.1. Seawater Intrusion to an Unconfined Aquifer. A general conceptual model for describing a groundwater flow system near a coastal boundary is shown in Figure 3.5.1. As shown in the figure, the higher density sea water has a tendency to intrude inland beneath the fresh groundwater. The spatial extent of the intruded saltwater wedge would depend on several factors including recharge rate, regional aquifer discharge rate, hydraulic properties, and sea level (Chang, 2011).

Freshwater lenses with varying volumes and water quality exist (or at least, existed at one time) beneath Santa Rosa Island, a barrier island. Groundwater level and salinity are important factors for the security of the Air Force facilities in the island. For example, the water content in the sand dunes will significantly affect the dune growth or erosion processes, and the groundwater salinity increase will strengthen the facility erosion. Further, the freshwater is important for plants and animals, such as birds, in and around the islands. To keep or recover the freshwater lens, one needs to understand its characteristics and dynamics (Tarbox, 2003). Dupuit–Ghyben–Herzberg (DGH) theory indicates that an ideal freshwater lens (i.e., within a homogenous, isotropic, infinite-strip island) is symmetrical about an island's center and depth to the freshwater–saltwater/freshwater interface, and is directly proportional to the elevation of the

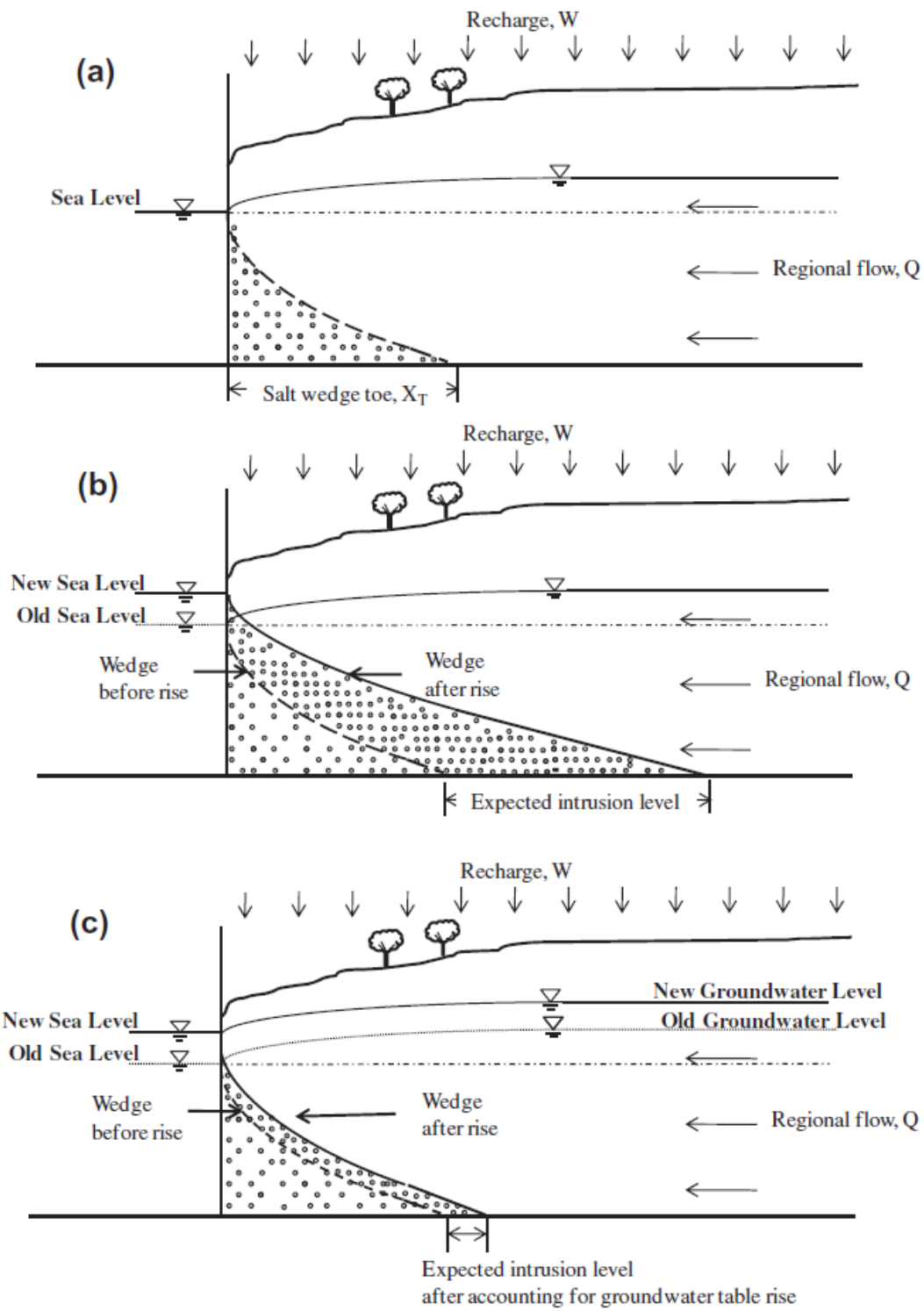

Figure 3.5.1. Comparison of conceptual models used for visualizing the impacts of sea-level rise on a saltwater wedge: (a) initial salt wedge before the sea-level rise, (b) salt wedge profile after sea-level rise based on a traditional conceptual model that ignores the lifting effect, and (c) a new conceptual model that includes the lifting effect. (Chang, 2011).

water table above mean sea level. A freshwater lens increases as precipitation percolates into the water table. Dune elevation and vegetation can affect the spatial patterns of recharge. The depth

and shape of a freshwater lens is primarily dependent on the medium's conductivity (K) and precipitation recharge rate (R). Tidal pumping is an additional factor which can change the shape of the freshwater-saltwater interface. Figure 3.5.2 shows the freshwater movement and the morphology of the freshwater lens on a barrier island (Vacher, 1988a).

3.5.1.2. Saltwater Intrusion into a Confined Aquifer. A regional groundwater flow model has been developed to describe the groundwater flow in the Eglin AFB area. Additionally, a density dependent flow and transport model has been developed to simulate the evolution of seawater intrusion into the confined aquifer in the area. Both models are initiated via a steady state flow in the original natural conditions, no pumping and sea level rise. The calculation results reflect the natural hydraulic head distribution and salt concentration distribution without human activities. Well pumping from the aquifer was then added to the system in a transient mode from initial pumping activity time to current time. The modeling simulation presents the effects of human activities on the groundwater system. In the third step, various sea level rise scenarios were added to the model to simulate the water flow and salt concentration variation from current time to the end of this century.

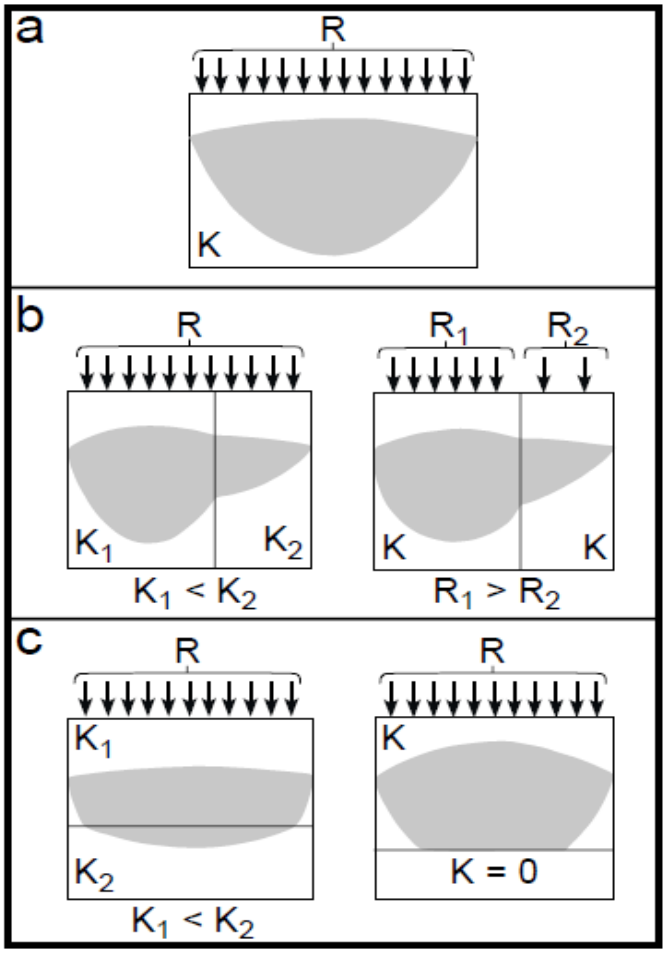

Figure 3.5.2. Distributions of freshwater lenses under various conditions: (a) Model with homogenous K and R; (b) Asymmetric lenses due to variability in K and R; (c) Thin lenses due to high K layer at depth and zero permeability K layer at depth. (Vacher, 1988a).

3.5.2. Numerical Modeling. Density-dependent numerical models are frequently used to address scientific, engineering, and water resources management problems (Voss and Wood 1993; Voss 1999; Voss and Anderson 1993; Simmons et al., 1999; Simmons et al., 2002; Shoemaker et al., 2003; Langevin, 2001). MODFLOW2000 (Harbaugh et al., 2000; Hill, 1992) and SEAWAT2000 (Guo and Langevin, 2000) were chosen as the groundwater flow and density-dependent ground water flow simulators for this study. SEAWAT2000 is a new version of the SEAWAT codes (Guo and Bennett, 1998; Guo and Langevin, 2002) that combines MODFLOW2000 (Harbaugh et al., 2000) and MT3Dms (Zheng and Wang 1999) to solve the coupled ground water flow and solute transport equations. The SEAWAT2000 was chosen since its simulation results match well with other density dependent flow models in terms of accuracy and execution time.

The variable-density ground-water flow simulation is usually developed and presented in terms of fluid pressure and fluid density. In this study, the variable-density groundwater flow equation was developed in terms of equivalent freshwater head and fluid density for coupling MODFLOW with MT3DMS. The mathematical equations for flow, solute transport and relationship between concentration and density are,

$$\begin{cases} Flow: \quad \nabla \cdot \left[\rho K_f \left(\nabla \cdot h_f + \dfrac{\rho - \rho_f}{\rho_f} \nabla z \right) \right] = \rho S_f \dfrac{\partial h_f}{\partial t} + \theta E \dfrac{\partial C}{\partial t} - \rho_s q_s \\ Density: \quad \rho = \rho_f + EC; \quad E = \dfrac{\partial \rho}{\partial C} \\ \qquad (i.e. \quad E = \dfrac{\rho_s - \rho_f}{C_s - C_f} = \dfrac{1025 - 1000}{35 - 0} = 0.7143) \\ Transport: \quad \dfrac{\partial(\theta C)}{\partial t} = \nabla \cdot (\theta D \cdot \nabla C) - \nabla \cdot (\theta \vec{v} C) - q_s C_s \end{cases} \tag{3.5.1}$$

In the Flow equation, h_f [L] is the equivalent freshwater head; ρ [ML^{-3}] is density of saline ground water; ρ_f [ML^{-3}] is density of freshwater; K_f(x,y,z) [LT^{-1}] is freshwater hydraulic conductivity; S_f [L^{-1}] is specific storage in terms of freshwater head; ρ_s [ML^{-3}] is the density of source or sink terms; q_s [T^{-1}] is the volumetric flow rate per unit volume of aquifer representing sources and sinks; θ [dimensionless] is porosity; t [T] is time. In the Density equation, C [ML^{-3}] is solute concentration; Cs[ML^{-3}] is the solute concentration of water entering from sources or sinks. In the Transport equation, D[L^2T^{-1}] is the hydrodynamic dispersion coefficient;$\vec{v}$ [LT^{-1}] is fluid velocity.

The governing equations for the movement of ground water and the solute transport of solutes are coupled. Fluid density is a function of solute concentration and fluid pore pressure.

3.5.3. Model Settings.

3.5.3.1. Model Setting for an Unconfined Aquifer. As shown in Figure 3.5.3, a 2D coastal model domain was selected for the unconfined aquifer on Santa Rosa Island. The domain is 100 m east-west, (along the coastline) and 210 m in north-south (perpendicular to the coastline). This model was used to estimate the saltwater wedge migration due to sea-level rise. The model was

first run in a steady state condition to achieve a balanced saltwater and freshwater interface. Subsequently the model was run in a time dependent mode.

Another 2D model domain extending 1000 m by 1500 m was created to simulate the freshwater lens on eastern Santa Rosa Island. This model is used to simulate the hydraulic head variation in the unconfined aquifer due to sea-level rise.

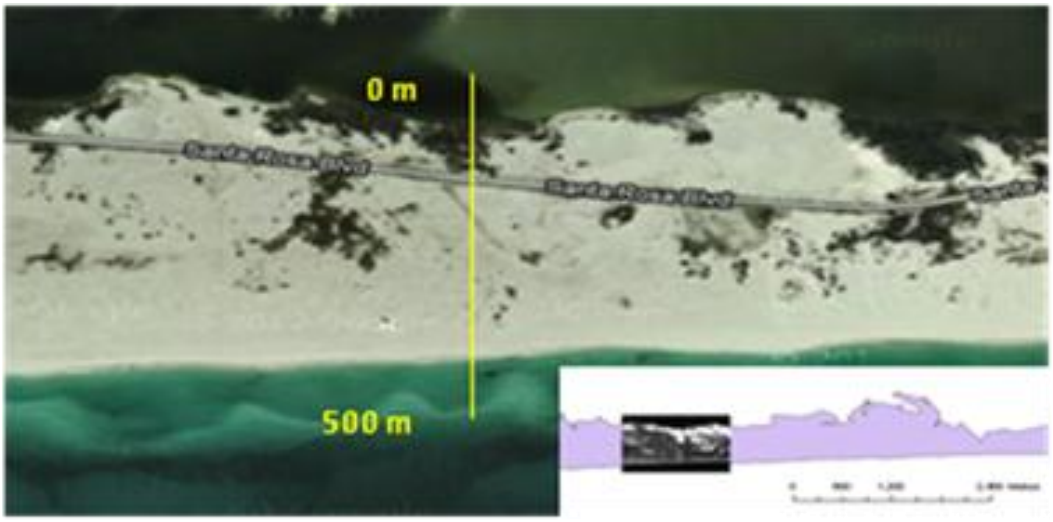

Figure 3.5.3. Location of transect used for 2D freshwater lens model on Santa Rosa Island.

3.5.3.2. Model Settings for a Regional 3D Saltwater Intrusion Model. The regional 3D groundwater flow model includes Santa Rosa, Okaloosa and Santa Rosa counties in Northwest Florida. For the numerical modeling, the following hydrogeological conditions were considered: site geometry, hydrogeologic characterization (hydraulic conductivity, porosity and thickness of layers), position and characterization of rivers and drainage canals, natural groundwater recharge, boundary and initial conditions, piezometric hydraulic heads based on freshwater, observation wells and distribution of salinity concentration in the system.

3.5.4. Hydrostratigraphic Units.

3.5.4.1. Hydrogeology and Stratigraphy. The hydrogeologic units in the study area are in the Middle Eocene to Recent Series as presented in the regional groundwater report published by Northwest Florida Water Management District (NWFWMD) (2000). The geologic units are further classified into hydrogeologic layers depending on their transmissive and storage properties. The principal hydrologic zones from top to bottom consists of the sand-and-gravel aquifer, which forms the surficial system, the intermediate system regional confining unit, the Upper Floridan Aquifer, the Bucatunna Clay confining unit (where present) and the Lower Floridan Aquifer. The detail hydrogeologic characteristics information could be found in the NWFWMD regional water resources report (2000). Figure 3.5.4 shows a typical hydrogeologic section within the study area depicting the hydrostratigraphic sequences in this study domain. The elevation of these aquifers had been interpreted by Pratt et al., (1996) on a regional scale. The elevations of each aquifer layer in this study are from this report.

3.5.4.2. Potentiometric Data. The water table in the surficial zone, the Sand-and-Gravel Aquifer, is generally a subdued replica of the topography, a few meters below land surface in

most of the Coastal Lowlands physiographic region (Hayes and Barr, 1983). The potentiometric surface of the Upper Floridan Aquifer within the study area is updated every year by NWFWMD since 1986 and a noticeable hydraulic head decline has been observed. Information on the Lower Floridan Aquifer in the study area is relatively sparse.

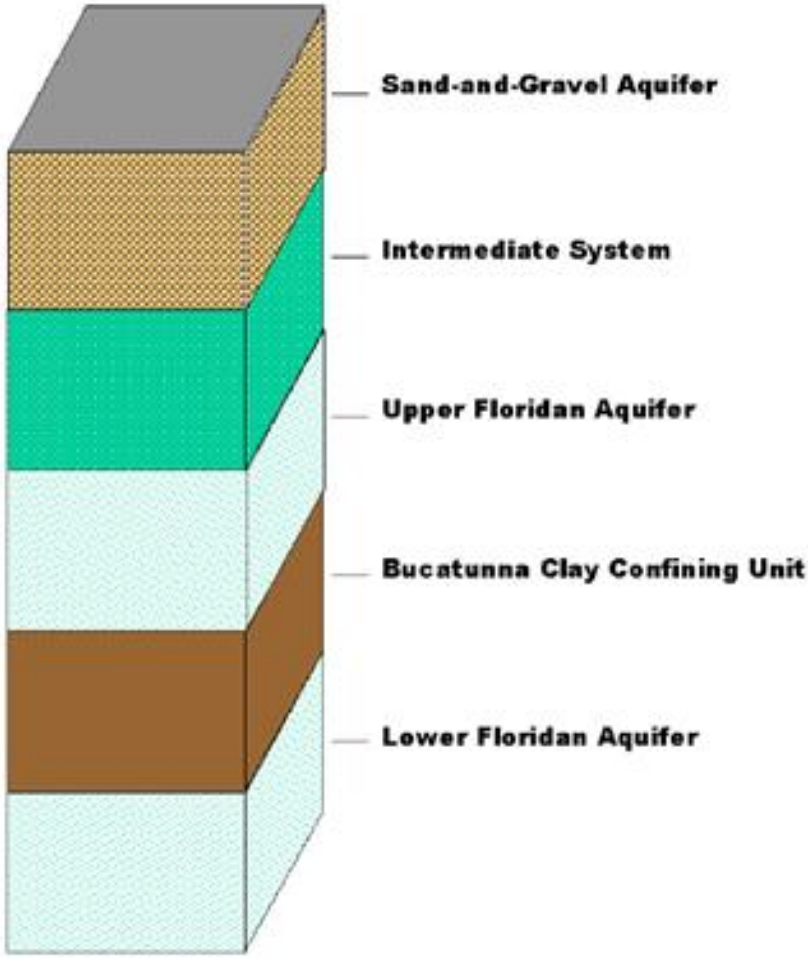

Figure 3.5.4. Hydrogeologic units in the study area (NWFWMD, 2000).

3.5.4.3. Recharge and Transport Parameters. Rainfall precipitation is the primary source of recharge to the area. Average rainfall in the study area is approximately 2 meters per year (m/yr), with 0.4 to 0.6 m/yr recharging to the Sand-and-Gravel aquifer. The transport parameters are adopted from the NWFWMD saltwater intrusion report. Effective porosity in the study area was set to 0.25. The longitudinal dispersivity was set to 30 m. The transverse dispersivity was set to 6 m. The vertical longitudinal dispersivity was set to 3 m and the vertical transverse dispersivity was set to 0.3 m. The molecular diffusion was set to 0.0001 m^2/d for the bottom layer of the sub-Floridan System and for the Bucatunna Clay confining unit.

3.5.4.4. Boundary and Initial Conditions. In the surface groundwater layer, the drainage boundary condition is used to discharge the excess recharge in case the modeled water levels

exceed the land surface. The river package is applied in the surface layer where rivers exist. The layer below the Lower Floridan Aquifer is set to be a no-flow boundary in the flow model, but a specified concentration and hydraulic head boundary is used in the saltwater intrusion model. For the lateral boundaries, the intermediate Confining Unit is a no-flow boundary. In the Floridan aquifer, specified hydraulic head conditions along the east and west boundaries are defined. No flow conditions are set in the north part for the updip portion of the Floridan Aquifer system. The south boundary is defined as constant head boundary and increases with depth due to the water density increasing with depth.

Groundwater is the principal source of freshwater in the study area. Over a hundred wells pump water from the Floridan Aquifer. The locations of these wells are plotted in Figure 3.5.5. Richards (1993) collected most of the pumping data in the study area for 1990 average daily rate withdrawals. These data have been augmented by NWFWMD (1999) to cover the current study area. The well pumping rate in the sea-level rise model has been set by the water management planners for Santa Rosa, Okaloosa, and Walton counties (NFWMD, 2012).

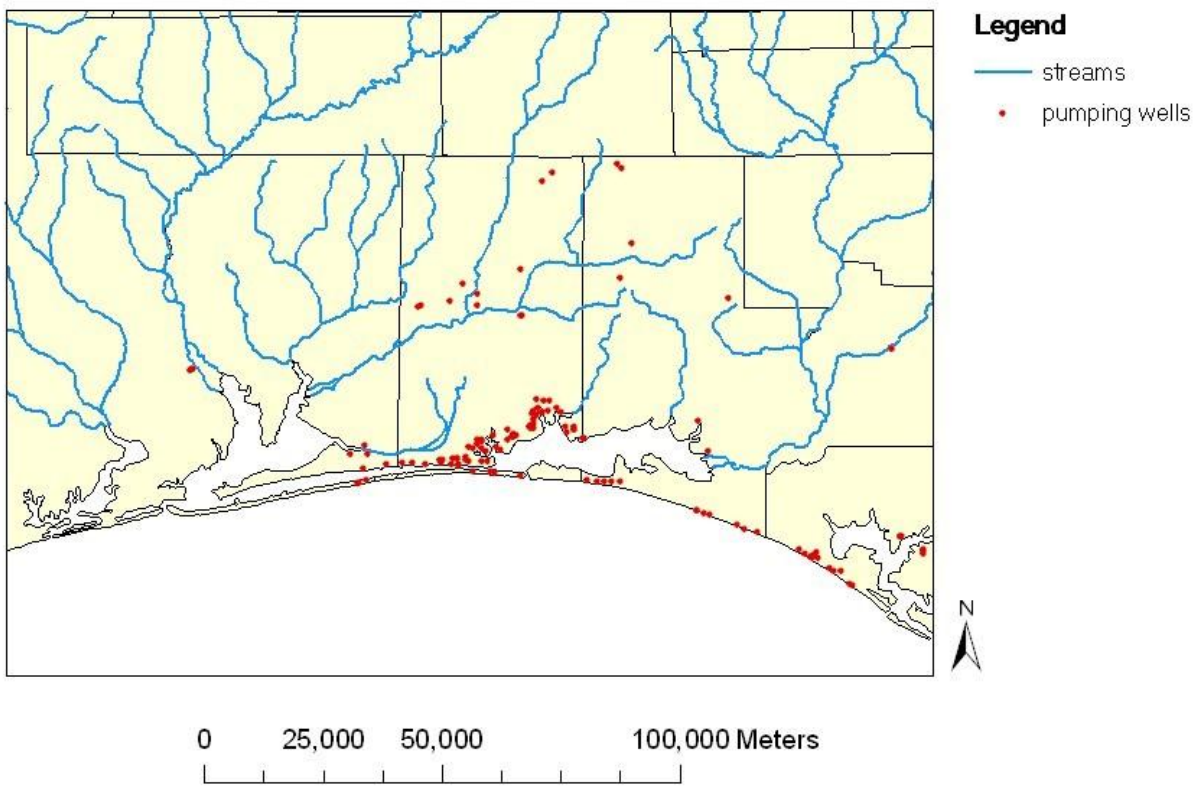

Figure 3.5.5. Surficial drainage units and pumping well locations in the study area (NWFWMD, 2000).

3.5.5. Sea-Level Rise Scenarios. Current literature indicates that the eustatic rise of sea level is progressing more rapidly than previously assumed, perhaps due to the dynamic changes in ice flow omitted in the most recent IPCC calculations (Monaghan et al., 2006). Sea-level rise will, in general, increase groundwater levels in a coastal aquifer and strengthen seawater incursion to

the aquifer. To predict the effect of sea level rise on groundwater flow and salinity variation in the Eglin AFB region, SERDP sea level rise scenarios were adopted in this report. According to our model results, the influence of a 0.5 meter sea level rise on the confined groundwater is trivial. As a result, the 1-meter and the 2-meter sea-level rise scenarios by 2100 are considered in the confined groundwater flow models.

3.6. Modeling Morphologic Change

An important tool to predict the effects of sea level rise on coastal military facilities and the dependence of these effects on the rate of rise is a numerical model capable of representing the processes that control the morphology of the many interacting coastal system components. These components include the mainland shore, beaches, barrier islands, coastal dunes, the surf zone, the shoreface tidal inlets and related features. It has been shown by several researchers that these components are dynamic on a time scale of years to decades, changing in response to changes in sediment supply, fluid power (wave and current climate), and sea level (DeVriend, 1991; Stive and DeVreind,1995; Stive et al., 1990; Niedoroda et al., 1995a). It is generally not appropriate to represent these components in isolation. They are continually interacting in non-linear ways as morphological changes in one component bring about changes in the sediment supply and dynamic forcing, which affect other components in the overall complex coastal system (Cowell et al., 2003a, b).

Eglin Air Force Base was selected as a prototype example of a complex coastal system because it occupies a portion of the Santa Rosa barrier island, with its dunes, overwash deposits and tidal inlet, along with a significant portion of the adjoining mainland shore. Santa Rosa Island is largely in a natural state, especially within the base. It is also one of the more heavily studied barrier islands on the U.S. coast (e.g., Stone, et al., 2004; Rosati, 2009).

The many advantages of using Eglin AFB and Santa Rosa Island as the prototype for developing, calibrating, testing and exercising a numerical model of complex coastal systems has not overshadowed the overall project aim to develop a mathematical model that can be applied in a wide variety of coastal settings around the country and around the world. At this time there are few such models available (Hinkel, 2005; Hinkel and Klein, 2003; Stive and Wang, 2003; Wang et al, 1995, Cowell et al., 1995; Nicholls et al., 1993). In general, these are all poorly suited to predicting the scales of coastal morphological change that are expected on the time scales of decades to centuries and on spatial scales of hundreds of meters to kilometers.

The assembling, reduction and processing of a large amount of existing data regarding the Santa Rosa barrier island and other components of the complex coastal system in and around Eglin AFB has been described in a previous section of this report (see Section 3.1). A conceptual model of the processes controlling the large-scale morphology of the complex coastal system in the vicinity of Eglin AFB has been developed.

The mainland shoreline is undergoing *in situ* or “bathtub” inundation except where marshes are established. The morphology inland of the shore of Choctawhatchee Bay is generally a low-relief landscape with a low bluff behind the narrow beaches. Sea level rise will cause continued erosion of the low bluffs and the narrow beaches will retreat accordingly. Because the inland area is above the highest 100-year sea level rise considered in this project, we expect that bluffs

will simply continue to erode without any of the dynamic changes of the nature of those along the open barrier beaches exposed to the Gulf of Mexico.

The coastal marshes respond to the combined effects of ongoing inundation and vegetation assemblage responses as explained in other sections of this report (see Sections 3.4 and 4.4). These future developments of the mainland shore contrast with those of the barrier island system. Historic data since 1855 clearly demonstrate the dynamic responses to the overall wind, wave and storm climate. The ocean shoreline has generally experienced long periods of relative stability and local minor shoreline progradation locally. Interspersed with these are periods where one or a sequence of major hurricanes has impacted the barrier island system. During these episodes, there is rapid and considerable shoreline retreat with a significant volume of sand being lost from the beach prism and deposited on, and even behind, the barrier island as overwash deposits. The sand dunes of the island are continuously evolving, with slow growth during periods of normal weather interrupted by sudden storm erosion, which occasionally brings about total destruction. Sand removed from the dunes by these storms is redistributed between the beach prism, the barrier island platform and in extreme storm events, as deposits along and beyond the bay shoreline. However, dunes are also resilient, with regrowth initiating shortly after the destructive storm events. The overall pattern is one of coastal dune growth along a primary dune system immediately landward of the beach prism, which leads to a volume of sand in temporary storage. Storms erode and redistribute these deposits leading to an upward growth of the barrier island platform and, in places, a progradation of the bay shoreline.

Not all of the barrier island features are explained by these ongoing dynamic processes. There are several places within Eglin AFB and along other portions of Santa Rosa Island where ancient sand dunes are evident. These represent features related to long-vanished shoreline positions and related processes. These are not part of the present system of coastal dynamics and they do not dynamically respond to the present storm climate or rate of sea level rise. Other portions of this barrier island system have undergone development that has altered the balance of coastal processes.

The conceptual model provides a starting point for the design of a numerical model of complex coastal systems. Clearly this model must be capable of representing a diverse set of typical components that are expected to be found in most coastal areas and that are represented in the Eglin AFB prototype area. The model should be based on the physics of processes that control the morphology of these components, their responses to changes in the physical forcing, and the interactions between the individual components. The complex coastal system at Eglin AFB gives a good representation of the variety of components that can be expected to be important in other coastal systems, to one degree or another. The model needs to be three-dimensional in its representation of the overall system because not all processes can be included in more simple representations and such absences would completely upset the balanced representation of the whole system.

It is also important that the model of the complex coastal system be adapted to the realities of input data and the stability of numerical procedures. It is readily envisioned that a comprehensive program of measurements to capture the full range of waves, currents, winds, sediment transport and their interactions over an area many tens of kilometers in scale and over time periods of decades to centuries would be an impractical undertaking. It is also necessary to avoid overly detailed representations of physical processes. As mentioned previously, the general

approach to mathematical modeling of complex coastal systems has been well described in the classic paper by de Vriend (1991). The point is that a proper model represents the features and processes at time- and length-scales that are relevant to problems of interest. Processes operating at small scales should be represented by generalized parameters. For example, in most fluid dynamic models the motions and effects of the small-scale, rapidly changing turbulent eddies are generalized to eddy coefficients. In morphodynamic modeling the hourly and daily fluctuations in the waves and currents must also be parameterized into time-, and space-averaged representations. Also, processes operating at scales larger than those of interest in the problem are treated as external factors that may be simply input as small overall trends or ignored completely. For example, most engineering models used to design beach nourishment projects ignore the slow changes in global sea level. On the other hand, it is necessary to retain the appropriate mathematical expressions for the large-scale physics of the processes that control sediment transport and the resulting morphologic changes so that the model is truly dynamic.

To assess morphological developments such as shoreline position, rates of beach erosion, changes in barrier island elevation and width, and other changes that are of interest in planning, engineering and operational decisions about base facilities, the relevant time scales are from several years to a century or more. The relevant length-scales are in the range of tens of meters to kilometers. These scales are quite different from those associated with the winds, waves and currents which are the agents of coastal change. Changes in the morphological features arise from patterns of net deposition or erosion of the transported sediment. Sediment transport from waves and currents respond on time-scales of seconds to hours and length-scale from millimeters to meters. Typically, the rate and direction of sediment motion varies over these short time scales with oscillations that are large in comparison to the small net transports that control the changes in morphology. Models representing these physical processes must be extremely accurate to resolve such small net differences and most cannot satisfy this requirement. This difficulty gives rise to morphodynamic models that seek to represent the sediment transport processes directly as time-, and spatial-averaged quantities. The rapidly varying aspects are parameterized rather than being resolved.

Morphodynamic models utilize a wide range of approaches to generalize the time-, and spatially averaged physical processes. Some rely on simple conservation of feature geometry during spatial migration controlled by large-scale forcing. The Roy and Cowell model of shoreface and nearshore response to rising sea level based on the application of the Bruun Rule (Cowell et al., 1995) is an example. Others, such as the nearshore, shoreface and shelf model described in Niedoroda et al, (1995a) and Niedoroda et al., (2011) are based on time-averaged variables and equations representing physical processes at large scales. Some morphodynamic models represent individual components of coastal systems, such as shoreline evolution, while others represent several components as they respond together to changes in large-scale forcing (see Cowell et al., 2003a, 2003b). In the latter the concept is that coastal systems that include river sources, bays, salt marshes, inlets, barrier islands, beaches and dunes form a linked dynamical system which responds with complex interactions to changes in the major forcing such as the storm and wave climate and sea level rise and sediment supply.

While morphologic changes of coastline and dunes have been studied extensively, the adaptation of dunes and general barrier island morphology to increasing rates of sea level rise is not well studied. To our knowledge, sea level rise has not been explicitly addressed in most of the previously developed coastal models. Dunes and barrier islands are of special importance for

coastal protection and restoration. As the final line of defense against storms, they protect the shore by absorbing storm energy and provide sediments to island platform and backshores. In addition to their role in shielding the mainland shores, barrier islands directly support military infrastructure and training facilities. Meaningful predictions of the long-term changes in both ocean and bay shoreline positions, island platform elevation and coastal dune morphology provide key inputs to decisions regarding the placement of new structures, the advisability of providing coastal defense structures to protect existing facilities and the degree to which natural processes can tolerate disruptions due to training or other military activities.

3.6.1. The MoCCS Model. The Model of Complex Coastal Systems (formerly named the PR-SL model) is a multi-line mathematical representation of the physical processes that control morphodynamic adjustments to ongoing and slowly varying changes in the major forcing parameters which include: 1) sediment supply, 2) general wave-current climate, 3) the storm climate, and 4) relative sea level. Although parts of the MoCCS model were based on the previously developed CST-ASMITA model (see Niedoroda et al., 2001 and Niedoroda et al., 2003) the model has been largely rewritten and expanded to include more coastal processes and morphological components. Unlike the more common models which are based on grid elements a multi-line model has the different morphodynamic components represented in different computational frameworks. This is more fully explained in the following section of this report. In the MoCCS model the sediment fluxes and morphological changes are modeled independently for the beach and surf zone, the shoreface, the inner continental shelf, the inlet(s), the bay and/or lagoon, and river sources. Sediment discharge fluxes and morphological changes are matched along the internal boundaries at each time step.

3.6.2. Overall Structure of the MoCCS Model. The MoCCS model represents two forcing regimes and eight morphological components. One forcing regime is used to represent the processes that control large scale and slow changes in the morphology of the system components in response to slowly varying forcing parameters such as changing sea level, wave-current climatology, and sediment supply. Because these changes are slow but persistent leading to differences that become noticeable on time scales of years-to-decades, this forcing regime is named the *Chronic Regime*. However, in addition to these slowly changing aspects of coastal morphology there are other changes that occur rapidly in response to the extreme forcing conditions during major hurricanes. Over long periods, the incremental morphological changes from individual storms combine sequentially into cumulative changes. The storm-driven processes and their cumulative morphological responses are represented by the *Acute Regime.* In the natural world, the Chronic and Acute processes are continually interacting. It is more appropriate to consider the processes and controls of these two forcing regimes separately in the MOCCS model, with the effect of these combined interactions taken into account once each model year. That is, processes that occur within a year are not resolved in detail but their average effects are included in the simulations.

It is important to recognize that the MoCCS model, like models in general, is designed to provide a quantitative representation of those natural processes that are relevant to a specific problem. In this case the goal is to represent processes that are important in reshaping the shoreline position and the morphology of the complex coastal system while avoiding details that are unimportant at long time scales. This is especially important because of the additional requirement that the model be relatively undemanding of computational resources so that it can be used to compute a large number of possible realizations of a century-long series of future system changes. The

ensemble of future realizations is then used to statistically describe morphological changes over the next century.

3.6.3. The MoCCS Chronic Regime. The morphological components that change slowly but persistently in response to changes in large-scale forcing from the wave-current climate, relative sea level and sediment supply include the open coast shoreline and surf-zone, the adjoining shoreface and inner continental shelf, and the tidal inlet. As shown in Figure 3.6.1, each of these components is represented differently in the MoCCS model. For example, the processes resulting in changing the morphology of the inner continental shelf and the shoreface are defined according to a depth-averaged model grid with elements measuring 250 m on each side. The processes controlling the shape and position of the open shoreline are represented as a one-line alongshore model component with elements also measuring 250 m on each side and with the shoreline position within each of these cells defined by a sub-grid element coordinate. In this way the one-line shoreline model component aligns with the corresponding representation of the adjacent shoreline grid along an internal boundary along which the morphology and sediment discharge fluxes are balanced at each time step. The use of the sub-grid element coordinate to track the time-varying location of the shoreline has been adopted to allow very detailed specification of the shoreline location, down to the sub-meter scale, without burdening the model computations with a huge number of very small grid elements. The processes resulting in slow and persistent changes in the bar deposits at the tidal inlet are represented as individual panels for the ebb-, and flood-tide shoals. As is common in the natural world, the inlet is maintained by dredging and it is assumed that this maintenance dredging will persist over the next century. Each of these parts of the MoCCS model is discussed individually.

The outer limit of the complex coastal system is taken to be the inner continental shelf. The sediment transport in this realm responsible for changes in the morphology is forced by complex and ever-changing patterns of waves and currents. For any given point on the sea bed at each instant in time there is a flow caused by the combined action of currents and waves. If this produces sufficient force on the sediment particles they will be in transport. However, seconds later the flow has changed as the pattern of interacting waves and currents has evolved. Clearly it is very difficult to represent the actual details of these processes in a large scale numerical model. It is also important to recognize that most of the sediment movement caused by the waves and currents is of an unsteady or oscillating nature. The spatial gradients in sediment transport that cause morphological change arise as very small net transport fluxes. Rather than accounting for these subtle effects arising from complex motions, the MoCCS model adopts large-scale time-averaged representations of the controlling physics.

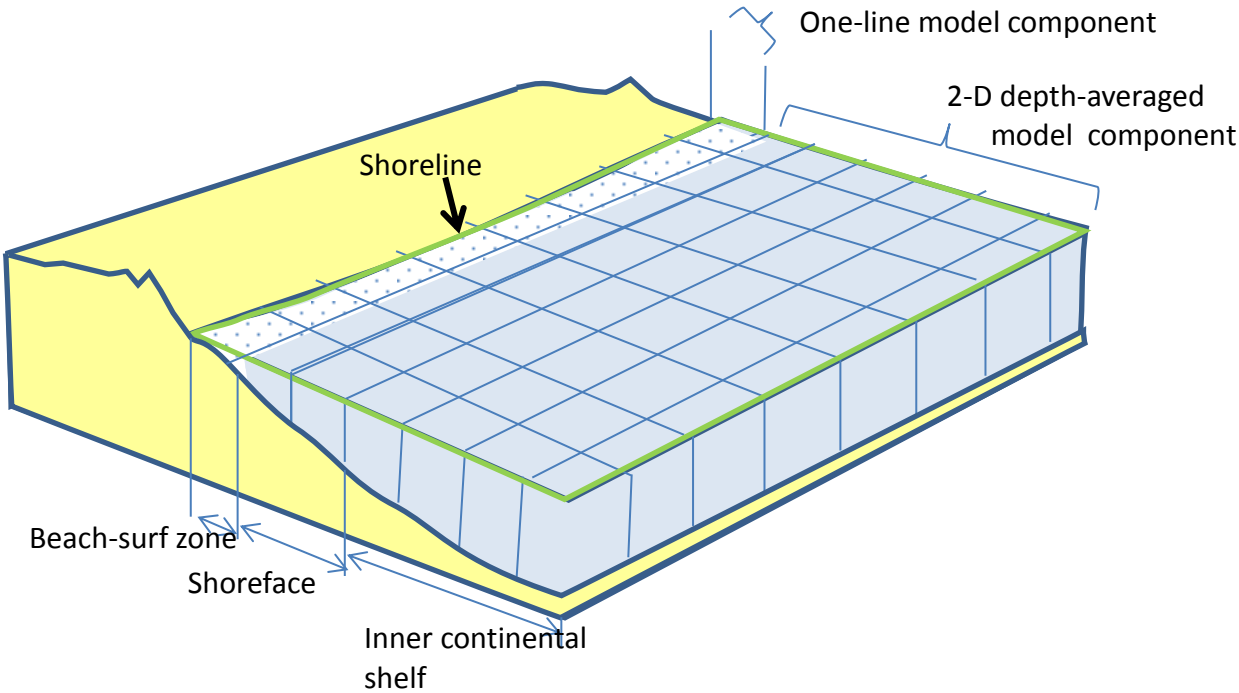

Figure 3.6.1. Schematic of the MoCCS model Chronic Component parts. Actual grid spacing is much more detailed than shown here.

The slow evolution of water depths and sea bed morphology on the inner continental shelf is modeled according to the Exner Equation which represents the conservation of volume. This is given as:

$$\frac{\partial h}{\partial t} = -\frac{1}{1-e}\nabla Q = -\frac{1}{1-e}\left(\frac{\partial Q_X}{\partial x} + \frac{\partial Q_y}{\partial y}\right) \tag{3.6.1}$$

Where h is the elevation of the sea bed, e is the porosity, Q is the time-averaged rate of sediment transport and $\boldsymbol{x}$ and $\boldsymbol{y}$ are the coordinate directions. In the MoCCS model, y is the cross-shore direction.

Flows on the continental shelf result from the interaction of time-varying wind stresses, astronomical tidal forces, and contrasts in the spatial patterns of water mass density. All of these components are continually changing so that the dominant feature of shelf currents is their variability in speed and direction. When viewed from a large-scale perspective, these varying flows resemble the chaotic motion of turbulence where the rotary current patterns that resemble eddies are very large and change at the time scales of the tidal and wind stress forcing variability. Also, waves are generally much more important than currents in causing bottom sediment to become entrained. This is caused by high fluid shear stress imparted to the sea floor by the steep instantaneous velocity gradient in the wave boundary layer. In the MoCCS model the approximation is made that the relative intensity of bottom sediment entrainment is a function of the wave orbital bottom stress. This too is represented in a time-averaged sense. When conditions are nearly calm small waves will cause entrainment of bottom sediments only in the relatively shallow depths close to the shore. In storms, this zone of entrained bottom sediments can expand across the whole model domain including the inner continent shelf. The actual temporal and spatial distribution of the time-averaged entrained sediment concentration is the

frequency-weighted sum of all of the full range of wave conditions that are encountered in a given area.

The sediment transport on the inner continental shelf is represented by the time-averaged equation first described in Niedoroda et al., (1995). Here the total depth-averaged sediment volume flux (Q) is given by,

$$Q = \overline{U}\,\overline{C} - K_1 \overline{D}_i \nabla \overline{C} - K_2 \frac{P}{\rho g h} e^{-\beta h} e^{-ds} \tag{3.6.2}$$

The first term on the right side of this equation represents the net advective transport flux taken as the product of the depth- and time-averaged entrained sediment concentration ($\overline{C}$) and the time-averaged depth mean current ($\overline{U}$). Typically, this is zero in the cross-shore direction and very small in the alongshore direction.

The second term represents the time-averaged net sediment flux due to the combined action of the waves acting to entrain the bottom sediment into the flow and the overall action of tidal, wind-driven and other currents. When viewed from a time-average perspective where the averaging time is on the order of a year, these currents are largely oscillating in nature, forming complex patterns resembling the chaotic eddies of turbulences, but at a very large scale. This is represented by the large-scale turbulence coefficients (D_x and D_y). Unlike normal shear-driven turbulence, which is isotropic, the intensities of these chaotic flows are not independent of direction. The alongshore coefficient values are generally much larger than the cross-shore values.

The depth- and time-averaged entrained sediment concentration is assumed to be controlled by the fluid stress in the wave boundary layer. Ordinarily, the exponential decay in the wave orbital flow speed makes this an inverse function of water depth in the domain of the MoCCS model. When considered in a time-averaged sense, this dependence is much stronger because only rare periods of large storm waves produce fluid stress adequate to entrain the bottom sediment of the inner shelf. The frequency of episodes where bottom sediment is entrained increases as the water depth decreases. Overall, the magnitude of the time-averaged entrained sediment concentration is a strong inverse function of the water depth.

The combination of chaotic flows and a strong entrained sediment concentration gradient represent the conditions of Fickian diffusion which maintains a time-averaged transport flux with the direction controlled by the concentration gradient.

The third term on the right hand side of the above equation represents an empirical relationship between a net onshore sediment flux caused by a combination of wave boundary layer stress asymmetry and net wave-driven bottom current and the offshore transport bias caused by the slope of the sea floor acting on back and forth entrainment of the sediment by the wave motion. This is expressed in the third term, which has exponents involving the local water depth (*h*), bottom slope (*ds*) and a scaling coefficient (β).

Sediment transport along shoreline in the surf zone is represented in two components. The shoreline erosion or advance is computed through the use of the Exner equation based on the time-averaged longshore sediment volume flux computed as long-term net transport and a

diffusive transport resulting from the sum of short-term up-and down-coast fluxes resulting in a gross transport. The net transport is computed from the equation,

$$q_{surf} = MH_b^{\frac{5}{2}} \sin 2\theta_b \tag{3.6.3}$$

Where M is a coefficient, H_b is the time-averaged breaking wave height and the time averaged θ_b is wave-breaking angle which is defined as the included angle between wave propagation direction and shoreline direction:

$$\theta_b = \beta_0 - \alpha \tag{3.6.4}$$

where α is the wave propagation angle in surf zone, β is defined as the azimuth of an outward normal to the shoreline:

$$\beta_0 = \mu - \frac{\pi}{2} - \tan^{-1}\left(\frac{\partial y}{\partial x}\right) \tag{3.6.5}$$

The time averaged wave parameters are first evaluated from measured data. In the case of the Santa Rosa modeling, these data came from NOAA Buoy 42040. These values were subsequently revised by calibrating the computed shoreline changes to a long-term data set as described later in this report.

The effect of the gross longshore sediment transport is to cause the shoreline to tend to straighten by slow erosion of convex curves and corresponding filling where the curvature is concave. This problem was addressed in a general way by a simplified form of the Pelnard-Considere relationship,

$$\frac{\partial y}{\partial t} = G\frac{\partial^2 y}{\partial x^2} \tag{3.6.6}$$

Where y is the shoreline position, x represents the cross-shore direction, t is the time and G is a scale coefficient (see Dean 2002, p.40). This relationship scales the rate of change of the shoreline position due to the back-and-forth variations in the longshore sediment transport according to the local shoreline curvature. It is commonly used in engineering beach sand nourishment projects to evaluate the long-term dispersal of the added sediment to beaches adjacent to where the fill is placed. The coefficient G is called the 'longshore diffusivity' and it scales according to the time averaged wave conditions, bottom slope and sand size. In our application the length scale over which the curvature is represented is on the order of several kilometers and the scaling coefficient value is determined as a fitted parameter using a comparison of the model results to the measured shoreline change over a period of decades.

The MoCCS model uses a relatively coarse model grid which favors computational efficiency. However, long-term shoreline changes over long stretches of beach can be quite small. That is, it is necessary to represent shoreline position changes on the order of a meter or less over distances of many tens of kilometers. This is accomplished within the relatively coarse grid of the MoCCS model by representing the shoreline position as a sub-grid element. The position of the shoreline within each grid cell is scaled according to a relative 'fullness'. The grid cell containing the shoreline has a relative volume defined by its area and an upper and lower limit to

its vertical dimension. The upper limit corresponds to the elevation of the adjacent land cell (nominally 2 m) and the lower limit represents the maximum normal depth within the surf zone (nominally –2 m). If the computed volume of this cell is half the maximum volume, the shoreline is placed at the cell center. If the volume within this cell increases during a portion of the simulation, the shoreline position advances accordingly until it reaches the outer face of the cell as the maximum volume is reached. If the sediment volume continues to increase the shoreline-containing cell is redefined (i.e., stepped seaward) and the shoreline position is redefined according to the relative 'fullness' of this new cell. If the trend is towards erosion this process works in reverse with the cell stepping landward as its volume becomes depleted. The advance or retreat of the shoreline is controlled by the relative convergence or divergence of the computed surf-zone sediment fluxes according to the net and diffusive relationship explained above.

Another component of long-term shoreline change is included in the MoCCS model to account for the time-averaged effect of individual large storms. The Chronic Regime model component normally represents processes averaged over time scales that are large compared to the characteristic duration of major storms. In general, storms tend to flatten the beach profile, although this is not always the case. It is also generally observed that beach profiles tend to re-establish their pre-storm shape during the conditions of normal weather between events. The shoreline position shifts over these cycles. For most storms, these variations in shoreline conditions can be taken as part of the overall short-term variability of the shoreline position that is ignored in this large-scale model.

However, major hurricanes and other storms can produce very significant changes in the shoreline. In many cases, the sand volume removed from the beach prism by the storm is redistributed between the offshore areas of the outer surf zone and shoreface and onshore through passes in the primary dune line to form overwash deposits. Even if all of the sand volume stored in the offshore deposits eventually works its way back to the rebuilding beach prism, there is net loss in the volume largely due to sediment sequestered in the overwash deposits. From the time-averaged perspective, this net loss in the beach prism volume and its corresponding retreat in the shoreline need to be taken into account. In the MoCCS model, net-loss volumes are assigned to different storm intensities, and these are distributed along the shoreline according to distance from the point of landfall. The values are assigned from empirical observations as explained later in this report.

As shown on Figure 3.6.1 the shoreface is the zone between the inner continental shelf and the surf zone. It has been shown by Bruun (1962, 1988) and Moody (1964) that the geometry of the sea bed profile in this depth range varies according to recent wave conditions becoming more steep in storms and less steep during prolonged conditions of smaller waves. However, over periods of time on the order of a year or longer there is a characteristic average depth profile within the shoreface zone. The well-known Bruun Rule (1962, 1988) asserts that this time-averaged characteristic depth profile persists on time scales relevant to sea level change. This causes the whole profile to shift landward and upward where the shoreline retreats due to sea level rise. In the MoCCS model, this relationship is used to provide a transition zone between the one-dimensional representation of the surf-zone process and the two-dimensional representation of the inner shelf regime. Upper and lower depth limits are given for the shoreface with the upper limit corresponding to the maximum depth of the surf zone. If there is a relative convergence of the time-averaged longshore sediment volume flux in the surf zone the shoreline

advances. A typical difference in the height (i.e. water depth) of the sediment within the surf zone cell and the next seaward cell is set based on the characteristic depth profile of the shoreface. An advancing shoreline can cause this computed difference to exceed this depth limit. At this point a sediment volume adequate to correct this difference is taken from the surf zone cell and transferred to the adjacent shoreface cells in a cascade that tends to preserve the characteristic depth profile. The outer portion of the shoreface cells exchange sediment volume with the adjacent inner shelf cells according to the representation of the inner shelf sediment transport processes.

In practice, it is necessary to determine the values of several of the model parameters. This is accomplished in one of two ways. Where appropriate, a system of cross-scale modeling is used. For other parameters, it is necessary to adjust their scale until the model produces simulations of morphological changes that are in agreement with changes determined from detailed long-term measurements.

Cross-scale modeling is a convenience used to avoid the need for expensive and elaborate programs of wave and current meter deployments to obtain long-term detailed measurements. Only recently detailed numerical models representing coastal hydrodynamics and related sediment dynamics have been developed with the capability of simulating natural conditions for periods of many months, and in some cases, more than a year. These models have detailed representations for coastal waves, tides and currents, and they typically operate with time steps on the order of seconds. Their depth grids are typically dense and detailed so that their requirements for computer resources are high. As a consequence, the time needed for a year-long simulation with a model desktop computer is on the order of several days. Such models are capable of making detailed time-series outputs of wave and current conditions at many places within their domains, but they are also poorly suited for the multiple long-term simulations of the MoCCS model.

The U.S. Army Corps of Engineers CMS-Flow and CMS-Wave models have been used to simulate the details of hourly current and wave conditions over a model domain similar to that of the MoCCS model. Wind and wave data from NOAA Buoy 42040, taken every six hours for calendar year 2003, were input. The tidal-component of the currents was determined using CMS-Flow imposing dominating tidal constituents of this domain to the open boundary of the model. The computed currents and waves were taken as typical representations of a long time series of observations. Although these models have been used in many other places (Reed et al., 2011), they have not been calibrated against measured data in the Eglin project area. However, with the reliability of these models demonstrated elsewhere, it is reasonable to use them to provide examples of detailed long-term data sets, because the goal of the MoCCS model development is to produce a method for estimating large-scale and long-term morphological changes and not to evaluate precise changes in particular examples. Thus, these outputs from the detailed models would need to be replaced by actual long-term measurements or with results from well-calibrated model set-ups when it becomes necessary to make accurate and specific large-scale predictions. In fact, the general wave and current parameters developed from these long and detailed simulations are not especially sensitive to a reasonable amount of variation in the inputs. This is further emphasized by the fact that morphological changes in the deeper portions of the MoCCS model domain are slow and small. They have very little effect on the more interesting results regarding shoreline change and barrier island morphology.

The six-hour input data to the CMS Flow Model resulted in year-long hourly output of depth-averaged currents at 192 locations, distributed over the offshore portion of the model domain. At each location, four outputs were developed for adjoining model cells so that local gradients in both the longshore and cross-shore flows were expressed. These were used to compute the large-scale diffusion coefficients using equations,

$$D_x = \frac{|u'v'|}{\frac{d\bar{U}}{dy}} \tag{3.6.7}$$

$$D_y = \frac{|u'v'|}{\frac{d\bar{V}}{dx}} \tag{3.6.8}$$

The CMS Wave model was used with the same input data set to represent the hourly wave parameters at a series of points distributed over the offshore portion of the model grid. These time series were reduced to monochromatic power-equivalent wave heights and periods. A separate post-processor was used along with bottom sediment grain size data obtained from the ROSS database (Ross.urs-tally.com) to convert the time series of wave conditions to corresponding time series of entrained bottom sediment. These provided the time-averaged entrained bottom sediment concentrations that are used with the following equation (Van Rijn, 1989).

$$c_a = 0.015\rho_s \frac{d_{50}}{a} \frac{T_a^{1.5}}{D_*^{0.3}} \tag{3.6.9}$$

Where, c_a = reference concentration (kg/m3), ρ_s = sediment density (kg/m3), d_{50} = particle diameter (m), a = reference level (minimum =0.01 m), D_* = particle size parameter, T_a = bed-shear stress parameter.

The 2003 wave data from NOAA Buoy 42040 were used as a representative of the time-averaged wave conditions. The individual six-hour data were binned and averaged to produce a monochromatic power-equivalent mean annual wave, characterized by single values for the wave height, wave period and propagation direction. These were used as initial values for the computation of shoreline change over a 60-year period between 1934 and 1994.

The methods for assembling an accurate record of shoreline change at Eglin AFB and along Santa Rosa Island have been explained in an earlier section of this report (Section 3.1). A series of 15 to 20 (depending on which subsection) historic shore positions were determined from historic maps, aerial photographs and LiDAR surveys. This effort developed a time history of the Santa Rosa Island shoreline position between 1857 and 2007. As described in Section 3.1 of this report, these data can be presented in a variety of formats. Exploration of these data has shown that there are two multi-year periods of special interest to the MoCCS modeling. One is a 60-year period between 1934 and 1994 where the shoreline position shows deposition and shoreline progradation along most of the Eglin AFB portion and most of the center portion of Santa Rosa Island. This corresponds to a period where only small or distant cyclonic storms impacted the island. The second period is between 1995 and 2007. Three major hurricanes (Opal 1995, Ivan 2004, and Dennis 2005) impacted the island and there were large measured shoreline erosion changes. Section 4.1.4 of this report provides a complete discussion of these

changes and Figure 4.1.10 presents the results of comparisons of shoreline positions over more than a century.

The tidal inlet into Choctawhatchee Bay is armored by jetties and maintained with dredging controlled by the U.S. Army Corps of Engineers. Therefore the inlet does not have its natural cross section. The history of this inlet is described in Section 4.1.3 of this report. The inlet introduced considerable variability in the position of the Gulf shoreline on adjacent beaches, before it was stabilized by the jetties. Even with stabilization the inlet has considerable interaction with the longshore transport of sand in the surf zone of the Gulf beaches. In representing this inlet in the MoCCS model it was assumed that its position and entrance channel will continue to be stabilized by the jetties and the program of periodic dredging. However, sand sediment will continue to move within the inlet in such a way that some sand transfers across the inlet mouth to the adjacent beaches and some becomes part of the permanent deposits in the ebb and flood tide inlet bars and within the inlet itself. That is, it is assumed that the area of the inlet mouth and the adjoining ebb and flood tide deltas remain the same as sea level rises as shown in Figure 3.6.2. However, sand is deposited so as to maintain the overall depths of the inlet and over the inlet shoal. For each annual increment in sea level rise a volume of sand is removed from the longshore sand drift along the Gulf shoreline. This volume is computed by multiplying the whole rise by the inlet area summed with half of the rise increment multiplied by the combined shoal areas. This assumes that the outer edges of the shoals do not change in depth as the deposits taper from a maximum thickness at their inner margins.

Figure 3.6.2. East Pass Inlet, at the eastern end of Santa Rosa Island, with the areas of the inlet mouth (yellow), flood tide shoal (red) and ebb tide shoal (blue) outlined.

The measured shoreline changes along Santa Rosa Island provide an excellent data set for the calibration of the Chronic Component of the MoCCS model. This model does not include processes that control the shape of the very western end of this barrier island, but these locations are more than 35 km from the western border of Eglin AFB. Therefore, data from this portion of the measured shoreline changes are not included in the comparison with the model results.

Figure 3.6.3 is a representation of the shoreline in map view (upper panel) with a graph of measured shoreline position change over the period between 1934 and 1994. Several scales of spatial variability are shown but the overall pattern of change is clear and readily associated with the varying orientation and curvature of the shoreline shape. The third panel on Figure 3.6.3 shows the results from a MoCCS model simulation of this same 60 year period. The wave parameters have been adjusted through a process of successive trials to produce this simulation, which has the closest agreement between modeled and measured results. Unfortunately, there is no other long period of shoreline positions during a prolonged interval of good conditions matching the assumptions of the Chronic model component from which a verification test can be performed. Subdividing this period is not a good option because variability in results is largely a function of how the division boundaries are defined, rather than being a measure of model skill. Subject to this shortcoming, the time-averaged wave parameters and the parameters that scale the net transport and longshore diffusion process taken from this simulation are used in the modeling of the future shoreline locations in response to different scenarios of sea level rise and storm conditions.

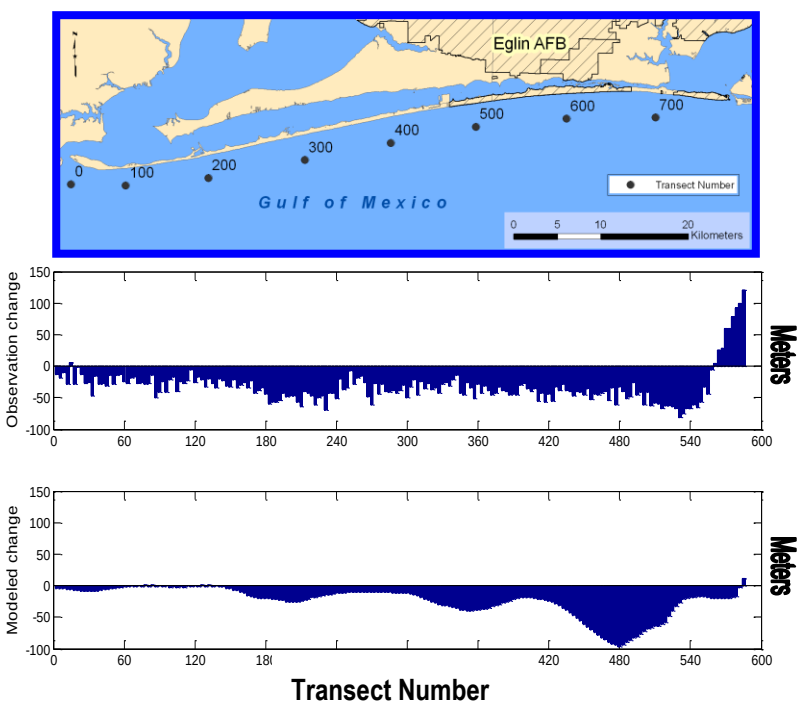

Figure 3.6.3. Comparison of measured (middle panel) and modeled (lower panel) shoreline change along Santa Rosa Island during the period of mild storm activity with negative shoreline changes indicating beach deposition and growth.

The inclusion of the time-averaged shoreline changes due to net beach prism volume loss resulting from major hurricanes within the Chronic component of the MoCCS model were described previously. Although this behavior is commonly observed, no systematic data relating these net volume losses to storm wave and beach geometry parameters have been located in the literature. To complete the MoCCS model it was necessary to estimate these net volume changes from measured data. Figure 3.6.4 shows a series of shoreline positions for the period 1993 to 2009 at a representative section in the Eglin AFB position of Santa Rosa Island. This is a period characterized by a sequence of major hurricane impacts. The trend line shows a roughly defined pattern of shoreline retreat during the storm and shoreline stabilization or re-establishment during the intervening periods. The detailed patterns do not show relationships between storm intensity and net shoreline retreat. Instead, a review of these patterns at several of the measured transects resulted in a judgment-based estimate of the overall scales of storm-induced net shoreline retreat according to the storm intensity. These values are listed in Table 3.6.1.

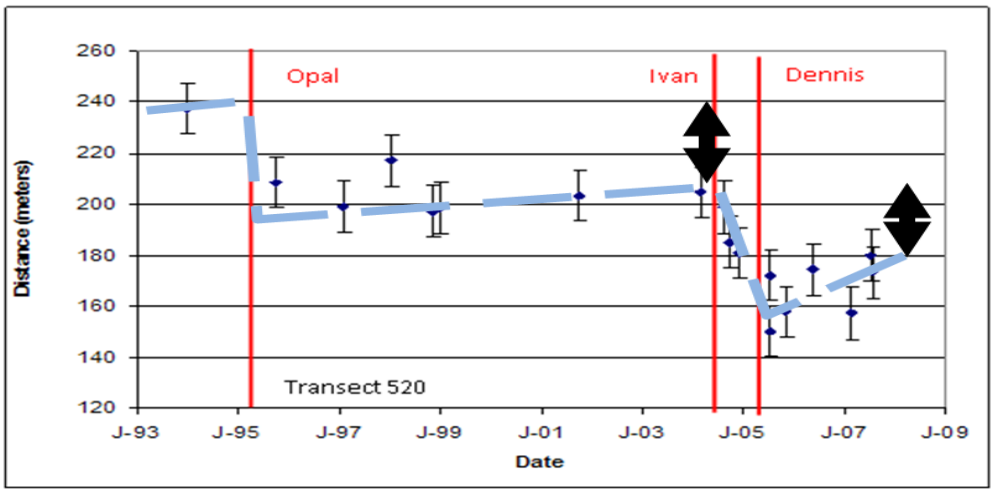

Figure 3.6.4. Beach shoreline changes during the period of major hurricane landfalls showing a trend line (dashed blue) that indicates major retreat during, and shortly after the storms, followed by partial recovery. This leads to the storm-induced net changes indicated by the heavy black arrows.

Table 3.6.1. Time-averaged net shoreline change in response to storm intensity.

Relative Storm Intensity	Net Storm-induced Shoreline Retreat (m)
1	10
2	20
3	30
4	40

The values given in Table 3.6.1 represent the net storm-induced time-averaged shoreline retreat for different storm intensities as applied at the point of storm landfall. When applied in the MoCCS model these values are tapered downward with distance to either side of the landfall location. The tapering function is the same used with the relative values of the storm surge and this is explained later in the section of this report on the Acute component.

It is well to recognize the approximate nature of the values shown in Table 3.6.1. The measured data suggest that they are reasonable estimates based on the measured data from Santa Rosa Island over the interval 1993 to 2009 but these have proved difficult to properly quantify, in part because the intervals between some of the hurricanes was not adequate for the full recovery of the shoreline to develop. This is identified as one of the subjects that will greatly add to the validity of the MoCCS model when future research provides better values.

3.6.4. The MoCCS Acute Regime. In the MoCCS model, the beach, dune, barrier island platform and bay shoreline are the morphological components that are most responsive to storm-driven processes. A series of width-averaged, one-dimensional shore-normal profiles are used to yield a two-dimensional (2-D) representation of the geomorphologic response of barrier islands to changes in the rates of sea level rise and storm climate. As illustrated in Figure 3.6.5 the barrier island section consists of beach, dune, island platform, and backshore features. The length of the barrier island is divided into a large number of representative sections, each characterizing the cross-shore morphology of an island slice. The slices are 250 m wide in longshore extent. The elevation profile in each slice represents the width-averaged topography, with narrow features such as dune passes and overwash channels represented as sub-panel elements. This allows representation of considerable detail along the island. These characteristics change along the length of the barrier island providing a quasi-three-dimensional representation as shown in Figure 3.6.6. The beach has a sloped face intersecting the mean water line on the beach face (Yoff) and a beach berm and back-beach platform ending at the dune. Yoff is a parameter defining shoreline position and is the internal boundary link between the Acute and Chronic components of the model. That is, both of these components affect the time-varying position of the shoreline as represented by the value of this parameter. The beach berm and back-beach platform starts at DBoff and their height is determined by the variable Z_0.

The dune is represented as a ridge characterized by a seaward face slope (AFace) and a slip face angle (ARepose). These slopes are considered to remain constant as the dune volume varies through changes of dune height (DHT) relative to Z_0. Sediment transport across the dune due to overwash is characterized by the dune pass elevation relative to Z_0 (DunePass), which will be explained later. The dune base positions are determined using DBoff and Backoff. To account for ranges of dune heights that are characteristic of individual coastal reaches, a maximum dune height is defined. When a growing dune reaches this height, secondary dunes are developed and a dune field is created. The dune field geometry is characterized as a trapezoid cross-section. Although this does not attempt to represent the true cross-section of a dune field it does provide a representation of the sand volume storage.

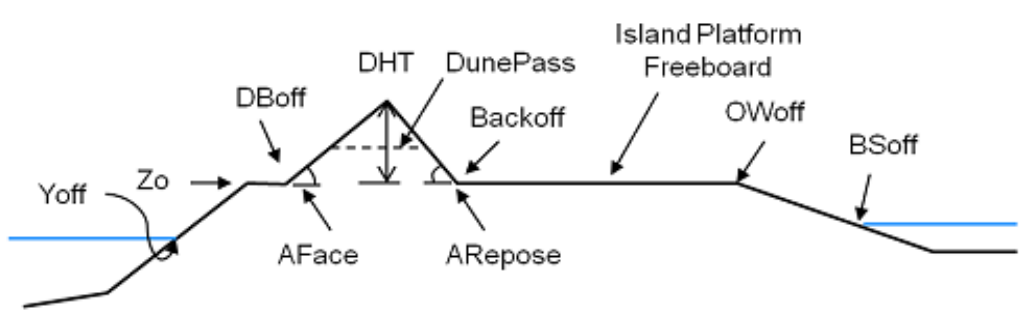

Figure 3.6.5. Definition sketch for a cross-section profile of a barrier island with a single dune.

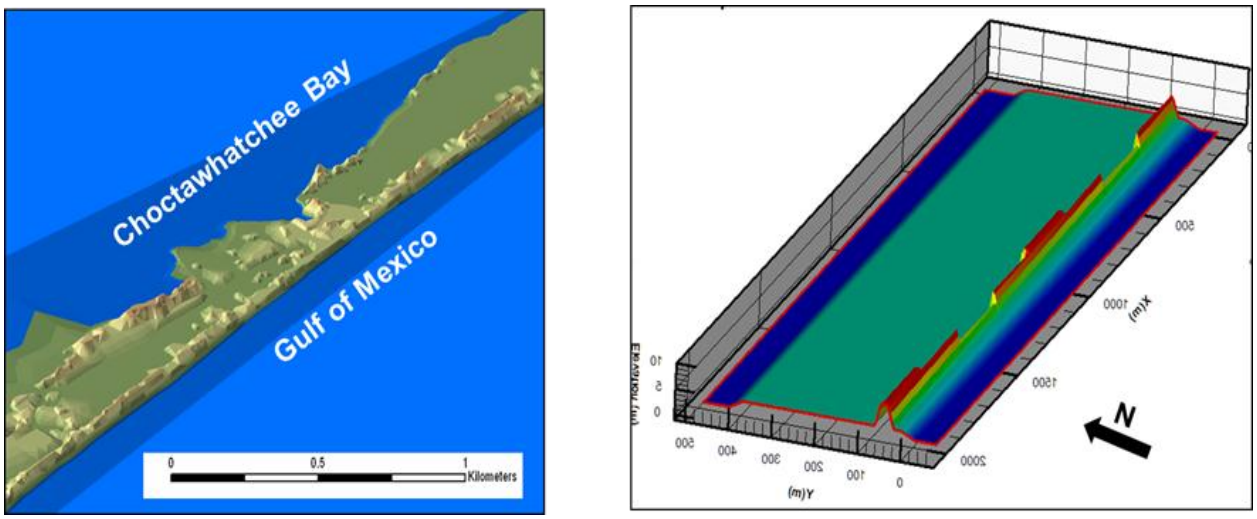

Figure 3.6.6. Representative oblique views of Santa Rosa Island from LIDAR imagery and equivalent MoCCS model.

The island platform and backshore are behind the dune and end at the bay. The platform remains horizontal during simulation but its elevation (Island Platform Freeboard) varies relative to the time-varying mean sea level. The island platform freeboard ends at OWoff; a gentle slope beyond OWoff represents the bay shoreline characterized by the bay mean water line (BSoff).

While in reality the beach prism, the portion of the profile between DBoff and Yoff, changes on time scales of days due to changes in wave and tide conditions, these variations are not resolved from their mean-annual condition in our model. Instead, the short-term sand volume exchanges between the beach prism and offshore bars are assumed to be balanced on seasonal and annual time scales. Because the change in mean sea level during each short-term sand volume exchange between the beach prism and offshore sand bars cycle is imperceptible we assume that the vertical elevations of beach face and berm height (Z_o) track the slowly changing mean sea level. In other words, the beach prism rises with increasing mean sea level at the same rate. Heights of all the other elements of the barrier island are not adjusted to sea level rise, which may lead to lower island platform freeboard (relative to sea level) and a narrower island due to the bay shoreline transgressing, depending on sand volume of overwash deposited on the island platform.

The volume of dune erosion is simulated using the method adopted from Larson et al., (2006) and Hanson et al., (2010) to incorporate surge height according to the equation:

$$\Delta V_E = 4C_s(R + \Delta h - Z_0)^2 \frac{t}{T} \tag{3.6.10}$$

where ΔV_E is volume of dune eroded per unit beach length, C_s is a coefficient with a value between 1×10^{-3} and 2.5×10^{-3}, T is period of the deep water wave, t is surge duration of the erosion, Z_0 is elevation difference between dune foot and beginning of the swash (i.e., the mean water line), Δh is surge height, and R is wave bore runup height given by:

$$R = 0.10\sqrt{H_0 L_0} \tag{3.6.11}$$

H_0 and L_0 being deep water RMS wave height and length, respectively. Astronomical tide is ignored in the calculation due to its small magnitude in the prototype area (it could be added as an adjustment to the duration of the dune erosion).

There are three determinations of where the eroded dune volume is deposited, depending on values of surge height, wave runup height, dune height, and dune pass elevation. In the first, as shown in Figure 3.6.7 if the sum of surge height and runup height is smaller than the sum of dune pass height and Z_0, all of the eroded dune volume deposits on the beach prism,. If the former sum is larger than the latter one, but smaller than the whole dune height plus Z_0, then the eroded volume is partitioned between the beach prism and the overwash. The portion of sand returning to the beach prism is determined by an empirical ratio between excessive runup height (relative to the dune pass) and the difference between dune height and dune pass height. If the sum of surge height and runup height exceeds the sum of dune height and Z_0, then all of the eroded volume is carried beyond the dune and deposits on the island platform. The volume of overwashed sand in the latter two cases is assumed to be deposited uniformly across the island platform, leading to increased island platform freeboard. When the resulting elevation of the island platform could exceed the elevation of the dune foot (Z_0) an excess volume is set aside rather than allowing the island platform to grow higher. This excessive volume is transferred to the backslope of the island and is uniformly distributed. This, in turn displaces the bay shoreline outward into the bay. If dune height is smaller than dune pass elevation, overwash occurs when runup height is larger than dune height, and all eroded sand is overwashed and deposited on the island platform in the manner described above. An internal link also provides that the volume of sand lost to the beach prism due to the net time-averaged storm-induced shoreline retreat is taken to be carried inland by storm overwash processes, so in the model it is redistributed to the island platform landward of the dunes.

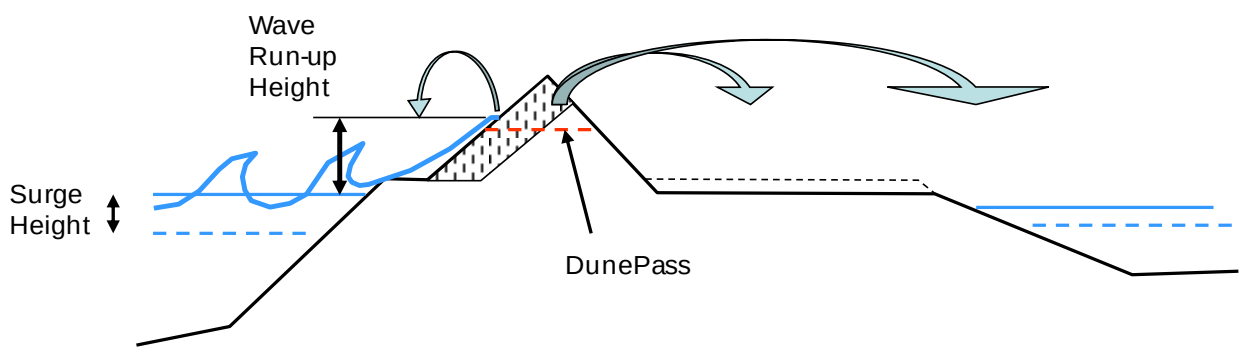

Figure 3.6.7. Partitioning mechanisms of eroded dune sediment deposits. Three possible processes are considered: 1. all the eroded sediment is deposited on the front beach prism; 2. besides front beach deposition, part of the eroded sediment is deposited on the island platform and backshore; 3. all the eroded sediment is deposited on the island platform and backshore.

The annual rate of dune growth is also considered in the model by incorporating aeolian volume flux, calculated externally and treated as a model input. The entire volume is added to the dune face by adjusting the dune height (DHT) and width (between DBoff and Backoff) but keeping AFace and ARepose constant, without considering deposit of aeolian volume on the island platform.

3.6.5. Approach for Predicting Future Morphology. The representations of physical processes in the MoCCS model have been deliberately cast in a simple form to allow the model to be effectively used in Monte Carlo simulations. This overcomes the problem of selecting a particular sequence of future storm intensities and occurrence because these are varied according to their statistical characterization in each individual Monte Carlo simulation. The results of these simulations consist of statistical descriptions of the future development of the barrier island for each of the four sea level rise rates defined in the overall project.

3.6.6. Analyzing Uncertainty. Two sources of uncertainty are considered for modeling morphological changes of barrier islands and shorelines. One is uncertainty in the parameters related to modeling effects of storms on barrier islands, which are: storm number for single year, storm magnitude, and storm track. The parametric uncertainty is typically characterized by probability distributions of the parameters; its propagation through numerical models can be quantified using Monte Carlo (MC) methods. The other source of uncertainty is the scenario uncertainty due to unknown scenarios of sea-level rise. This uncertainty must be quantified, because sea-level rise is one of the driving forces of the MoCCS and ACUTE model and has significant impact on the model simulation. The scenario uncertainty is addressed by considering a group of scenarios. After conducting modeling analysis for each scenario, the scenario uncertainty is quantified using the scenario averaging method. The parametric and scenario uncertainties are in a hierarchical structure in that different scenarios may have different parameters. In other words, the parametric uncertainty should be quantified for each scenario before the scenario uncertainty is quantified.

In this project, only major storms such as hurricanes are considered, and information needed to characterize uncertainty of the hurricanes is taken from the historic climatology developed by the Federal Emergency Management Agency (FEMA) for the West Florida Central Panhandle coast (FEMA, 2002). Although this area is under more comprehensive study by FEMA, FEMA (2002) is adequate for the illustration purpose of this study. The Poisson distribution:

$$P(k;\lambda) = \frac{\lambda^k e^{-\lambda}}{k!} \tag{3.6.12}$$

is used to generate storm numbers for a given year, where k is storm number, and λ is the expected occurrence in certain interval. Given that the average annual rate of hurricane occurrence is 0.001327/km (FEMA, 2002), the annual storm rate for the modeled 45 km-long coastline is 0.06 per year. Therefore the expected occurrence, λ, in the 100 years of simulation period is 6. Using a standard random number generator, 1,000 random samples of storm numbers in 100 years are generated, and the histogram of the random samples is plotted in Figure 3.6.8. The mean (λ) of the fitted Poisson distribution is 5.93, close to the theoretical value of 6, given that only 1000 samples are generated.

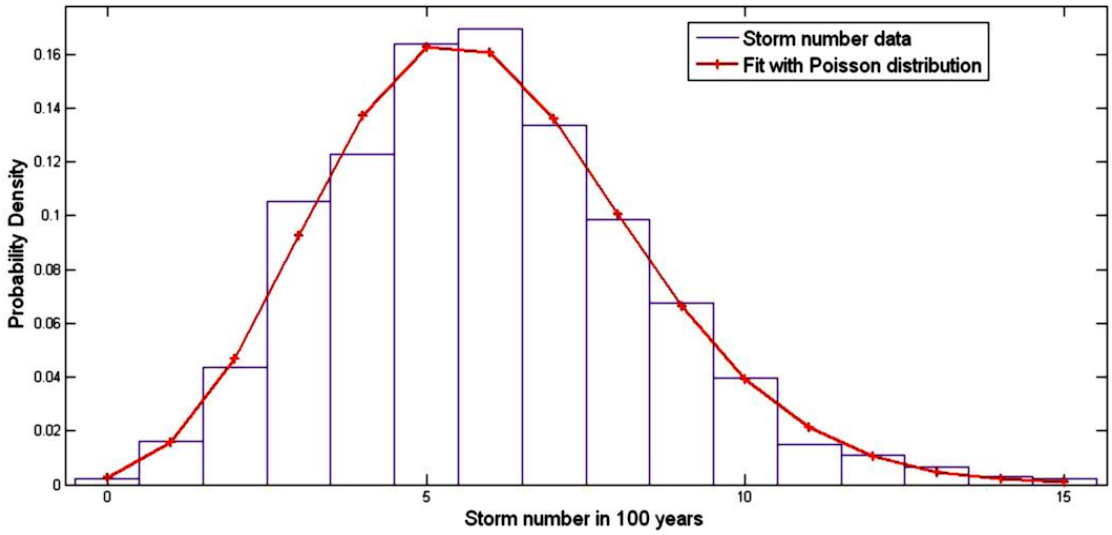

Figure 3.6.8. Generated storm numbers fitted with Poisson distribution.

If the generated storm number for a given year is larger than 0, storm magnitudes and tracks need to be generated. The storm tracks can be obtained by analyzing historical data. In this study, three tracks were arranged perpendicular to the shoreline and placed at the two ends (Tracks 1 and 3) and the center (Track 2) of the barrier island. By assuming that a hurricane makes the landfall with equal probability along the three tracks, random storm tracks were generated using a random number generator of the Intel FORTRAN compiler, and their histogram is shown in Figure 3.6.9. The distribution can be updated if more information of hurricane landfall becomes available. The method of uncertainty analysis is flexible with any distribution of the storm tracks.

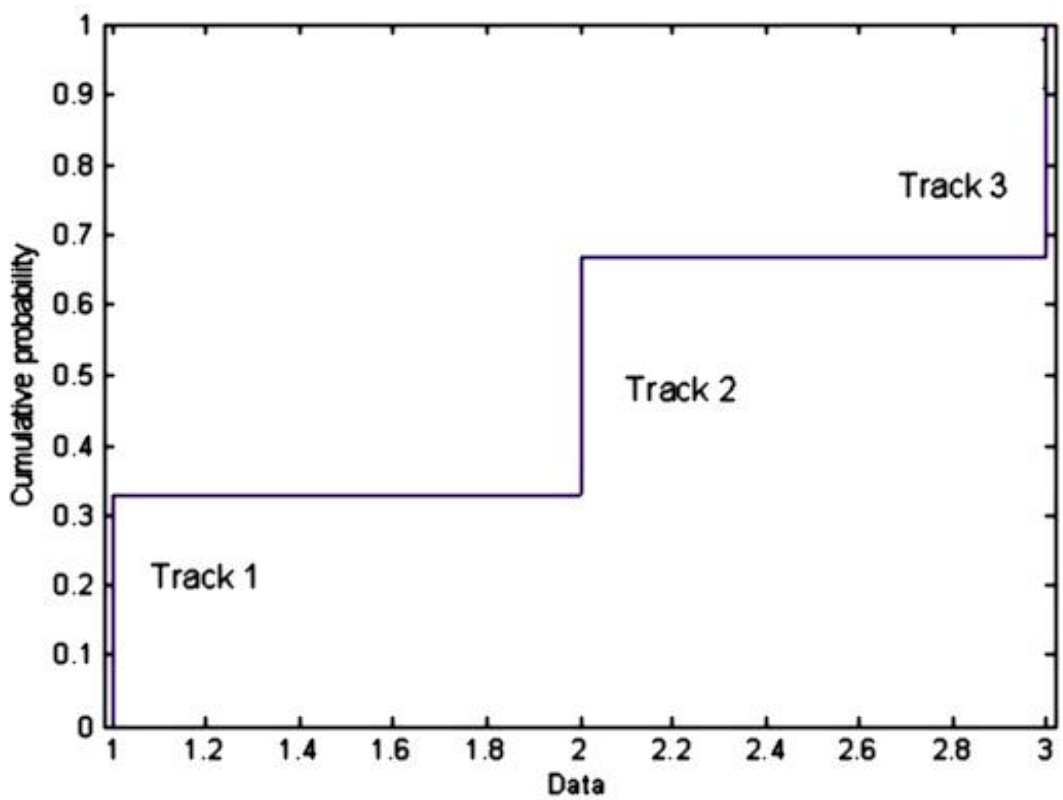

Figure 3.6.9. Uniform distribution used to generate storm tracks.

The random values of storm magnitude, measured by maximum surge height, are generated using an empirical method so that an explicit probability density function is not needed. This makes the uncertainty analysis flexible because the probability density function is largely unknown. For each storm, one needs to determine the maximum surge heights for running SLOSH to obtain the lookup table of surge heights and other quantities needed to calculate the sediment transport. Four maximum surge heights are considered for four storm sizes that include all possible events of storm erosion and sediment transport (ranging from limited beach flooding to severe dune attack). Because the prototype area is the central Florida Panhandle, the values of the maximum surge heights were determined empirically based on the cumulative probability of surge height obtained from the Okaloosa County flood study (FEMA 2002). Four ranges of exceedance probabilities were selected as 0 to 0.5, 0.5 to 0.75, 0.75 to 0.95 and greater than 0.95 so that small storms correspond to larger exceedance probabilities. Each range of the exceedance probability corresponds to a range of maximum surge heights, and the representative maximum surge height is taken as the value of the average exceedance probability of the range. Take the third range of 0.75 – 0.95 as an example, its representative maximum surge height is 1.16 corresponding to the probability of 0.85, as shown in Figure 3.6.10. The four representative surge heights are thus determined as 0.3 m, 0.64 m, 1.16 m and 2.1 m. The point here is to represent a series of storm surge elevations in discrete intervals rather than as a continuium. Each class is associated with a probability density. The number of these classes could be increased to as many as is practical and the procedure would remain the same. In this case four classes are sufficient because these will be used to represent conditions within 100-yr time intervals. If many more classes were used the highest representative discrete surge height would keep on increasing towards whatever maximum credible surge elevation characterizes the area. This might be well above the highest values shown on Figure 3.6.10. However, the probability density associated with the highest class would become so low that it would be very unlikely to occur in any future 100-yr interval. In future applications of the MoCCS model another number of discrete classes may be selected if such an increase in resolution is warranted.

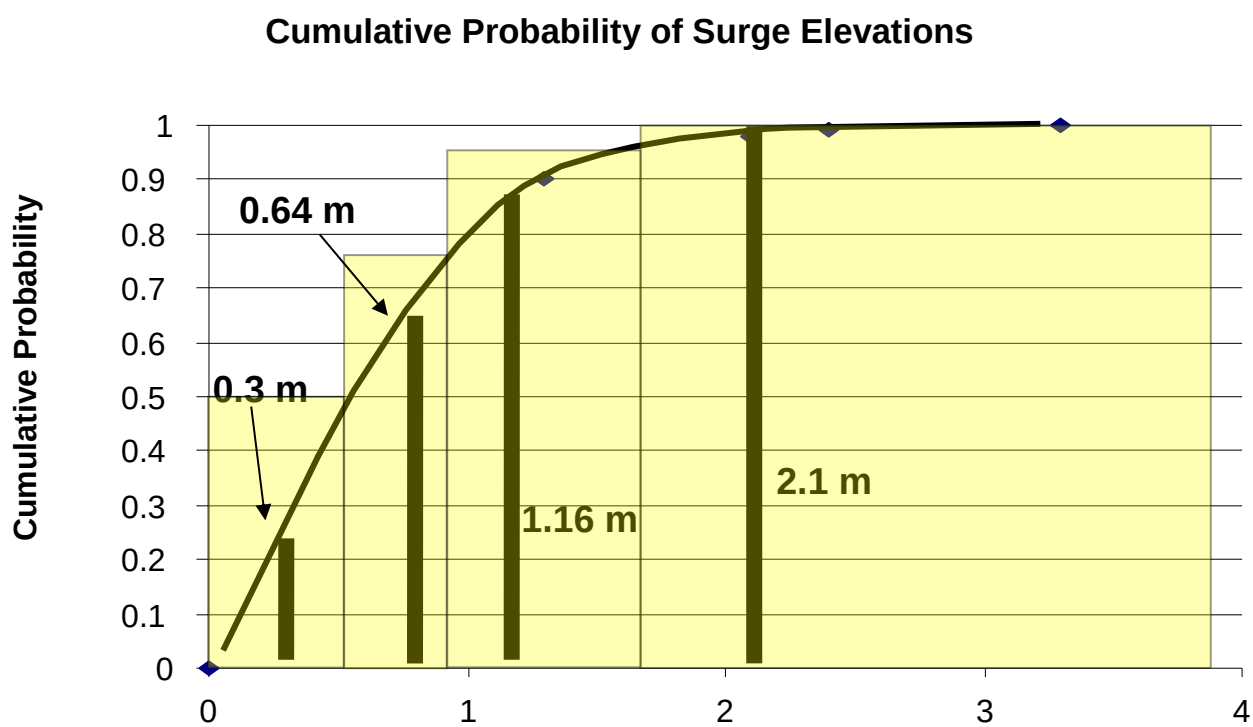

Figure 3.6.10. Maximum storm surge height values and probabilities for different storm sizes.

While this procedure is empirical, it is general and can be applied to other number of storm magnitudes and surge heights by adjusting the exceedance probabilities. It should also be recognized that the specific values used for the Santa Rosa Island area are likely to be quite different from other locations. Therefore, to apply the model elsewhere an independent analysis of the type just described would be needed. When running ACUTE and MoCCS for the MC simulation, in each realization, one first generates a random number from the uniform distribution (using the random number generator in Intel FORTRAN compiler) and then determines the storm size, which is used together with the SLOSH-based lookup table to simulate storm erosion and sediment transport.

After the random numbers of storms numbers, surge heights, and storm tracks were generated, by assuming that the three random variables are independent, the random numbers were permutated randomly and used in the MC simulation. This allows evaluation of the joint effect of storm number, landfall position, and storm magnitude on the morphological responses under sea-level rise scenarios.

A total of five sea-level rise scenarios were considered in this study. One was a continuation of the present rate (baseline scenario). The other four were arranged to bracket the range of sea-level rise predicted for the next 100-yrs. The scenarios project sea-level rise of 15 cm, 50 cm, 100 cm, 150 cm, and 200 cm elevation by 2100. These are referred to as the baseline scenario, Scenario 1, Scenario 2, Scenario 3 and Scenario 4. The five scenarios were treated as a discrete random variables and each scenario was associated with a discrete probability. Summation of the five probabilities was required to equal one. Since estimating the probabilities of sea-level rise is beyond the scope of this study, we used various sets of scenario probabilities to represent the possible occurrence of the five sea-level rises.

Uncertainty in model parameters and modeling scenarios propagates through the numerical models into uncertainty of model predictions. Parametric uncertainty propagation is quantified using the MC method, in which the random samples of storm numbers, storm sizes, and storm tracks are used for conducting multiple model simulations to produce probability distributions of model predictions. The MC simulation is conducted for each sea-level rise scenario, and the scenario uncertainty is quantified further using the scenario averaging method for jointly quantifying parametric and scenario uncertainty. Denote Δ as model predictions and S_k as the k-th possible scenario. The probability distribution of Δ under scenario uncertainty is estimated via

$$P(\Delta) = \sum_{k=1}^{K} P(\Delta \mid S_k) P(S_k), \tag{3.6.13}$$

where $P(\Delta \mid S_k)$ is probability distribution due to parametric uncertainty under a given scenario. Based on (3), the mean and variance of Δ can be calculated via

$$E[\Delta] = \sum_{k=1}^{K} E[\Delta \mid S_k] P(S_k) \tag{3.6.14}$$

$$Var[\Delta] = \sum_{k=1}^{K} Var[\Delta \mid S_k] P(S_k) + \sum_{k=1}^{K} (E[\Delta \mid S_k] - E[\Delta])^2 P(S_k) \tag{3.6.15}$$

These two quantities are used more often than the distribution function (equation 3.6.13) in uncertainty analysis. Derivation of the above three equations can be found in Meyer et al.,

(2007). While the derivation is in the context of groundwater modeling, the mathematical basis is general rending the equations applicable to coastal modeling under sea-level rise scenarios.

4. Results and Discussion

4.1. Analyzing Historic Coastal Change and Remote Sensing Data

4.1.1. Geomorphic Setting and Eglin Air Force Base Island Infrastructure. Santa Rosa Island is a 70 kilometer long barrier island located along the northwestern coast of Florida (Figure 3.1.1). The island is narrow, ranging from 0.5 to 1.0 kilometers in width. A coastal section of Eglin Air Force Base occupies the eastern portion of the island, extending for approximately 38 kilometers from East Pass near Destin, Florida, westward to Navarre Beach, Florida (Figure 4.1.1). The town of Fort Walton Beach separates the base into an eastern and western segment. The coastal segments of Eglin AFB have a large number of test facilities, dominated by radar and communication systems, a missile test facility and a 100-meter high "open-air-hardware-in-the-loop" tower test facility. A paved road system is present along much of the western segment of the base facilities on the island (Figure 4.1.1). Many of the test and monitoring facilities are located within 50 meters of the Gulf shoreline.

Historically, the physical setting of the island has included prominent foredunes of 5-7 meters height, stabilized by vegetation. The interior consists of a low lying (~2 meter) zone consisting of local overwash fans and localized freshwater ponds and wetlands. On the bayside of the island are irregularly distributed, 10-15 meter-high, stable dunes covered with maritime pines and shrubs (Figures 4.1.2 and 4.1.3). Freshwater and brackish water marshes are also present, adjacent to Santa Rosa Sound (Figure 4.1.3). The percentage and total acreage of major geomorphologic and land use subdivisions of the eastern portion of Santa Rosa Island are reported in Table 4.1.1.

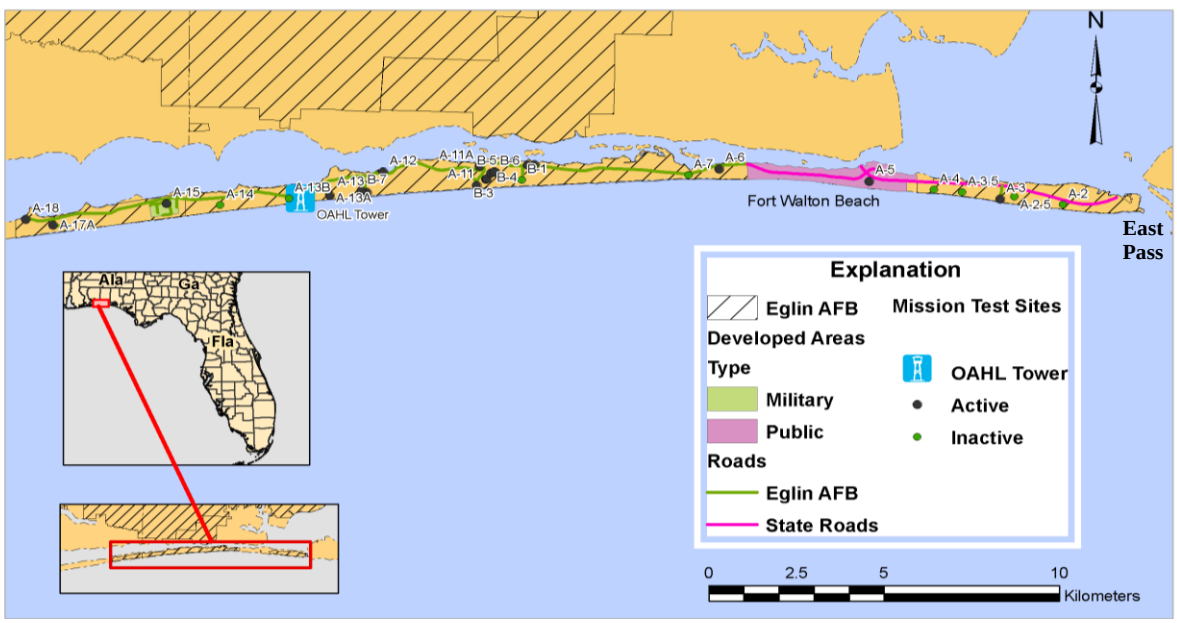

Figure 4.1.1. Eglin Air Force Base infrastructure on Santa Rosa Island. Sites with the "A" designation are primary mission test facilities. Sites with the "B" designation represent ancillary facilities. Some of the inactive sites have been impacted by shoreline erosion.

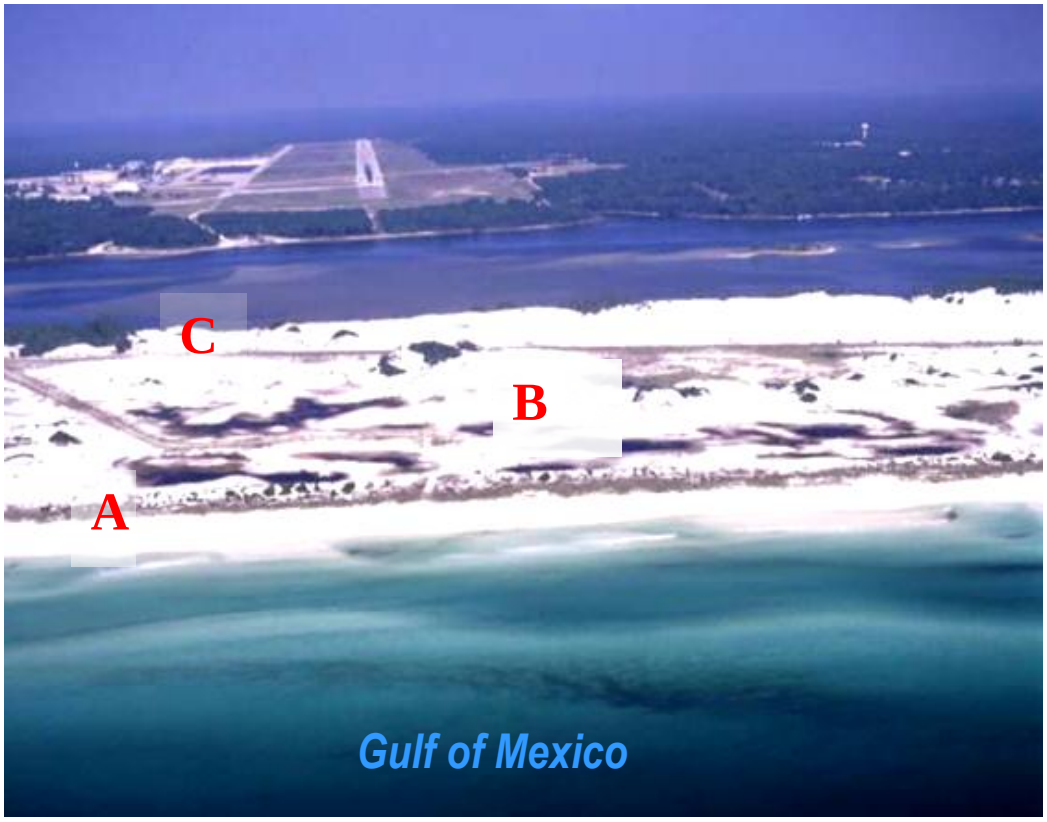

Figure 4.1.2. Northward-oriented, oblique aerial image of Santa Rosa Island near test site A-10. Geomorphic subdivisions visible in the image are: (a) vegetated, 5-meter foredunes, (b) interior stabilized overwash zone and freshwater ponds, (c) stabilized bayside dunes with tree cover. Hurlbert Airfield is visible on the mainland. This image was taken in 1989, before the destruction of the foredunes by Hurricane Opal in 1995.
(Source: State archives of Florida, http://floridamemory.com/items/show/131981.)

Table 4.1.1. Major geomorphic units and land cover for the eastern half of Santa Rosa Island (from Navarre Beach to East Pass).

Type	Area (hectares)	Percent
Active Dune Complex	6.2	0.3
Artificial Dune	0.2	nil
Beach	109.5	5.8
Dredged Material	16.3	0.9
Inactive and Active Overwash Zones	871.8	46.2
Interior Wetland	1.9	0.1
Marsh	79.4	4.2
Stable Dune Complex	130.7	6.9
Vegetated Barrier Core	302.8	16.1
Water	13.6	0.7
Modified Land †	343.4	18.2
Structures	8.9	0.5

† Includes Fort Walton Beach (civilian).
Source: Morton and Montgomery (2010).

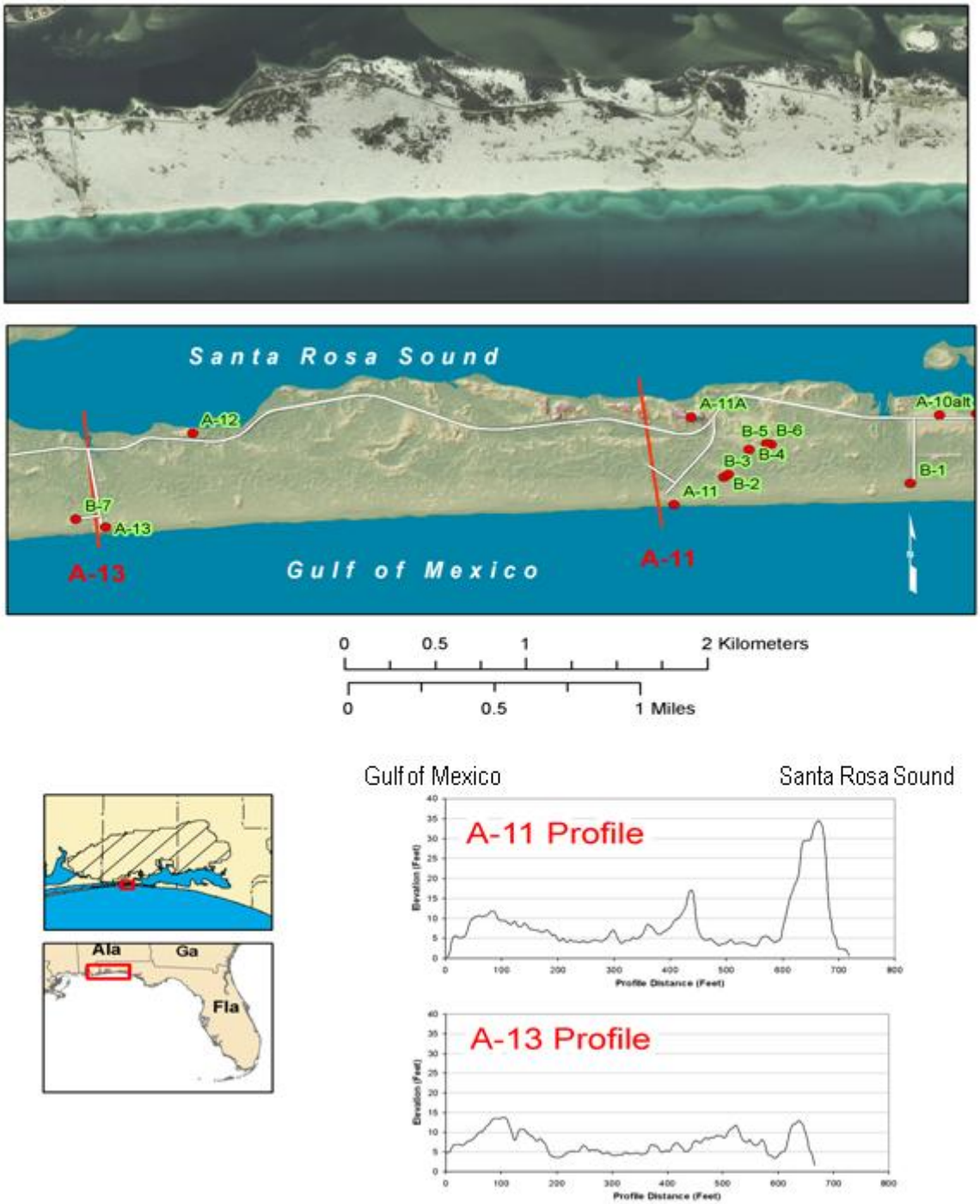

Figure 4.1.3. Topography of Santa Rosa Island approximately 1 kilometer east of the Eglin Air Force Base OAHL tower. Low-elevation, foredunes (3-4 meters high) merge with a low-elevation (<2 meters) overwash zone, which also contains freshwater ponds and marsh. Stabilized, discontinuous, bayside dunes 4-15 meters high are present on the northern portion of the island.

4.1.2. Shoreline Change – Overview. Stapor (1975) noted that, with the exception of the western portion of Santa Rosa Island, most the island coastline has exhibited a long-term rate of change of less than one meter per year. Stone and Stapor (1996) provided corroboration for the near-equilibrium sediment transport for Santa Rosa Island. Morton et al., (2004, 2005) utilized

the DSAS program to analyze erosion along the Gulf Coast from the late 19th century up to 2001. They observed that for the western Florida Gulf Coast, the average long-term shoreline change was -0.8 ± 0.9 meters per year. Significantly higher rates of erosion occur at inlets (Clark, 1991; Morton et al., 2004). Starting with Hurricane Opal in 1995, three major category 3 hurricanes have produced significant shoreline erosion along the length Santa Rosa Island. These storms include Opal (1995), Ivan (2004) and Dennis (2005). All of these storms have produced significant shoreline retreat due to storm surge erosion (Leadon et al., 1998; Leadon et al., 2004, Clark and LaGrone, 2006). For the western portion of Santa Rosa Island, Hapke and Christaiano (2007) noted that the shoreline was eroded as much as 60 meters during Hurricane Ivan, and a total of up to 88 meters following the 2005 storm season, which included hurricanes Dennis, Katrina and Rita..

The eastern portion of Santa Rosa Island has a shoreline that was stable for at least 125 years (~1870-1995). Most of the Eglin Air Force Base infrastructure was established during this period of stability (~1950-1995). Starting with Hurricane Opal and the following major hurricanes during 2004-2005, there has been a major retreat of the Gulf shoreline (Figure 4.1.4), development of extensive overwash fans (Figure 4.1.5) and extensive damage to building and roads (Figure 4.1.6). A $112 million program to rebuild roads, armor test sites and initiate local beach renourishment (Figure 4.1.6.F) on the island is currently in progress (Eglin AFB, 2010).

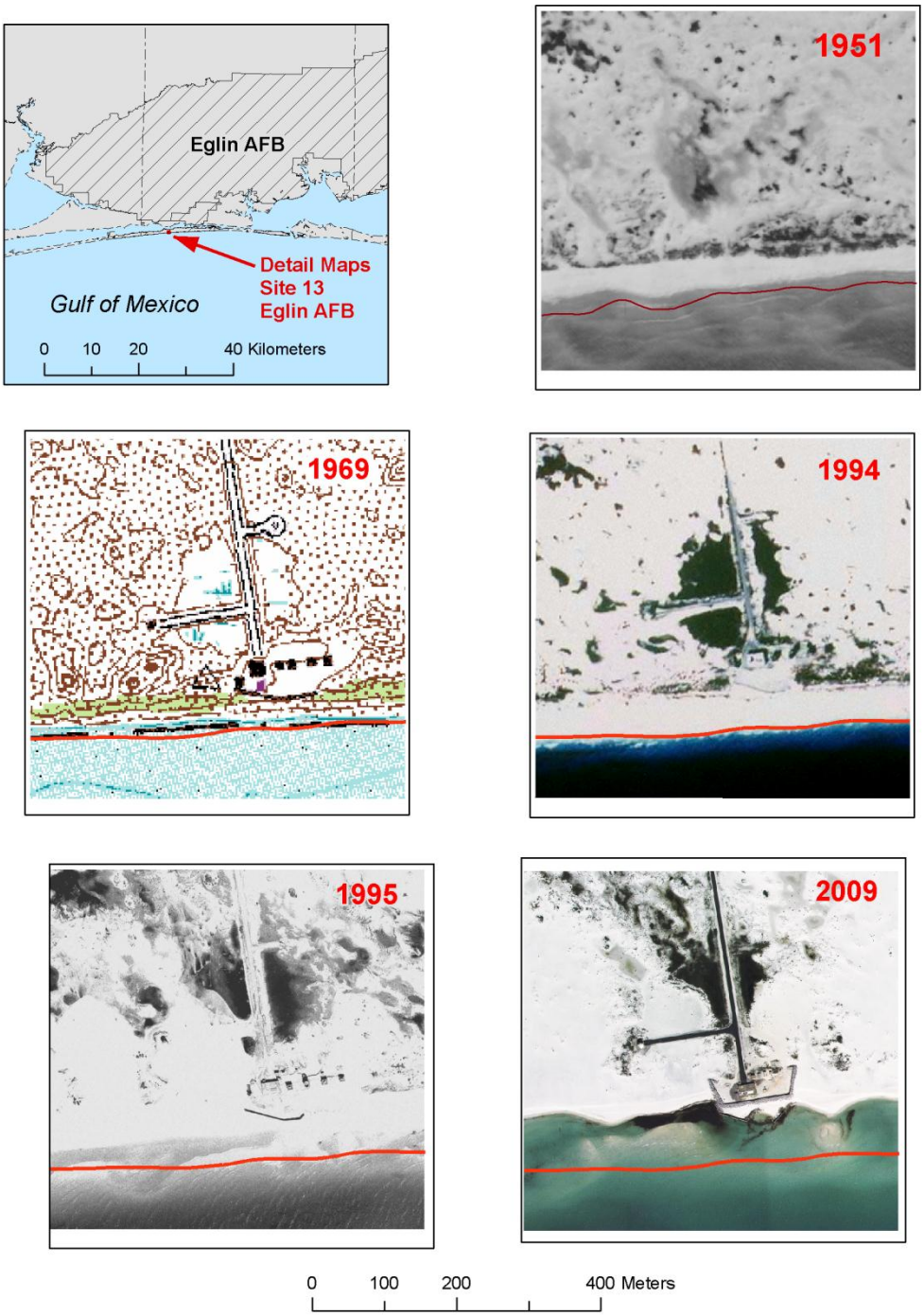

Figure 4.1.4. Long-term changes of the shoreline of Santa Rosa Island in the vicinity of Eglin Air Force Base test site A-13. The red line represents the shoreline position in 1870. Prominent foredunes (5-7 meters in elevation) are visible as the dark strip of vegetation adjacent to the beach (dates 1961-1994). The image for 1995 indicates a dramatic retreat of the shoreline and the destruction of the foredune complex following Hurricane Opal. Subsequent major storms – Ivan (2004) and Dennis (2005) -- have produced additional recession of the shoreline. Locally the beach has retreated up to 90 meters compared to the pre-Opal position.

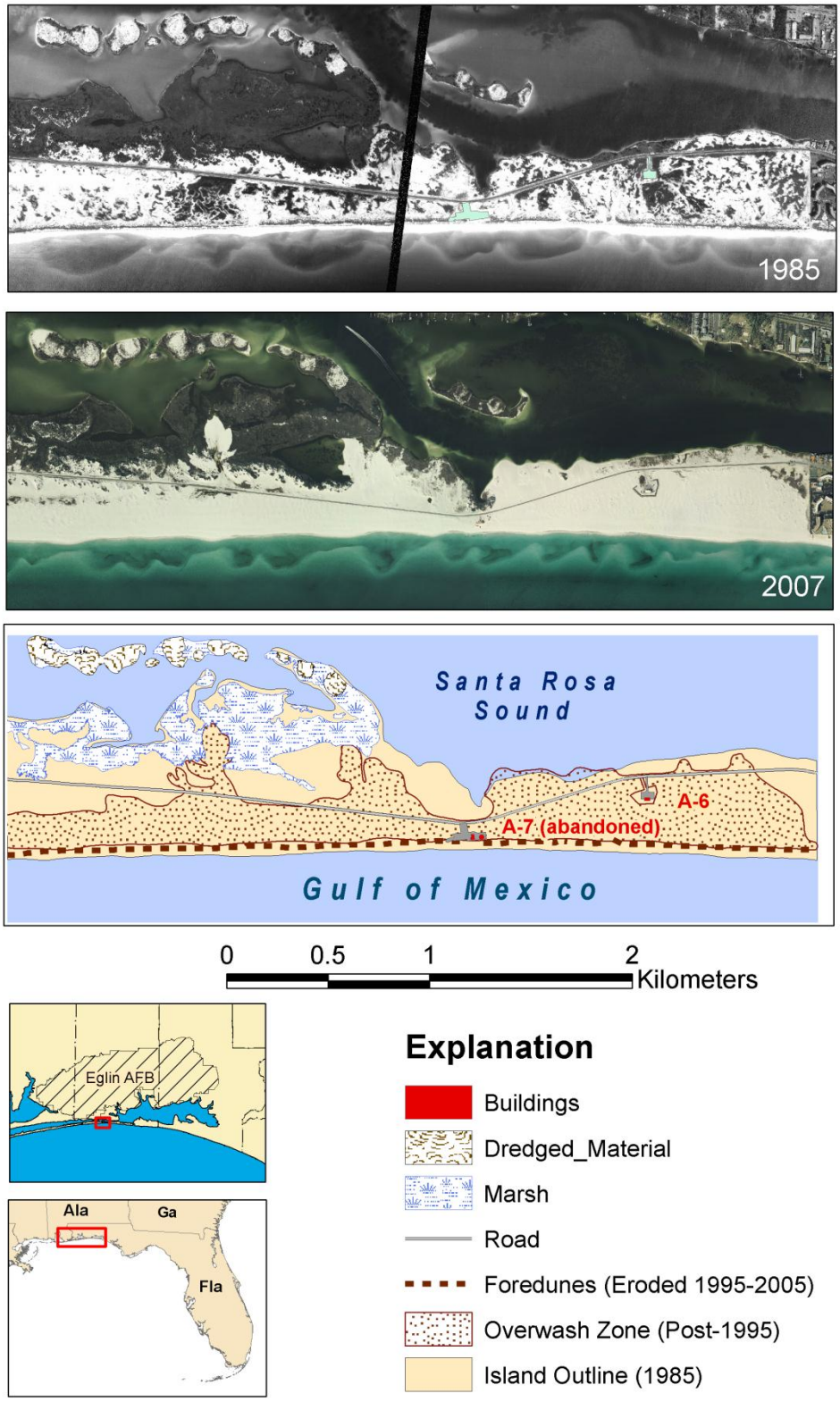

Figure 4.1.5. Development of major overwash fans on a narrow section of Santa Rosa Island near test site A-6. Foredunes have been eroded by Hurricane Opal (1995). The overwash fans have advanced across the island due to major Category 3 and 4 storms since 1995.

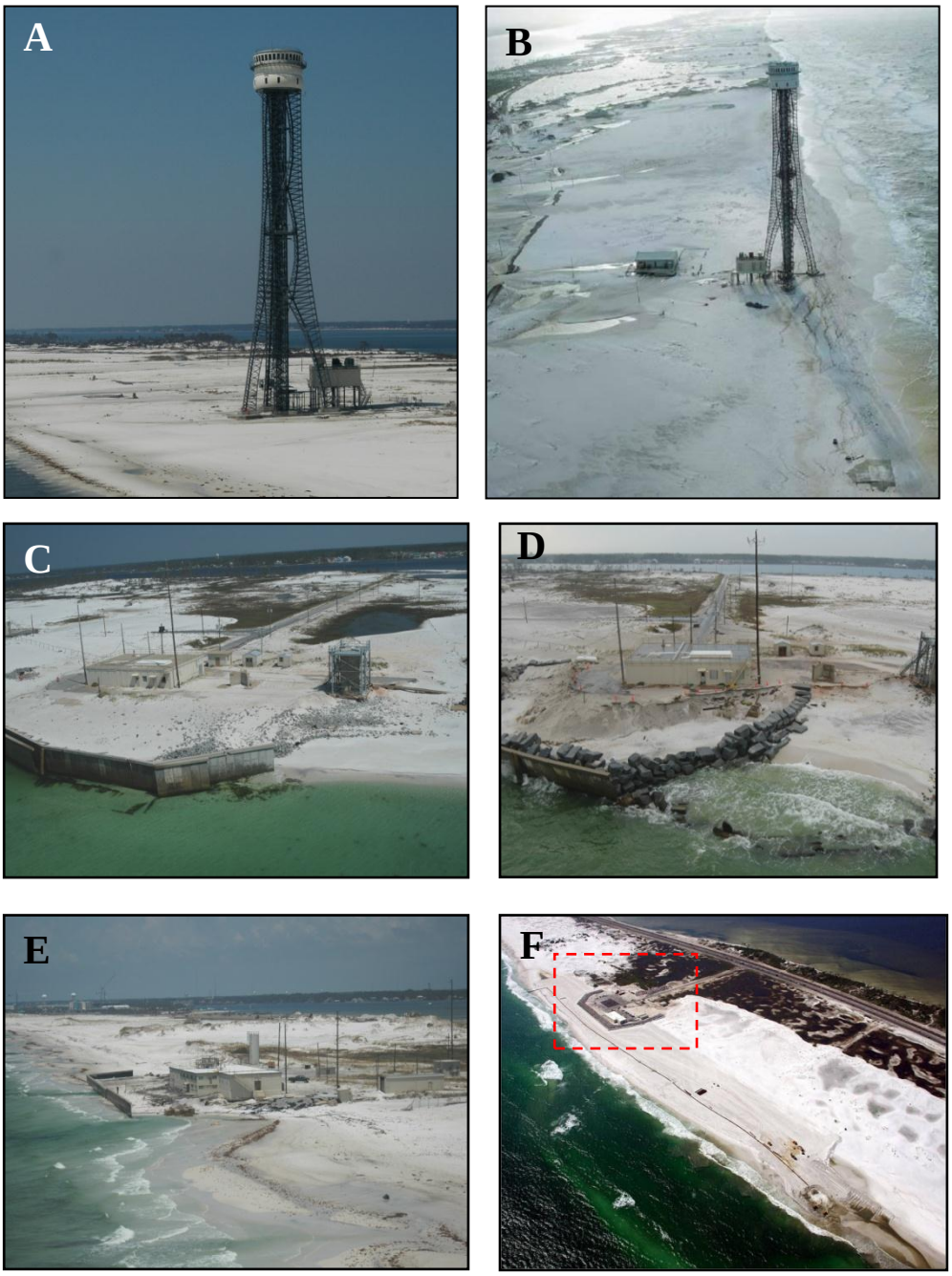

Figure 4.1.6. Damage to Eglin Air Force Base test sites following Hurricanes Ivan (2004) and Dennis (2005). A. One hundred meter high "open-air-hardware-in-the-loop" tower test facility (OAHL) prior to the recent hurricanes. B. OAHL tower following Hurricane Dennis. Facilities at the base of the tower have been flooded and the paved access road has been damaged by overwash. C. Test site A-13 prior to Hurricane Ivan. D. Post-Ivan image of site A-13. The concrete sea wall protecting the facility building has been destroyed and is protect by a temporary wall of riprap. E. Post hurricane image of Eglin Air Force Base test site A-3. The sea wall protecting the facility building has been destroyed. F. Beach restoration in the vicinity of test site A-3. A major wall of riprap surrounds the site facilities and the beach is being renourished with sand pumped from an offshore borrow site. The dashed, red box shows the location of Figure 4.1.6E. Source: Images A, C-F – Florida DEP Bureau of Beaches and Coastal Systems; Image B - http://news.webshots.com/photo/ 1393139711028585130cejmlN.

4.1.3. Inlet Morphologic Change. In contrast to most of the island shoreline, throughout much of the 19th and 20th centuries Santa Rosa Island has exhibited dramatic changes at the inlets bounding the island at its eastern and western ends. East Pass, the current inlet at the eastern end of the island, was formed by a breach of the island during storms in 1928 and 1929 (Morang, 1992). The previous inlet was located approximately 2.5 kilometers to the east of the present inlet (Figure 4.1.7A). Following the 1928-1929 breach, the old inlet shoaled and by 1935 only a narrow channel remained (Figure 4.1.7B). Littoral sediment transported into the inlet by flood tides has produced the Norriego Point spit on the eastern side of the East Pass (Morang, 1992) (Figure 4.1.7C). At the present time the main channel of the pass is migrating eastward, producing erosion along Norriego Point. Morang (1992) proposed that the eastern end of the island undergoes periodic cycling of the position of the inlet, with gradual return to the more easterly, northwest-southeast trending channel.

The western end of Santa Rosa Island has been the site of progressive growth for over 250 years (Figure 4.1.8A). Shoreline positions from 1856-1970 suggest a nearly constant rate of areal growth of 0.62 hectares per year (Figure 4.1.8B). The earliest available navigation chart of the area, Gauld's 1766 survey of Pensacola Bay (Gauld, 1780), places the western end of the island 600 meters southeast of the 1856 position. This would suggest an approximately 6 meters per year rate of growth during the late 18th and early 19th century. In the years following 1970, the terminus of the island has lost area, as shown in Figure 4.1.8B. This may be due in part to increased dredging by the U.S. Army Corps of Engineers in the adjacent entrance channel to Pensacola Bay (Figure 4.1.9). From 1880 to 1960 annual dredging removed an average of 176,000 cubic meters per year from the channel. The dredging volume increased to approximately 424,000 cubic meters per year between 1960 and 1994, and 32 to 35 million cubic meters per year for the years 1988-1990 (Browder and Dean, 1999; Rosati, 2005). The inlet dredge spoil was disposed offshore and in the bay north of Santa Rosa Island, elevating the land surface south and west of Fort Pickens or employed for beach renourishment on Perdido Key, west of Pensacola Pass. Browder and Dean (1999) reported that the 1988-1991 dredging of Pensacola Pass may have reduced the western end of Santa Rosa Island by 180 meters. Stone and Stapor (1996) proposed that for the western portion of the island the net littoral transport was westward with an annual volume of approximately 58, 0000 cubic meters per year. If sediment infill into Pensacola Pass is dominated by littoral transport from the island, the available dredging data may indicate a significantly higher rate of sediment transport. Post-2000 aerial images of the island indicate a moderate decrease in the area of the end of the island (Figure 4.1.8) and a 400-meter northeast shift in the position of the island's westernmost end.

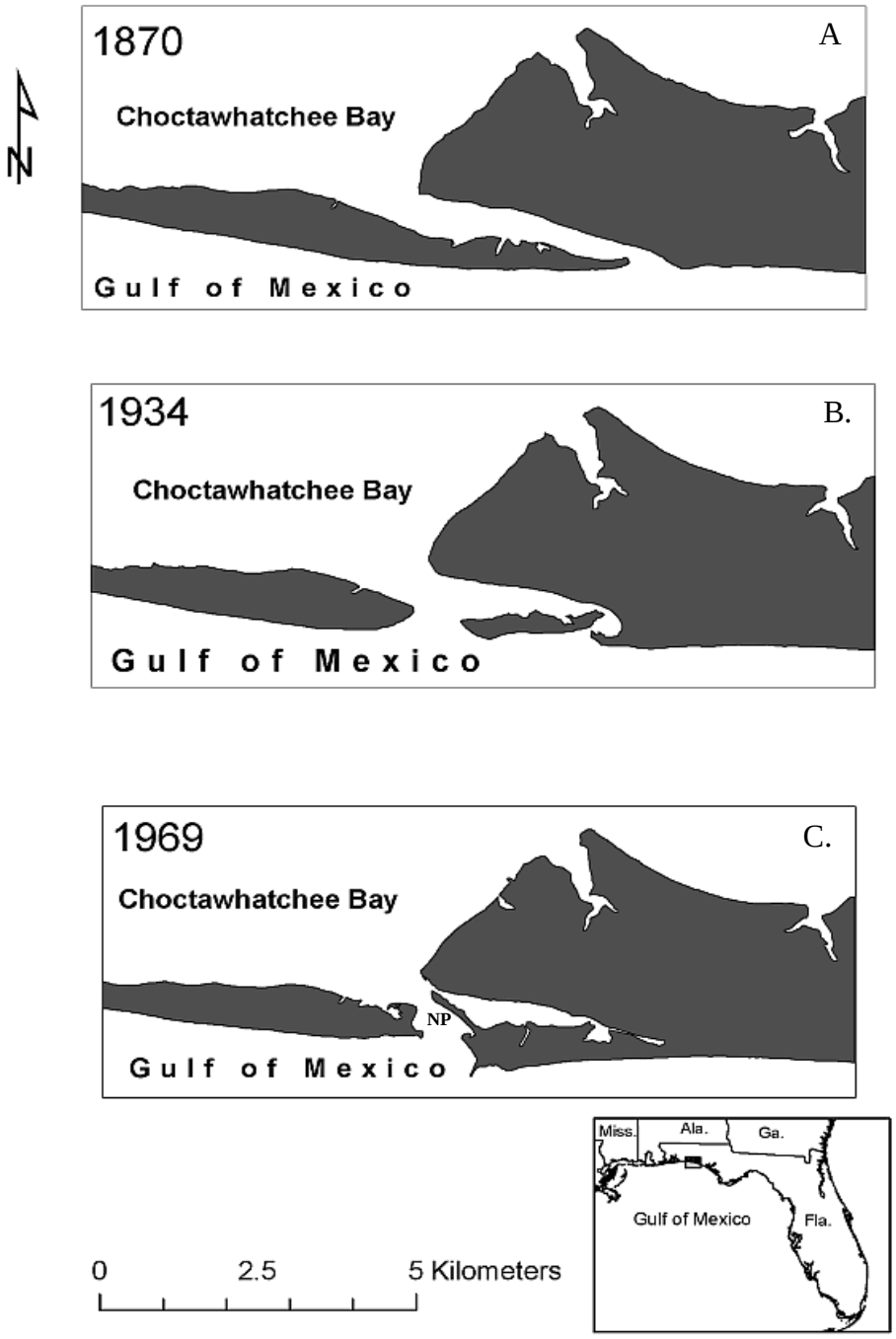

Figure 4.1.7. Major change in the position of the eastern terminus of Santa Rosa Island. Location of East Pass is shown in Figure 4.1.1. **A.** Configuration of East Pass prior to storm activity in 1928 (Morang, 1992). **B.** Configuration of East Pass in 1934. **C.** Configuration of East Pass in 1969. A major spit, Norriego Point (NP) has developed on the eastern side of the pass since the opening of the new channel.

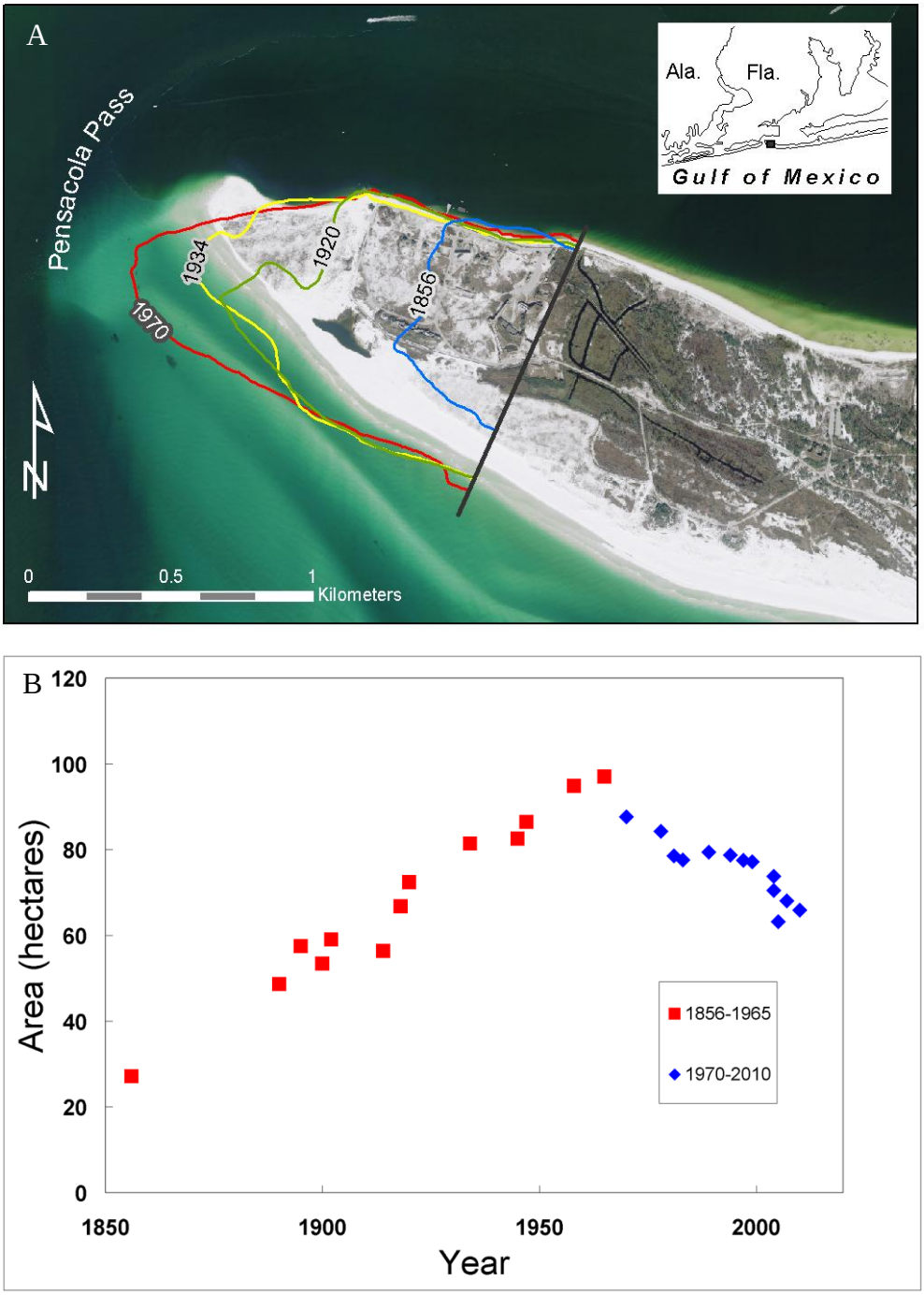

Figure 4.1.8. A. Long-term changes in the shoreline position of the western terminus of Santa Rosa Island and Pensacola Pass (1856-2007). Earlier shoreline positions, based on historic surveys and air photos, are superimposed on a Florida DOT 2007 air photo image. **B.** From the period 1856 to approximately 1970 the area of the end of the island grew at a rate of approximately 0.62 hectares/yr), with a net linear growth of approximately 6.4 meters/yr. Since 1970 the island has undergone little additional westward extension. Losses since 1970 may be associated with an increase in inlet dredging volumes.

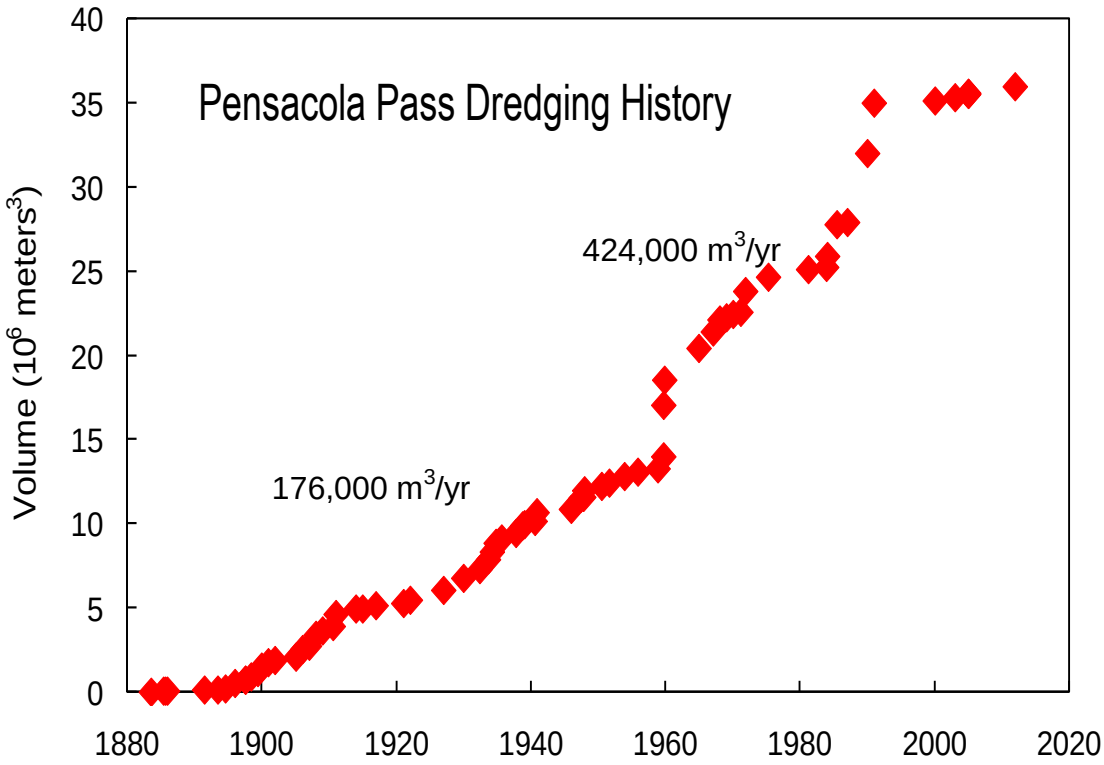

Figure 4.1.9. Cumulative dredging volume for Pensacola Pass at the western end of Santa Rosa Island (Browder and Dean, 1999; Rosati, 2005).

4.1.4. Shoreline Change – DSAS Analysis. The current investigation represents the most comprehensive compilation to date of historic shoreline data for the northwest Florida coast. The shoreline data, from the late 1850's to 2010, includes georeferenced historic charts, air photos and Lidar data. The long-term (1856-2010) net shoreline change (Figure 4.1.10A) is moderately to strongly erosional. Much of this change is due to erosion associated with storm surge during 1995-2005 hurricanes. The greatest shoreline change (~300 meters of coastal retreat), near transect 740, is associated with the rerouting for the East Pass Inlet beginning in 1929. The narrow, western portion of the island (transects 50-150) has also experienced erosion greater than 200 meters. Detailed analysis of the timing of erosion (Figure 4.1.12A) suggest that acute erosion (>150 meters) occurred during the early twentieth century, possible as a result of four major category 3 hurricanes in the Pensacola area in between 1906 and 1917 (Eglin AFB, 2005). A 1926 category 3 hurricane may be responsible for minor erosion that took place along the western portion of the island (Figure 4.1.12A).

During the mid- to late-twentieth century (1934-1994) there was modest shoreline growth (20-50 meters) along most of the length of the island (Figure 4.1.10B). This period of growth may have been associated with the absence of major hurricane activity in the region during that time period. Rates of growth varied from near zero along the western portion of the island to 0.5-1.0 meters per year along the eastern half of the island (Figure 4.1.11). Moderate erosion (2 meters per year) occurred near the inlets of the island; however, some of this erosion was associated with single events (such as the formation of the modern East Pass) rather than long-term, chronic change.

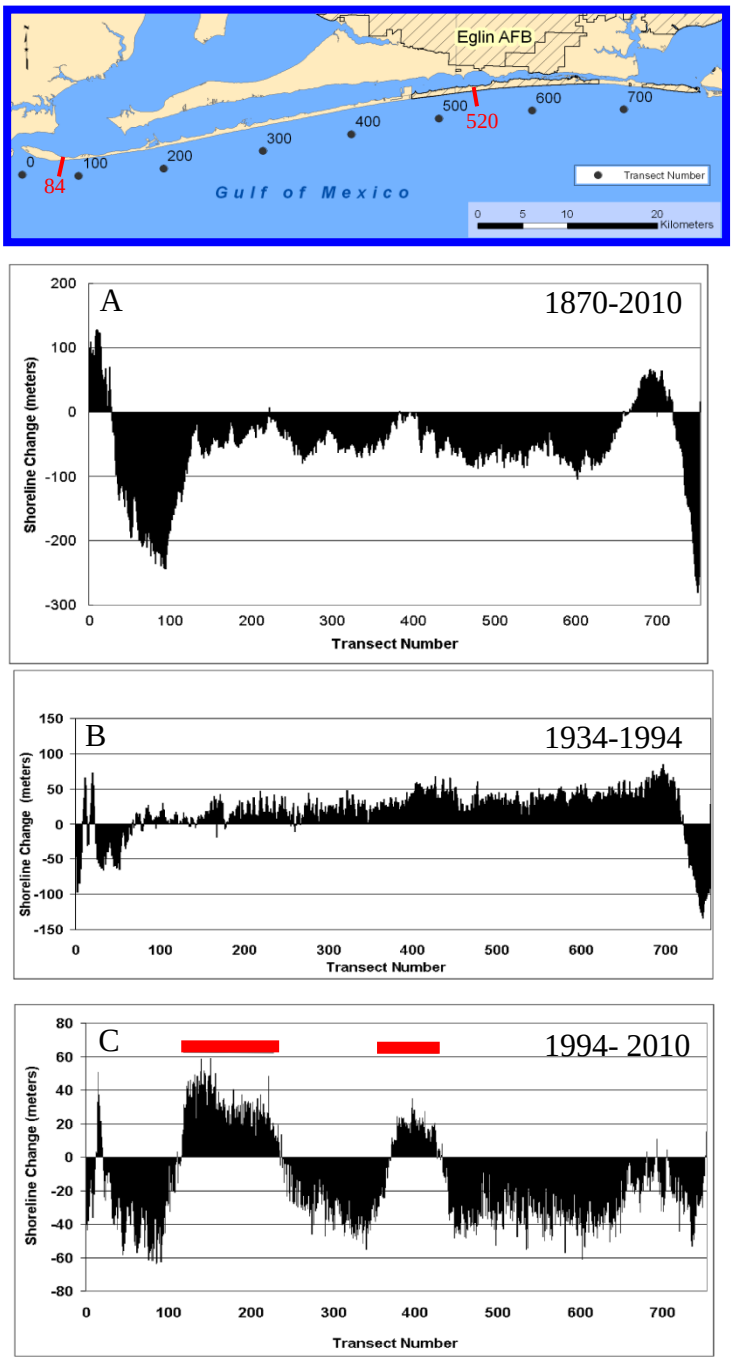

Figure 4.1.10. Net shoreline change along Santa Rosa Island for selected time periods. Transect locations are shown in the map at top. Note that vertical scale (shoreline change) range is different in each panel. **A.** Net shoreline change for the period 1856-2010. Values based upon DSAS analysis of approximately 25 separate time periods. **B.** Net shoreline change for the period of minimal storminess, 1934-1994. Values based upon DSAS analysis of approximately 10 separate time periods. **C.** Net shoreline change for the period of intense storminess, 1994-2010. Values are based upon DSAS analysis of approximately 14 separate time periods. Shoreline accretion (red bars) between transects number 111-243 and 368-432 is the result of recent beach renourishment projects. Shoreline trends for highlighted transects 84 and 520 are shown in Figures 4.1.12 and 4.1.13.

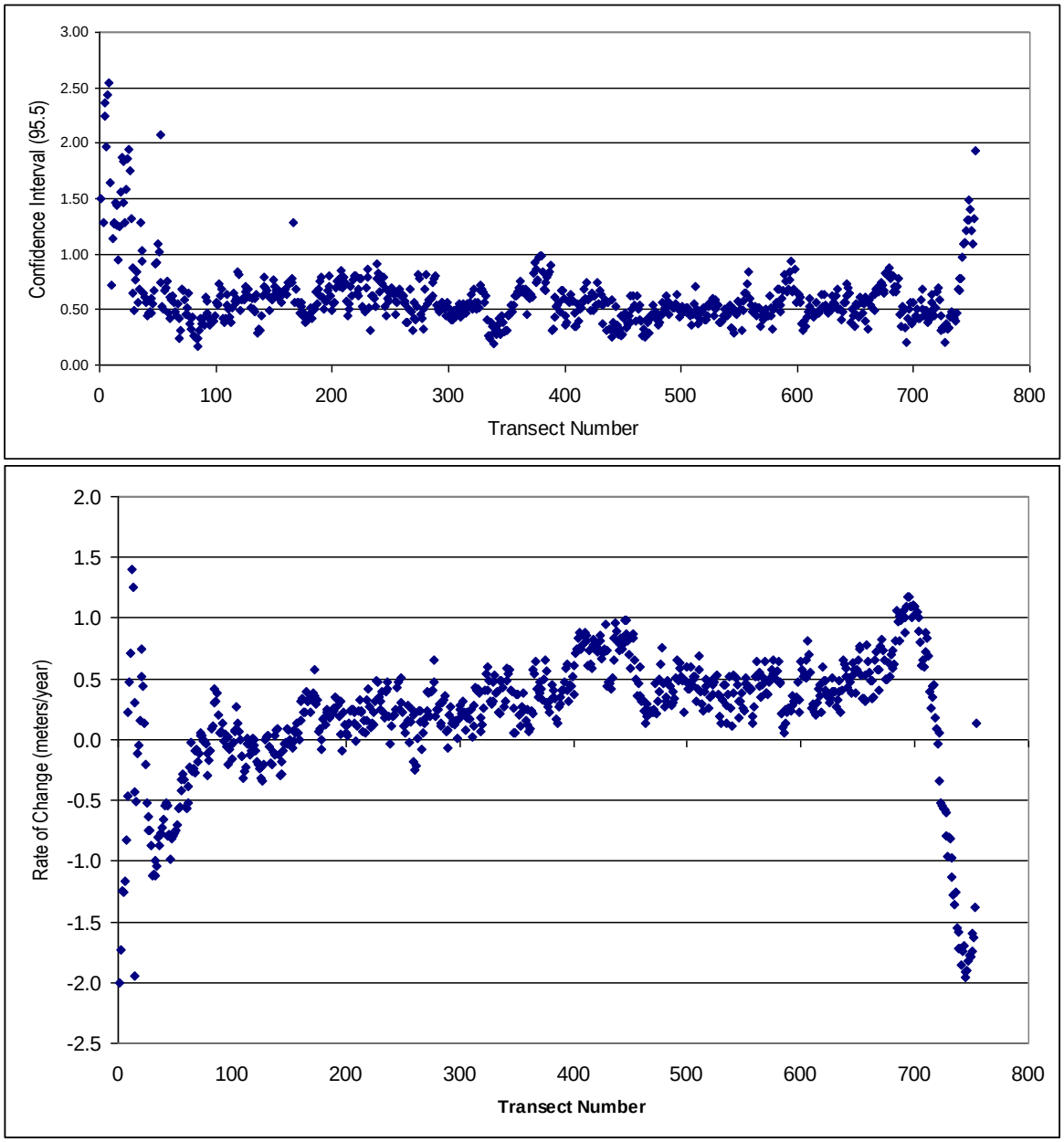

Figure 4.1.11. Lower panel shows net shoreline change along Santa Rosa Island for the time period 1934-1994. The confidence interval (95.5 percent) for each transect measurement is shown in the upper panel.

Recent hurricane activity in the vicinity of Santa Rosa Island during the period 1995-2005 has included three major category 3 storms, Opal (1995), Ivan (2004), and Dennis (2005), plus several minor hurricanes and tropic storms.. During this period the entire island underwent significant shoreline erosion, with a net change of -50 to -60 meters taken place during the combined period of storm activity (Figure 4.1.10C). Beach renourishment at Pensacola Beach (transects 111-243) and Navarre Beach (transects 368-432) has restored the shoreline to its 1994 (pre-Opal) position.

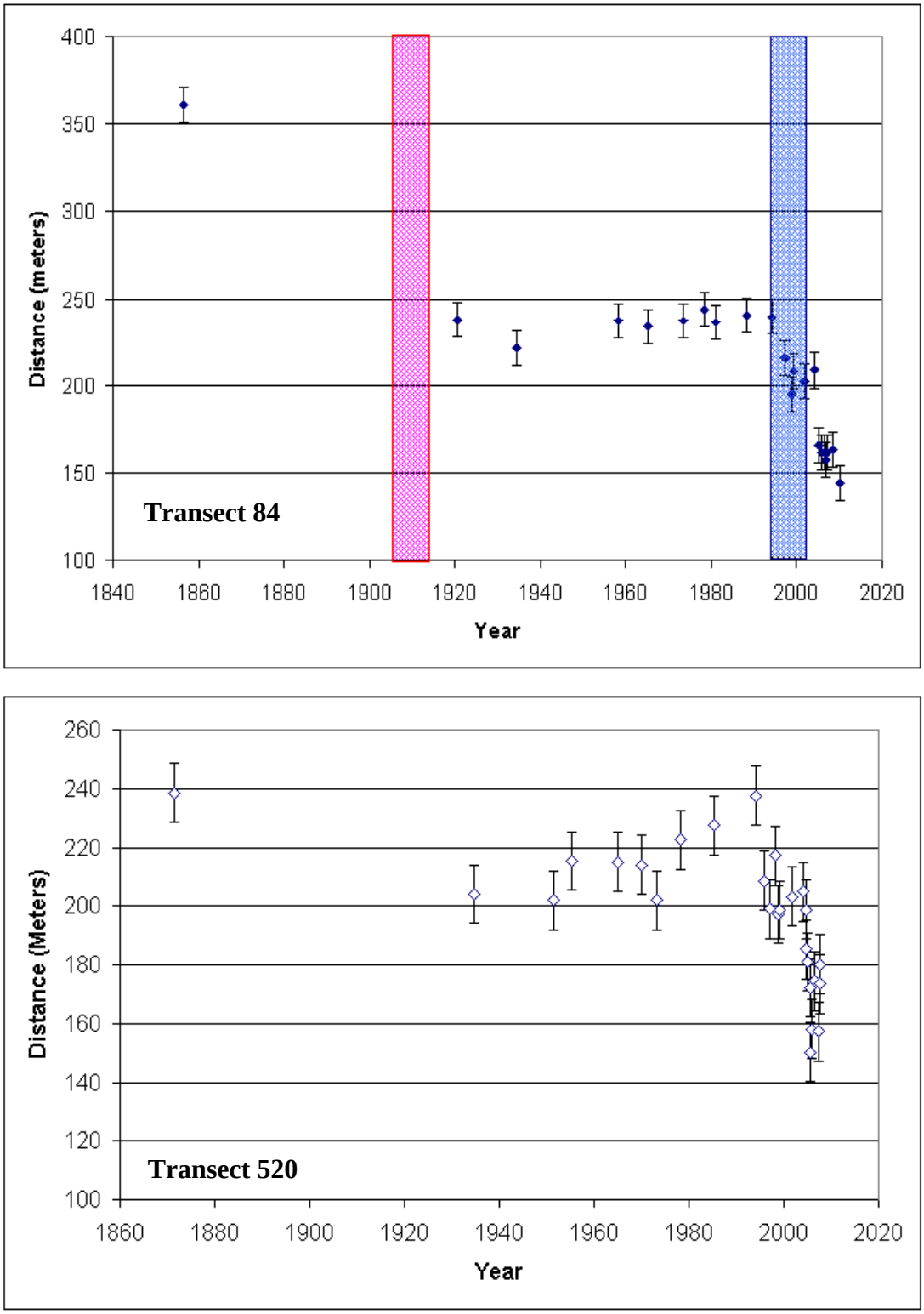

Figure 4.1.12. Detail of shoreline changes for two selected locations - western (Fort Pickens - transect 84) and eastern (Eglin Air Force Base – transect 520) portions of Santa Rosa Island. Note the difference is vertical scales for the two different locations. The transect locations are shown in the upper portion of Figure 4.1.10. Error bars indicate the estimated shoreline position uncertainty of ± 10 meters. The colored bars in the upper figure represent periods of known major hurricane activity associated with significant (>2 meters) storm surge activity (Eglin AFB, 2005, Leadon et al, 1998, Leadon et al., 2004, Clark and LaGrone, 2006.

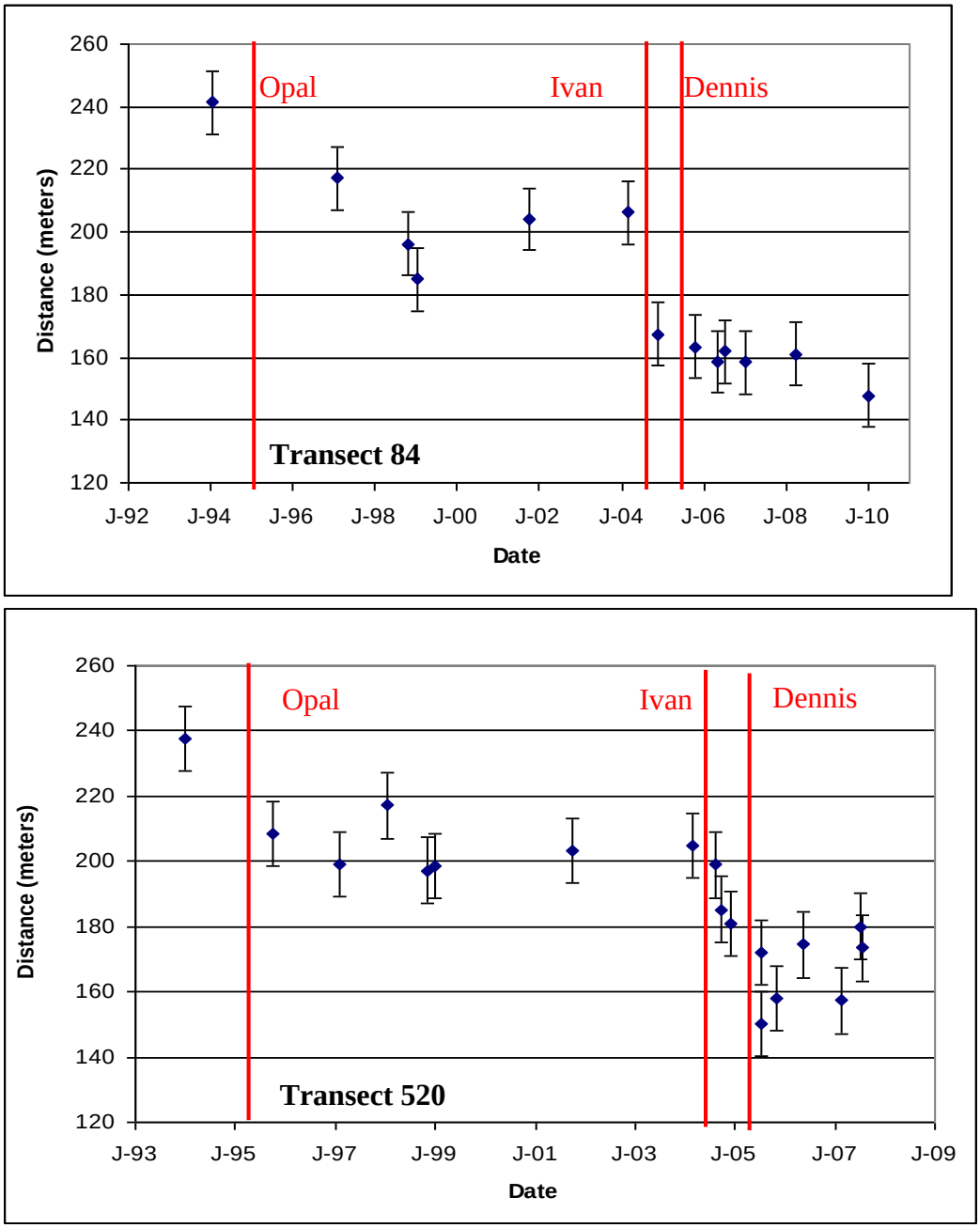

Figure 4.1.13. Detail of shoreline changes for two selected locations - western (Fort Pickens - transect 84) and eastern (Eglin Air Force Base – transect 520) portions of Santa Rosa Island for the period 1994-2010. Note the difference in scales for the two different locations. The "J" indicates January for a given year. The transect locations are shown in the upper portion of Figure 4.1.10. Error bars indicate the estimated shoreline position uncertainty of ± 10 meters. Major category 3 hurricanes affecting Santa Rosa Island (Leadon et al, 1998; Leadon et al., 2004, Clark and LaGrone, 2006) are shown as red vertical bars.

Detailed examination of the long-term shoreline history of the island (Figures 4.1.12 and 4.1.13) reveals that, for most of this period, the island's shorelines were relatively stable. The greatest change – primarily retreat – has taken place during two periods: severe erosion along the western portion of the island during the early 20th century and the island-wide erosion during the period

1995-2005. The earlier erosion period may be associated with four Category 3 storms that passed near Santa Rosa Island during the period (1906-1917). Detailed observational evidence (Clark and LaGrone, 2006; Morton et al., 2004b) provides evidence for the beach erosion associated with Hurricanes Opal, Ivan and Dennis, affecting the island during 1995-2005.

4.2. Modeling Future Storms. There is academic, commercial, and public interest in estimating loss from hurricanes striking land and understanding how loss might change as a result of future variations in climate. We have captured the uncertainty about the maximum possible future loss by modeling the uncertainty about the event frequency and the event magnitude. The results are described below. The biggest concern for EAFB is the tail of the distribution where managers are making decisions about new and existing buildings. Having a robust treatment of uncertainty translates into better-informed decision-making.

4.2.1. Storm Losses versus Wind Speed. Hurricane wind speed is the sole variable that is both theoretically and statistically linked to climate change. For a given set of hurricanes, average wind speed increases with increasing ocean temperature. Climate model projections of 21st century anthropogenic warming indicate the possibility of greater wind shear across parts of the tropical Atlantic leading to fewer and/or less intense hurricanes (Vecchi and Soden 2007), but observations over the past 5-10 years indicate that shear has not increased.Damage loss amounts as a function of wind speed alone allow us to project future wind damage losses from hurricanes at Eglin AFB.

The relationship between damage (D) from a hurricane's size, forward motion, precipitation, and wind speed (V) remains poorly constrained and often characterized using a power-law relationship where $D = \alpha V\beta$ and β ranges between 3 and 9 (Howard et al., 1972; Nordhaus, 2010; Bouwer and Botzen, 2011). In contrast, we find a simple exponential dependence of aggregate economic losses from hurricanes on wind speed at the time of United States landfall.

A time series of normalized losses is shown in Figure 4.2.1. Note that the largest normalized economic loss is associated with the 1926 Miami hurricane. The frequency distributions of loss and wind speed are shown in Figure 4.2.2. The loss data vary by nearly six orders of magnitude whereas wind speeds vary by just over a factor of four. Several factors contribute to the variability in loss including: population density in the area affected by the storm, the nonlinear response of damage to wind speed, and the amount of precipitation and flooding. This variability can be seen in a scatter plot of wind speed versus loss (Figure 4.2.3).

Estimates of how aggregate damage and loss increase with wind are usually based on a power law relationship. However, the rationale for this choice is not clear to us. We expect a plot of damage to a structure versus wind speed to have an S-shaped profile with no loss at low wind speed and complete loss at a high wind speed (Vickery et al., 2006a, 2006b). The losses to contents, appurtenance structures, and additional living expenses or business interruption can be more complicated, but they are also included in loss estimates. Regardless, it can be difficult to confirm a power law relationship with small sets of data.

We model the log (base 10) of aggregate normalized loss as a function of wind speed using quantile regression (Koenker and Bassett, 1978). The fits for the 0.10, 0.25, 0.50, 0.75 and 0.90 quantiles are shown as colored lines in scatter plots for all losses, and for losses in three landfall regions (Figure 4.2.3). The regions are based on an analysis showing that landfalls in Florida

depart from a Poisson rate process and are clustered (Jagger and Elsner, 2012). Regression results are shown in Table 4.2.1. Interestingly, within the uncertainty of the results, a slope of ~5% per m/s seems appropriate for most quantiles and regions. Higher quantiles with lower slopes have a large uncertainty and appear to be associated with East Coast storms. However, a test of significance using the Wald approach (Hendricks and Koenker, 1991) indicates little evidence to reject the null hypothesis of equal slopes for the different regions. The relative constancy in slopes suggests the possibility of an inherent relationship that causes losses to increase by 5% for each m/s increase in wind speed.

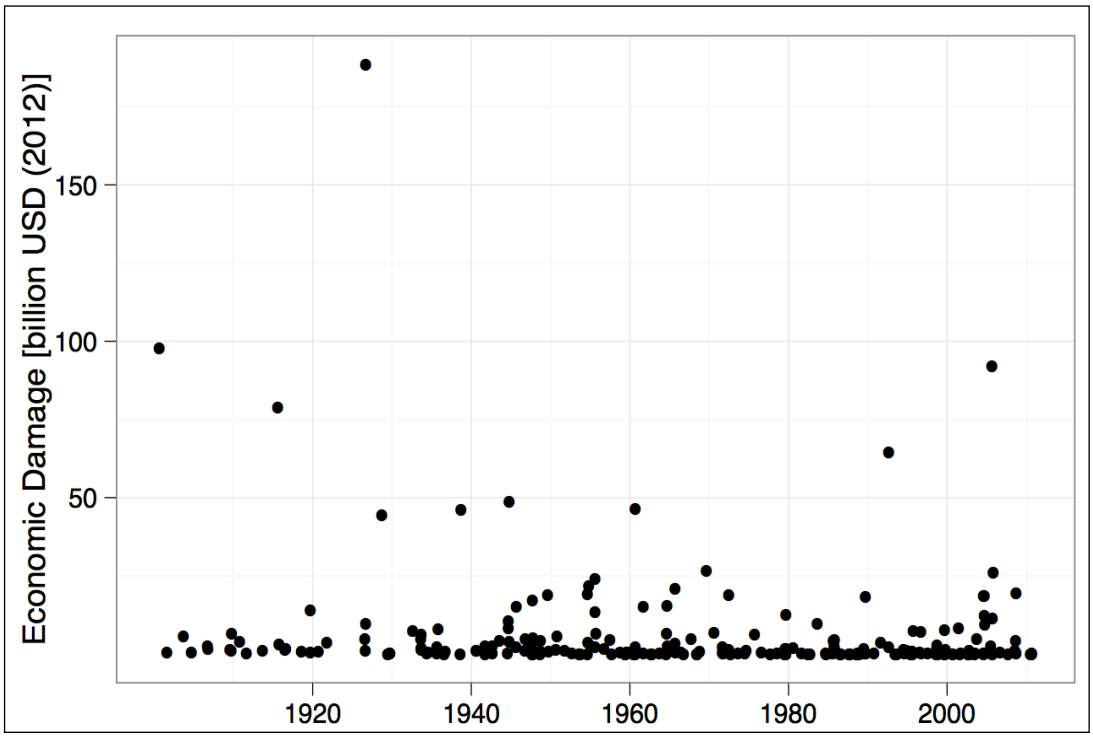

Figure 4.2.1. Time series of normalized losses. Loss data are obtained from http://www.icatdamageestimator.com/.

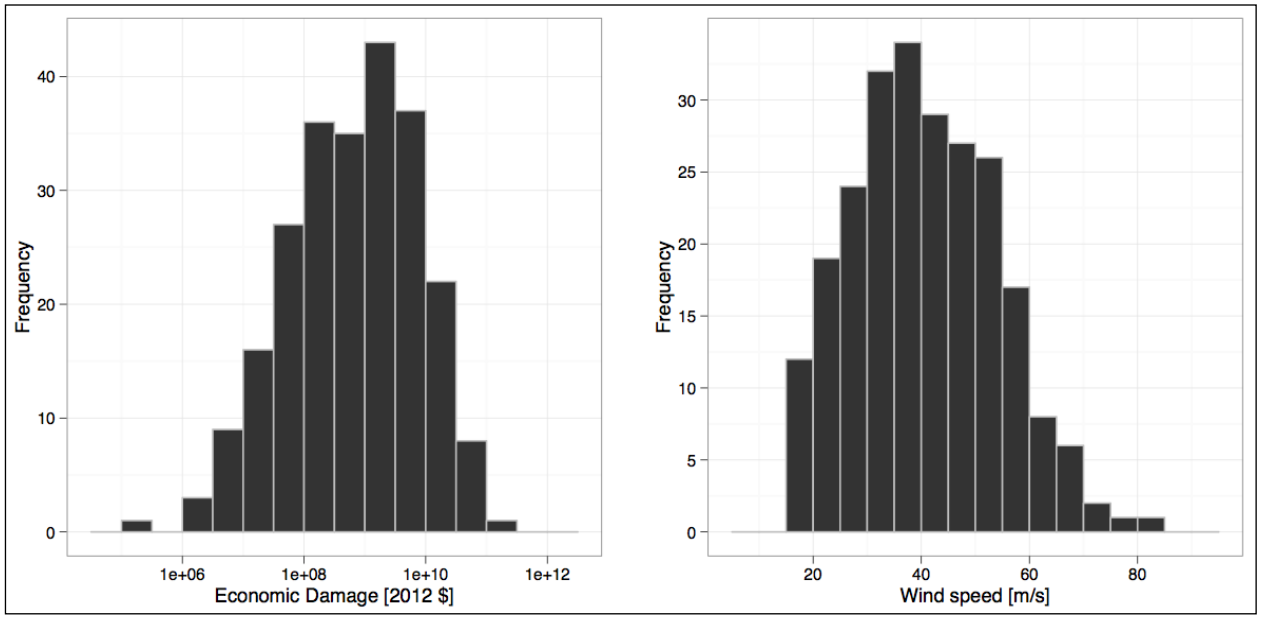

Figure 4.2.2. Frequency distribution of wind speeds (right) and damage (left) of all U.S. hurricanes since 1900.

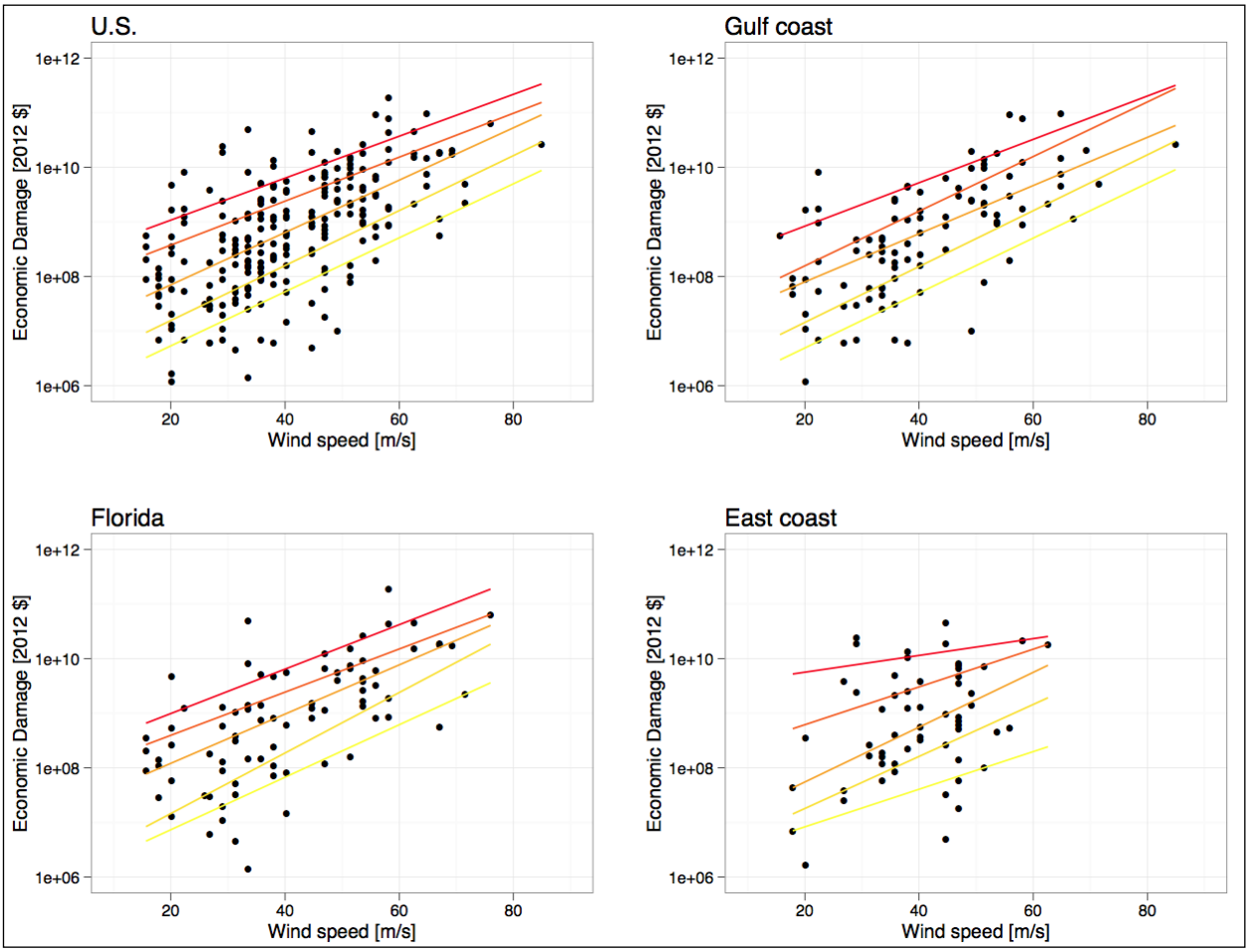

Figure 4.2.3. Quantile fits of economic damage as a function of wind speed. Statistics for the fits at the 0.10, 0.25, 0.50, 0.75, and 0.90 quantiles are given in **Table 4.2.1.**

Table 4.2.1. Statistics from the quantile regressions. Values in parentheses are the 95% confidence intervals.

Quantile	Damage at $\overline{W}$ [$\log_{10}$]	Slope [%/m s^{-1}]
0.10	7.72 (7.467,7.902)	5.0 (3.9,6.4)
0.25	8.218 (8.156,8.397)	5.1 (4.5,5.9)
0.50	8.820 (8.739,8.948)	4.9 (3.7,5.4)
0.75	9.400 (9.297,9.551)	4.0 (3.2,5.3)
0.90	9.820 (9.746,9.978)	3.8 (2.8,4.6)

We suggest that the centercepts (the quantile losses for the mean wind speed) for the different quantiles be interpreted as the loss produced by a combination of essentially random factors that characterize a storm's impact (e.g., size, shape, precipitation, location, surface roughness and surge). Once these factors are accounted for, the loss from a storm will be dominated by wind speed and the response should be relatively consistent across quantiles. The quantile slopes for

the exponential relationship are constant (Table 4.2.1) and consistent with this interpretation of the centercepts. In contrast, we find a significant variation in quantile slopes for model based on the power-law relationship (not shown). In addition, using Kolmogorov-Smirnov statistics (Clauset et al., 2009) we find a low p-value (0.08) that suggests the power-law relationship provides a poor fit to the data.

The 5% per m/s relationship derived using the exponential relationship can be used to estimate how loss might vary with a change in wind speed. Elsner et al., (2008) show that the strongest storms are getting stronger at a rate of 0.1 m/s/yr. At the end of 10 years, assuming this trend is maintained, there will be a 1 m/s increase in hurricane wind speeds, and thus, we would expect a 5% increase in loss independent of any change in exposure.

4.2.2. Effect of Sea Surface Temperature on Storms. Estimates of the sensitivity of hurricane strength to ocean heat are needed to better understand how fierce hurricanes might become in the future. This is fundamental in establishing the limits on the utility of GCMs in projecting future changes to storm climatology across the North Atlantic. Most hurricanes that influence Eglin AFB originate and intensify over the western Caribbean and Gulf of Mexico as part of the North Atlantic basin.

Maximum intensities are increasing especially over the warming Atlantic, but reliable estimates of sensitivity are not possible with time-series data. Sensitivity estimates for the most intense hurricanes are made using quantile regression (Elsner et al., 2008), but the variation of SST over time is rather small making it difficult to get a precise value. Studies using paired values of intensity and SST are also limited since most pairs represent hurricanes in an environment less than thermodynamically optimal. Here we overcome these limitations by using a spatial tessellation of the hurricane data and a statistical model for the limiting intensity to obtain robust estimates of the sensitivity of hurricane intensity to sea-surface temperature (SST).

Figure 4.2.4a shows the spatial tessellation of the North Atlantic and the color shading indicates the number of hurricanes in each hexagon over the period 1981--2010. We only consider grids having at least 15 hurricanes (at least one hurricane every other year on average). Figure 4.2.4b shows the highest hurricane intensity within each of the 24 hexagon grids. Intensity is given by the maximum sustained near-surface wind speed estimated within the hurricane eyewall less 60% of the forward speed. We restrict our analysis to the North Atlantic using the period 1981--2010 because data records over this region and time are most reliably consistent. Areas across the central Atlantic have the highest number of hurricanes, while areas farther south especially the Caribbean and Gulf of Mexico have seen the strongest hurricanes.

As two examples, histograms of the highest per hurricane intensity for grids labeled c and d are shown in Figure 4.2.4c, d. The bar width is 5 m/s and the range is 25 to 75 m/s. Grid c has 20 hurricanes and grid d has 27. The 75th percentile intensity is 54.7 m/s in grid c compared to 40.2 m/s in grid d. Grid c has fewer, but stronger hurricanes compared with grid d. The set of highest intensities in each grid provides the data and extreme-value theory provides the rationale for a statistical model to estimate each grid's limiting intensity. The statistical model (solid curve) is shown in Figure 4.2.4e, f for the data in grids c and d. The method of maximum likelihood is used to estimate the model parameters. The gray points are empirical estimates of the return level as a function of return period. The dotted line is the 25th percentile intensity (threshold) and the red line is the limiting intensity given the data and the model, which amounts to 72.1 m/s for the set of hurricanes in grid c and 51.3 m/s for the hurricanes in grid *d*.

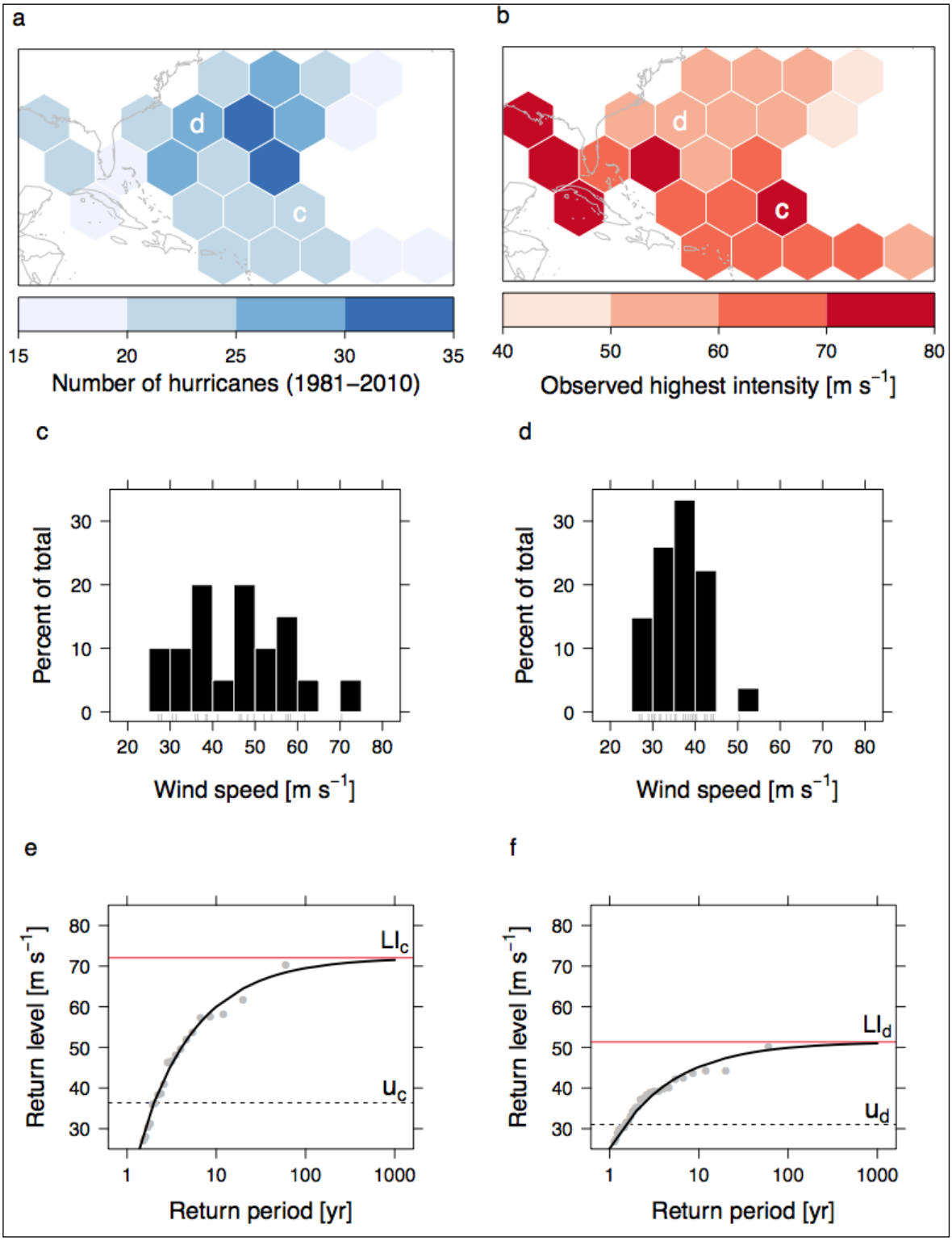

Figure 4.2.4. Hurricane frequency and intensity over the period 1981 - 2010. (a) Number of hurricanes in equal-area hexagons and (b) highest intensity of all hurricanes in each hexagon grid. (c, d), Histogram of per hurricane maximum wind speeds from grids c and d. Bin width is 5 m/s (e, f), Statistical model (solid line) for the data in grids c and d. The gray points are empirical estimates. The dotted line is the threshold intensity (u) and the red line is the limiting intensity (LI).

Models are fit to the intensity values in each grid and the parameters mapped in Figure 4.2.5. Threshold (u) values range from 26 m/s in grids along the far northern part of the basin to 44 m/s for the grid near Hispaniola. Wind speeds exceeding the threshold are used in the statistical model. The scale parameter (sigma) is the spread of intensities above the threshold and controls how fast the cumulative probability function decays for values near u. Larger values indicate slower decay. Spreads are largest in grids over the Caribbean, Gulf of Mexico, and tropical central Atlantic and smallest in grids farther north. The shape parameter (xi) describes the tail behavior with negative values indicating a limiting intensity (LI) given by:

$$LI = u - sigma/xi \tag{4.2.1}$$

Limiting intensities are highest over the western Caribbean and Gulf of Mexico where the ocean surface is the hottest.

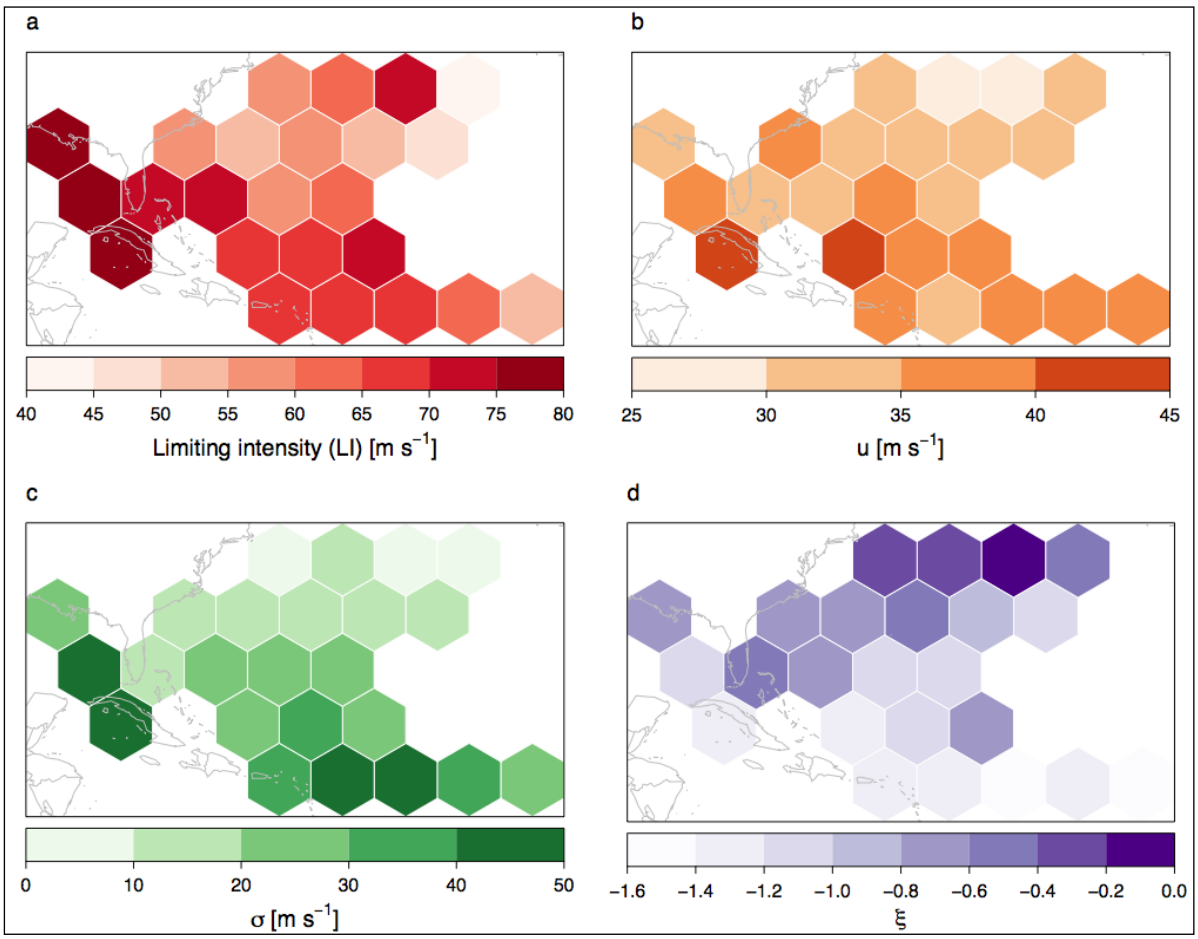

Figure 4.2.5. Limiting intensities (a) and model parameters (b-d). Limiting intensities are highest in grids over the western Caribbean Sea and Gulf of Mexico. Higher LIs are associated with higher threshold and higher scale values.

Limiting hurricane intensity is rooted in the statistical theory of extreme values. Other factors like wind shear have been minimized by considering only the strongest possible hurricanes. The threshold wind speed is a compromise between having enough winds to accurately estimate the parameters of the statistical model, but not too many that the intensities fail to be described by extreme value theory.

We average the SST values within each of the hexagons from the period 1981-2010 during the months of August-October and then separately regress each of the model parameters onto them. Details are given in the Methods summary section. Results are shown in Figure 4.2.6. Each point represents the LI-SST pair for a particular hexagon. The limiting intensity (panel a) shows a significant trend with increasing SST indicating a sensitivity of 8.2 +/- 1.19 m/s/K (s.e.). The value is consistent with an inferred estimate of 8.7 m/s/K from (DeMaria and Kaplan, 1994). The sensitivity results from an increase in both the threshold and scale with increasing SST over the range between 25 and 30C (four grids having SST less than 25C are removed). The shape parameter is largely independent of ocean temperature. As the ocean warms, the distribution of hurricane winds shifts to higher values and there is a greater spread of values above the increasing threshold. Uncertainty about the sensitivity estimate assumes the regression residuals are spatially uncorrelated. We test this using Moran's I and a contiguity neighborhood for each grid and find no evidence of residual spatial correlation (P = .439 under the null hypothesis of no correlation). We also find no relationship between LI and latitude.

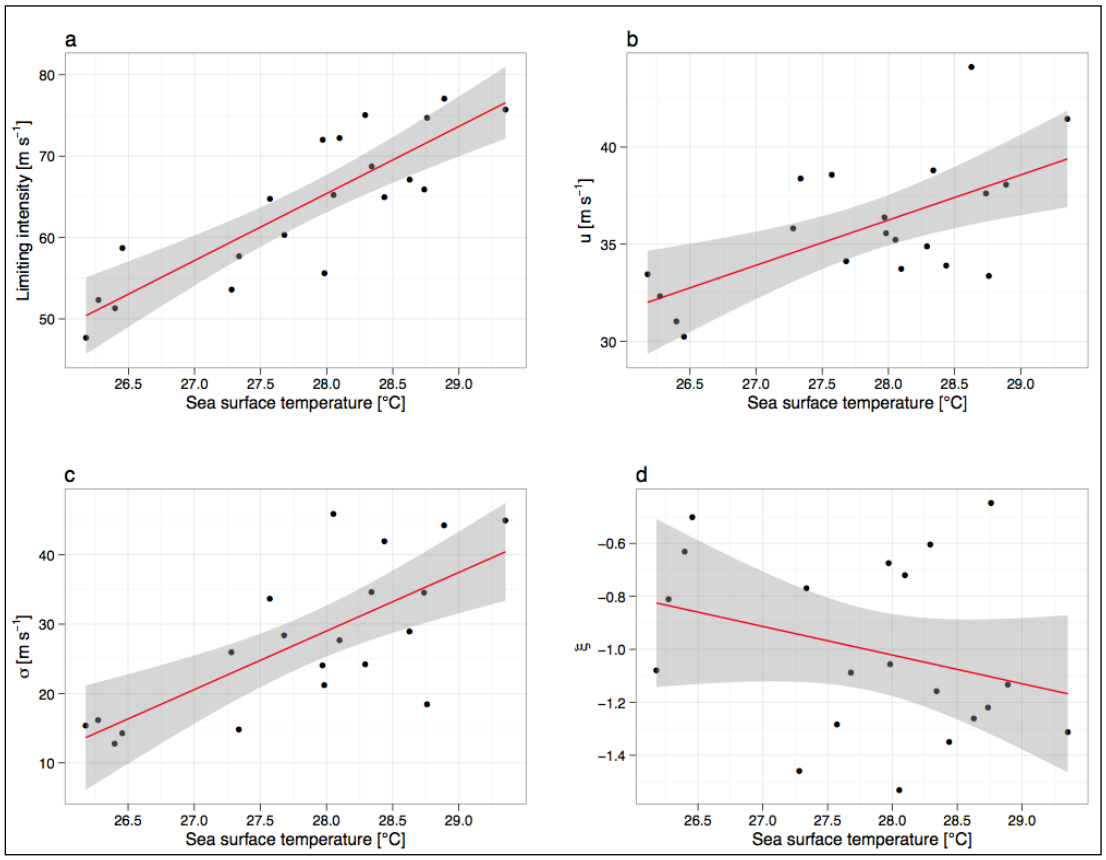

Figure 4.2.6. Scatter plots of limiting intensity (a) and model parameters (b-d) versus SST for grids having SST values greater than 26C. A best-fit linear regression line (blue) represents the sensitivity of hurricane intensity to SST. The 95% confidence interval about the sensitivity is shown as a gray band.

The analysis for determining sensitivity of intensity to SST is repeated using tropical cyclone track data from the HiRAM dynamical model (Zhao et al., 2009) and results shown for one realization in Figure 4.2.7. HiRAM is run as a control simulation forced with prescribed sea-surface temperature from the Hadley Centre Global Sea Ice and Sea Surface Temperature dataset (Rayner et al., 2003). The model features a 50 km horizontal resolution with 32 levels in the

vertical. The sea-surface temperatures used to estimate observed sensitivity of limiting intensity to ocean warmth are from NOAA's extended reconstructed version 3b data set for the North Atlantic Ocean.

Here we estimate uncertainty on the limiting intensity using a bootstrap resampling of the wind speed data independently for each hexagon. The sensitivity from the observations (best-track) is shown by the slope in the left panel and the sensitivity from the HiRAM model is shown by the slope in the right panel. The sensitivity from the model is only 1.5 +/- 0.60 m/s/K (s.e.) and is significantly less than that computed from the observations. The difference arises primarily due to the lack of sensitivity in the scale parameter. As the ocean warms the distribution of modeled hurricane winds shifts to higher values similar to the observed hurricane winds but, unlike the observed winds, there is no change in the spread of modeled winds above the increasing threshold. Similar results are obtained using tropical cyclone tracks from two other HiRAM climatology simulations and from a simulation of the Florida State University-Center for Ocean and Atmosphere Prediction Studies (FSU-COAPS) GCM (LaRow et al., 2008).

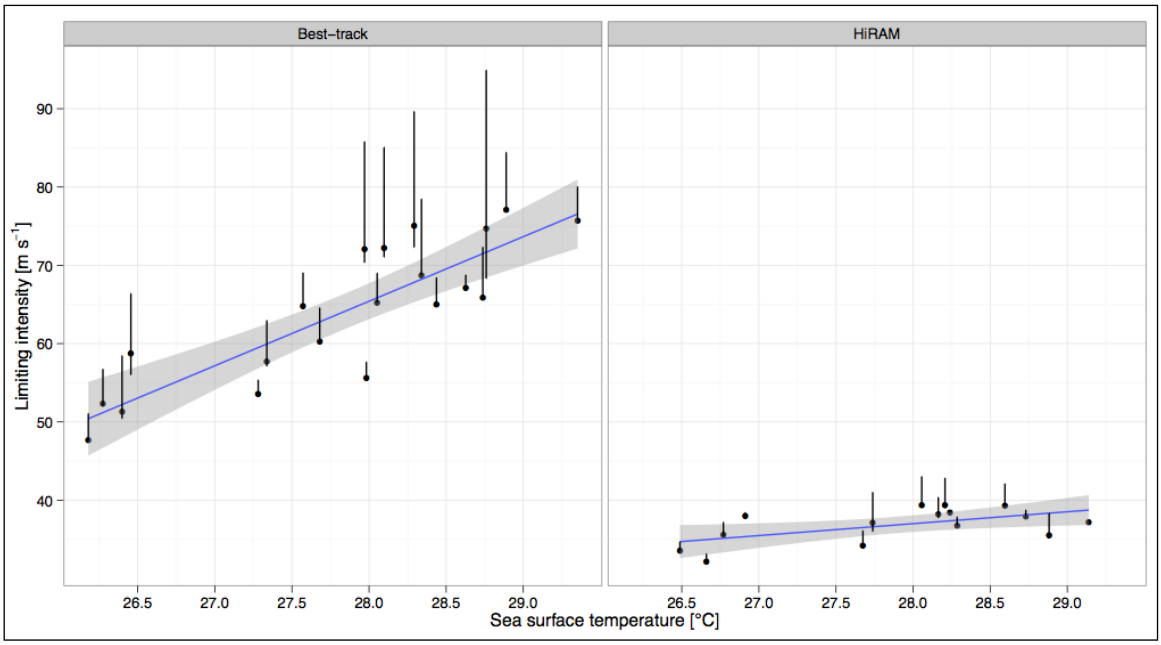

Figure 4.2.7. Scatter plots of limiting intensity versus SST. (a), Observations and (b), HiRAM model. The 80% confidence interval (10% on the upper limit) on the points are based on a bootstrap resampling of the wind speed values in each grid.

The relationship between ocean warmth and hurricane intensity is well known, but estimates of the sensitivity of this relationship relative to future climate scenarios have not been attempted in a statistically rigorous way. This has hampered progress toward understanding our future risk to these potentially catastrophic events in the warmer world of tomorrow. The method demonstrated here is capable of producing reliable estimates of sensitivity including quantitative levels of uncertainty on the estimates. Results indicate that real hurricanes are five times more sensitive to warming seas over the North Atlantic than their counterparts from a numerical simulation calling into question the usefulness of current models for projecting future hurricane activity in this part of the world. This insensitivity of limiting intensity to ocean warming precludes the use of GCM information to estimate future storminess over Eglin AFB.

4.2.3. Modeling Hurricane Intensity Changes.

Figure 4.2.8 shows the percent change in maximum tropical cyclone intensity with respect to a 1 degree C change in SST as a function of tropical cyclone intensity over the Gulf of Mexico using quantile regression (Elsner et al., 2008; Jagger and Elsner 2009). The points indicate the trend estimate computed from a quantile regression model for intensity quantiles from 0.01 to 0.99 by 0.01 and the vertical bar indicates the one standard error about the estimate based on the assumption of independent and identically distributed residuals as is commonly used with normal linear regression. The non-linear trend line is shown in red and the 95% confidence band around this trend is shown in gray.

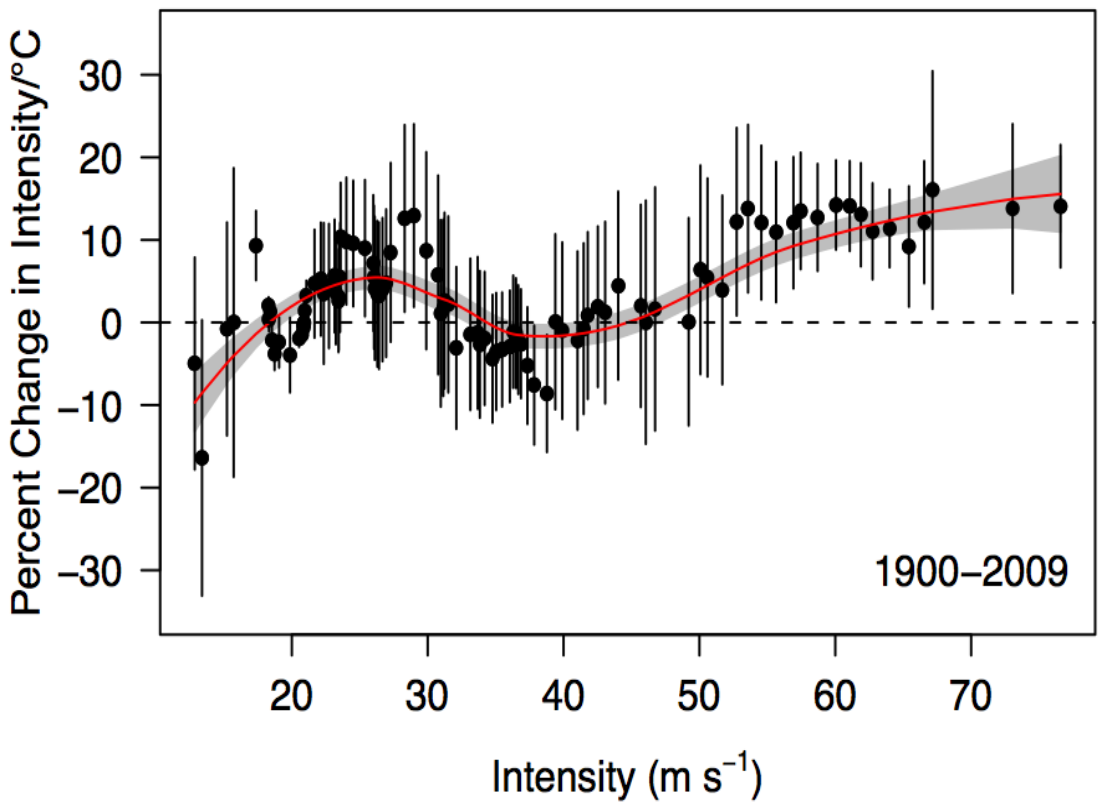

Figure 4.2.8. Change in Gulf of Mexico tropical cyclone intensity from 1900–2009. The percentage change in intensity is with respect to a 1C change in SST over the Gulf of Mexico and is a function of storm intensity. The dot and vertical line indicate the best estimate of the change and the one standard error. The red line is a local regression through the set of points and the gray region defines the 95% confidence band on the trend.

The overall tendency is clear in showing little change in intensity for the weaker tropical cyclones, but a large and, for some quantiles, statistically significant upward trend in intensity for the stronger tropical cyclones. The red line indicates a local polynomial regression fit through the points. The regression fit at a given intensity is made using points in the neighborhood of this intensity weighted by the distance from the particular intensity. The neighborhood size is set at a constant of 75% of the points. The non-linear trend line does not change much when the early 20th century storms are removed, although the percentage increases are somewhat larger. In fact, the increase at the 90th percentile storm intensity is 14% using storms back to 1900 compared with 21% using storms only back to 1944.

Next, we quantify the trend in SST and get an estimate of the increase in Gulf warmth by the year 2100. Estimates of global SST increases by the year 2100 range from 1 to 3 degrees C based on numerical climate models. We take a similar approach as with hurricane intensity and examine the July SST data over the Gulf of Mexico and show how it is changing over time.

Figure 4.2.9 shows the time trend in Gulf of Mexico SST since 1900. The warming is pronounced and statistically significant. The trend estimate shown as the black line amounts to 0.68 degree C per century. The significance can be seen by the 95% confidence band (between the two red lines). This warming is consistent with reports of between 0.4 and 1.0 degree C per century for global tropical ocean warming (Deser et al., 2010).

It should be noted that we do not necessarily expect an extrapolation (linear at that) to represent the future. Yet, the method provides a quantitative estimate of what Gulf of Mexico hurricanes might encounter in the 22nd century that is consistent with estimates of anthropogenic global warming.

Our approach of using the SST-hurricane relationship may be less applicable for military installations at higher latitudes where storm intensity is complicated by baroclinic processes associated with Rossby waves. It might also be less applicable in areas such as the western North Pacific where the monsoon trough plays a dominant role in typhoon intensity.

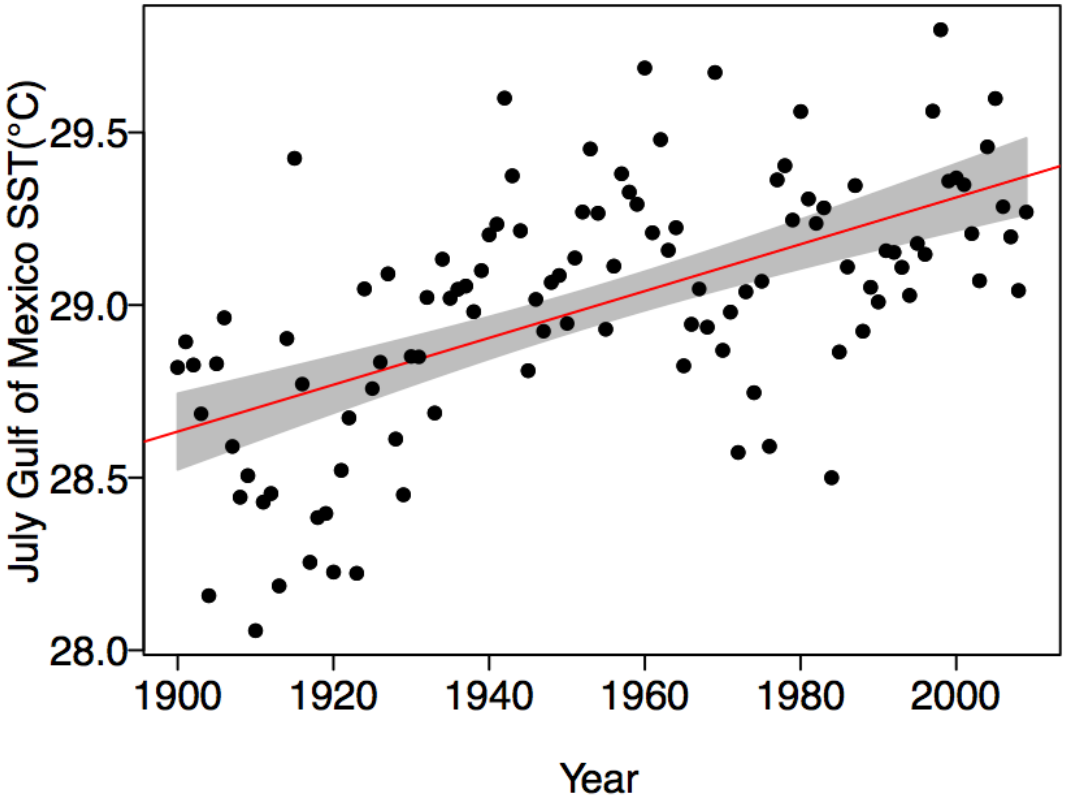

Figure 4.2.9. Gulf of Mexico SST trend. The change in SST is the time trend over the past 110 years. The points indicate the area-averaged SST value for the month of July each year over the period (1900–2009). The red line is the least-squares regression line through the data and the gray region defines the 95% confidence band on the trend.

An estimate of the per degree C increase in hurricane intensities (as a function of intensity) together with an estimate of the SST warming by 2100 allows us to estimate the increase in wind speeds for each historical hurricane. The assumption is that the set of historical hurricanes is a representative sample of the frequency and intensity of future hurricanes, but the strongest hurricanes will be stronger due to the additional warmth in the Gulf of Mexico. The approach is similar to that used in Mousavi et al., (2010) to estimate the potential impact of hurricane intensification and sea level rise on coastal flooding, but here we use wind speed instead of central pressure deficit for the change in hurricane intensity.

Let *w* be the observed wind speed along the track of a hurricane today, then the equation for representing the wind speed for the same hurricane in the year 2100 is given by:

$$w_{2100} = [1 + \Delta w(w)\ \Delta SST\ 90]\ w \qquad (4.2.2)$$

where $\Delta w(w)$ represents the fractional change in wind speed per degree C change in SST as a function of wind speed described by the red curve in Figure 4.2.8a, represents the time trend in SST expressed per year and 90 is the number of years into the future.

Our model for intensities to the year 2100 is applied to wind speeds along the track for each historical hurricane affecting EAFB. For the weaker winds the difference between today's and tomorrow's speeds are quite small, but for the strongest winds the future is windier.

Our method does not include structural uncertainty associated with the choice of using other models that include wind shear, etc. Qualitatively we suggest that this uncertainty is much smaller than the uncertainty associated with sampling as there is no credible evidence that wind shear or other factors that might inhibit hurricanes will change in the future, at least not relative to increases in ocean warmth. While there have been reports that wind shear across the area will increase, thereby curtailing the intensity of the strongest hurricanes (Vecchi and Soden 2007), those results are based on scenarios from GCMs that have little, if any, credibility.

4.2.4. Modeling Future Wind and Surge Damage Losses. The wind speeds along the hurricane track points are adjusted according to the model described in the previous section. However, the track point locations and all other storm vitals remain the same as there is no observational, theoretical, or model evidence for changes to these storm characteristics in a warmer world. The new storm vitals together with sea-level rise projections are subsequently used by HAZUS to generate future loss estimates. Loss estimates can be done for wind and surge damage separately or as a combination. We further assume (obviously unrealistically) no change in the general building stock (GBS) and all losses are in 2006 dollars.

Wind speeds are available along each historical hurricane track at one-hour intervals (Jagger and Elsner 2006) so there is no need to have a landfalling wind speed. Future SSTs are generated by extrapolating the trend observed in the data using SST values only over the Gulf of Mexico (Fig. 4.2.9). The percentage change in SST per degree warming is obtained by the curve in Fig. 4.2.8. The two changes are used Eq. 4.2.2 to obtain a change in wind speed along the entire hurricane track. The uncertainty on the SST is obtained from the prediction interval on the regression. The bounds on this uncertainty are used as input to the HAZUS wind damage model.

4.2.4.1. Building Stock Data. Our analysis uses data from the GBS. These data are most reliable for non-military infrastructure. The HAZUS literature notes that military reservations

are not well represented by the GBS because of the unique nature of some military construction and lack of building inventory/survey on parts of the bases.

According to FEMA, military facilities are not available in the current HAZUS default inventory (http://www.fema.gov/plan/prevent/hazus/hz_database.shtm). Furthermore, the HAZUS Technical Manual (MR-4) states that High Potential Loss Inventory (HPLF) for facilities categories such as levees, nuclear power plants and military installations do not have specific damage curve functions like that of other structures.

This is not to say that loss estimates cannot be performed for a military base in its entirety. This can be done, but the estimates for the selected study area in this investigation are considerably more reliable. Hence, we made the assumption that the aforementioned tracts would be a good segment of EAFB on which to determine damage loss estimates because these tracts were census designated places. The assumption is that the GBS data for those two tracts are more dependable, and produces a more reliable result. This is not to say that GBS data does not exist for the other four census tracts in question. In fact, we can model damage loss estimates for the entire base. The reliability of the results would be considerably lower. Table 4.2.2 depicts the six census tracts that comprise Eglin AFB.

Table 4.2.2. Census tract number and total area (acres) of the tracts used on our wind loss model.

Tract Number	Tract Area (acres)
12091021400	1928
12091023200	4424
12091021200	8236
12113010802	74359
12131950300	193102
12091020800	235467

The full tract numbers are 12091021400 and 12091021200. The numbers are a concatenation of several FIPS codes that identify the state, county and tract number. The 212 and 214 are part of that number. We picked the tracts to most closely match the main base residential areas.

The GBS data intrinsic to the HAZUS model is in a specified format. The Eglin AFB real property data obtained from the DoD is in a different format. Building types, construction techniques and building uses are classified using a different scheme making it impossible to replace the GBS with DoD property data without making assumptions about the actual buildings at the base. Contact with researchers from the Army Corps of Engineers, including Jose Rullan-Rodriguez of ERDC-GSL-MS, indicates that they have encountered similar issues with trying to create a building inventory for naval facilities in Virginia. Their method of creating a building inventory could be applied to EAFB, with considerable effort and data input.

Data in the SDSFIE format, together with a tool called SDSFIE Geobuilder might allow definitions of all the occupancy types in the data set. Geobuilder is a customized application developed by Gulf Engineers and Consultants, Baton Rouge, LA.

According to Steven Ward, of Gulf Engineers and Consultants, this should be searchable in the domains tab of the tool. Once the user identifies the occupancy types of the structures in question, he would then need to make a subjective call as to which one they match in the HAZUS occupancy type class. Once that relationship is identified, the user would then be able to import this information into HAZUS using the Comprehensive Data Management System (CDMS). Due to the complexity of this process, carrying out the analysis was deemed beyond the scope of this project. It should, however, be attempted on a prototype basis.

4.2.4.2. Wind Losses. First a comparison is made between landfall wind speed, peak gusts, and wind-damage loss estimates for the 1975 Eloise and a storm similar to Eloise occurring in 2100. The difference in landfall wind speed amounts to an increase of only 0.6%, however the peak census tract wind speed increases by 3.9%. This increase in wind speed results in a 45% increase in total wind-loss damage across the region. The amplification of wind speed increases by approximately an order of magnitude is higher than the five-fold amplification based on historical hurricane winds and damage in the United States. The greater damage might be a manifestation of the relative differences in housing construction for this part of Florida compared with elsewhere, especially the Northeast.

Statistical models of loss estimates for contemporary and future hurricanes are compared in Figure 4.2.10. The loss curve using the historical hurricanes (contemporary) is in black. All dollar amounts are normalized to the year 2006. The values are transformed to the common logarithm (log base 10) of dollar amounts. The loss curve for future hurricanes is in blue and it is based on the wind speed model of the previous section. Both the contemporary and future loss model use a threshold of $5 million for the minimum loss event. No adjustment is made for future inflation, wealth, or building stock.

As expected, the probability of future losses is higher, but particularly for the largest loss events. For annual exceedance probabilities less than 1 in 11 years, future losses are projected to be greater than contemporary losses, assuming all else remains the same. The 90% confidence band around the percent increase is based on running the loss model using winds estimated from the upper and lower values of the 95% confidence limits on the nonlinear trend line of wind speed as a function of SST and the upper and lower values of the 95% confidence limits on the trend is SST. The results show that if future projections of hurricane intensity are realized, coastal losses on the 1-in-100 year (1-in-500 year) storm will increase by 36% (52%) relative to today's losses making EAFB more vulnerable to future wind losses from the strongest hurricanes.

4.2.4.3. Storm Surge Losses. Damage loss estimates from future storm surge can be done in a similar way. Here it is necessary to add tides and projected increase in sea-level. Figure 4.2.11 shows the projected surge of a future hurricane Opal where the winds have been increased according to our model above and where the sea-level is 60 cm above today's height coming ashore at a projected high tide two feet above MSL. The scenario below models a significant storm surge on Santa Rosa Island. In fact, the Eglin portion of the island is almost totally inundated. The east side of the pass near Destin also experiences inundation, while the areas near the main base experience some minor flood inundation. The main base area is buffered by the

barrier island that bears the brunt of a storm surge and thus offering protection from storm events. However, in this scenario any military structures or infrastructure especially on the barrier island would undoubtedly be impacted by storm conditions like those modeled below. If IPCC SLR projections are considered possible and future storminess is expected to increase

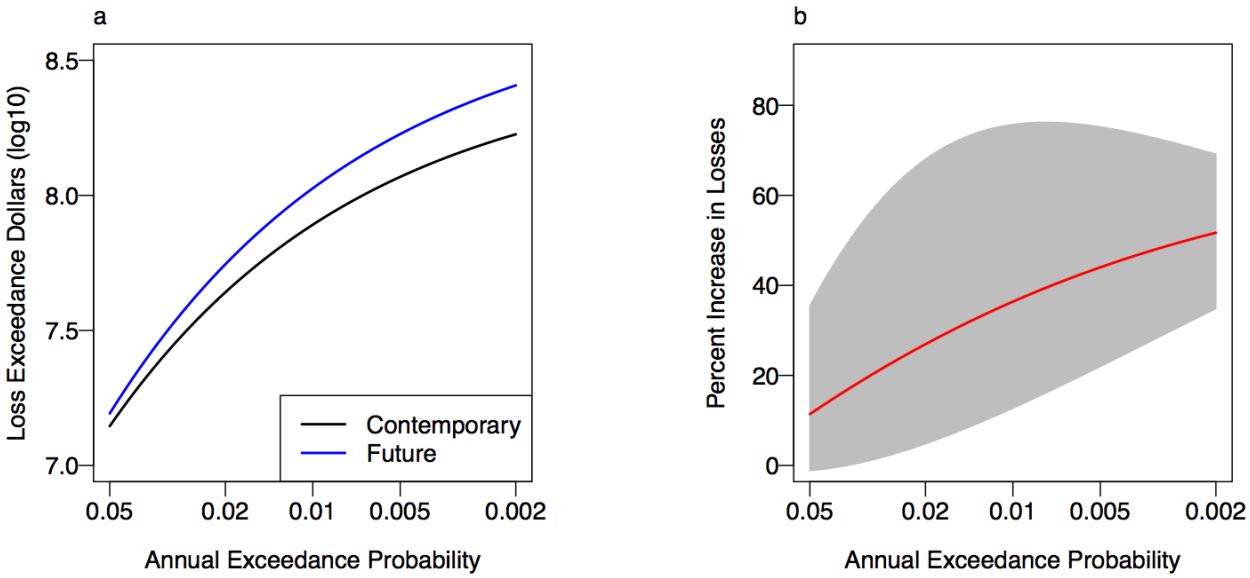

Figure 4.2.10. Modeled wind loss curves and percentage increase in losses. For the modeled loss curves (a), the black line represents loss exceedances based on the historical record of hurricanes affecting the two main census tracts in EAFB (contemporary losses) and the blue line represents loss exceedances based on our model for the same set of hurricanes but with intensities modeled on projected changes for storms in the Gulf of Mexico (future losses). The percentage increase in losses is displayed as a function of annual exceedance probability (log base 10 scale) (b). The gray region defines the 90% confidence band based on the estimated uncertainty of the change in wind speed as a function of SST and on the uncertainty on the trend in SST.

based on modeled changes in SST then the scenario depicted below is within the realm of future possibilities.

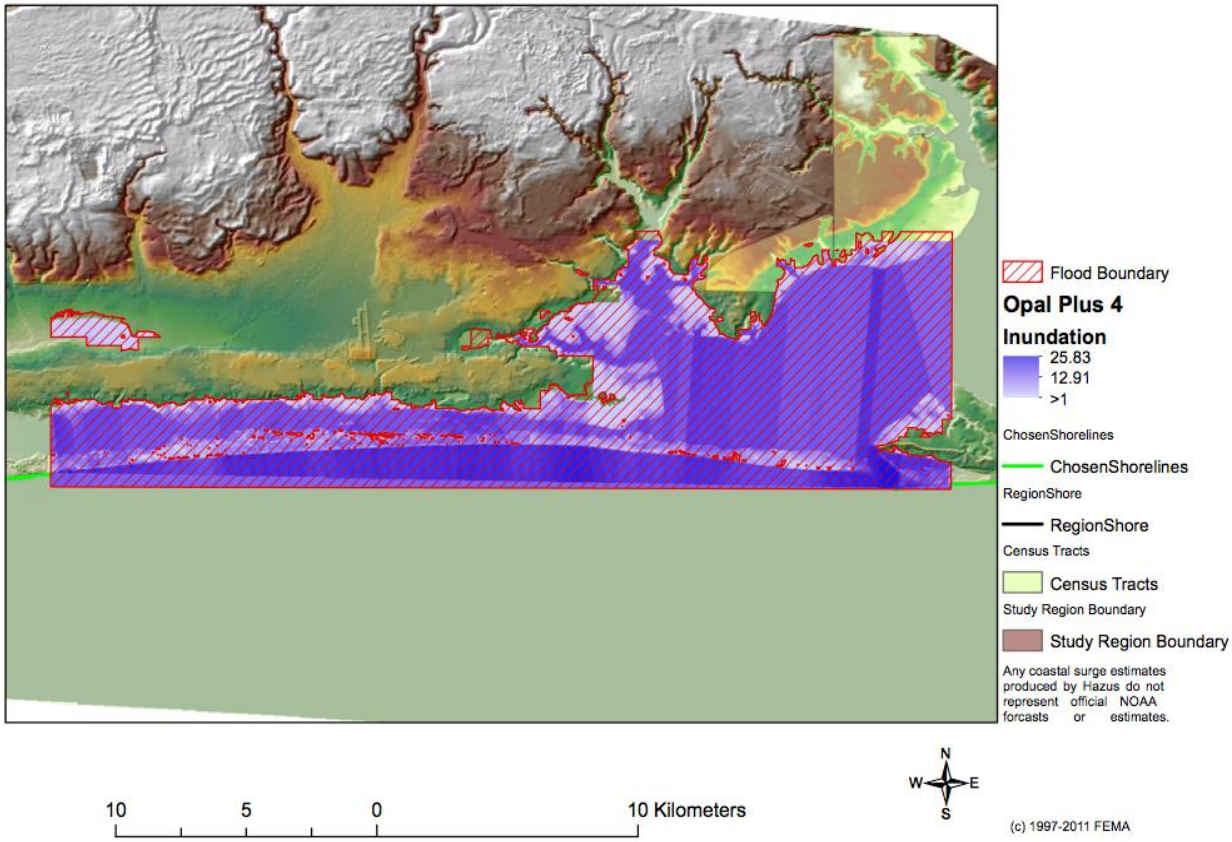

Figure 4.2.11. Future Hurricane Opal with stronger winds and higher sea level.

4.3. Analyzing Paleostorm History in Coastal Sediments

4.3.1. Lake Data. Western Lake (Figure 4.3.1) is approximately 0.2 km north of the Gulf of Mexico shoreline, located just landward of the foredunes. The lake surface has an elevation of approximately 0.75 m (Figure 4.3.2). Western Lake is divided into two parts, arranged east to west. The east side includes a natural slough, which opens up to the Gulf of Mexico when either lake levels become too high due to periods of intense rainfall, or hurricanes and related surge inundate the lake. The eastern portion of the lake, which is the most exposed to storm surge, has two possible areas which are subject to dune breach and inundation by storm surge: one to the south at approximately 2.3 m and one to the southeast at approximately 3 m. The storm surge associated with Hurricane Dennis, in 2005, caused a minor breach in the dunes south of the eastern portion of Western Lake, creating a small overwash fan (CBA, 2012).

The coastal dune lakes of Northwest Florida are typically closed to marine influence, and normally experience low salinity conditions. They are open to the sea through small, natural inlets following the impact of strong storms. As a result, the lake water can range from fresh to highly brackish, resulting in complex and diverse ecosystems during the transition periods. Long-term monitoring of the water quality shows that the lake conditions can vary between mesotrophic and oligotrophic nutrient conditions (Florida Lakewatch 2008; CBA, 2012). Total phosphorus levels over the past 15 years have ranged from 3 µg/L to 31 µg/L, with a mean value of 7.2 µg/L. Total nitrogen has ranged from 80 µg/L to 600 µg/L, with a mean value of 266 µg/L. Dissolved oxygen has ranged from 0.2 mg/L to 17.3 mg/L, with a mean value of 5.4 mg/L. pH levels ranged up to 8.4, with a mean pH of 7.2. The salinity in Western Lake has

varied from fresh (1.0 ppt) to nearly marine (24.8 ppt), with a mean value of 11.1 ppt, and has been largely dependent on the amount of saltwater inundation experienced during storm events and precipitation received by the lake.

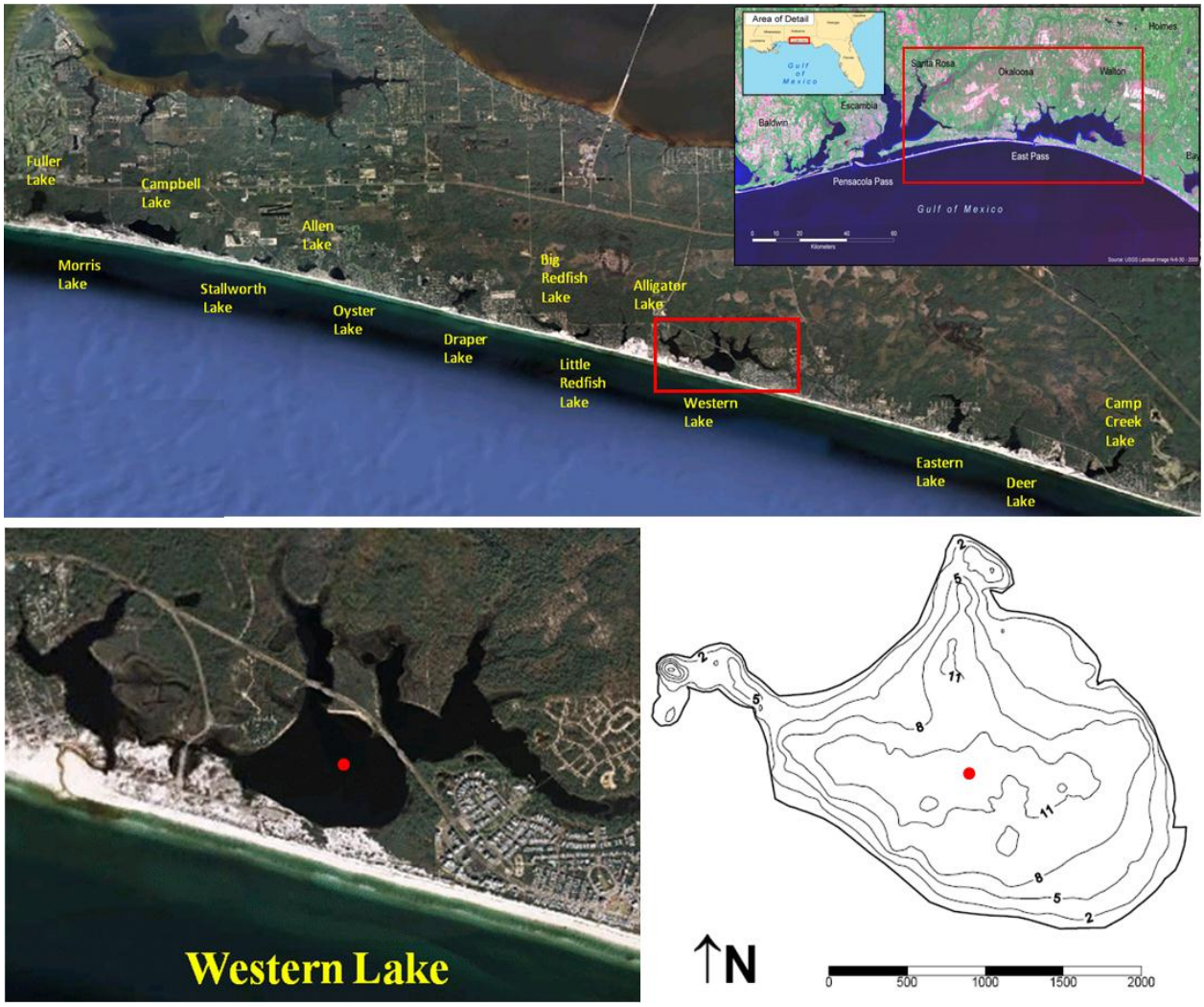

Figure 4.3.1. Location map of Western Lake, on the NW Florida coast. The upper figure shows all of the coastal dune lakes of NW Florida. The lower figures show an image and a bathymetric map (contours in feet) of Western Lake. Inset map from Choctawhatchee Basin Alliance. Red circle indicates core location. Image source: Google Earth.

4.3.2. Core Description. Several sediment cores were collected from the coastal lakes of the EAFB region. The sediment core selected for intensive paleostorm analyses, core 070910-03, was collected in approximately 3 meters water depth from Western Lake, FL. Core location is shown in Figure 4.3.1. An x-radiograph of the core is shown in Figure 4.3.3. The original length of the core was 131.4 cm. The upper 10 cm consisted of fluid mud. The muddy texture was dominant throughout the core. Horizontal laminations were visible throughout the core, indicating minimal bioturbation. The sand laminae are exceptionally clear in the core x-radiograph, providing good evidence that there was minimal bioturbation in the core.

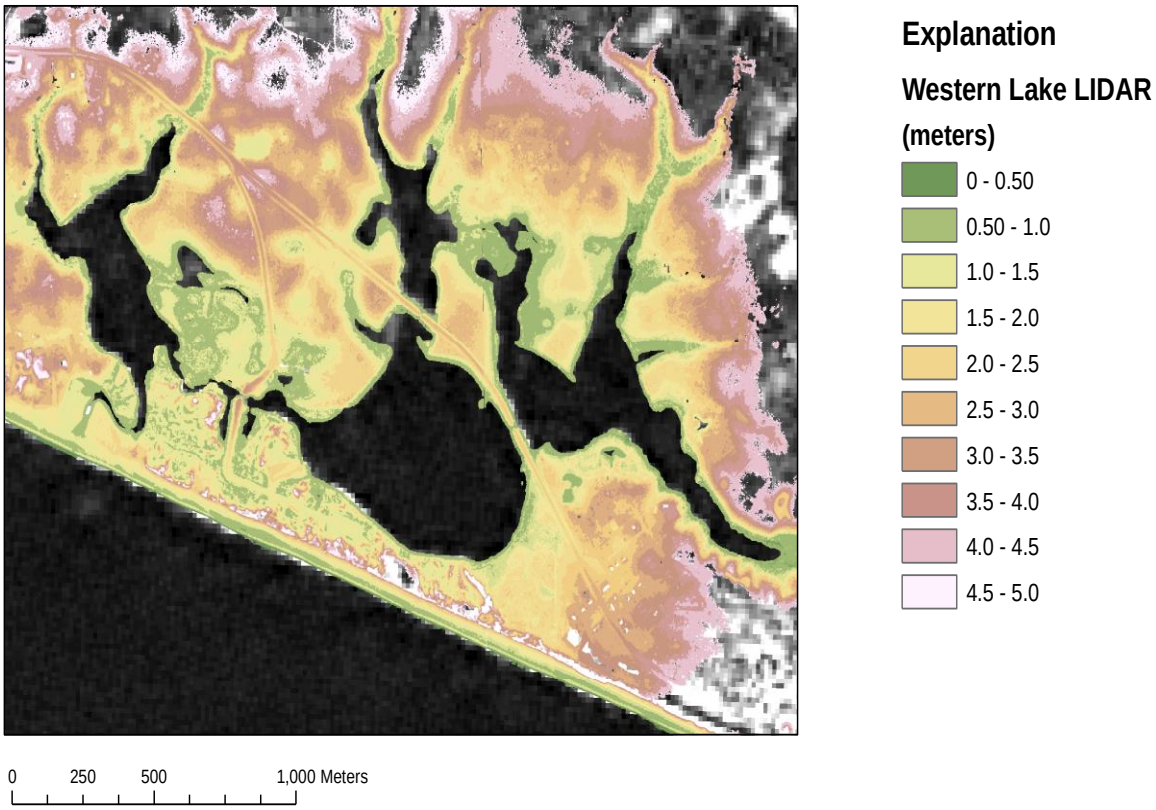

Figure 4.3.2. LIDAR imagery of the Western Lake area, NW Florida. Location is shown in Figure 4.3.1. Elevations are in meters.

4.3.3. Sedimentologic and Isotopic Data. Organic geochemical proxies (OGP) have been analyzed (including $\delta^{13}C$, $\delta^{15}N$, C/N, %C, %N) in sediment cores from two coastal lakes (Western Lake and Eastern Lake) in the study area. In order to better understand the isotopic signatures of the lake sediments, we have analyzed the isotopic signatures of various potential sources that contribute organic matter to the lake. As shown in Figure 4.3.4, organic matter of marine origin typically has high $\delta^{13}C$ and $\delta^{15}N$ values and low C/N values compared to terrestrial organic matter in the study area. Thus, a positive shift in $\delta^{15}N$ of lake sedimentary organic matter, if concurrent with a positive shift in $\delta^{13}C$ and a negative shift in C/N, can be interpreted as indicating seawater flooding or an overwash event (Figure 4.3.4, Das et al., in review).

The primary isotopic and sedimentologic variables of interest are those which comprise the storm identification model (Figure 4.3.3): percent sand, %N′, and $\delta^{13}C$. The values for percent sand ranged from 7.3 % to 69.5 %, with a mean value of 37.1 %. There are 24 peaks above the mean value, 19 of which exceed + 1 standard deviation, and 5 of which exceed + 2 standard deviations. The $\delta^{13}C$ values ranged from -26.2‰ to -23.1‰, with a mean value of - 24.4‰. There were significant shifts both in the positive and negative directions. The %N′, the first derivative of %N, ranged from - 0.2% to 0.2%, with a mean value of 0.0%.

In addition to the 19 significant peaks identified in the percent sand profile, the x-radiograph (Figure 4.3.3) showed 14 sand laminae, representing potential storm events. Two relatively thick sand layers can be discerned in the core, in addition to approximately twelve thinner laminate.

The majority of the peaks in the percent sand profile correspond to sand layers visible in the x-radiograph.

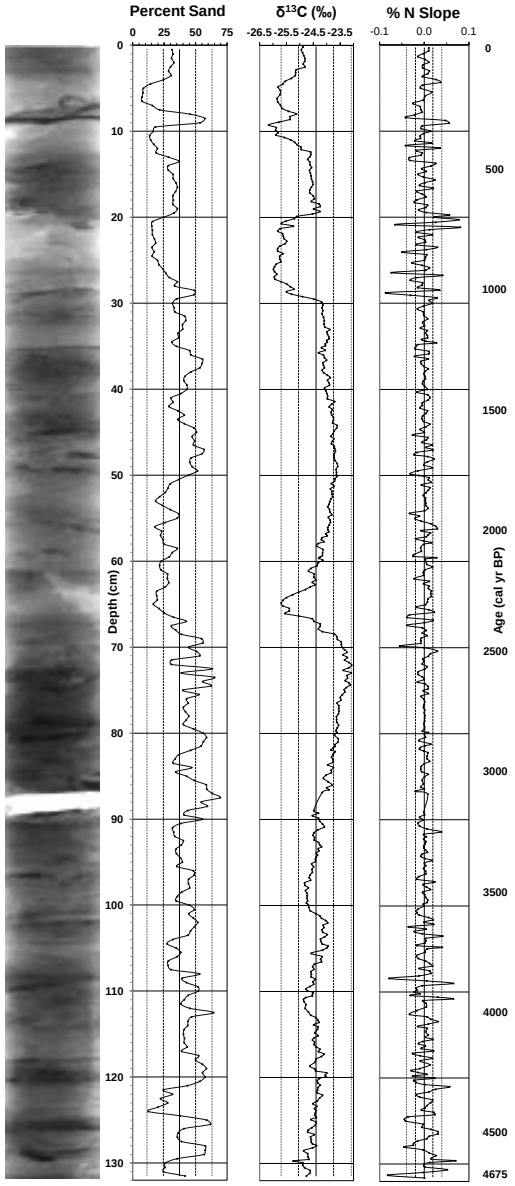

Figure 4.3.3. (From left) x-radiograph, and profiles of percent sand, $\delta^{13}C$, and % N' for core 070910-03. Depth in core is shown in cm on the left vertical axis. Age, based on radiocarbon time-depth model, is shown on the right vertical axis. "Storm" events typically have percent sand and $\delta^{13}C$ values above the mean. The solid vertical lines represent the mean of each data set. Dashed vertical lines represent ± 1 standard deviation. Dashed vertical lines represent ± 2 standard deviation. Core location is shown in Figure 4.3.1.

4.3.4. Micropaleontological Data. Samples were collected from 14 sand layers within core 070910-03: 7-9 cm, 35-36 cm, 48-49 cm, 55-56 cm, 69 cm, 74 cm, 79 cm, 81 cm, 84 cm, 86 cm, 89 cm, 96 cm, 117-118 cm, and 128-129 cm. Once collected, the samples were dried and subjected to microscopic analysis for the presence of foraminifera. The majority of the sand samples were shown to be barren. However, the sample collected at 79 cm had 12 *Ammonia sp.*

individuals and various small molluscan fragments that could not be identified. Other samples also had molluscan fragments, some of which appeared to be the bivalve *Rangia sp.*

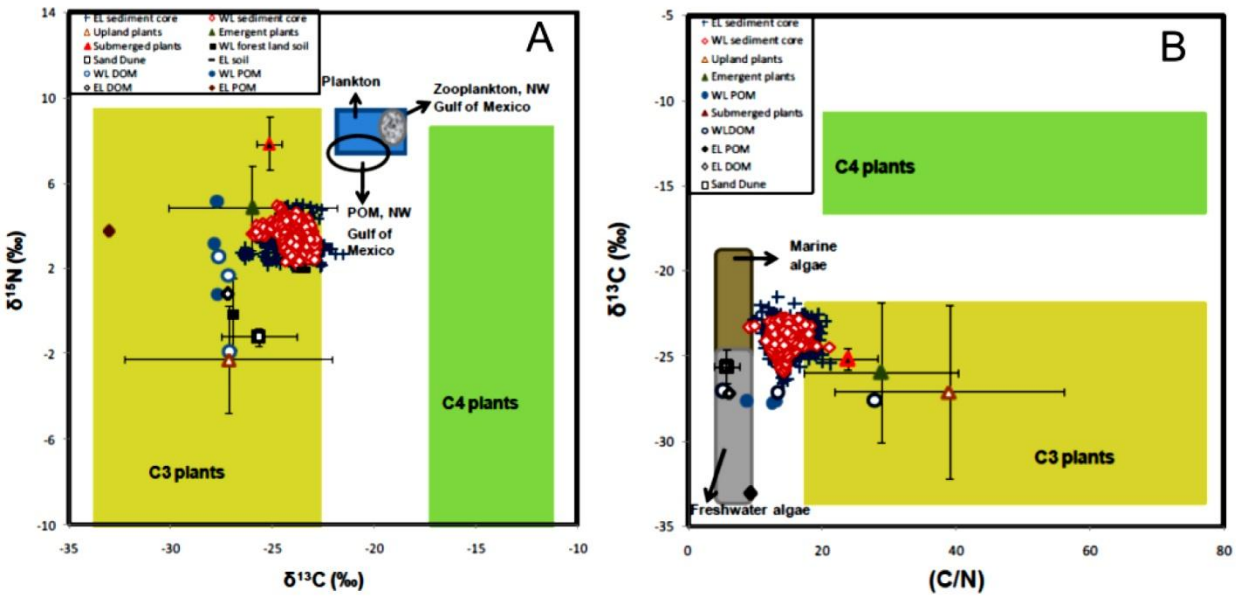

Figure 4.3.4. (A) Comparison of $\delta^{13}C$ and $\delta^{15}N$ values of organic matter in lake sediment, POM and DOM the study area, with the mean $\delta^{13}C$ and $\delta^{15}N$ values of plants and soil in the lake watershed, as well as the typical range of marine and terrestrial plants and organics (Macko et al, 1984). **(B)** Comparison of $\delta^{13}C$ and C/N values of organic matter in lake sediment, POM and DOM with the mean $\delta^{13}C$ and mean C/N values of plants and soil in the lake watershed as well as the typical values of marine and terrestrial plants and organics (Meyers, 1994; Lamb et al., 2006).

Rangia cuneata, the most common Rangia species in the region, is native to the coastal waters of the northern Gulf of Mexico (LaSelle and de la Cruz, 1985). *Rangia cuneata* inhabits low salinity estuarine habitats, making it an indicator of brackish or estuarine environments, (Parker, 1966). It is most commonly found in areas with salinities from 5-15 ppt (Swingle and Bland, 1974). Similarly, *Ammonia parkinsoniana*, a common form of *Ammonia sp.* found in the northern Gulf of Mexico, represents a primarily brackish to estuarine environment, typical of the mid-region and mouth of an estuary (Puckett, 1992). Although none of the samples appear to be strictly marine, they do all appear to represent bay/estuarine conditions, suggesting that water from the Gulf of Mexico has entered Western Lake, most likely during inundation during storm events.

4.3.5. Geochronology. Samples for radiocarbon dating were collected from 9 cm, 36 cm, 75 cm, 88 cm, and 127 cm depths in the core. The radiocarbon dates were converted using the CALIB 6.0 calibration scheme (Stuvier et al., 2012). An additional surface skim sample was collected from the sediment/water interface to determine the reservoir age of the lake. The raw radiocarbon date for the surface sample, 230 +/- 15 yr BP, was taken as the reservoir age, which was used in calibrating the samples. The raw and calibrated dates are shown in Table 4.3.1. A time-depth curve is shown in Figure 4.3.5.

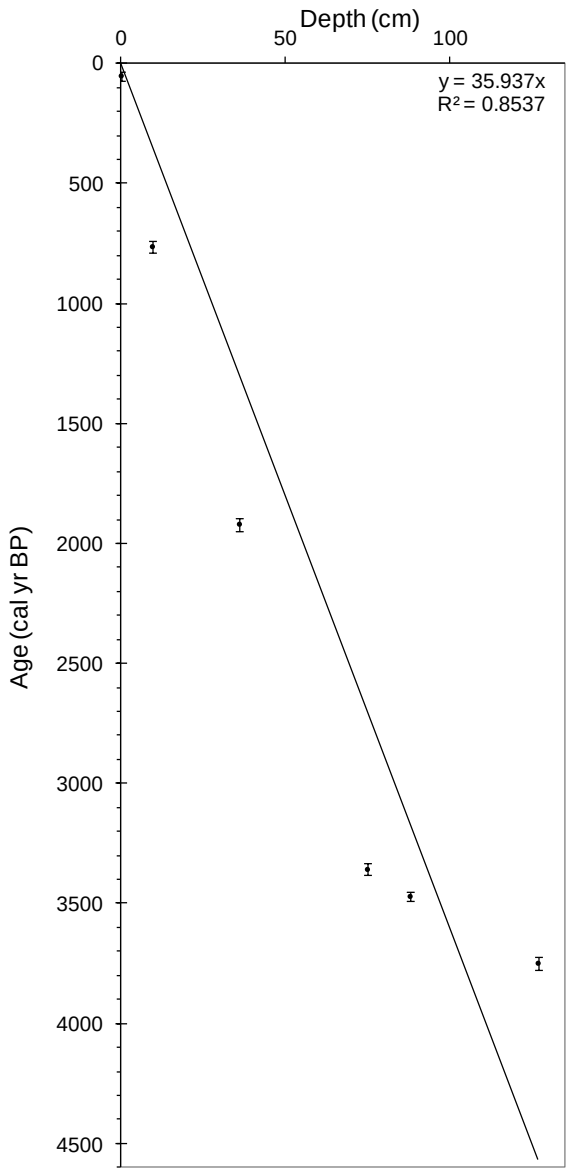

Figure 4.3.5. The time-depth curve derived from the radiocarbon dates from Core 070910-03. The vertical error bars represent the one-sigma range of the calibrated radiocarbon dates.

Table 4.3.1. Radiocarbon data for Western Lake core.

Lab Number	Depth in core (cm)	Radiocarbon Date	
		(yr BP)	(cal yr BP)
OS-83029	0	230 ± 15	52 ± 20
OS-83030	9.5	1020 ± 20	764 ± 24
OS-83031	36	2120 ± 20	1920 ± 28
OS-83032	75	3270 ± 25	3359 ± 25
OS-83033	88	3410 ± 25	3471 ± 20
OS-83034	127	3630 ± 25	3750 ± 29

4.3.6. Storm Surge Heights from SLOSH. The NOAA/NWS SLOSH model was used to estimate storm surge elevation for historic storms. SLOSH was run using the regional historic hurricane tracks and other pertinent data from the HURDAT database, as shown in Table 3.3.1, in order to estimate the surge values in the vicinity of Western Lake for storms of known magnitude (NOAA, 2012b). SLOSH input parameters for the fourteen landfalling storms in this study are listed in Table 3.3.1, along with the modeled surge height data. Hurricane Opal (1995), a Category 3 storm when passing closest to Western Lake, had the largest modeled surge of 2.7 meters. The calculated surge associated with Category 3 storms ranged from 0 to 2.7 meters.

Hurricane Opal (1995) had the largest surge of 2.7 m. While Opal was a category 4 storm; at its most intense, it was a category 3 storm when it passed closest to Western Lake. None of the lesser storms produced enough surge to overtop the dunes that front the lake. The LIDAR topographic data show that the lowest point on the barrier dunes seaward of the lake is 2.3 meters (Figure 4.3.2). The historic storm data, indicate that a major (cat. 3 or greater) storm would be necessary to breach the dunes and inundate the lake. The paleostorm model results, therefore, may be taken to represent the impact of major storms on the lake.

4.3.7. Storm Model Results. A storm event, as identified by the storm model, typically exhibits percent sand and $\delta^{13}C$ values above the mean, and a neutral %N′ value. Other studies have also shown storm signals corresponding to $\delta^{13}C$ values significantly above the mean, indicating inundation with marine water, enriched in the heavier isotope. Storm signals are also occasionally represented by negative excursions in $\delta^{13}C$ values, which are interpreted as inundation events caused by heavy rainfall and coastal flooding, rather than marine surge (Lambert, 2003; Lambert et al., 2008).

In the Western Lake core, the result after each inundation event resulted in a period of enhanced productivity in the lake, and a marine/estuarine geochemical signature in the lake sediments for a brief period. The paleostorm model described above was applied to the Western Lake data. The model resulted in 53 peaks above the cutoff probability during the last five millennia (Figure 4.3.6).

4.3.7.1. Storm Identification and Storm Frequency. The storm model identified 53 separate segments in the core record, each representing an anomalous geochemical environment in Western Lake over the last ~5000 years (Figure 4.3.6). This is taken to represent episodes when storm surge had inundated the relatively freshwater lake, altering the lake's chemistry for some period of time. It should be noted that some of these segments are broad, indicating an extended period during which the lake chemistry remained out of equilibrium.

On average, each 3-mm sample collected for isotopic analysis represented approximately 11 years of lake history (Figure 4.3.3). An autocorrelation analysis showed each successive sediment sample to be statistically independent. Among the 439 original samples, 229 lie under the 53 anomalous segments. It is reasonable to conclude, therefore, that the model has identified a minimum of 229 storm events over the approximately 5000-year lake history represented by the core.

4.3.7.2. Paleostorm Return Periods and Cycles. The return period, and therefore the number of storm events per century, was determined for the 53 storm-influenced segments identified from the storm model (Coor, et al., submitted), as shown in Figure 4.3.7. Samples which

exceeded the 50% cutoff interval, resulting in one of the 53 storm-influenced segments, was assigned a value of 1, given that the model predicts a high probability that at least 1 storm occurred during the approximately 11 years represented by the sampling resolution. Samples which did not exceed the 50% cutoff interval were assigned a value of 0, given that the model predicts a low probability of a storm having occurred during the period represented by the sample. The resulting minimum number of storms was summed and normalized per century.

Of the 53 segments that did exceed the cutoff frequency, four distinct periods are visible, demonstrating a cyclicity in relative storminess over time. The first active period observed, from approximately 4800 to 4400 cal yr BP, exhibiting a mean of 6.6 storms per century, ranging from 4 to 10 storms per century. The second period, lasting from approximately 4100 to 3200 cal yr BP, averaged 5.8 storms per century, ranging from 4 to 8 storms per century. The third period, from approximately 2500 to 1800 cal yr BP, shows a slightly shorter return period with mean of 7.6 storms per century, ranging from 4 to 9 storms per century. The fourth period, ranging from approximately 1300 cal yr BP to the present, exhibits a mean of 7.4 storms per century, ranging from 3 to 10 storms per century. The overall mean for active storm periods is 6.9 storm events per century, while the overall mean over the 5 millennia is 5.0 storm events per century. Three inactive periods of several centuries duration separate the four periods of higher storm activity.

The model results can be viewed in the larger context of the northern Gulf of Mexico during the latter half of the Holocene. Hodell et al., (1991) noted that orbital changes have resulted in solar insolation for 10 degrees north latitude reaching a modern peak at about 7 ka and decreasing up to the present. Poore et al., (2003) analyzed high-resolution faunal and isotope data for two cores from the northern and western Gulf of Mexico. They concluded that, based on proxy evidence, sea surface temperature (SST) in the Gulf has decreased since the mid-Holocene. This would result in a southward movement of the Intertropical Convergence Zone (ITCZ), a decrease in the influence of easterly winds, and less incursion of warm surface waters into the Gulf of Mexico (Poore et al., 2003). Poore et al., (2003) also found evidence of century-scale variability in climate proxy date for the Gulf of Mexico, especially for the period from 7 to 2.5 yr BP. The modeled data also exhibit century-scale variability in storminess. The model results (Figure 4.3.7) reflect stability in the level of storminess over the past 5000 years, which is reflected in the similarity between the historic mean number of storms per century, 6.2, and the long-term mean of storms per century during the “active” periods, 6.9, both of which are higher than the overall long-term mean of 5.0 storms per century. The results, therefore, appear to be consistent with Wallace and Anderson’s (2010) finding of relative stability of climate in the Gulf of Mexico during the late Holocene.

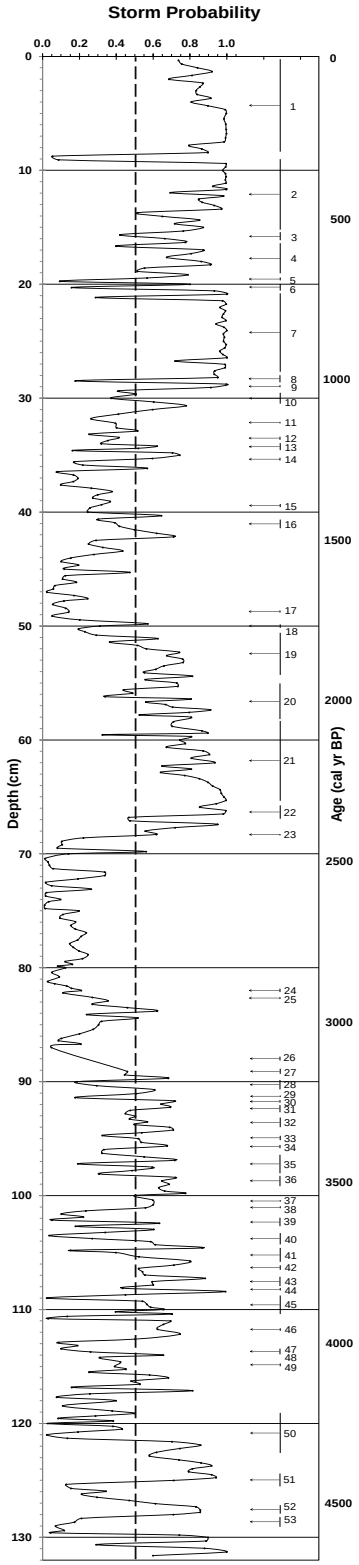

Figure 4.3.6. Results of the storm model applied to the Western Lake core data. The horizontal axis shows the probability of a storm event, where 0 represents the minimum chance of a storm having occurred and 1 represents maximum probability of storm occurrence. The 0.50 probability cutoff is shown by the dashed line. The left vertical axis depicts depth in core, in cm, and the right vertical axis represents time, as derived from the radiocarbon time-depth model. Horizontal arrows indicate the 53 storm activity episodes identified by the model.

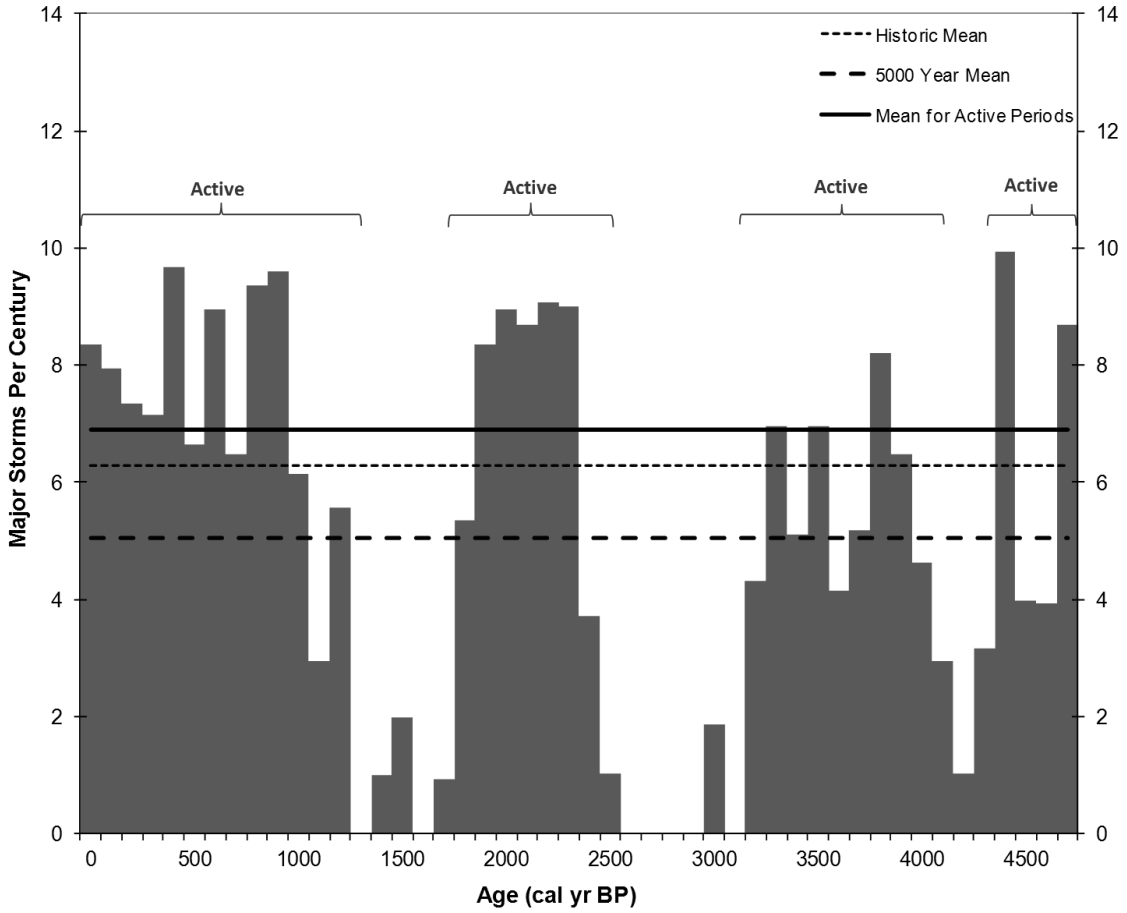

Figure 4.3.7. Major storm history for the northwest Florida coast, based on the paleostorm model. The minimum value for storm occurrence per century is shown for the past five millennia. Four periods of increased activity are separated by shorter periods of low activity. An active period is defined as one averaging 4 or more major storms per century. The mean of the active periods is indicated by the solid black line. The historic mean for the past ~150 years is shown by the dotted line. The overall mean over the last five millennia is indicated by the heavy dashed line.

4.4. Modeling Coastal Wetlands

The wetland system that is the focus of this study is located at the mouth of the Yellow River and an adjacent embayment (Catfish Basin). This area is the most extensive wetland associated with Eglin Air Force Base (Figure 4.4.1). The wetlands are associated with the multi-distributary delta of the Yellow River. The aerial extent of the wetlands at this location, excluding estuarine open water, is approximately 2500 hectares (Table 4.4.1). Freshwater swamps and marsh make up approximately 60 percent of the wetlands. Tidal marsh and tidal swamps comprise approximately 30 percent of the wetland area. The remaining wetland environments have very limited total areas.

4.4.1. SLAMM Modeling. The parameters used in SLAMM modeling (Table 3.4.1) are modified from the Warren Pinnacle (2011a) SLAMM study of the Choctawhatchee Bay marsh system, located 85 kilometers east of Yellow River (Figure 3.4.3). Modifications of the

Choctawhatchee parameters include a higher historical trend for sea-level change (2.1 mm/yr) and MHW (0.309 meters). As noted in the Warren Pinnacle (2011a) study, site-specific sediment accretion values are not available for the northwest Florida coast. Surface Elevation Table (SET) sedimentation measurements are available from estuary systems located along the Florida Big Bend and sediment accumulation rates for rivers similar to the Yellow and Choctawhatchee Rivers were used in Warren Pinnacle study. These values are incorporated into the SLAMM parameters used for his study. Northwest Florida Water Management District (NFWMD) – FEMA Lidar data, flown in 2006, was used for elevation component of the SLAMM model. Estimated vertical accuracy of the lidar data is 15 centimeters. Wetland classification is based upon the latest (1990) National Wetland Inventory (NWI) dataset. The 1990 data was used as the base for the 2000 SLAMM initial layer.

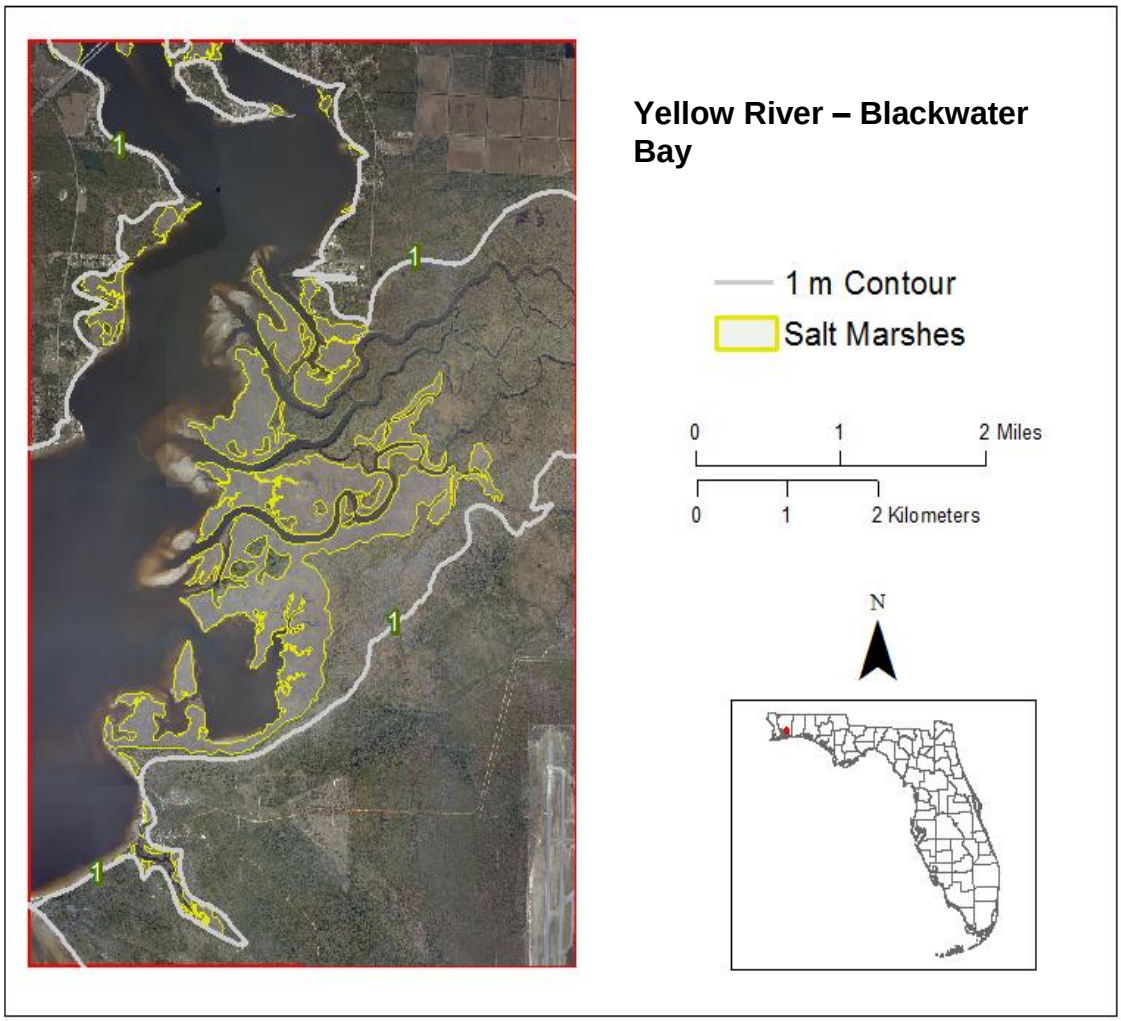

Figure 4.4.1. Digital orthophoto mosaic of the Yellow River, Blackwater Bay and Catfish Basin salt marsh estuary system. The one meter contour, represent the maximum sea level value used for the SLAMM model is shown as a gray line. Eglin Air Force Basin Auxiliary Field 10 is in the lower right-hand portion of the image.

Table 4.4.1. Predicted change in wetland habitats associated with a one-meter sea level rise (2000-2100) for Yellow River delta and adjacent Catfish Basin, Santa Rosa County, Florida.

Habitat	2000	2025	2050	2075	2100
Swamp	1290.36	1240.96	1057.23	884.29	818.16
Cypress Swamp	1.98	1.98	1.97	1.41	0.75
Inland Fresh Marsh	232.24	231.64	226.08	216.91	213.06
Tidal Fresh Marsh	3.79	3.74	3.53	3.18	2.85
Transitional Salt Marsh	48.48	50.01	189.29	182.63	71
Regularly Flooded Marsh	159.08	450.97	176.71	228.96	235.91
Mangrove	13.84	13.84	12.26	5.36	1.05
Estuarine Beach	0.57	0.57	0.52	0.39	0.25
Tidal Flat	2	58.37	475.47	363.04	225.53
Inland Open Water	16.57	16.56	11.94	11.47	11.11
Riverine Tidal	20.09	19.08	9.89	8.74	7.23
Estuarine Open Water	1544.67	1550.39	1581.7	1879.45	2251.81
Irregularly Flooded Marsh	394.66	108.69	39.67	53.28	57.01
Tidal Swamp	349.1	328.63	289.18	236.32	179.7
Note: Values are reported in hectares. Modeling calculations utilize SLAMM6.					

4.4.2. Results – Yellow River. The SLAMM modeling results for a one meter rise in sea level between the periods 2000 and 2100 is presented in Table 4.4.1 and Figures 4.4.2 and 4.4.3.

The areal changes for different wetland types are presented on a logarithmic scale in Figure 4.4.2. The log scale is used in order to emphasize changes in tidally-influenced habitats, which have limited total areas. The most noteworthy change in the different wetland classes is the dramatic increase in the area of tidal flats (from "0" to 226 hectares) and regularly flooded marsh (+77 hectares) and the prominent decrease in the extent of irregularly flooded marsh (-338 hectares). The dramatic development of the tidal flat environment, from zero in 2000 to 226 hectares in 2100 may be an artifact of the SLAMM modeling algorithms. The Yellow River delta has well-developed, deep channels suggesting that sediment may be carried further offshore rather than forming a tidal flat near the delta mouth. Swamp areas have decreased approximately 472 hectares or approximately 35 percent, probably due to conversion to marsh environments (Figure 4.4.3). Some locations have been completely converted to estuarine open water. The best example of this is the complete flooding of the Catfish Basin, shown in the lower, southwest corner of the maps in Figure 4.4.2. SLAMM models for ICCP A1B Max (0.69 meters) and a two meter sea level change are presented in Tables 4.4.2 and 4.4.3. For the two-meter sea-level rise scenario tidal flat areas reach very high values (~700 hectares).

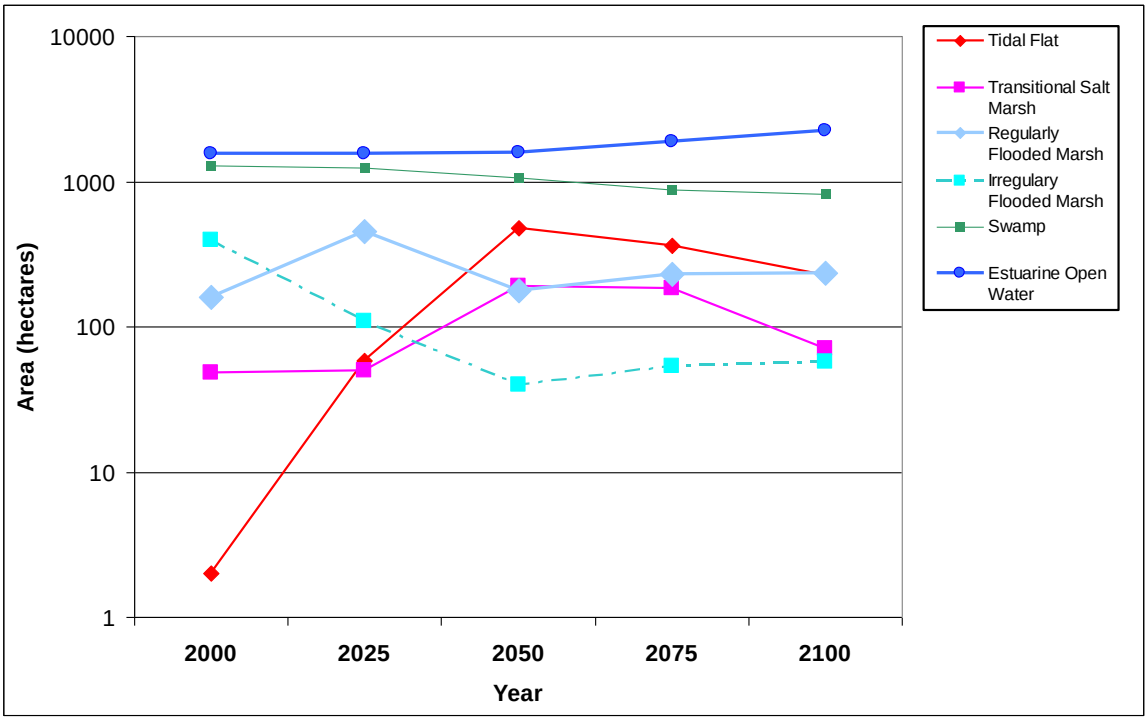

Figure 4.4.2. Change in the area of wetland habitats for the Yellow River delta and adjacent Catfish Basin between 2000 and 2100. Minor habitats have been omitted from the graph.

Table 4.4.2. Predicted change in wetland habitats associated with a 0.69-meter sea level rise (IPCC A-1B maximum scenario) for Yellow River delta and adjacent Catfish Basin, Santa Rosa County, Florida for the time period 2000-2100.

Habitat	2000	2025	2050	2075	2100
Swamp	1290.4	1139.8	864.7	736.4	579.0
Cypress Swamp	2.0	2.0	1.2	0.4	0.1
Inland Fresh Marsh	232.2	226.3	213.9	209.6	202.3
Tidal Fresh Marsh	3.8	3.5	2.9	2.2	1.5
Transitional Salt Marsh	48.5	156.5	287.4	133.4	165.9
Regularly Flooded Marsh	159.1	466.5	202.3	372.1	244.6
Mangrove	13.8	8.1	0.0	0.0	0.0
Estuarine Beach	0.6	0.5	0.2	0.0	0.0
Tidal Flat	0.0	130.9	455.3	195.3	364.7
Inland Open Water	16.6	16.5	11.5	11.0	10.6
Riverine Tidal	20.1	18.6	9.1	7.1	7.0
Estuarine Open Water	1544.7	1556.8	1722.7	2187.6	2389.9
Irregularly Flooded Marsh	394.7	45.8	84.6	111.2	54.4
Tidal Swamp	349.1	303.6	219.6	109.1	55.5
Note: Values are reported in hectares. Modeling calculations utilize SLAMM6.					

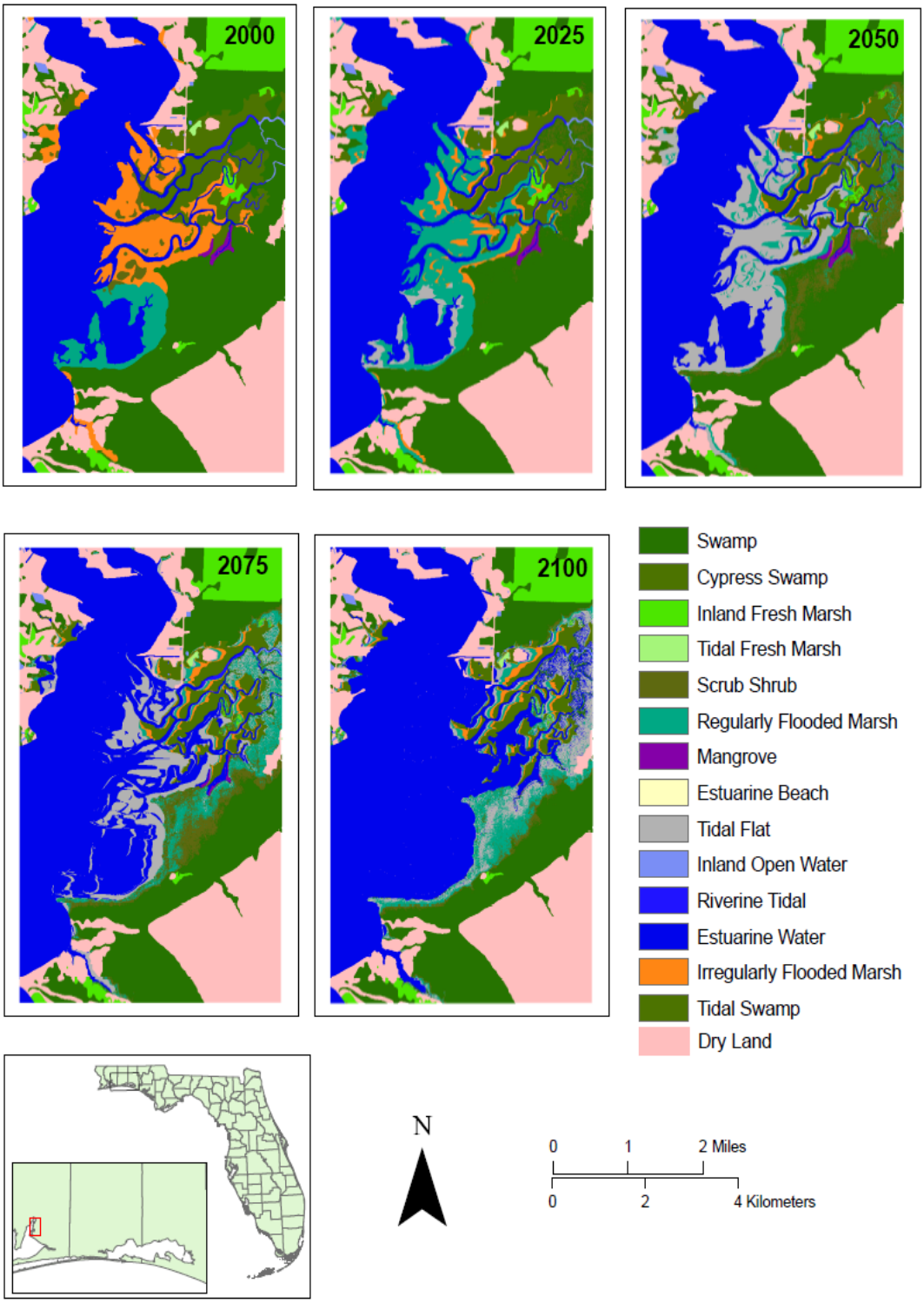

Figure 4.4.3. Change in wetland habitats for the Yellow River delta and adjacent Catfish Basin between the years 2000 and 21000. Habitat distribution based upon SLAMM 6 modeling.

Table 4.4.3. Predicted change in wetland habitats associated with a two-meter sea level rise (2000-2100 for Yellow River delta and adjacent Catfish Basin, Santa Rosa County, Florida.

Habitat	2000	2025	2050	2075	2100
Swamp	1290.4	1264.3	1151.7	989.4	879.2
Cypress Swamp	2.0	2.0	2.0	1.9	1.4
Inland Fresh Marsh	232.2	232.2	230.9	226.0	219.7
Tidal Fresh Marsh	3.8	3.8	3.7	3.5	3.3
Transitional Salt Marsh	48.5	26.1	114.0	167.5	117.4
Regularly Flooded Marsh	159.1	421.1	315.4	155.6	203.7
Mangrove	13.8	13.8	13.8	13.8	13.8
Estuarine Beach	0.6	0.6	0.6	0.6	0.5
Tidal Flat	0.0	26.7	300.5	587.8	701.3
Inland Open Water	16.6	16.6	12.2	11.7	11.5
Riverine Tidal	20.1	19.3	10.9	9.3	8.4
Estuarine Open Water	1544.7	1549.9	1576.8	1597.3	1640.1
Irregularly Flooded Marsh	394.7	162.7	33.0	36.2	37.9
Tidal Swamp	349.1	336.3	310.0	274.9	237.4
Note: Values are reported in hectares. Modeling calculations utilize SLAMM6.					

4.4.3. Results – Choctawhatchee Bay. Warren Pinnacle (2011a) recently completed a SLAMM study for the wetlands along the eastern portion of Choctawhatchee Bay (Figure 3.4.3). The total area of wetlands is approximately 98000 hectares, which is about 40 times the extent of wetlands in the Yellow River estuary system. In the Warren Pinnacle study a separate land cover database, the Florida Natural Areas Inventory (FNAI), was converted to NWI classification categories. For a one-meter sea-level rise scenario, the Choctawhatchee Bay wetlands SLAMM modeling produces results that are similar to the Yellow River system. Tidal flat area increases from 1202 hectares to 4682 hectares (Table 4.4.4), while transitional salt marsh increases from "0" to 7288 hectares in 2100. Irregularly flooded marsh decreases from 4431 to 2653 hectares, while regularly flooded marsh increases from "0" to 4903 hectares for the 100-year period. Estuarine open water shows a moderate increase in area, going from 63,749 to 69,065 hectares. There appears to be only modest loss of marsh habitat, with much of the change associated with conversion of one marsh type to a more water-dominated marsh habitat setting (Figures 4.4.4a and 4.4.4b).

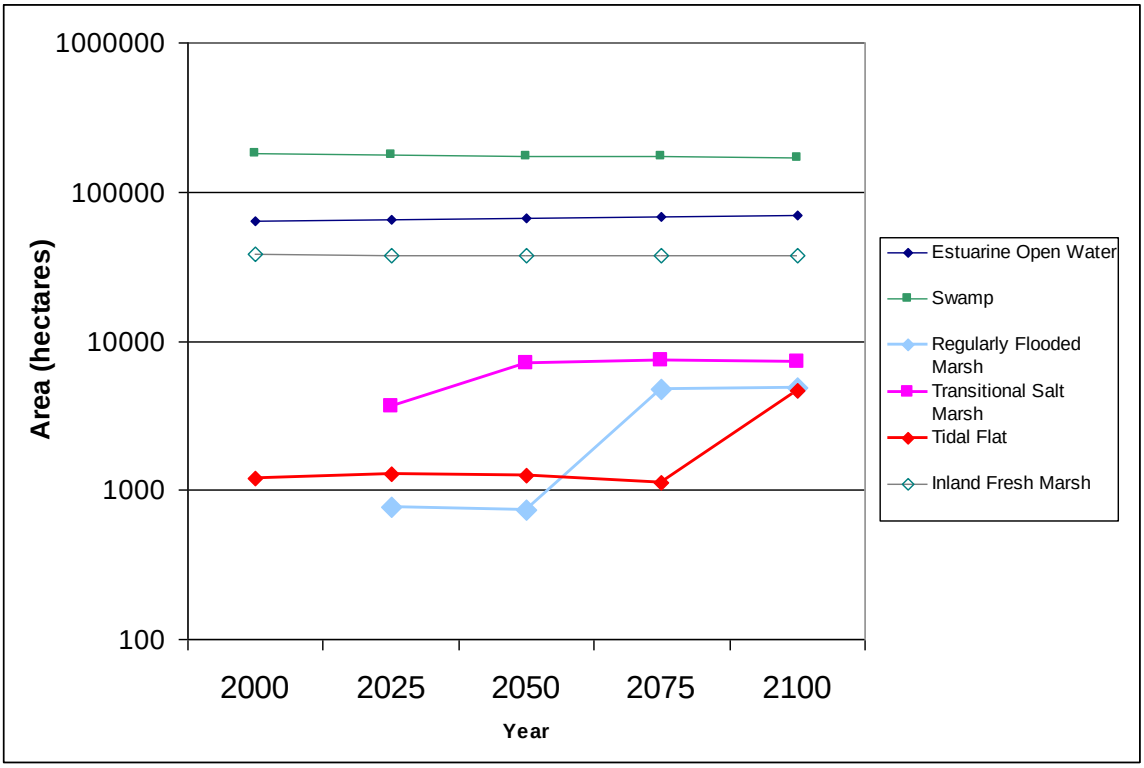

Figure 4.4.4a. Change in the area of wetland habitats for the Choctawhatchee Bay, Walton County, Florida for the period 2004-2100. Minor habitats have been omitted from the graph. Data from Warren Pinnacle (2011).

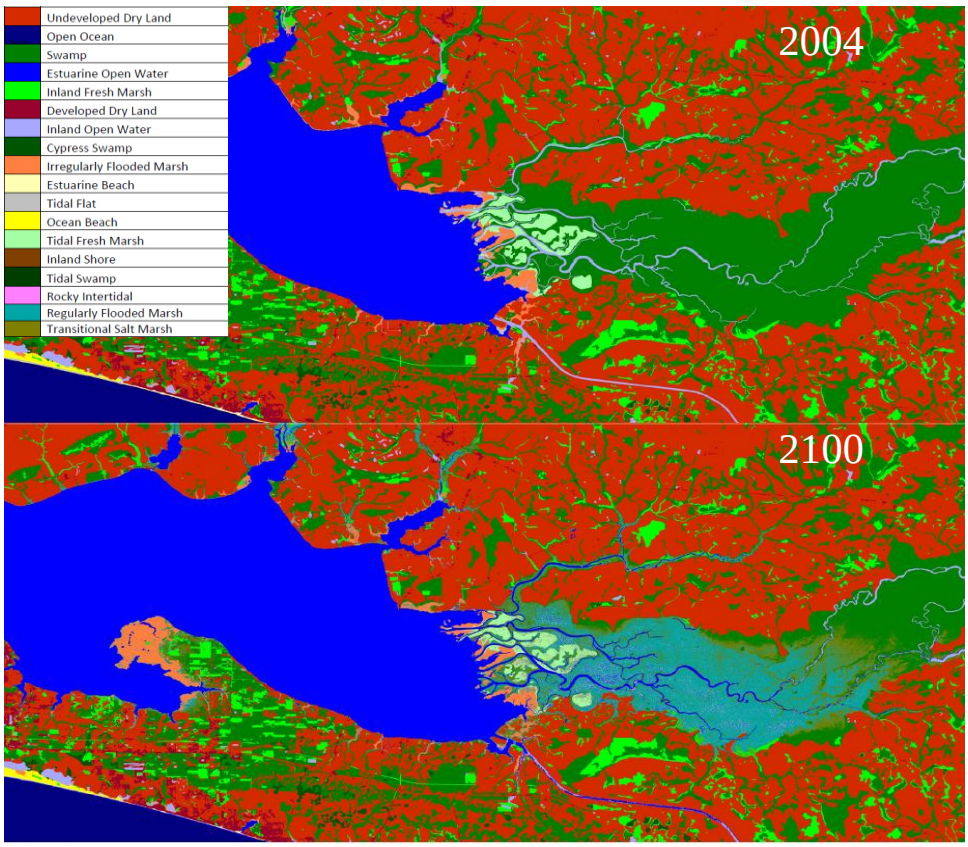

Figure 4.4.4b. Change in wetland habitats for the Choctawhatchee Bay, Walton County, Florida between the years 2004 and 2100. Habitat distribution based upon SLAMM 6 modeling. Data from Warren Pinnacle (2011).

Table 4.4.4. Predicted change in wetland habitats associated with a one-meter sea level rise (2000-2100 for Choctawhatchee Bay, Walton County, Florida.

Habitat	2004	2025	2050	2075	2100
Undeveloped Dry Land	675563.1	674645.8	673835.4	672499.3	670928.3
Open Ocean	565160.1	565167.4	565174.3	565193.7	565233.4
Swamp	180334.8	177375.4	174390.2	171551.9	169686.5
Estuarine Open Water	63749.4	65330.1	66401.0	67622.0	69064.7
Inland Fresh Marsh	38121.4	37775.6	37741.1	37580.8	37295.2
Developed Dry Land	26813.4	26761.2	26723.9	26630.4	26451.4
Inland Open Water	13359.3	12118.4	11828.8	11561.5	11340.0
Cypress Swamp	11415.7	11407.2	11396.7	11374.0	11330.7
Irregularly Flooded Marsh	4431.1	4061.7	3918.8	3449.4	2652.8
Estuarine Beach	1794.6	1632.2	1468.5	1334.5	1200.8
Tidal Flat	1201.6	1279.8	1262.8	1123.5	4681.8
Ocean Beach	774.4	769.9	772.7	803.9	853.3
Tidal Fresh Marsh	461.7	422.0	415.5	360.0	273.0
Inland Shore	5.7	5.7	5.7	5.7	5.7
Tidal Swamp	1.6	1.6	1.6	1.6	1.6
Rocky Intertidal	1.2	1.2	0.8	0.4	0.4
Regularly Flooded Marsh	0.0	777.6	735.9	4717.0	4902.9
Transitional Salt Marsh	0.0	3657.2	7115.9	7379.9	7288.4
Notes: Values are reported in hectares. Modeling calculations utilize SLAMM6. Data from Warren Pinnacle (2011a).					

4.4.4. Results – Eglin AFB Portion of Santa Rosa Island. At the present time, salt water marsh and tidal flats occupy on very minor portions of Santa Rosa Island. The narrow width of the island (0.5 kilometers), susceptibility of the island to storm surge overwash sediments and the maintenance of the Intracoastal Waterway navigation channel on the north side of the island, combine to limit the locations where back-barrier marshes can develop. The most extensive salt water marsh system on the Eglin Air Force Base segment of the island is a 40 hectare area located approximately 0.2 kilometers west of test site A-6, near the Fort Walton entrance to the base (Figure 4.4.5). At this location, the marsh area has been recently covered by overwash sediments from 1995-2005 hurricanes. The bay-facing side of the marsh is enclosed by dredging piles from the maintenance of the Intracoastal Waterway. Due to the complexities of these factors, SLAMM modeling was applied only in a reconnaissance manner to Santa Rosa Island.

Figure 4.4.5. Limited fresh and tidal marsh located on the north side of Santa Rosa Island. Eglin Air Force Base Test Site A-6 is located on the eastern portion of the aerial image.

4.4.5. Shoreline Orientation and Erosion. Current marsh erosion modeling in SLAMM assigns a fixed erosional rate (meters/year) for shorelines exposed to open water with a least nine kilometer of fetch. Measurements of shoreline erosion for the Yellow River delta for the period 1946-2007 suggest that erosional patterns may be more complex that what is currently utilized in the SLAMM model. In some portions the Catfish Basin erosion rates of up to one meter/year occur in a protected embayment with less than one kilometer of open water (Figure 4.4.6B). Projecting peninsulas are especially prone to differential erosion on the open-water side of the shore (Figure 4.4.6A). This effect may be important in some delta systems, which have "birdfoot" channels. Future versions of SLAMM may need to include the complex geometry of marshes into the modeling parameters for erosion.

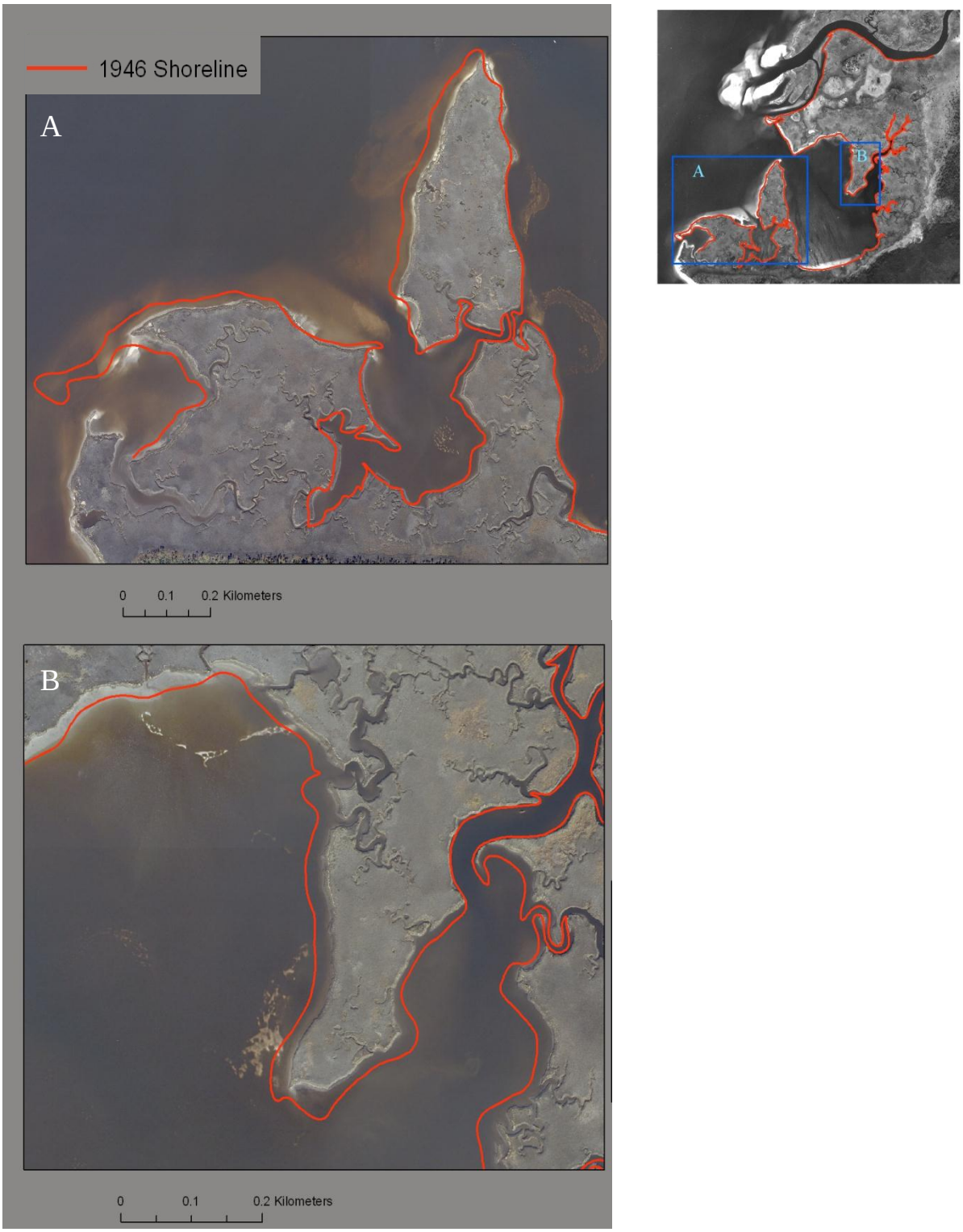

Figure 4.4.6. Variation in shoreline erosion in the Catfish Basin, located along the southern edge of the Yellow River delta. Image base is 2007 Florida DOT aerial orthophotograph. Red line is the 1946 shoreline derived from USDA – APFO air photographs. West-facing shorelines have undergone up to 50 meters of erosion (~ 1 meter/year). South- and east-facing shorelines have limited or no erosion during the same time period.

4.5. Modeling Coastal Groundwater

As noted in Section 3.5, the effects of the different future sea-level rise scenarios on both the major confined aquifers of the Eglin Air Force Base area and the surficial aquifers on the portion of the base on Santa Rosa Island were analyzed. The analysis was carried out using a set of numerical models that have been described in the previous report section. The results of these analyses are presented separately starting with consideration of the effects of future sea-level rise on the surficial aquifers.

4.5.1. Impacts of Sea-Level Rise on Unconfined Aquifers. A steady-state simulation for the unconfined system is established first to generate the initial conditions that existed prior to the sea level rise. Then, a transient groundwater flow and transport model is established to simulate saltwater and freshwater interface migration. Sea level rise is introduced into the model simulation by changing the parameter in the Cauchy boundary condition that represents the surface water level. Figure 4.5.1 is used to compare the current saltwater wedge with the predicted wedge in 2100 with sea-level rise. It is shown in the figure that the initial and final locations of saltwater wedge are distinctly different. The wedge has been moved toward inland about 10 meters, indicating that sea-level rise has significantly intruded into the surface aquifer system. This can be explained as that, under unconfined conditions, the sea-level rise would increase the saturated thickness the aquifer, so increase the hydraulic head of the saltwater. This increased pressure allows the wedge to penetrate further into the system, resulting in a new saltwater wedge location. The initial and final salt-wedge profile results indicate the initial salt wedge has been approximately raised by 4 m in vertical direction, similar to the level of sea level rise.

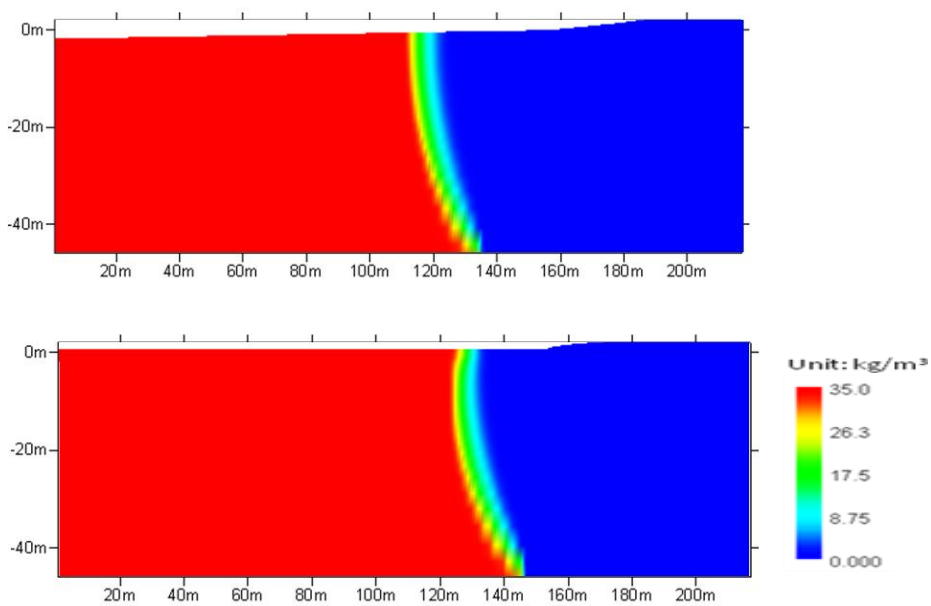

Figure 4.5.1. Comparison of steady-state salt wedges in the unconfined aquifer before sea-level rise (upper), and after sea-level rise (lower).

The 1.0 meter sea-level rise scenario is also used to simulate seawater intrusion into the surface aquifer in the barrier land. Figure 4.5.2 shows the distributions of hydraulic head above mean sea levels before and after sea level rise. With the sea level rise, the hydraulic heads in the

middle and lower side of the island increase, but the heads on the top side decrease. The head distribution is more symmetric about the middle of the island. In reality, the erosion and accretion would affect the barrier island geometry, which is not considered in our case study. Figure 4.5.3 compares freshwater lens locations in steady state condition before and after sea level rise. A noticeable decrease of the freshwater lens thickness is observed. The freshwater storage significantly decreases due to the sea level rise.

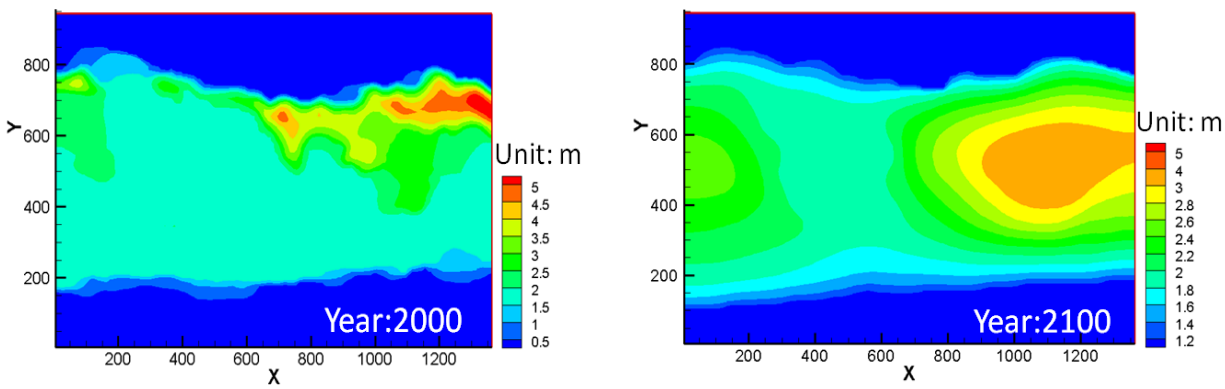

Figure 4.5.2. Comparison of hydraulic head distributions in the barrier island before (left) and after (right) the sea-level rise.

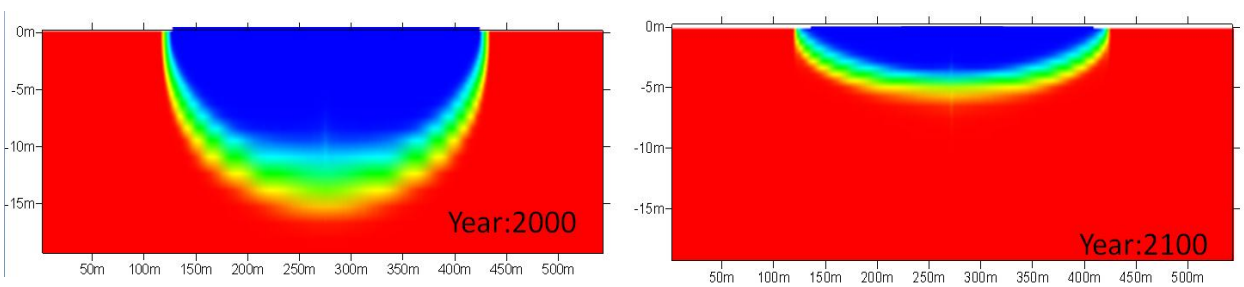

Figure 4.5.3. Comparison of freshwater lens predicted before the sea-level rise on the barrier inland (left), and after the sea-level rise on the barrier inland (right).

4.5.2. Impacts of Sea-Level Rise on Confined Aquifers. The impacts of sea- level rise on confined aquifers have been studied according to pre-development and post-development conditions. These are discussed separately.

4.5.2.1. Simulation of Groundwater Level in Pre-Development Condition. The regional groundwater flow model and density-dependent saltwater intrusion model are developed in two phases, pre-development and post-development. In the pre-development case, a steady state groundwater flow without any pumping in the area. The hydraulic parameter values calibrated by NWFWMD (2000) are also adopted in this study. Figures 4.5.4, 4.5.5 and 4.5.6 show the simulated pre-development water levels in surface aquifer, Upper Floridan Aquifer and lower Floridan Aquifer, respectively. The pre-development water levels in the surface aquifer similar to the topography. The water level distribution in the Lower Floridan Aquifer is similar to the distribution in the Upper Floridan Aquifer.

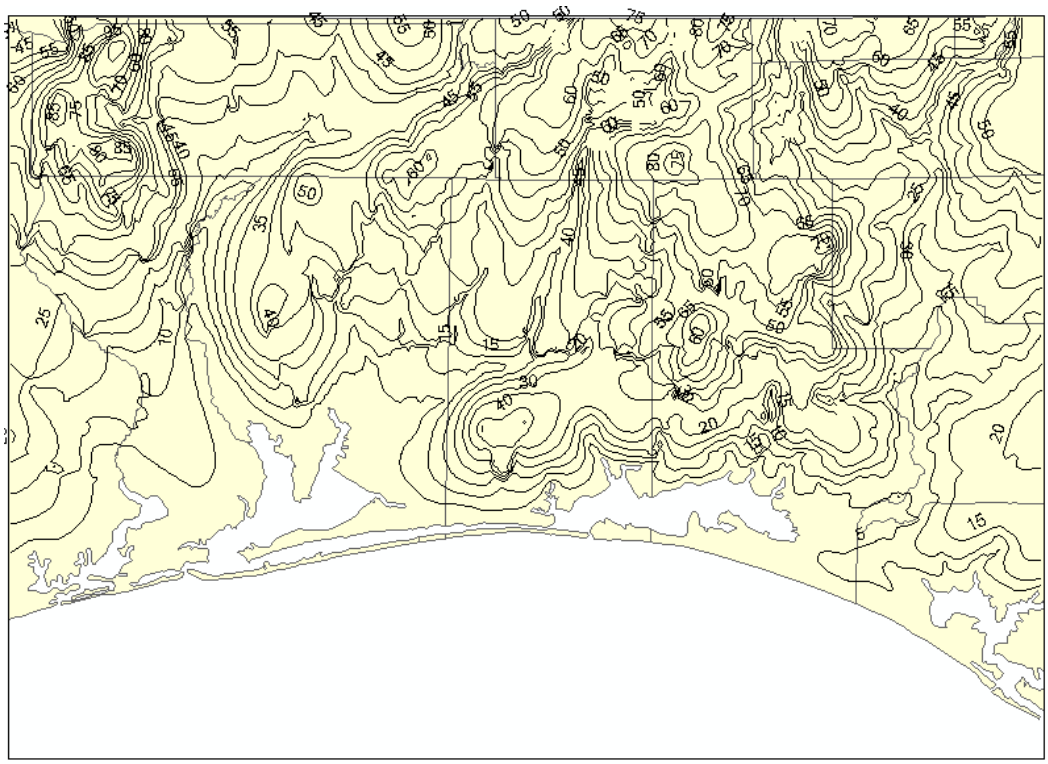

Figure 4.5.4. Hydraulic head distribution of surface aquifer in pre-development condition (contours in meters).

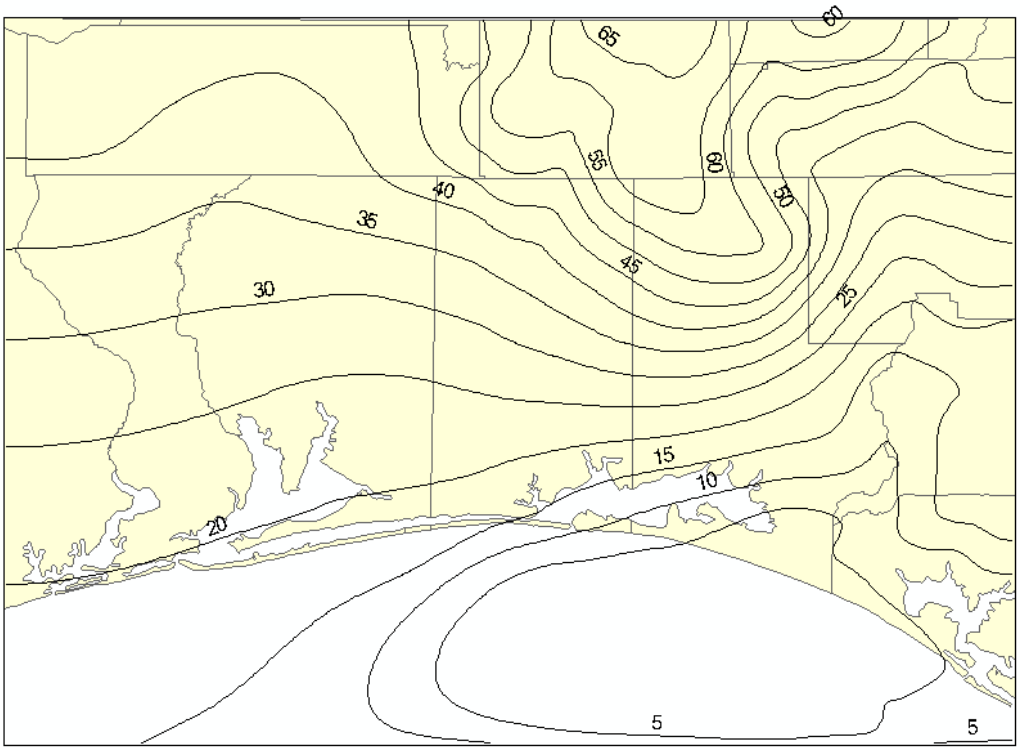

Figure 4.5.5. Hydraulic head distribution of upper Floridian aquifer in pre-development condition (contours in meters).

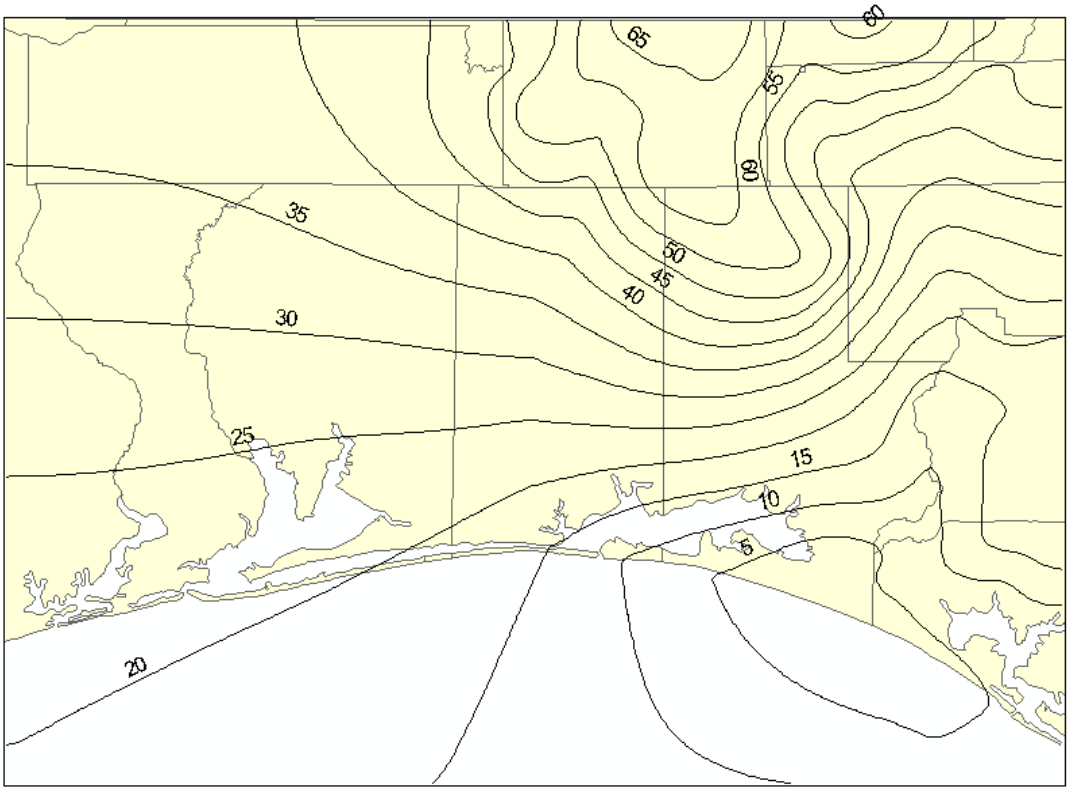

Figure 4.5.6. Hydraulic head distribution of lower Floridan aquifer in pre-development condition (contours in meters).

The pre-development salinity distributions in the Upper Floridan Aquifer and Lower Floridan Aquifer are shown in Figures 4.5.7, and 4.5.8, respectively. It is shown from the figures that the salinity gradually increases from the top layer to the bottom layer and from the north to the south of study area.

4.5.2.2. Post-development Simulation Results from 1942 to 1998. 107 wells pumping rate data were incorporated in a transient model from 1942 to 1998 to simulate groundwater flow and salinity transport during this period. Pre-development results were used as initial condition for the transient model. The simulated post-development water levels in upper Floridan Aquifer and lower Floridan Aquifer are shown in Figure 4.5.9 and 4.5.11, respectively. An observed water level distribution from Maloney et al. (1998) is shown in Figure 4.5.10. Compared the figures, one could tell that the simulated results are consistent with the observations and well capture the drawdown center in the Santa Rosa coast area. The differences in water level between pre- and post-development conditions represent the hydraulic head drawdown caused by pumping. In the upper Floridan Aquifer, the pumping has led to the drawdown as high as 35 m around the concentrated pumping area in the Choctawhatchee Bay, shown in Figures 4.5.9 and 4.5.10.

The 1998 salinity distributions in the Upper Floridan Aquifer and the Lower Floridan Aquifer are very similar to the pre-development salinity distributions in the two aquifers. The differences of salinity distributions in the pre-development time and in 1998 for the Upper Floridan Aquifer and Lower Floridan Aquifer are shown in Figures 4.5.12 and 4.5.13, respectively. These show that salinity change from the pre-development time to 1998 increases from west and east boundary, which is consistent with historical observations.

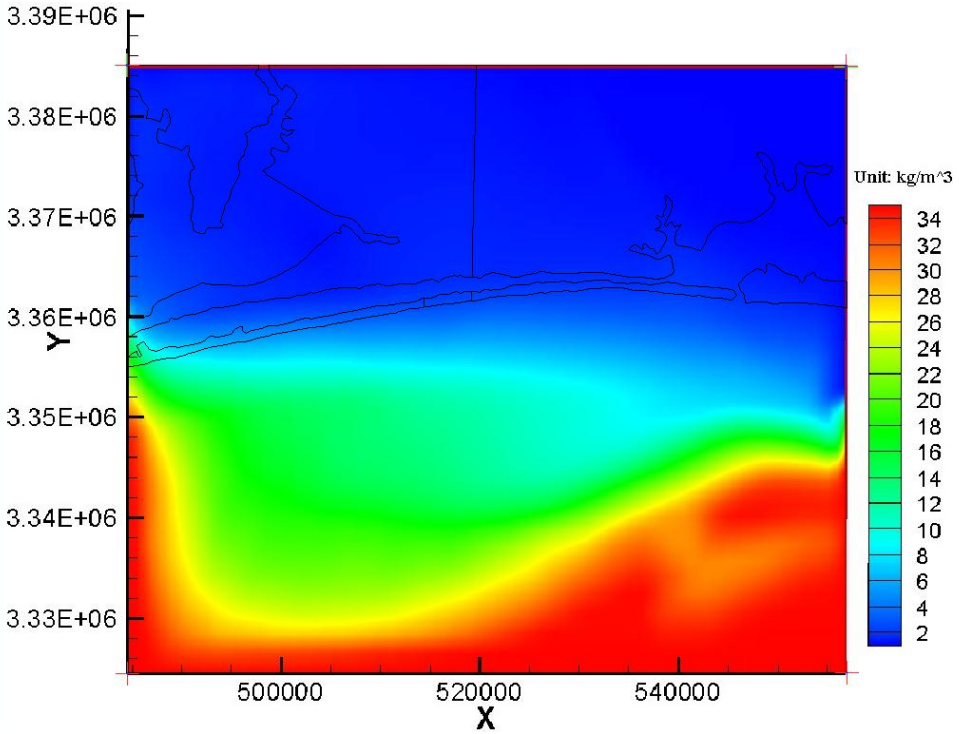

Figure 4.5.7. Pre-development salinity distribution in the upper Floridan Aquifer.

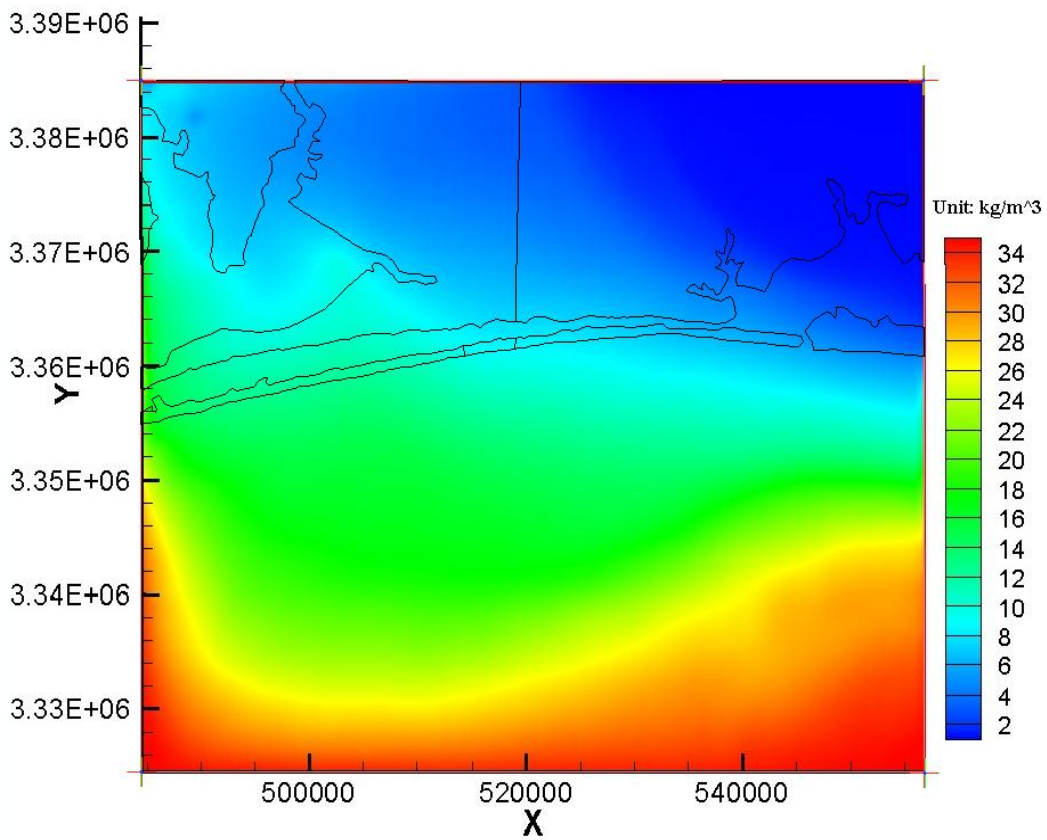

Figure 4.5.8. Pre-development salinity distribution in the lower Floridan Aquifer.

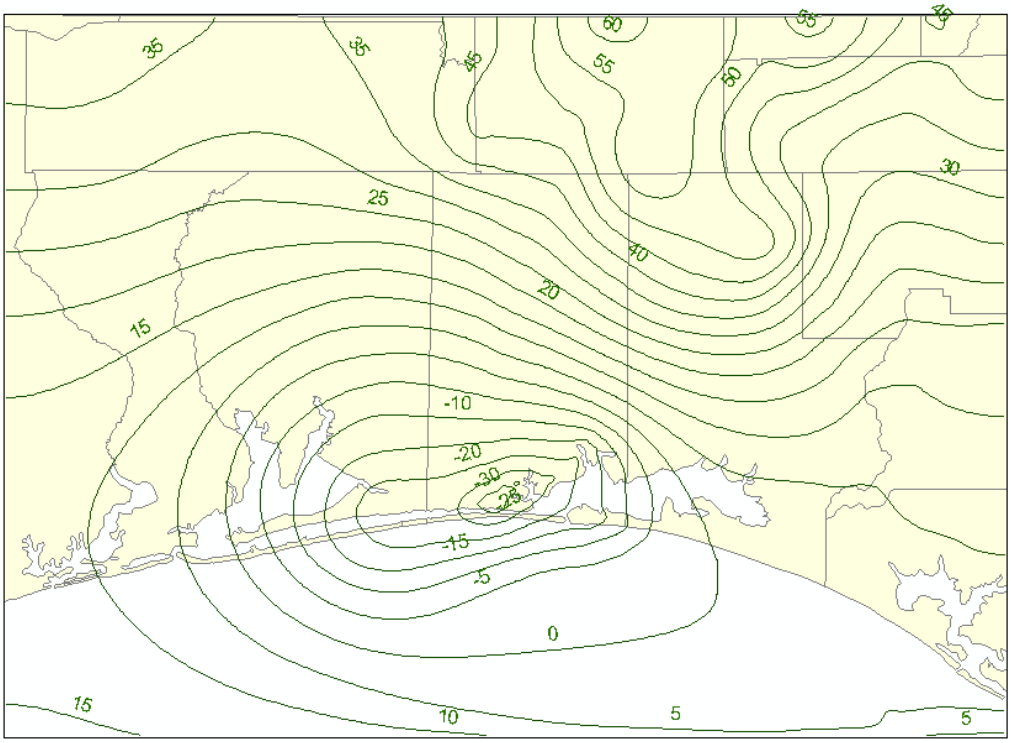

Figure 4.5.9. The hydraulic head distribution in upper Floridan Aquifer, 1998 (contours in meters).

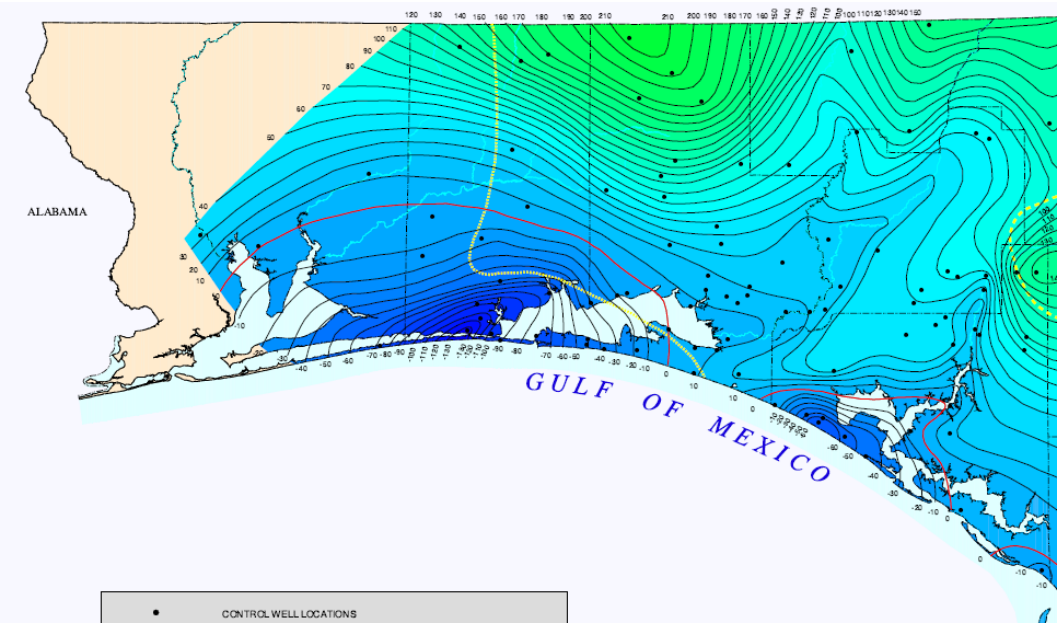

Figure 4.5.10. Potentiometric surface of the Floridan Aquifer system, 1998 (contours in feet) (Maloney et al., 1998).

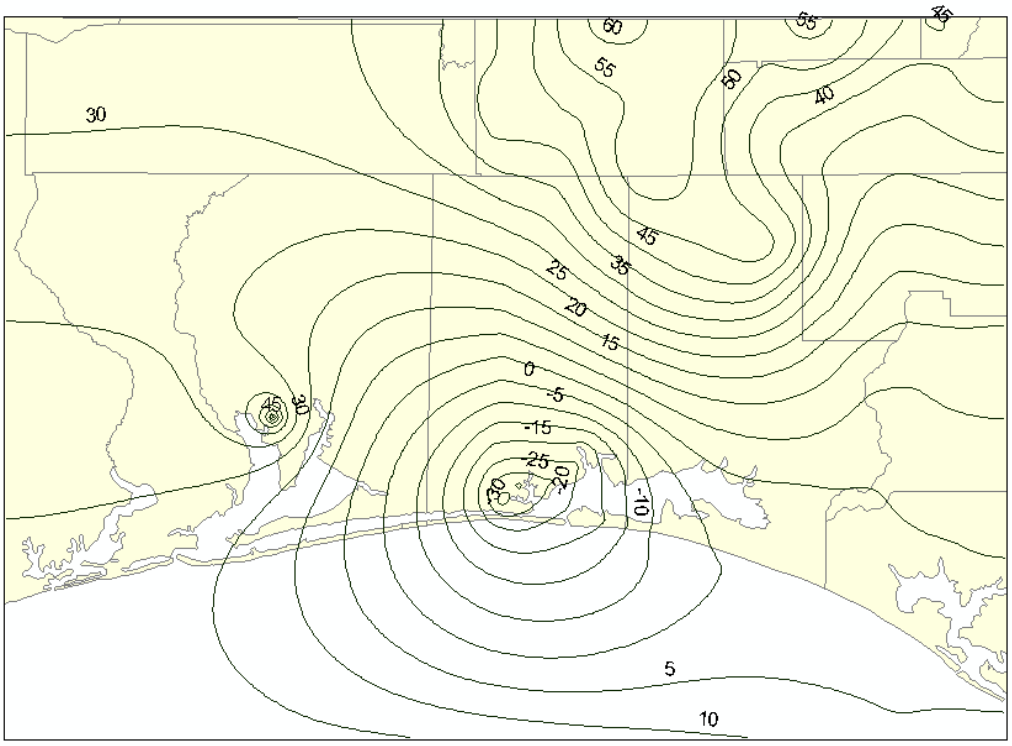

Figure 4.5.11. The hydraulic head distribution in lower Floridan Aquifer, 1998 (contours in meters).

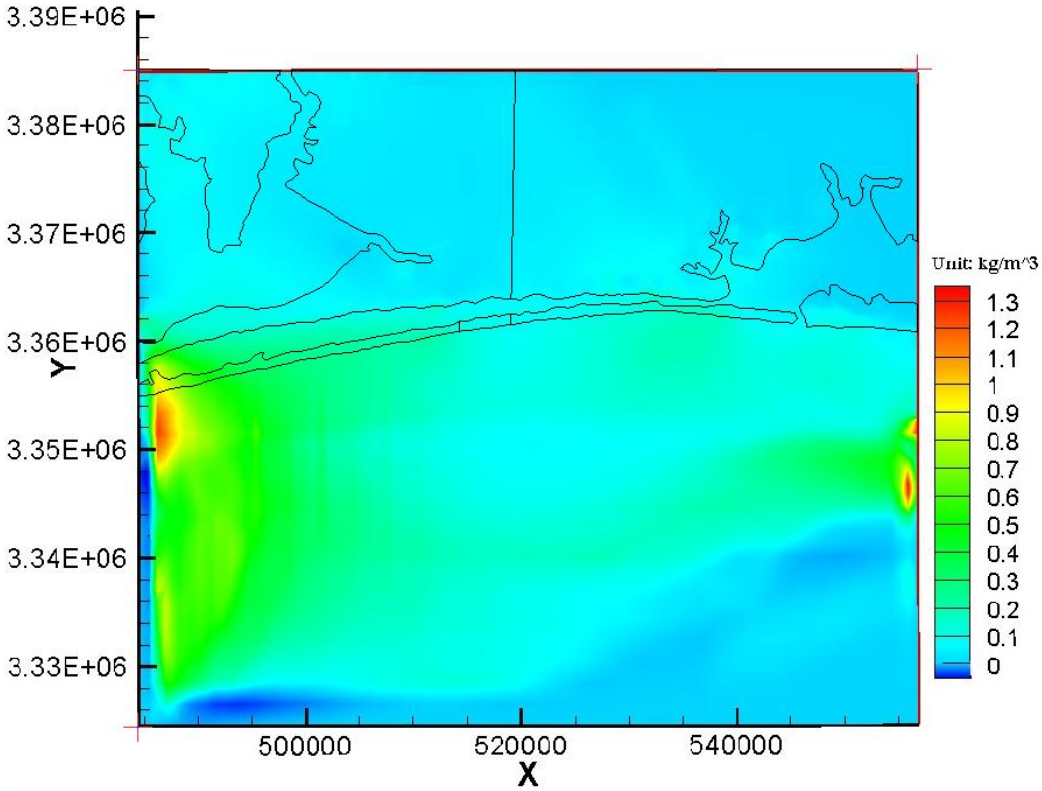

Figure 4.5.12. The distribution of salinity difference between 1942 and 1998 in Upper Floridan Aquifer.

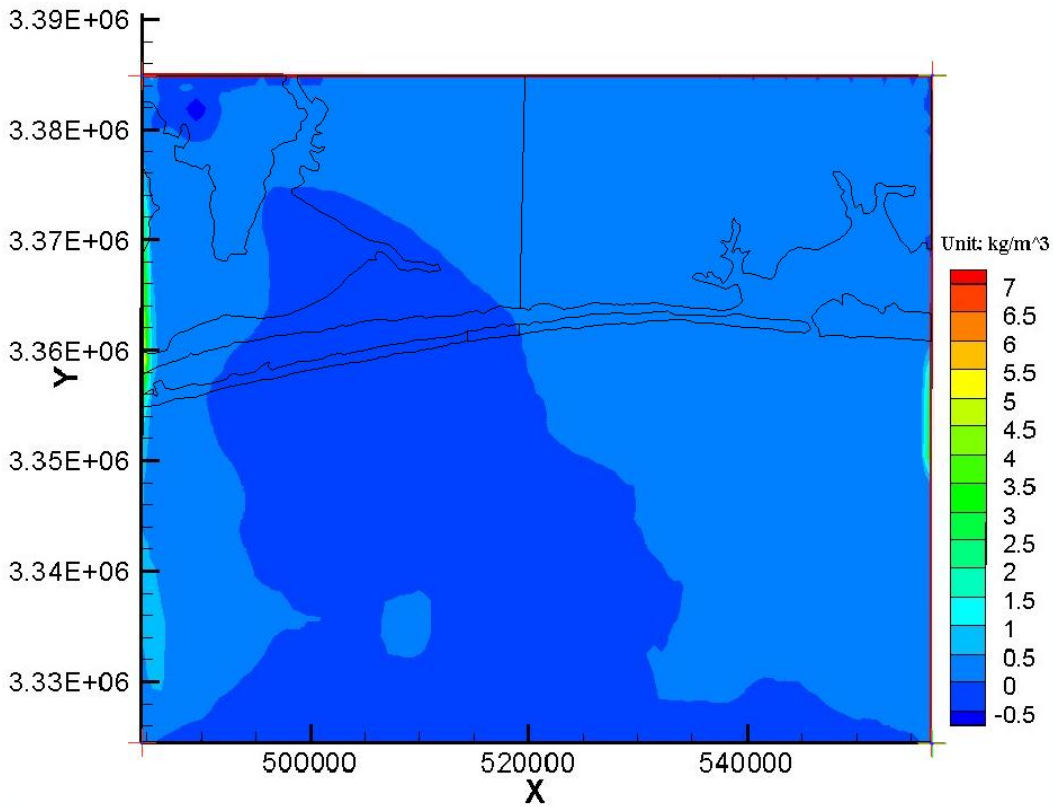

Figure 4.5.13. The distribution of salinity difference between 1942 and 1998 in Lower Floridan Aquifer.

4.5.3. Groundwater Simulation Results for 2100. In the above study, the groundwater flow and seawater intrusion models reasonably agree with the observations. Now the calibrated models are used to predict groundwater flow and seawater intrusion in 2100, in which the sea level rise condition is incorporated in the regional model for the surface aquifer. The coast line is treated as time dependent constant boundary in the model. NWFWMD in 2008 made the district-wide water supply assessment (approved in May 2009), planed the well pumping rates and evaluated groundwater resources through 2030 in the management document. The pumping rates planned by NWFWMD (2012) are used in this study. It is shown in Figure 4.5.14 the surface water level difference between 1 meter and 2 meter sea level rise scenarios. The sea level rise has little effect on the water level in the inland area. However, 2 meters sea level rise will lead to a one-meter water level rise in the coastal area. The simulated water levels in 2100 and in 1998 for Upper Floridan Aquifer and Lower Floridan Aquifer are shown in Figures 4.5.15 and 4.5.16, respectively. Compare to the hydraulic head distribution in 1998, the simulated water levels in 2100 are 1 meter higher in the two aquifers. The hydraulic heads change dramatically around the pumping wells in Upper Floridan Aquifer and Lower Floridan Aquifer, indicating the drawdown is mainly due to the pumping rather than sea level rise. A drawdown of 1 meter is simulated around the pumping cone center in next 100 years.

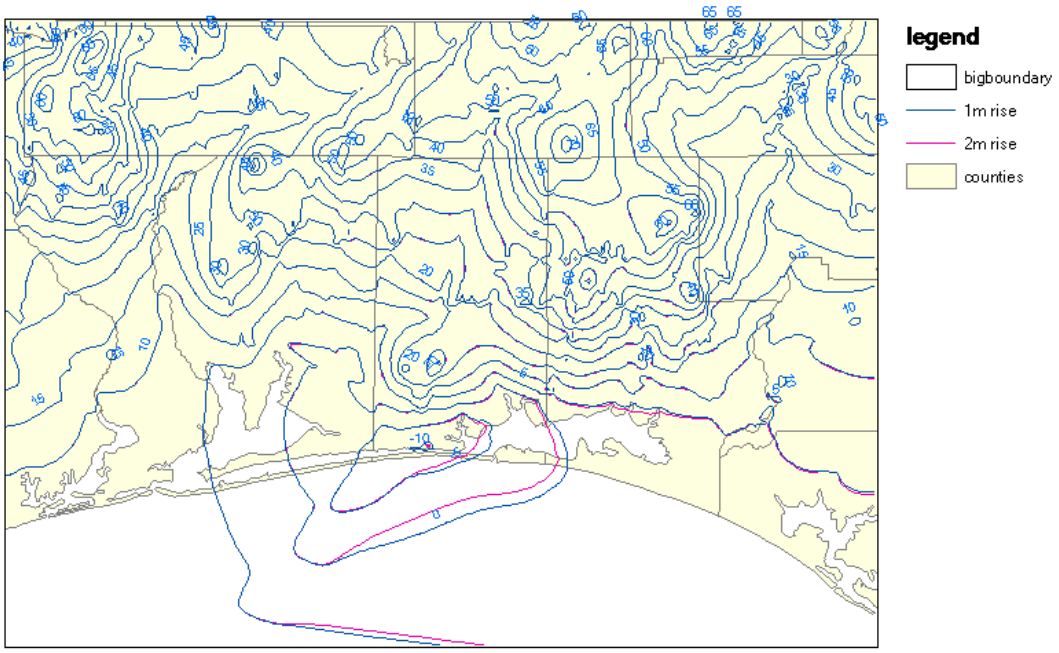

Figure 4.5.14. Hydraulic head difference of surface aquifer from 1998 to 2010 (contours in meters).

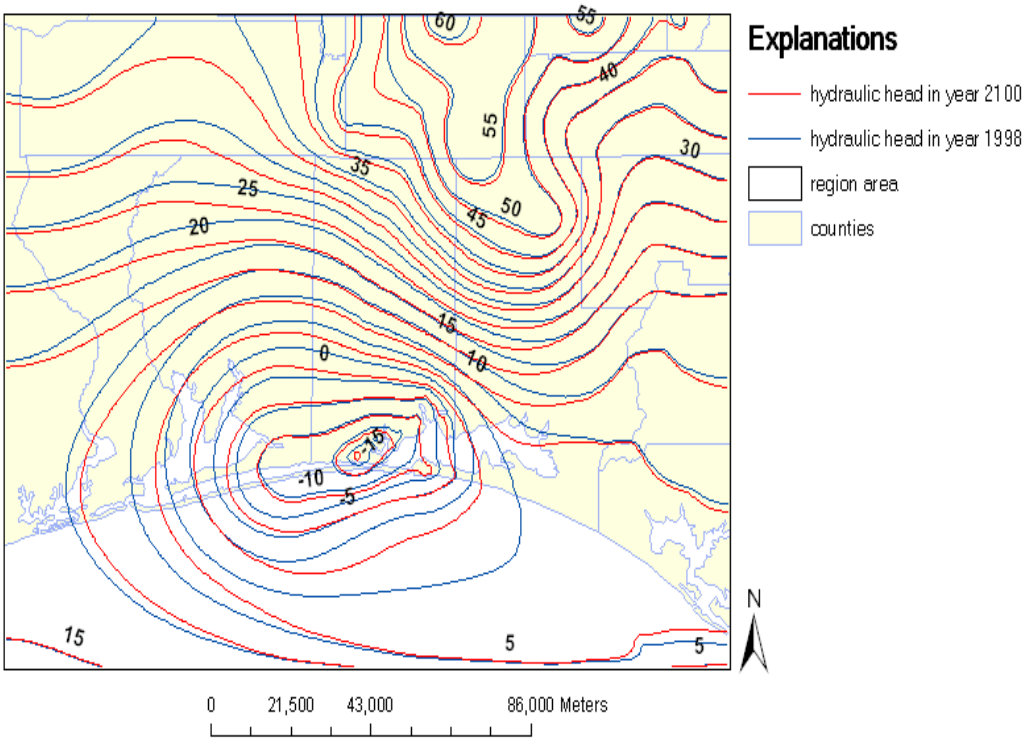

Figure 4.5.15. Hydraulic head distributions in 1998 (blue line) and in 2100 (red line) with +1m sea level rise in Upper Floridan Aquifer.

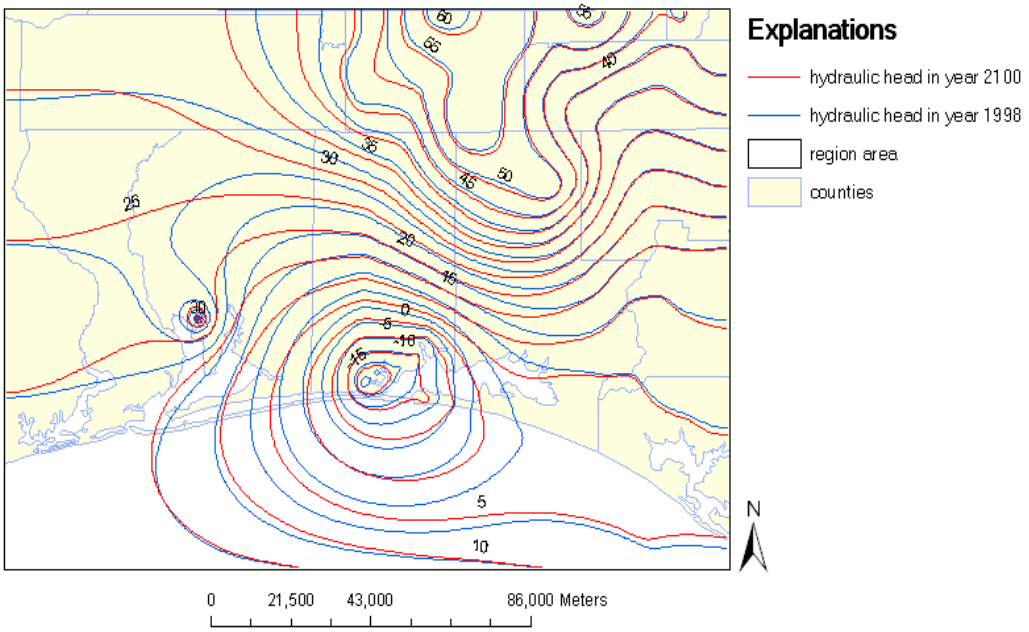

Figure 4.5.16. Hydraulic head distributions in 1998 (blue line) and in 2100 (red line) with +1m sea level rise in the Lower Floridan Aquifer.

Figure 4.5.17 presents the salinity variation in the Upper Floridan Aquifer from 1998 to 2100 with 1 meter sea level rise. A comparison of the contour lines in 1998 and 2100 shows that salinity increase in the inland area could be observed, indicating seawater intrusion in the area. The salinity differences between the two years in Upper Floridan Aquifer and Lower Floridan Aquifer are separately shown in Figure 4.5.18 and Figure 4.5.19, respectively. The maximal salinity change area is in the Santa Rosa Island. The figures show that the pumping would cause inward flow from the south to north in the study area. The figures show the sea level rise has slightly impact on the salinity change. Compared with 1 meter sea level rise, the 2 meters sea level rise can slightly increase salt concentration, less than 0.05 kg/m^3.

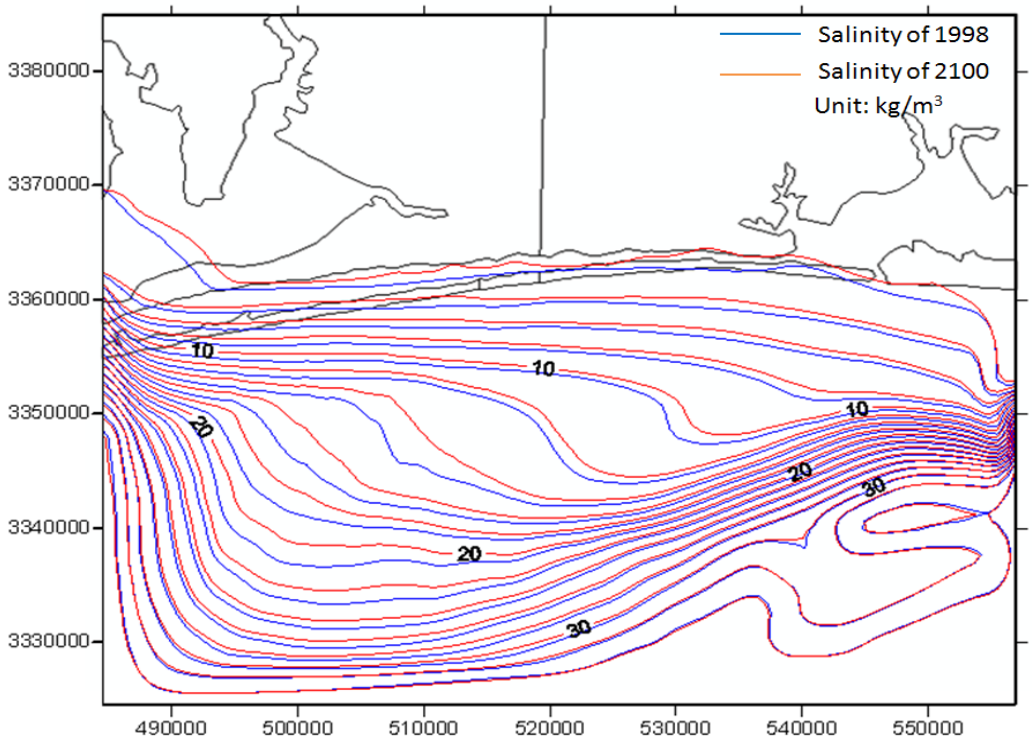

Figure 4.5.17. The salinity distributions in 1998 and in 2100 after +1m sea level rise in the Lower Floridan Aquifer.

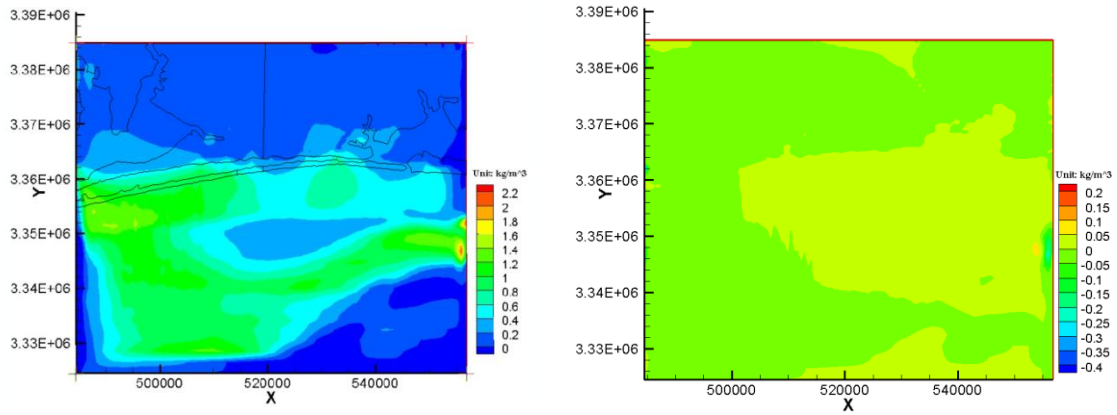

Figure 4.5.18. a) Salinity difference between 1998 and 2100 with +1m sea level rise in the Upper Floridan Aquifer; b) Salinity difference between +1 m and +2 m sea level rise by 2100.

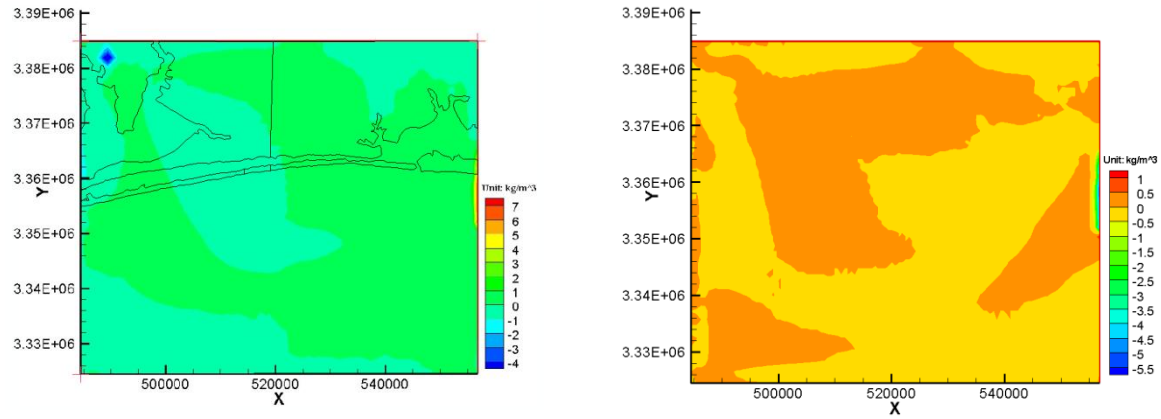

Figure 4.5.19. a) Salinity difference between 1998 and 2100 with +1m sea level rise in the Lower Floridan Aquifer; b) Salinity difference between +1 m and +2 m sea level rise by 2100.

4.6. Modeling Morphologic Change

The development of the MoCCS model has been described in Section 3.6. The model is especially designed to efficiently represent the physical processes that control the large-scale and long-term changes over periods of decades to centuries so that future morphologies can be predicted. Unlike most other models of shoreline and coastal morphologies, the MoCCS model is relatively undemanding of computational resources. This allows it to be run for hundreds of simulations representing alternative scenarios of the next 100 years with sea level rise and a variable sequence of major hurricanes. From these simulations, the central trends, variability and relative uncertainty can be established. The model has been set up and operated for the coastal area containing Eglin Air Force Base and much of the adjoining portion of Santa Rosa Island. This area has been selected largely because of the availability of a large amount of data regarding physical processes and the long-term historical changes in coastal morphology. The purpose of the model simulations that are described in this section of the report is to demonstrate the operation and capabilities of the MoCCS model and not to produce reliable and accurate predictions of coastal change. As demonstrated, such predictions are possible but will need more refined processing of the measured data, more complete model calibration and verification and better processing of the results, so that they can be easily understood and utilized by military facility managers, planners and engineers.

4.6.1. Projecting Shoreline Change. The MoCCS model has been used to project the changes in shoreline position, sand dune height and morphology, island profile elevation and bay shoreline location over the next 100 years with consideration of five different sea level rise scenarios and representation of the natural variability in the possible sequence of major hurricane intensities and landfalls. The model operates in an integrated fashion. However, for clarity it is best to discuss the results according to the individual morphological components.

As discussed previously, both the Chronic and Acute components of the MoCCS model rely on characterizations of both future sea levels and the sequence of major storms over the next 100 years. To evaluate effects of storm magnitude and landfall position, as well as the sequence and possible occurrence of multiple storms in a given year on morphological responses, storms in each year were characterized by relative storm magnitude and track. Only dominant storms such

as hurricanes are considered. Based on a FEMA study of the West Florida Central Panhandle coast (FEMA 2002), the storm rate was estimated as 0.06 per year for the whole domain, which gives the expected number of occurrence of 0.06 × 100 = 6 storms in the 100 year simulation period.

The MoCCS model can be used with wide range hurricane climate representations. However, for the purpose of developing the model and for making as set of illustrative results only a continuation of the current hurricane climate has been considered. Four different storm magnitudes were used. Based on the open coast surge flood heights obtained from the Okaloosa County flood study (FEMA 2002), the values of 0.3 m, 0.64 m, 1.16 m and 2.1 m were chosen as representative maximum surge heights. Using the four values to interpolate the curve of cumulative occurrence probability of surge heights leads to four probability ranges, each of which centers on the chosen surge heights. The corresponding cumulative exceedance probabilities for each range were 0 to 0.5, 0.5 to 0.75, 0.75 to 0.95 and greater than 0.95. Based on this distribution of exceedance probabilities, storm magnitudes with central pressures and radius to maximum wind values were determined that produce these surge heights in the SLOSH model operating on a grid that covers the Santa Rosa Island project area. A two-stage storm sequence algorithm was then applied once in each model-year. First, a random number was used along with the Poisson distribution function to determine the number of storms that would occur in the year. As noted earlier, the most common result was zero storms but values of one or more occur at the proper rate within the 100-yr simulation periods. For each year designated to have one or more storms, the algorithm uses the storm probability density data and another value of a random number to select the storm magnitude(s) and its (their) associated central pressure and radius to maximum wind value(s). Finally, a third random number value is used to select the storm track. These inputs are selected based on an assumption that the track probability density values are uniform along the shoreline. These tracks are adequate at this stage of model development, testing and general application. The number of tracks can be increased in the later more refined applications. Table 4.6.1 gives an example of the storm sequence for a single 100-year realization.

Table 4.6.1. One example of a storm series for a 100-year simulation.

Year	6	16	21	52	70	70	87
Annual number of storms	1	1	1	1	2	2	1
Storm track	2	1	3	3	2	2	2
Storm magnitude	2	4	3	1	3	2	1

In order to predict the future shoreline positions with the MoCCS model, separate simulation sets were developed for each of the five sea level rise scenarios. As discussed in Section 1.2, the project definitions include a period of interest of the next 100 years and four possible rates of future sea level rise. These result in total eustatic sea level rises of 0.5, 1.0, 1.5 and 2.0 m over the next century. Also, referring back to Section 1.2, the annual rates of sea level change are defined by parabolic functions.

In the MoCCS prognostic simulations, a set of model runs were made for a 100 year period and each of the sea level rise scenarios. A fifth scenario based on the simple continuation of the present rate of rise extended over the future as a linear trend. In each sea level rate simulation a large number of 100-year storm sequence scenarios were created. The number varies somewhat

depending on the projections that were made with the range between 100 and 700 realizations. The actual number of individual 100-year storm sequences used in each simulation is included in the discussion of the individual results.

The MoCCS model projections of shoreline change were based on applying the wave and scaling parameter values that were established in the calibration phase. These were based on simulating a 60-year long period of measured shoreline change during a period of relatively minor storm activity. To this was added the net storm-induced shoreline changes appropriate to each of the four storm magnitudes and scaled along the shore by distance to the landfall. In each individual 100-year simulation a distinct sequence of storms was represented. Consequently, the resulting series of projections of shoreline positions show realistic variability which permits characterizations of the 100-year projections according to mean values and measures of variability.

Direct mapping of shoreline changes over shores that are many 10's of km long results in unsatisfactory graphics because even changes on the order of 100's of meters are difficult to discern. To illustrate the use of the MoCCS model to forecast changes is shoreline position along a major portion of Santa Rosa Island, including all of the shoreline in Eglin AFB, we use the same type of data presentation as was used in Figure 3.6.3. Here straight horizontal lines represent the initial shoreline position and the changes over the stated time interval are shown with bars extending upward for erosion and downward for shoreline advance. Each bar represents a 250 m length of the shore so that when all are plotted a nearly continuous curve results. Owing to conventions used in setting up the MoCCS model shoreline erosion is indicated by positive values and shore advance by negative values.

Values of shoreline change for the five sea level rise scenarios are compared in Figure 4.6.1. For this illustration a single realization of the next 100-year time interval was use to avoid the complications that arise in representing results statistically as is necessary for multiple realizations. In fact, this particular 100-yr scenario simply represents a continuation of the mild storm interval used in calibrating the model. In a subsequent discussion we will present results from the multiple realization predictions.

The results shown on Figure 4.6.1 show that the expected shoreline change will be different along the shoreline length. Much of the shore of Eglin AFB is located where the mapped shoreline has a concave curvature, which favors long term deposition. Further westward a continuation of the present rate of sea level rise would result in some deposition alternating with shoreline intervals of little change or slight erosion. In the eastern portion of the island erosion associated with the natural withdrawal of sand by the stabilized inlet is indicated. The shoreline change pattern has somewhat of an undulation along the length of the island. A similar pattern can vaguely be recognized in the measured changes shown in Figure 3.6.3. It is thought that these spatial variations result from subtle differences in longshore sand transport that may be related to the system of shoreface-connected sand ridges in the proto-type that are not represented in the MoCCS model. Even for this mild-storm 100-yr scenario quite significant shoreline retreats are predicted for the higher potential rates of sea level rise.

As described earlier, the MoCCS model has been especially designed to be operated for a large ensemble of future 100-year realizations of ordinary conditions and major hurricanes. The number, magnitude, intervening durations and sequences of hurricanes can only be represented stochastically. The model generates these individual sequences in a series of randomized processes that are statistically equivalent to a continuation of the present storm climate for this

portion of the Gulf of Mexico. Although it would be a simple matter to change these operations so that an increased rate of major storms, such as described in Sections 4.2 and 4.3 of this report could be represented, such increases have not been included for the scenarios that produced the results given in the following figures.

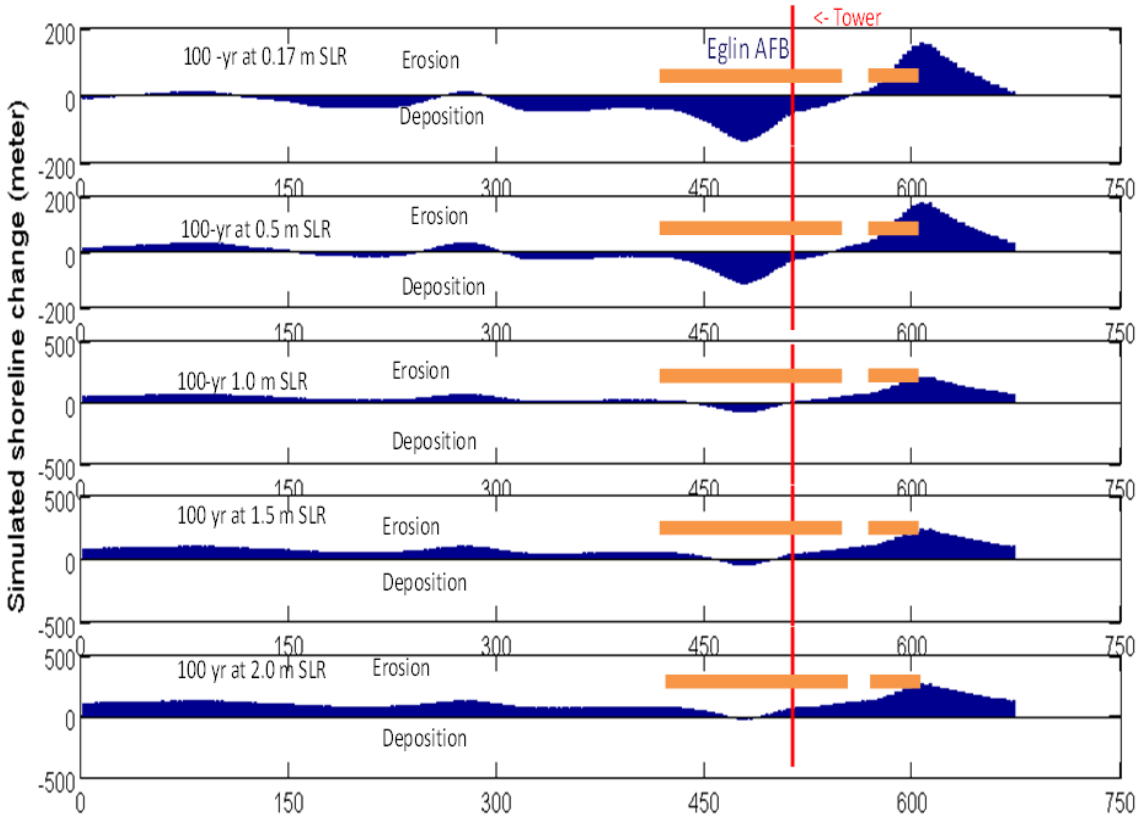

Figure 4.6.1. MoCCS model predictions of relative shoreline changes over the central portion of Santa Rosa Island for a future 100-year scenario for different rates of sea level rise. The approximate location of Eglin AFB is indicated by the orange bars and that of the Test Area 13B tower as a red vertical line. The top panel is for a continuation of the present SLR rate with others for rates leading to 100-yr rises of 0.5, 1.0, 1.5 and 2.0 m.

The variability in the results for each sea level rise rate simulation scenario is best shown at specific locations. The position of three of these locations is shown on Figure 4.6.2.

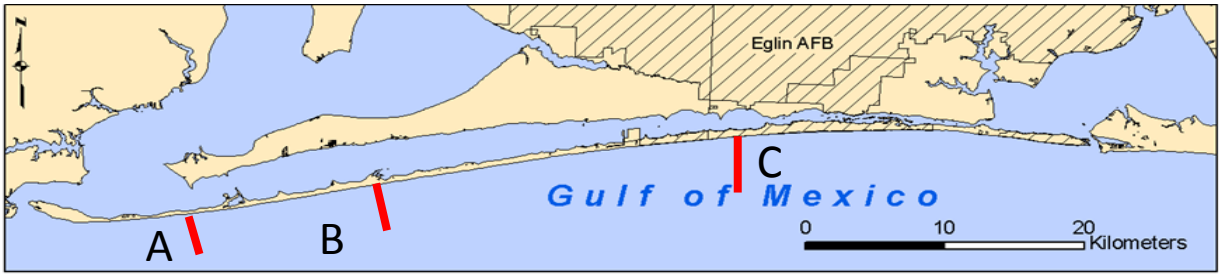

Figure 4.6.2. Locations of the results given in the next three figures.

The projections for the shoreline position for each of the representative profile locations are shown for the different sea level rise scenarios on Figures 4.6.3 through 4.6.5. These results are based on MoCCS model runs simulating a total of one hundred realizations of the 100-year future sequence of hurricanes. The ordinary wave climate and the hurricane climate are assumed to remain constant in these scenarios. As noted in Section 1.2 of this report the rates of sea level rise are considered to vary according to a parabolic function over the 100-year intervals. An exception is made for the simulations where the present rate of sea level rise is simply continued.

Figure 4.6.3 has four panels, which show the location of the shoreline at the end of the 100-year simulation period according to a probability density function. This allows the most likely position to be identified along with a measure of the potential variability of the results. Low variability is indicated by the distributions shown by probability density functions that have a sharp peak and a narrow spread. In the case of the result shown for location A (Figure 4.6.2) and a 100-year sea level rise of 0.5 m the peak is located at +45 m, which indicates retreat of the shoreline by 45 m. However, according to the range of storm events developed in the simulations, shoreline changes range between an advance of 40 m to a retreat of 230 m. The 10-percentile and 90-percentile values correspond to retreats of 33 m to 115 m.

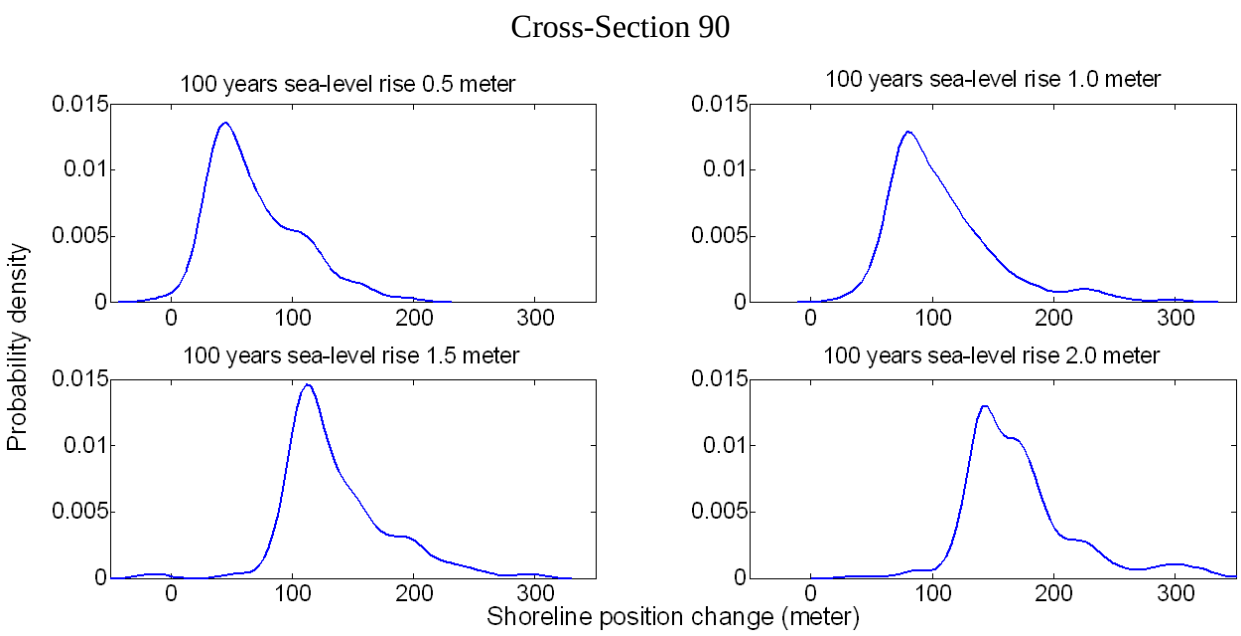

Figure 4.6.3. Projections of shoreline change at Location A (Fig. 4.6.2) (Section 90).

The other panels of Figure 4.6.3 show the MoCCS simulation results for the 1.0, 1.5 and 2.0 m sea level rise cases. A comparison clearly shows that the peaks of the distributions shift towards shoreline retreat. For the sea level rise scenarios of 1.0 m, 1.5 m and 2.0 m the peaks shift over the range +80 m, +112 m, and +140 m respectively. All these values are positive and thus indicate shoreline retreat. Also, there is a general increase in the variability of the predicted shoreline change which is indicated by a broadening of the area beneath the probability density function curve. These trends are also expressed by the values in Table 4.6.2.

By referring back to Figure 4.6.1 it can be noted that this location is predicted to have very little change over the next 100-years if the present rate of sea level rise is maintained. That is, the sand

supply and the slight decreasing-to-the-west gradient in the average rate of longshore sand transport which would cause the shoreline to advance are in near balance with the general effect of the present sea level rise which would cause the shoreline to retreat. The results from the other sea level rise scenarios indicate that the sea level rise effect progressively dominates and the retreat of the shoreline increases with the rate of sea level rise.

Table 4.6.2. Predicted shoreline change at Location A for four sea level rise scenarios simulated by one hundred realizations of the next 100 years.

100-yr Sea Level Rise (m) Scenario	PDF Peak	Dominant Change	Full Range (m)	10-percentile (m)	90-percentile (m)
0.5	45	Retreat	-45 to +230	+33	+115
1.0	80	Retreat	-10 to +333	+70	+160
1.5	112	Retreat	-50 to +330	+97	+195
2.0	140	Retreat	0 to +420	+130	+230

Figure 4.6.4 and Table 4.6.3 show the results of the MoCCS simulations for the four sea level rise scenarios that represent the predicted shoreline changes at Location B (section 140). Although this is 10 km to the east of Location A, it is still in the portion of Santa Rosa Island that is projected to have little shoreline change if the present rate of sea level rise continues. Accordingly, these results are very similar to those discussed for Location A.

Cross-Section 140

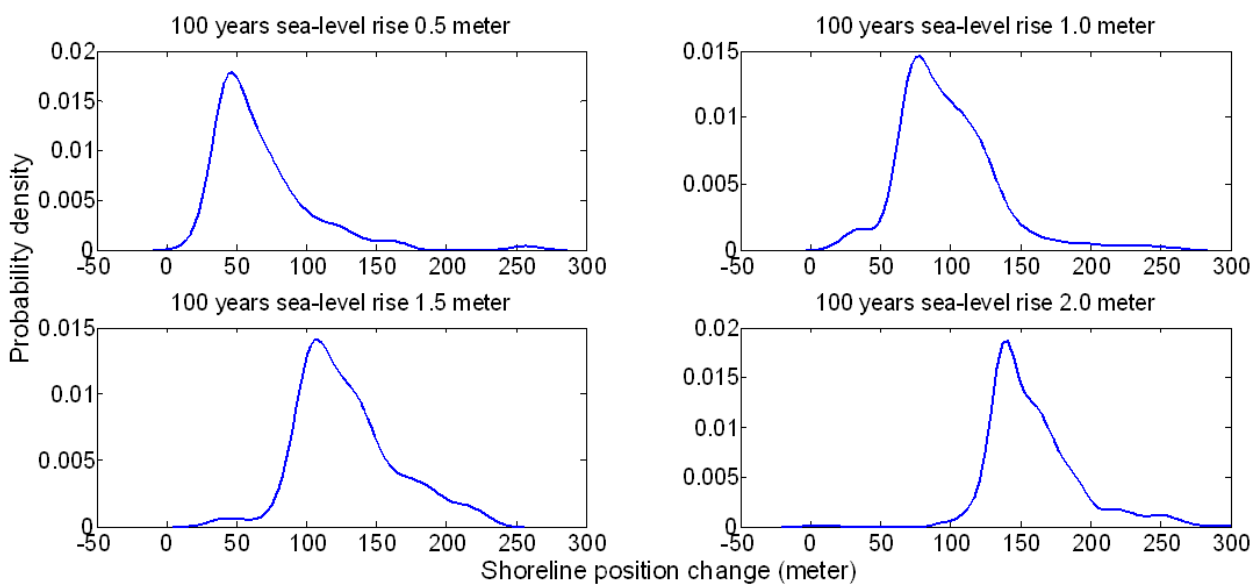

Figure 4.6.4. Projection of shoreline change at Location B (Fig. 4.6.2) (Section 140).

Figure 4.6.5 and Table 4.6.4 show the results of the MoCCS simulations for Location C. This section of Santa Rosa Island, which includes most of the Gulf shoreline of Eglin AFB has a more pronounced concave curvature compared with the shoreline further west. This, and its

orientation relative to the dominant wave approach direction, favors long-term sand deposition and shoreline advance. Reference to Figure 4.6.1 demonstrates this for scenarios including the continuation of the present rate of sea level rise. The positions of the probability density function peaks in the four panels of Figure 4.6.5 are at negative values indicating shoreline advance. The pattern seen for the results at locations A and B, is evident here as well. However, here there is considerable shoreline advance predicted for the 0.5 m sea level rise scenario and this decreases markedly in the results of the MoCCS simulation for the high sea level rise rate scenarios. It is interesting to note that the variability of the results increases according to the magnitude of the sea level rise scenario but this variability is noticeably less than in the results for the previous two locations.

Table 4.6.3. Predicted shoreline change at Location B for four sea level rise scenarios simulated by one hundred realizations of the next 100 years.

100-yr Sea Level Rise (m) Scenario	PDF Peak	Dominant Change	Full Range (m)	10-percentile (m)	90-percentile (m)
0.5	45	Retreat	-10 to +290	+38	+110
1.0	75	Retreat	0 to +280	+70	+132
1.5	108	Retreat	-3 to +258	+100	+180
2.0	140	Retreat	-20 to +385	+133	+200

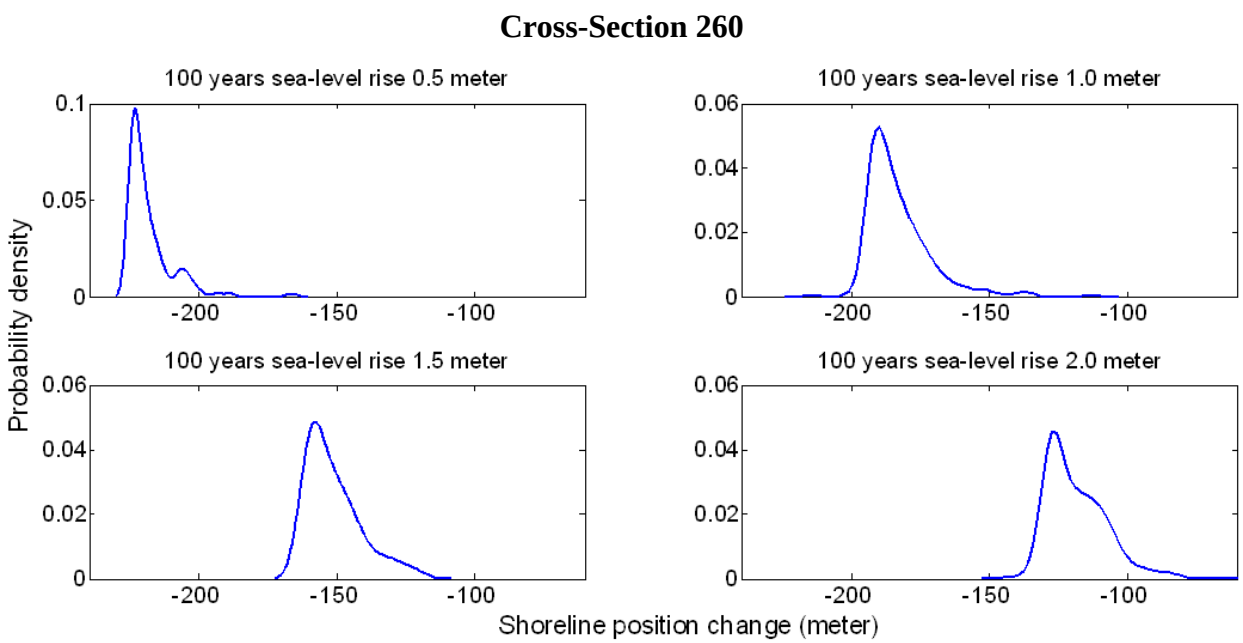

Figure 4.6.5. Projection of shoreline change at Location C (Fig. 4.6.2) (Section 260).

The results shown on Figures 4.6.3 through 4.6.5 can be compared to those shown on Figure 4.6.6 which represents the case where the present rate of sea level rise is considered to continue for the next 100 years for a location just east of the Test Area 13 B tower. The purpose of this figure is to illustrate how the predicted location and the variability of the predictions vary as the

duration of the prediction interval increases. From this comparison it is clear that the shoreline system at this place is generally in a depositional regime and that this is expected to continue at this rate of sea level rise. The most probable shoreline change in 25 years is a growth of 19 m with growths increasing to 28 m, 56 m and 65 m in the following three 25 year intervals. However, the projection for the next 25 years includes a significant potential for erosion (positive values). This low potential for erosion occurs in all but the fourth panel on this figure. These results do not include conditional probabilities so it is not possible to discern whether the results would change after the first 25 years if it was observed that growth had continued over that period.

Table 4.6.4. Predicted shoreline change at Location C for four sea level rise scenarios simulated by one hundred realizations of the next 100 years.

100-yr Sea Level Rise (m) Scenario	PDF Peak	Dominant Change	Full Range (m)	10-percentile (m)	90-percentile (m)
0.5	-223	Advance	-160 to -230	-207	-225
1.0	- 190	Advance	-115 to -225	-170	-193
1.5	- 158	Advance	-108 to -173	-137	-161
2.0 - 128 Advance +15 to - 158	-105		-128		

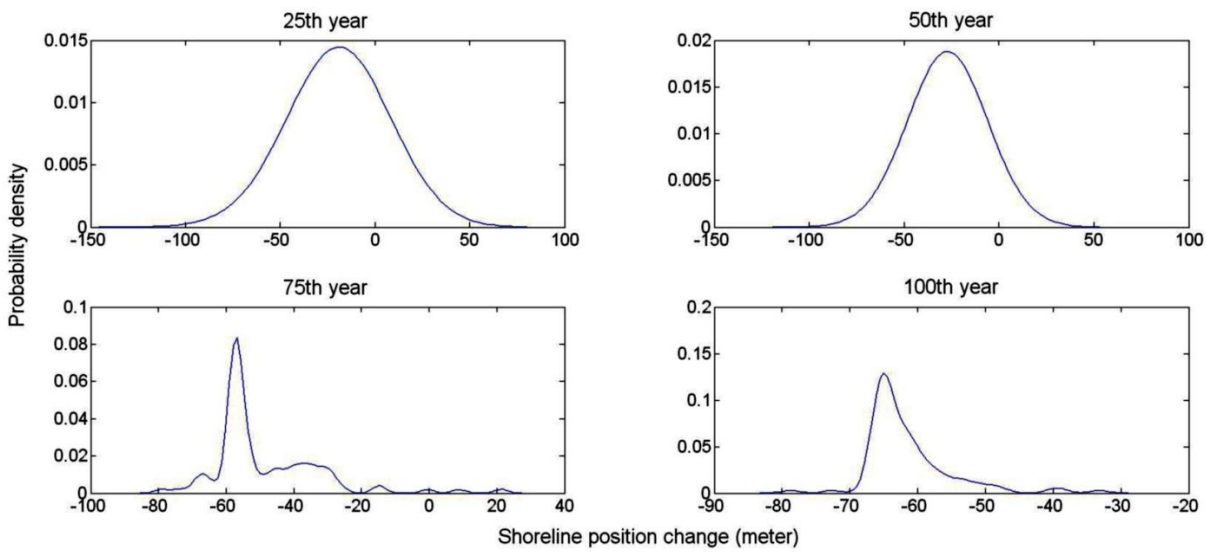

Figure 4.6.6. Projected shoreline changes near the Test Area 13B Tower for the scenario in which the present rate of sea-level rise continues.

Figure 4.6.7 shows the mean rate of projected shoreline advance near the test structure. Comparison of this with the more complete portrayal of results shown on Figure 4.6.6 emphasizes the value of full statistical representations. The results shown on Figure 4.6.6 are of special interest because of an expensive facility located there that is used in the testing and calibration of new ordinance. This provides an interesting example of the potential application of the MoCCS modeling results. Base managers are currently faced with decisions regarding the

continued use of this tower. During the sequence of storms between 1995 and 2005 the adjacent shoreline retreated dramatically. Shore erosion control structures have been emplaced but the question remains. Should the erosion control structures be repaired and possibly extended to protect the tower if substantial shoreline retreat continues into the future? Perhaps this is ultimately futile and the sooner this can be recognized the better. Perhaps the tower will need to be abandoned with the test equipment relocated onto another type of platform. Candidate platforms include a deployment on a specialize aircraft. A decision of this nature must be made years in advance due to the lead time needed to design, engineer and manufacture the new types

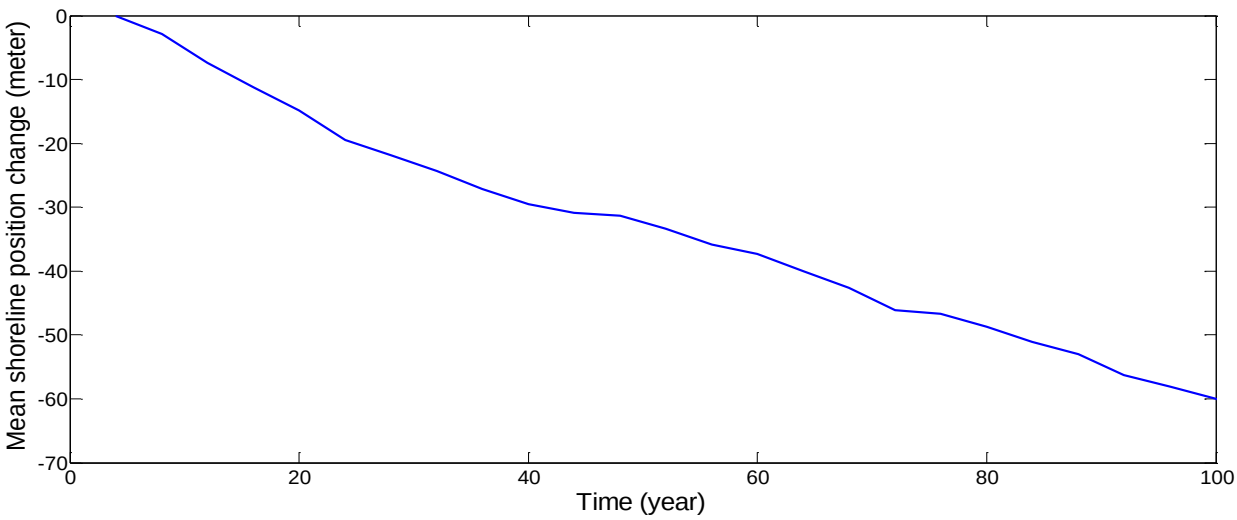

Figure 4.6.7. Projected mean values of the shoreline position change at the Test Area 13B Tower for the scenario in which the present rate of sea level rise continues. Negative values indicate that the shoreline is prograding.

of measuring equipment.

At this time, it must be stressed that these results are intended only to show a representation of the type of results that can be produced by this modeling analysis and are not highly reliable predictions upon which real decisions can be based. To make the more reliable predictions, several of the simplifications in determining modeling parameters will need to be restudied and improved. Nevertheless, these illustrative results show that the relative rate of sea level rise is an important determinant of the long-term projection of the shoreline position. This approach is far better than could be arrived at by simple projection of the rate of shoreline retreat determined from the decade containing a rare sequence of major storms.

4.6.2. Projecting Island Morphology Change. The MoCCS model was used to simulate the geomorphologic response of the dunes, island platform elevation and bay shoreline on Santa Rosa Island to different rates of sea level rise in 100 years. The annual rate of aeolian sand transport from the beach towards the dunes was taken as 1.3 m^3/yr/m from a study for Okaloosa County (Taylor Engineering, 2007). Three island cross-sections are used to illustrate the results. Section 1 is initially 500 m across from the ocean beach to the bay shore. This represents a wide portion of the island with an initial condition representative of where pre-existing dunes have been recently destroyed. Section 2 is initially 400 m long and represents a somewhat less wide portion of the island where the principal dune ridge is initially 6 m high and 32 m wide. Section

3 is initially only 100 m wide and it represents the narrowest portion of Santa Rosa Island. This section also has a primary dune with an initial height and width of 1.5 m and 7 m, respectively.

To calculate the volume of erosion using Equation (3.6.1), it is necessary to determine runup height (R), based on the wave period (T), and surge height (Δh). As mentioned earlier, the Okaloosa County FEMA flood study results were used to determine the maximum surge heights associated with four different occurrence probability densities. The NOAA SLOSH Model (Jelesnianski et al., 1992) with the Panama City (FL) grid was used to estimate the hurricane central pressure deviations, radii to maximum wind and forward speeds that would result in the four maximum surge heights through an iteration procedure. Running SLOSH gave surge height and maximum wind speed for each of the four storms; the latter was used to estimate H_0 and L_0 of Equation (3.6.2) based on the Shore Protection Manual (USACOE, 1984). The surge duration (t) in Equation (3.6.1) was estimated based on a sine function of surge hydrograph, island elevation (Z_0), and maximum surge heights. Following Larson et al., (2006), the C_s value was taken as 1.8×10^{-3}.

The model was operated for all sea level rise scenarios and a single century-long realization to illustrate the range of morphological responses. It was also used to define the trend and variability of future predictions with a series of multiple realization tests. These results are also used to assess the prediction uncertainty. The results from the individual 100-yr realizations are described first.

To demonstrate the morphological responses a series of individual 100-yr simulations were performed. Unless otherwise specified, the single realization results shown here are for the same series of six hurricanes as listed in Table 4.6.1 and sea level rise scenario SL – 1.0. Figure 4.6.8 shows time series plots of dune height (DHT), bayshore position (BP) and island platform freeboard (IPF) at three representative island sections. The three profiles were selected to represent difference in the initial morphology. These were defined previously and are labeled as profiles 1, 2 and 3. In Figure 4.6.8, the sets of three panels are arranged one below the next with those for Profile 1 at the top and Profile 3 at the bottom.

The relative impact of each storm as well as the importance of the recovering dunes in withstanding the next event is clear. Profiles 1 and 3 show initial growth of the dune heights before the arrival of the first storm. The initial dune height on Profile 2 is near the upper limit so it does not increase. Instead, the sand added before the first storm goes into storage in a dune field. This provides a sufficient reservoir of sand volume to greatly reduce the impact of the storms compared to the way the dunes on the other two profiles respond. Some storms devastate the dunes and there are long periods where dunes grow to their maximum heights. The relatively long width at Profile 1 causes it to trap all of the eroded dune sand on the island platform with none available to balance against the encroachment of the bayshore. The results for the island platform freeboard show that the volume added to the island platform from the eroded dune is also inadequate to keep pace with this rate of sea level rise. The third panel shows a nearly uniform decrease of the island platform freeboard that is close to the total rise in sea level.

The results for Profile 2 show that the initial dune height is important throughout the 100-yr simulation. Although the dune is eroded, it is never erased. It provides an important volume of sand to the bay shoreline, which results in offsetting the transgression due to the sea level rise. However, this occurs in one event early in the sequence of the storms. Subsequent events do not

provide sand to the bay shoreline and even fail to provide enough volume to the island platform to keep up with the rate of sea level rise. This contrasts with the results for Profile 3 at the narrow waist of the island. Although the dunes are small initially and they are erased three times in the first sequence of storms, the dune eventually grows to heights similar to the other places. The narrow width of the island allows the island platform freeboard and the bay shoreline to keep pace with sea level rise or slightly exceed it.

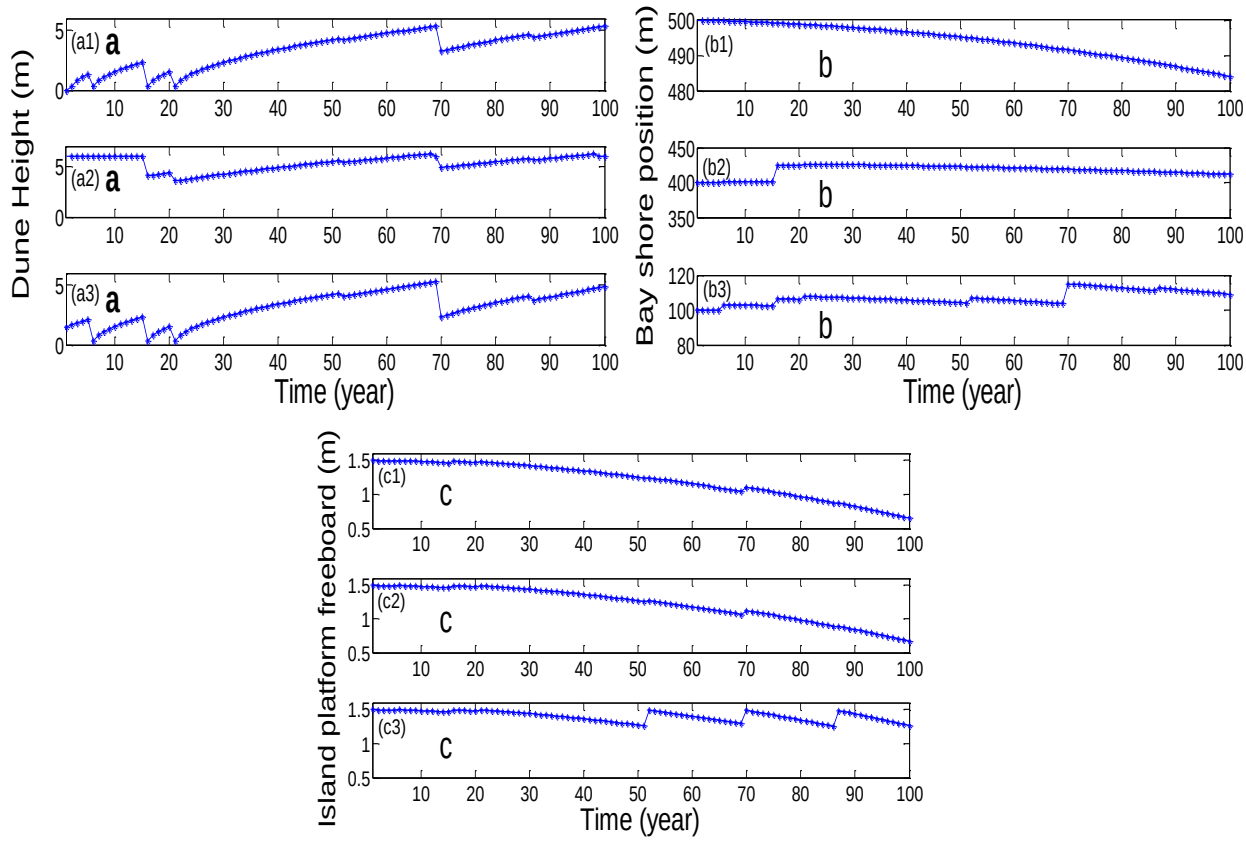

Figure 4.6.8. Changes over three island cross-sections of dune height (a1- a3), bay shore (b1-b3) and island platform freeboard (c1-c3) for a 100-yr simulation containing six hurricane events.

Figure 4.6.9 illustrates the impacts of the different sea level rise rates on the evolution of the dune heights, bay shoreline and island platform freeboard for Profile 3 (100 m wide). The different rates of sea level rise have little effect on the dune height because the dune building processes remain constant in all of the sea level rise scenarios. Predictably, the bay shoreline advances and the island platform freeboard are best maintained during the lowest rates of sea level rise.

Individual realizations of future conditions are obviously of limited value when dealing with a natural coastal system that is strongly forced by a highly variable set of storms and with multiple interacting non-linear responses. The MoCCS model permits a large number of Monte Carlo (MC) simulations to be run in both the Chronic and Acute components. Convergence of the simulations was investigated using the block average method, and it was found that 1,000

realizations are sufficient over the domain during the entire simulation period under all five sea-level rise scenarios.

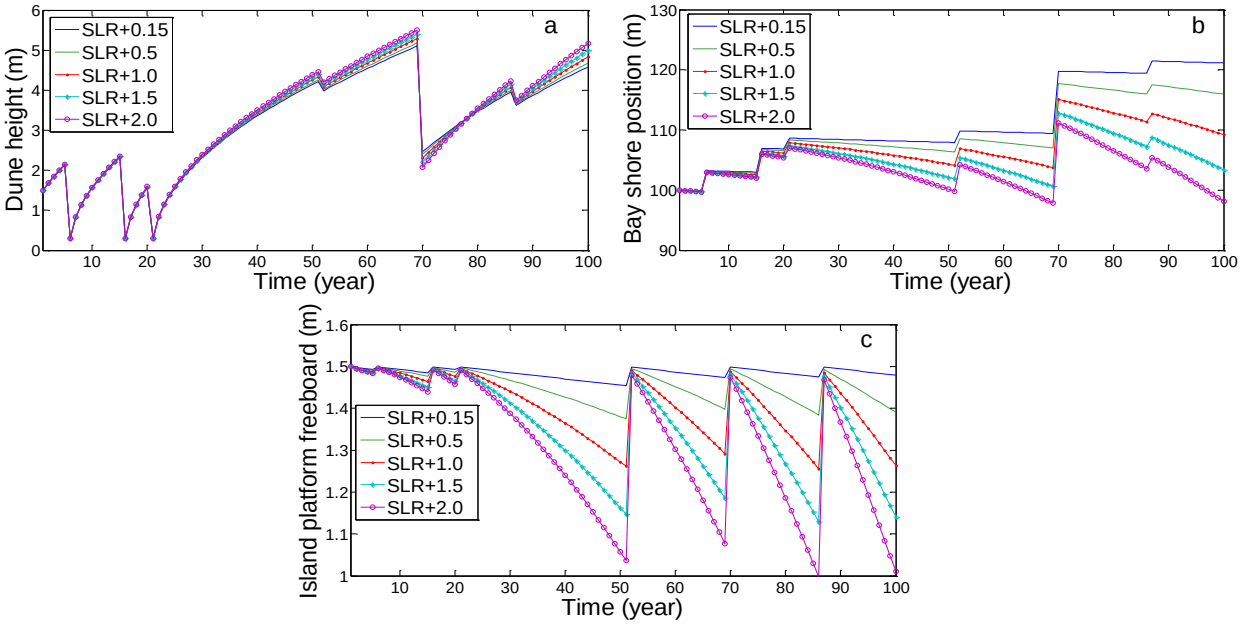

Figure 4.6.9. Comparison of the island response to five 100-yr sea level rise scenarios for the narrow (100 m) cross section.

The predictive uncertainty was quantified by examining mean prediction, prediction variance, and probability density functions (PDFs) of variables of interest such as dune height and bay-shore position. Figure 4.6.10 plots temporal variation of the mean and variance of bay-shore positions at Profile 3 under the five sea-level rise scenario. These are designated as SLR+0.15, through SLR+2.0 corresponding to total sea level rises over the 100-year interval of 0.15, 0.5, 1.0, 1.5 and 2 m respectively. Temporal variations of the mean and variance are different under different scenarios. The mean increases with time in the first three scenarios but decrease under the last two scenarios with higher rates of sea level change. The variance increases with time under all the five scenarios, with the smallest increasing rate under the baseline scenario. This variability poses large prediction uncertainty, particularly under the scenarios of large sea-level rise. It is therefore uncertain whether island erosion or accretion will occur, especially under the scenarios with larger sea-level rise. Decision-making or engineering design based on a single realization or the mean is risky, and the substantial variability should be addressed in coastal engineering design and long-term management. In comparison with the mean and variance, the PDFs are more comprehensive and quantitative for quantifying predictive uncertainty, which however are not presented due to the page limit.

In comparison with the mean and variance, the probability density functions (PDFs) are more comprehensive and quantitative for quantifying predictive uncertainty. Figure 4.6.11 plots the PDFs of the bay-shore position at cross-section 60 at 25, 50, 75, and 100 years. The figure also shows that the PDFs are significantly different under different sea-level rise scenarios. Evolution of the PDFs is of particular interest. The PDFs show two modes under each scenario in early

time (e.g., 25 years). For the baseline scenarios, the peak of small values becomes less and less dominant when time increases. At 100 years, only one peak exists. It is similar for scenario 1. For scenarios 2-4, when time increases, the mode of large value shifts to right and becomes dominant; the other model shift to left and becomes relatively less significant. The shifting indicates increase of prediction uncertainty. If the peak of smaller value is still significant (e.g., for scenario 4 at 100 years), it should be considered in engineering design and decision-making. The PDF is of particular use, because it can be used to easily evaluate the probability of island erosion or accretion by calculating the area below of the PDFs for a given threshold.

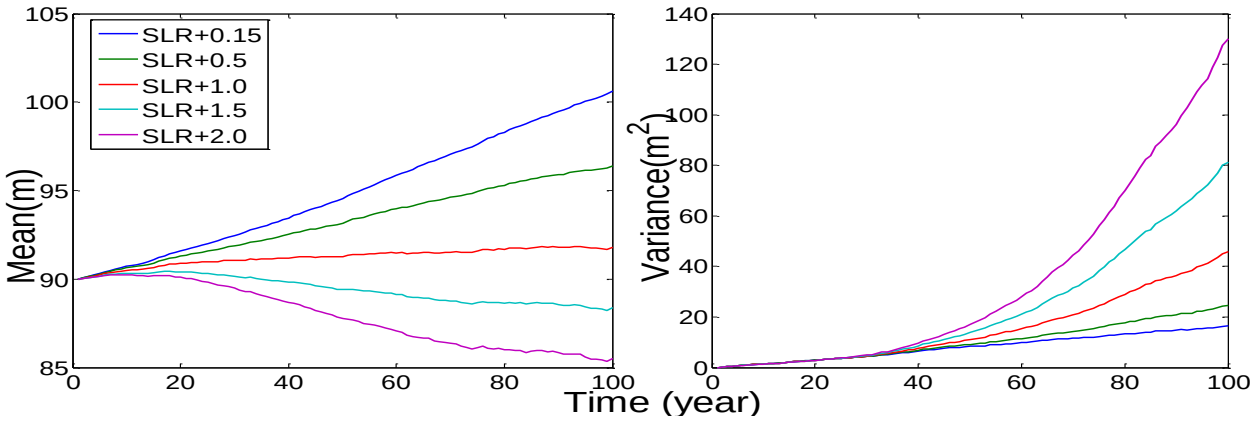

Figure 4.6.10. Temporal variation of mean (left) and variance (right) of bay-shore position under the five sea-level rise scenarios at Profile 3.

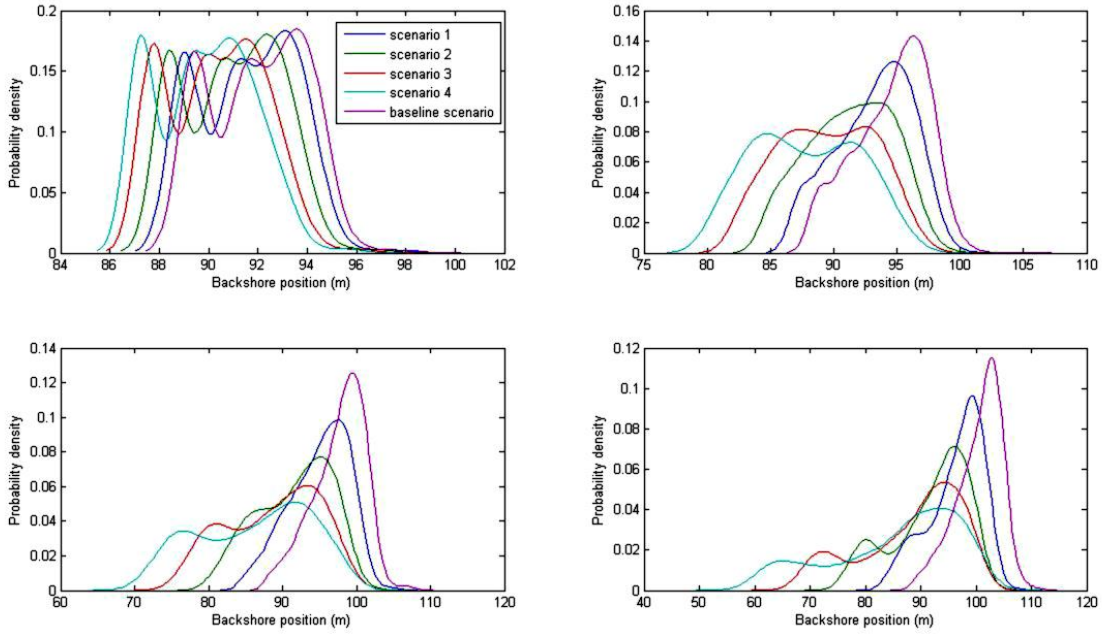

Figure 4.6.11. Probability density function (PDF) of bay-shore position at cross-section 60 at (a) 25 years, (b) 50 years, (c) 75 years, and (d) 100 years.

Based on the quantification of parametric uncertainty under individual scenarios, the scenario uncertainty is quantified using the model averaging method. The first task is to estimate scenario probability $p(S_k)$ based on historical data and/or expert judgment. As part of a sensitivity analysis, the scenario averaging is conducted for various sets of scenario probability. A total 126 sets of scenario probabilities are obtained by first discretizing the probability of each scenario at 10% increment and then conducting a permutation according to $\sum_{k=1}^{n} p(S_k) = 1$; combinations of the probability of the five scenarios that do not satisfy this condition are discarded. The extreme cases are that (1) one scenario has 60% probability of occurrence but each of the other four individual scenarios has 10% probability; and (2) each scenario has 20% probability. The form case indicates that there is a dominant scenario, while the latter case that all the scenarios have the same probability of occurrence.

Figure 4.6.12, in the manner of Figure 4.6.10, plots the mean and variance of backshore position obtained from scenario averaging using the 126 sets of scenario probabilities. While Figure 4.6.10 shows that different scenarios have different effects on dune height predictions, Figure 4.6.12 suggests that the mean and variance of scenario averaging are within those of baseline and Scenario 4, i.e., the smallest and the largest sea-level rise. Figure 4.6.12 shows that, after the averaging, despite of variability of the scenario probabilities, the predictive uncertainty (measured by the variance) is smaller than that of individual scenario. It suggests that, if the scenario probability can be determined, predictive uncertainty can be reduced and more science-informed decision-making can be made.

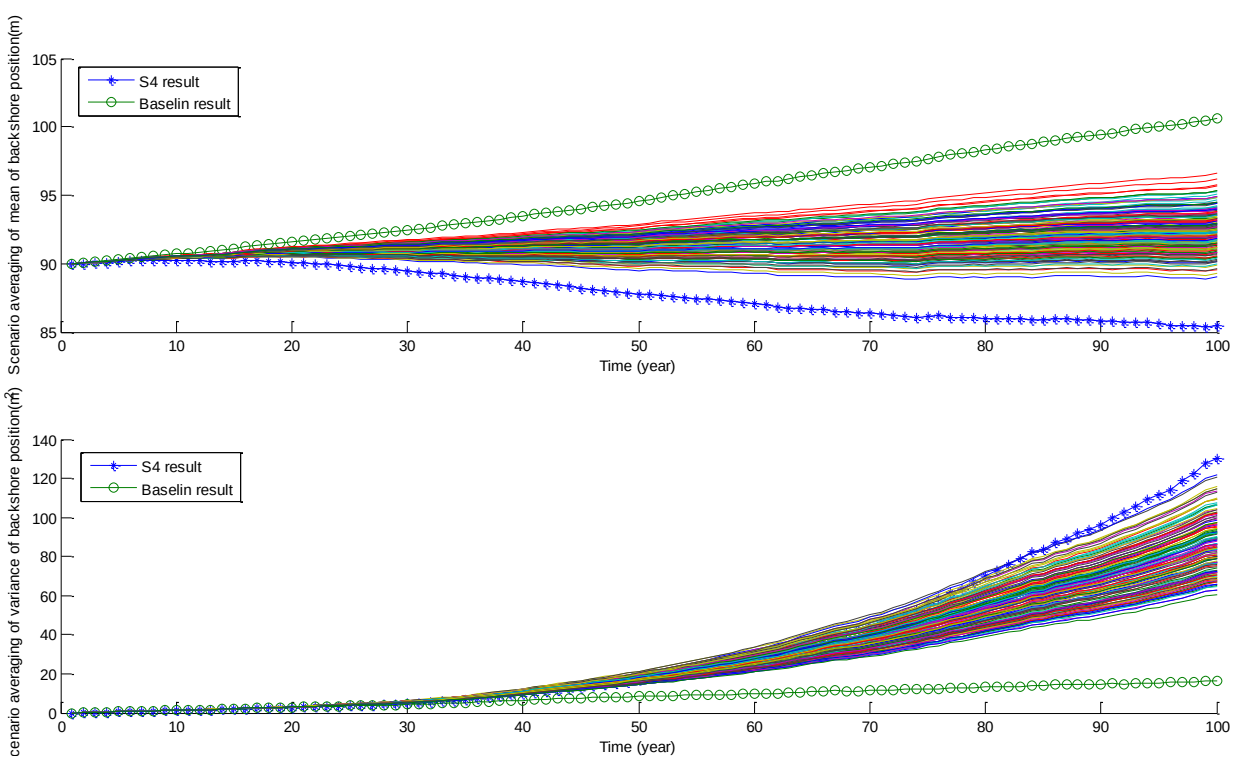

Figure 4.6.12. Scenario averaging of (a) mean and (b) variance of backshore position prediction at cross-section 60 using 126 scenario probability sets.

Similar to Figure 4.6.11, Figure 4.6.13 plots the PDFs of the backshore position obtained from scenario averaging. The figure also shows that the averaged PDFs are within the PDFs of the baseline scenario and Scenario 4. When examining the ranges of the distributions, the predictive

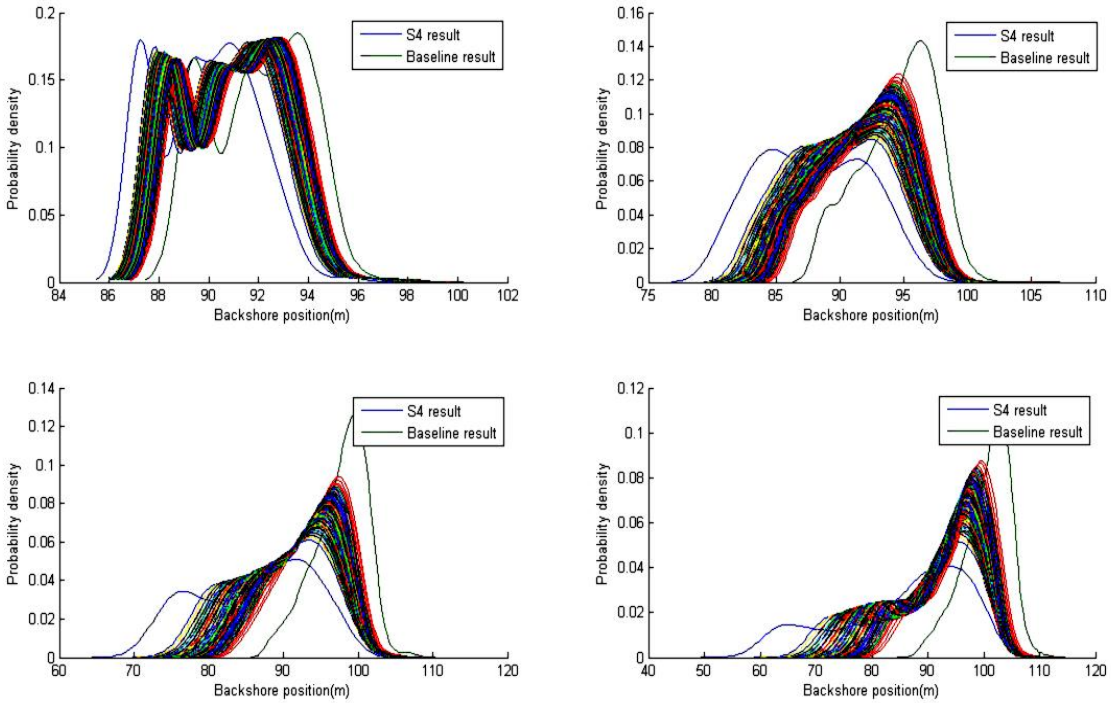

Figure 4.6.13. PDFs of backshore position prediction at cross-section 60 on year (a) 25, (b) 50, (c) 75, and (d) 100 using scenario averaging.

uncertainty corresponding to the baseline scenario is the smallest and that to Scenario 4, the largest. This figure suggests again that considering scenario uncertainty is expected to reduce risk and, at the same time, help decision-makers optimize limited resources in coastal management.

4.6.3. Projected Inlet Zone Changes. As noted earlier the East Pass Inlet to Choctawhatchee Bay is maintained by the U.S. Army Corps of Engineers though a program of periodic dredging and is stabilized in position by jetties. It is assume that these jetties will be maintained and that the dredging will continue over the next century. However, the inlet will continue to be a sink for longshore sand working its way across the inlet mouth and the effect of this will be to withdraw the sand necessary to promulgate the inlet shoals and the pass at their same depth below sea level and with their same areas. Figure 4.6.14 shows how these withdrawals of sand to the inlet deposits due to rising sea level affects the adjoining beaches for different rates of sea level rise. These results are for the simple case representing a somewhat unlikely continuation of mild storm conditions for the entire 100-year simulation. This gives a clear indication of the trends without complications that would arise in illustrating stochastic results.

These forecasts of accelerated beach erosion show that the effects may be evident as far as 10 km to the west of the inlet in the most extreme case. However, these may not be realized because beach nourishments or other forms of shoreline stabilization may be used to offset the natural

trend. Nevertheless, these results show the potential threat to the eastern portion of the Eglin AFB shoreline which lies within this potentially impacted zone.

4.6.4. Discussion of Results. The goal of this research has been to develop a method based on a new numerical model that allows useful predictions of the relative effects of different potential rates of sea level rise over the coming century on the morphology of complex coastal systems where military bases and infrastructures are, or can be located. The governing design philosophy has been to "get it done". That is, there are a tremendous number of interacting processes forced by constantly varying winds, waves, tides, sediment supply, sea level and other parameters that control the long-term evolution of coastal morphological features. It has been critical to decide on the relative role of these processes to select proper physical definitions of the important factors and to parameterize or ignore those of lesser importance. It is also vital to understand that the different components of the complex coastal system, such as the beach, dunes, shoreface,

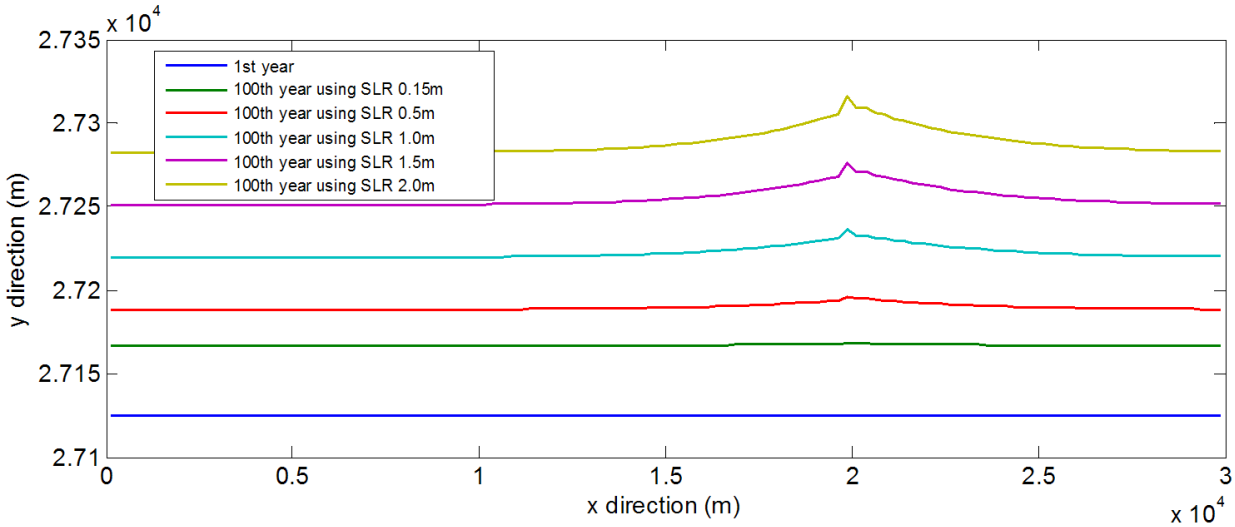

Figure 4.6.14. Computed relative changes on the shoreline adjoining the East Pass Inlet for different rates of future sea level rise. Inlet, at x = 2 x 10^4 m, is not resolved in these plots.

overwash, etc. must be quantitatively represented within the overall system because each interact with the other in strongly nonlinear balances.

The degree to which each of the physical processes represented within MoCCS model are fully understood is quite variable. For example, surf zone and beach sediment transport processes are generally considered to be well understood while the growth and development of coastal sand dunes is much more poorly known. In order to assemble the represent the sum of these processes in the interacting components of the MoCCS model it has been necessary to appeal to the governing design philosophy. Where things are well known they can be clearly represented in mathematical expresses and tested. In other cases, simple and even relatively primitive quantitative relationships had to be cast aside to avoid sidetracking the effort into resolving a detail at the expense of progressing the whole. The important point here is that if the whole can be developed and shown to operate in a meaningful and useful way then it should be possible to go back to the places where simplified representations have been adopted for expediency and to adequately improve these. In fact, the operation of the model as a whole helps to identify how such future efforts are best prioritized.

The MoCCS model can be expanded to include other coastal system components in the future. The routine now used to model the storm erosion and retreat of the frontal dunes provides a basis for a routine to represent similar storm erosion and retreat of a coastal bluff. The same can be said about the tidal inlet. The current version of MoCCS includes a jetty-stabilized and maintained inlet. This can be readily modified for shores where the inlet is natural.

The goals of this research do not include producing highly reliable predictions for specific locations or base facilities. This permitted the development of the MoCCS model without concern to specific detail. Where details have been given they are for illustrative purposes only. Again, the point has been to "get it done" with the understanding that if it proves to be meaningful and useful it, and its supporting data, can be refined to produce reliable results.

The results presented in this section of the report clearly show the usefulness of the MoCCS model in extending capabilities of evaluating the impacts of future accelerated rates of sea level rise to include real coastal morphological dynamics, not just "bathtub inundation". The model operates efficiently on readily available computer facilities so that predictions are based on stochastic rather than deterministic characterizations. The MoCCS model makes good use of existing legacy data and other numerical models. As discussed earlier, a system of cross-scale modeling is used to provide realistic proxies for what would be long and very expensive sets of field measurements of ocean currents and waves. Other existing models are used to parameterize complex processes such as the relationship between hurricane intensity and track on the heights of the storm surges. On the other hand it cannot be adequately emphasized how import it is to have a great amount of high quality data taken over an extremely long period of time to develop and test this morphodynamic model. The data collected with the several components of the overall project, as described previously in this report has been invaluable.

At this stage, the MoCCS model is far from perfect. There are a number of quantitative representations that are very general and not well support by either detailed theory or analyses of good data sets. The sensitivity of the results to the potential weaknesses of these approximations has not been tested. The multi-line structure of the model has been a great help to development of the underlying concepts for representing several of the model components and in permitting the model's timely completion. However, this structure is somewhat awkward and limiting to the full range of conditions for which it can be applied. Therefore, it would be well to replace this structure with a full grid-type model. Data sets from places other than the Eglin AFB and Santa Rosa area that are potentially available have not been accessed and analyzed. It is somewhat ironical that the ASMITA component of the model that provided some of the original basis for the MoCCS model has been found to be unsuitable to the conditions of Choctawhatchee Bay. This bay, and most others on U.S. coasts, do not have the systems of intertidal channels and mud flats that are the basis of ASMITA. ASMITA was originally intended to represent the bay, inlet and inlet bars. MoCCS retains representations of the inlet and the inlet bars but the development of a representation of the bay has lagged so much that it is not yet included in the model. This needs to be corrected. The guidelines for the operation of the MoCCS model have not been developed. Documentation consists of detailed comment statements within the Fortran and Matlab codes. Better documentation would help to take advantage of the present level of experience not only with model operation but also with the reduction and preparation of the supporting data. The model would benefit greatly from its application to other coastal settings. Finally there is a clear need to improve the data output graphics and results presentations so that they are more readily understood and appreciated by engineers, planners and facility managers

who are not specialists in coastal engineering and coastal morphodynamics. In spite of these shortcomings, it can still be confidently asserted that the encouraging results presented in this report clearly provide motivation for continued work and experimentation.

With these general comments having been made, we turn to an inventory of the specific research results. These are organized to roughly correspond to the order in which the results were described in the preceding report sections.

It has proved possible to produce a model that operates on appropriate time- and- space-scales to adequately represent the processes that control the large-scale evolution of the shoreline of open ocean beaches and barrier islands. This involved not only representing the general surf zone processes but included the interacting sediment transport processes of the shoreface, inner continental shelf, inlet and storm overwash components. The model shows good agreement between computed and measured shoreline changes over a historic period of nearly a century long duration.

The MoCCS model shows that the rates and directions of shoreline change vary considerably with location along the Santa Rosa barrier island. At the present rate of sea level rise there is an underlying tendency for beach deposition and shoreline advance over much of the island length; especially along the shore of Eglin AFB. An exception exists in the eastern portion of the base because of the influence of sand withdrawal into the tidal inlet. The model shows that this underlying trend for deposition along much of the island shoreline will change if the rate of sea level rise increases. Because of the spatial variability of the rates of shoreline position change it can be said that any acceleration in the rate of sea level rise will convert the present trend from deposition to erosion. At small increases in the rate this change is quite local and specific. At increasing rates this reversal in the direction of future shoreline change direction becomes more general. The present results from the model indicate that this “tipping point” for most of the island shoreline can occur at rates of sea level rise that are commensurate with a total rise of between 0.5 and 1.0 m over the coming century.

The results show that the basic model of the dune erosion, overwash and barrier island and changes to island morphology is capable of representing considerable practical information about the relative effects of different century-long sea level rise scenarios. At this point the model has been calibrated against some field calibrations. Comparisons of historic dune growth, erosion and shoreline change on Santa Rosa Island, based on comparisons of Florida Bureau of Beaches and Coastal Systems surveyed profiles and LiDAR images from a variety of sources, show that the relative rates of these changes are in general agreement with the corresponding rates derived from the model. It is clear that dunes are ephemeral features and that their main role is to provide a storage volume that is redistributed across the island in major storms. There appears to be a relationship between the annual flux of wind-blown sand and the hurricane climate such that the dunes only rarely grow to the height limit that is imposed in the model. The island translates both towards the bay and upward. Depending on the rate of sea rise and overwash sediment supply, the horizontal translation can be seen to either create or submerge a habitat suitable for coastal birds or for the backbarrier salt marshes.

The results also clearly show that there is no single response of a barrier island to sea level rise. The antecedent topography and the local island width are very important predictors of island response. On relatively narrow sections the island width and platform freeboard tend to track sea

level rise even up to the 2.0 m/100-yr scenario. Wider sections deposit overwash sand volumes over larger areas and do not keep up with even modestly accelerated sea level rise rates.

Where the island platform grows upward at a rate proportional to the island width, storm flooding of the island platform is less deep and shorter duration.

In closing this discussion of results, it is worthwhile to step back and take an overview of what the results mean from the point of view of understand the behavior of the complex coastal system and from the point of view the potential applications to base management. The general nature of barrier processes is well known and the subject of many textbook chapters. This study identifies the relative importance of the major processes specific to the Santa Rosa barrier island that are important in it maintenance in the presence of rising sea level. Both measurements of historic shoreline development and the results of the MoCCS model confirm that the shoreline is generally stable or advancing along most of the island length during extended periods that normally occur between landfalls of major hurricanes. Most of the shoreline of Eglin AFB is located where this trend towards advancing shoreline is most pronounced. The exception is the portion of the island and the base shoreline west of the East Pass tidal inlet. Even though this inlet has been stabilized by jetties and is maintaining by dredging it is still the cause of shoreline retreat along the easternmost reach of the island. Nearby landfalls of major hurricanes have are destructive on nearly all barrier island but they can be especially important in shaping Santa Rosa island because the primary dunes are of a scale that make them vulnerable to substantial destruction. The period between 1995 and 2005 is somewhat remarkable because of the impact of three major hurricane; Opal in 1995, Ivan in 2004 and Dennis in 2005. Significant shoreline retreat occurred along the entire length of the island and cumulative displacement overcame the previous decades of shoreline advance.

The results MoCCS model demonstrate that sand accumulated stored in the primary dune ridge during the prolong periods that normally separate major hurricane strikes provides a critical reservoir. The model emphasizes how this sand is redistributed over and across the much of the island as island platform and bayshore overwash deposits during the storms. The general effect is for the island to grow both upward and bay-ward. The MoCCS model indicates that there are critical balances in the long-term average occurrences of hurricane impacts and the morphology of the island. The dunes tend to grow up to heights around 6 m but are usually eroded by one or more major storm as they approach this crest elevation. This irregular cycle of dune growth and destruction with much of the sand being transferred onto and behind the island is shown by the MoCCS model to be balancing the island position and freeboard against the current rate of sea level rise. Not all of the island can be described this way. To the west of the base there are developments which seriously interfere with these natural processes. There are also several places along the island where inland dunes modify the routing of storm overwash. Nevertheless, the MoCC model does indicate that in general the island can be expected to be maintained at the present rate of sea level rise and even if this rate is increased modestly. On the other hand, the model also confirms that at some of the higher rates of sea level rise that have been test the island cannot maintain these balances and a general retreat of the Gulf shoreline, the bay shoreline and a lowering of the island platform freeboard relative to sea level can be expected. The model also shows that the sea level rise rate where changes in these critical balances is different at different places along the island depending on both local morphology and the general curvature of the Gulf shoreline.

There are several practical interpretations of the results. For example, the results show that the recently encountered period of intense storm erosion due to the landfall of three major hurricanes within a decade is anomalous. The destruction of the Gulf shoreline within Eglin AFB will probably be reversed if a more normal prolonged period of normal beach advance occurs before the next major hurricane. The probabilities of these changes and tends can be represented by the model. This suggests that facilities on eastern portion of the barrier island near the inlet will need continuous maintenance and shore defense structures are progressively less likely to be effective. Conversely, elsewhere along the Eglin AFB Gulf shoreline long-term beach stability or growth is most likely. This means that coastal defense structures can be effective against the occasions when major storms strike.

5. Conclusions and Implications for Future Research and Implementation

The outcomes of this investigation are most encouraging.

The project has been successful in modeling several different scientific components of the coastal system. The result has been the development of an integrated set of methods for predicting the impacts of different sea-level rise rates on a variety of different morphological features and natural resources of the prototype project area of EAFB, and more generally, coastal bases in many places with similar processes and natural features.

We have found that there are substantial differences in the type and magnitude of impacts to infrastructure and natural areas related to the different projected rates of sea level rise over the next century. For example, setting aside the issue of possible changes in the storm climate for the moment, the conceptual model resulting from the wide variety of existing data that has been collected and the purpose-built numerical morphodynamic model both show that the rates of beach erosion and barrier island change are strongly coupled to the sea-level rise rate. This, in turn, has a direct impact on the base facilities on Santa Rosa Island, on the coastal wetlands and on the island's groundwater resources. These responses are further affected by future scenarios that include changes in the hurricane climate.

The individual project components have been independently productive (several publications and conference presentations have been produced) and are proving to be mutually supportive. Each specific task has produced significant results and related scientific conclusions. These are described in the following subsections.

5.1. Analyzing Historic Coastal Change and Remote Sensing Data

Santa Rosa Island is representative of the narrow, low relief barrier islands located in the northern Gulf of Mexico. The foreshore of the island is exposed to a low tidal range and limited wave energy. The effective present day long-term average sea-level rise for the Florida Gulf Coast (2.3±0.3 mm near Pensacola, Florida) is lower than sections of the Gulf Coast near the Mississippi Delta, where barrier islands are effectively being destroyed by a combination of flooding and storm activity. The combined low energy environment for the Florida Gulf Coast, the absence of flooding due to rapid sea-level changes, plus a relative constant supply of littoral sediments, may be important factors in producing a shoreline that has remained stable throughout much of the 20th century.

GIS-DSAS analysis of historical charts, aerial images, and recent lidar data have made it possible to measure the foreshore position for the entire length of the island to a high degree of accuracy, covering the period 1870-2007. The large number of available data sets (up to 40) allows detailed studies of the rate of shoreline change. During the early 20th century (1906-1916), a cluster of four Category 3 hurricanes probably have produced significant erosion (up to 100 meters) along the narrow, western portion of Santa Rosa Island. During much of the remaining portion of the 20th century (1930s-1995), the foreshore of the island was stable or accreting. During this period, the eastern portion of the island accreted at rates of 0.5-1.0 meters/year. Three major Category 3 hurricanes that crossed the island at the end of the 20th and beginning of the 21st century, Dennis (1995), Ivan (2004) and Dennis(2005), produced profound changes in the island's morphology. Hurricane Dennis destroyed much of the foredune system along the

eastern portion of the island and produced significant shoreline erosion. Subsequent Category 3 storms continued to contribute to shoreline erosion and degradation of foredune systems. The absence of foredunes also allowed significant areas of overwash fans to develop and move sediment from the foreshore to the mid- and bayside of the island. Up to 100 meters of foreshore erosion occurred during the 1995-2007 period. Following hurricane Dennis (2005), there has been modest recovery (~30 meters) of the shoreline along the eastern portion of the island. Beach renourishment projects on the Eglin Air Force Base segments of the island will restore the shoreline to a position that preceded the cluster of hurricanes that affected the island in the past 20 years. Analysis of island growth near Pensacola Pass indicates an annular growth of 0.62 hectares/year. Dredging records from the inlet at Pensacola Pass suggest a westward littoral drift sediment load of at least 175 million cubic meters per year. This relatively constant supply of sediment has helped to maintain the stability of the island's shoreline.

Santa Rosa Island is currently in a nearly stable state between erosional and depositional processes. The island is prone to significant erosion at times when clusters of major hurricanes pass over or near the island. The clustering of storms produces a compounding effect by destroying foredune systems that prevent overwash fans from moving sediment from the foreshore to mid- and bayside of the island. This effect accelerates erosion during subsequent storms.

5.2. Modeling Future Storms

The strongest hurricanes are getting stronger as oceans continue to warm. This will lead to a greater loss potential to military infrastructure from high surge and winds from future storms that will be exacerbated by rising sea levels. Our work has led to a better understanding of the methods, models, and tools for conducting vulnerability and impact assessments related to future hurricane risk at EAFB. These methods can be applied to other locations along the Gulf coast and with some minor modifications along other hurricane-prone areas of Florida and the east coast. Our methods are an important step forward in aggregating losses from flood and wind damage rather than treating them as unrelated events.

As a proof of concept that future surge and wind events with their associated loss estimates can be modeled with a free toll as long as ArcGIS (ArcView) is available, Figure 5.2.1 is a future Hurricane Opal affecting the base. While most of the inundated developed areas are outside of the main base boundary, there are areas that are part of the main base that could potentially be flooded. This map was produced using the latest HAZUS 2.1 release that couples the SLOSH storm surge model with the previously mentioned HAZUS wind model. Hence, these flood models can produce combined wind and surge loss estimates for the study area.

5.3. Analyzing Paleostorm History in Coastal Sediments

The results of the paleostorm study demonstrate that a reliable storm history can be extracted from coastal sediment cores, based on a combination of isotopic and sedimentologic data, and using a statistical model which has been calibrated with the historic storm record. This new paleostorm identification method, and the model that has been developed, can be employed to identify storms in the sedimentary record that predate the historic storm database. A thorough investigation of the sedimentologic and isotopic properties of coastal lake sediments has shown that no single proxy is sufficient for identifying storm signatures. However, a combination of

isotopic and sedimentologic data has been proven to be sufficiently sensitive to detect major storm surge events that have impacted coastal lake sediments. As such, the newly developed methodology can provide paleo-storm frequency over the past several millennia.

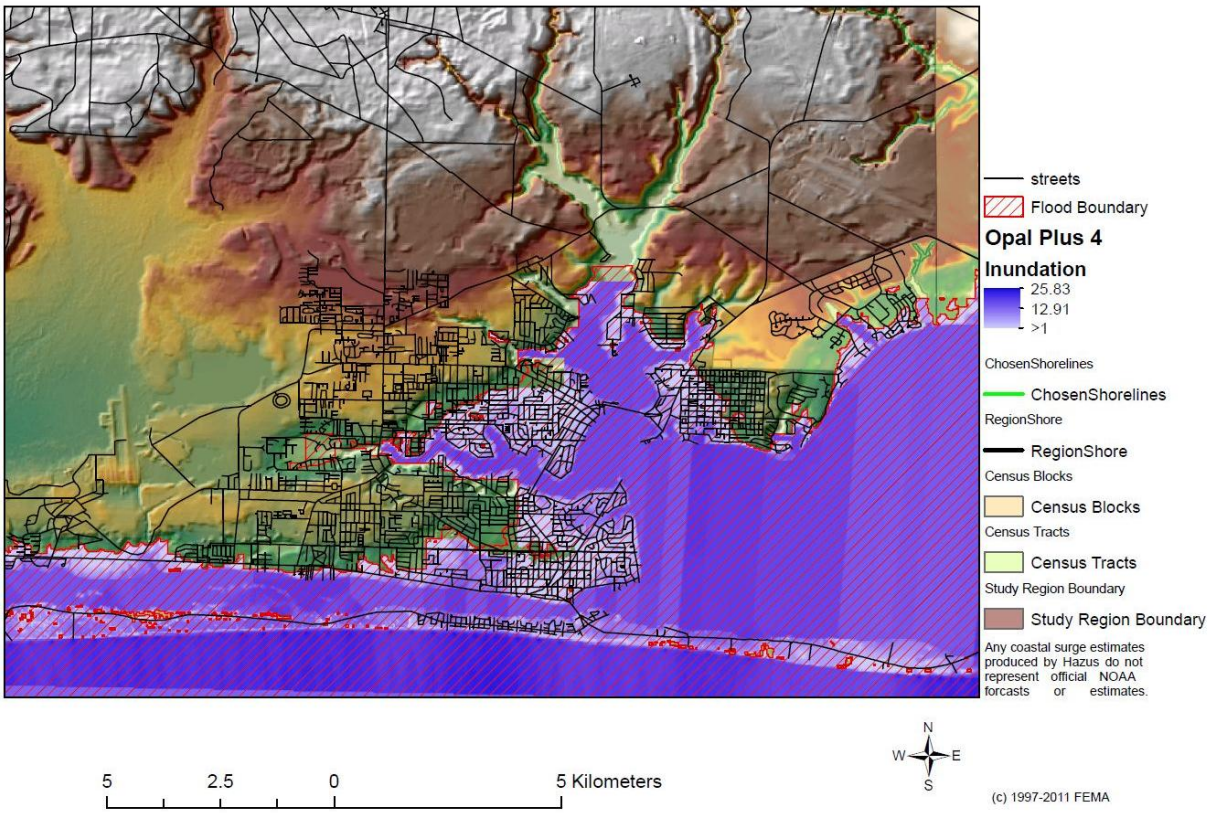

Figure 5.2.1. Future Hurricane Opal with stronger winds and higher sea level, showing roadway grid.

This new methodology is more objective, and more robust, than the standard methods of counting overwash sand layers or identifying marine microfossils in the sediments. The isotope model employed in this study identified 229 separate storm intervals spread the nearly 5,000-year lake history represented by the core. In addition, four periods of increased storminess were evident in the record, including the present period.

This region of northern Gulf of Mexico coast has experienced millennia-long cycles of increased storm activity, separated by quiescent periods of shorter duration. The level of major storm activity during the historic period of the past 150 years (6.2 storms per century) is significantly greater than the long-term mean storm frequency over the past five millennia (5.0 storms per century). The most recent "active" period is the longest in the observed record. Major storm frequency during the historic period is a continuation of a trend of increased storminess that began about 1,300 years ago. The mean frequency of major storms during the historic period is not significantly different from the mean level of storm frequency during the "active" periods of the past five millennia (6.9 storms per century).

This study has demonstrated that storm events, which carry only marine storm surge into a coastal lake, without sediment overwash, can be detected through their isotopic and sedimentologic signature. The method is robust and the results are comparable to those of other

studies using different storm proxies. The methodology employed during this investigation is capable of generating a storm history for any similar coastal region, and represents a quantitative basis for modeling storm risk in a warming future.

It should be noted that the storm models that have been investigated and developed for this project (e.g., the MOCCS model) require estimates of storm frequency and storm intensity. The original intent of the paleostorm investigation was to develop a complementary method for discerning both storm frequency and storm intensity for paleo-storms in order to incorporate the long-term storm record into the models. The paleostorm identification method that we have developed for this project, using geochemical proxies, allows us to quantify paleo-storm frequency. We have also investigated the use of geochemical proxy signatures in measuring paleo-storm intensity. The work on this aspect of the project is continuing. The new method can identify paleo-storm events as major storms, but thus far cannot discriminate in terms of wind speed or storm category.

5.4. Modeling Coastal Wetlands

Two major coastal wetlands are located in river deltas adjacent to Eglin Air Force Base. The Yellow River and Choctawhatchee River deltas are characterized by abundant freshwater swamps and limited areas of tidal or near-tidal marsh. In the Yellow River wetlands, for the present sea-level conditions and for areas below one meter NAVD88, tidal and near-tidal marshes comprise approximately 40 percent (990 hectares) of the coastal wetland. The remaining wetlands are freshwater swamps and marshes. Progressive sea-level rise (up to one meter for this study) results in a progressive flooding of the present tidal marshes. The location of the marshes migrates up river and there is a 30 percent decrease in fresh water swamps. The extent of the different tidal marsh environments change. The most noticeable change is a dramatic increase in the extent of tidal flats, going from near zero for the year 2000 to over 365 hectares in the year 2100. Tidal wetlands of the Choctawhatchee River delta have significantly greater area (19,000 hectares) but exhibit similar shifts in wetland habitat. For a one-meter rise in sea level, the extent of tidal flats increases dramatically from 1,200 hectares in the year 2000 to 4,700 hectares in the year 2100. Regularly flooded marsh increase from near zero in the year 2000 to 4,900 hectares in 2100. The increase in the extent of regularly flooded marsh is in part due to the loss of the irregularly flooded marsh, dropping from 4,400 hectares in the year 2000 to 2,800 hectares in 2100. Tidal flats increase from a present-day value of 1,200 hectares to 4,700 hectares in 2100. Due to the narrow width of Santa Rosa Island, the continued dynamic activity of erosion and overwash fans on the island, and the presence of an active navigation channel near the back-barrier portion of the shoreline, there is limited potential for the development of a larger tidal marsh system on the island.

As with any study, there are limitations associated with the data used in the SLAMM-SLR simulations. First, the model resolution is based on the accuracy of elevation and the wetland land-use data. Second, the SLAMM model places much weight on inundation and elevation change, and lacks feedback mechanisms that may come into play as SLR accelerates. Third, the parameters used in the model should be as specific as possible for the selected field sites, but accurate erosion and accretion data are not readily available. During this study it was possible to document that in a marsh system associated with a multiple channel delta, erosion of the marsh system can be highly variable and significant erosion can take place even in portions of the marsh that are not exposed to wide stretches of open water. Despite these disadvantages, our

approach provides first order and important insights into how accelerated SLR may affect tidal marshes and their delivery of ecosystem services in the future.

5.5. Modeling Coastal Groundwater

The objective of this study was to understand how the past and present conditions have affected the saltwater intrusion process in the coastal aquifer near Eglin AFB and how the future expected sea level rise will affect the groundwater flow and salinity evolution processes on Eglin Air Force Base, which includes parts of Santa Rosa Island and the main base area in the mainland. The groundwater flow on Santa Rose Island is at a local scale, while the flow in the main area is at a regional scale. This study provides an overview of the essential elements of the risk assessment guidelines for groundwater system in the Eglin Air Force basin. The study results could also be applied to other Department of Defense facility areas with similar groundwater flow conditions.

Various numerical simulations were conducted using the MODFLOW-family computer code, SEAWAT, to study the transient effects of sea level rise on saltwater intrusion into the confined and unconfined aquifers on Eglin Air Force Base with a vertical sea-land interface. The confined aquifers are located on the mainland, and the unconfined aquifers are on Santa Rosa Island and also on the mainland. The simulation results indicate that if the ambient recharge remains constant, the sea-level rise will have no impact on the steady-state salt wedge in the confined aquifers. The transient flow in the confined aquifer is mainly controlled by well pumping for water supply. Under the current well pumping conditions, hydraulic head will continuously decrease and seawater intrusion will increase. The sea level rises in both 1-meter and 2-meter scenarios have a slight influence on sea water intrusion into the confined aquifers. However, in the unconfined aquifer, the sea level rise and associated storm surges can lead to salinity intrusion into groundwater and the surface waters, which have negative impacts on human water usage and ecosystems, especially on Santa Rosa Island. If salt water covers the surface of the Santa Rosa barrier island in a large storm surge, the hydrologic environment will deteriorate significantly. It would require about 1.5 years for the system to entirely replace the intruded saltwater in groundwater aquifer. This has the potential to dramatically alter the habitat conditions in the barrier island.

Uncertainty analysis was conducted for the base on both Santa Rosa Island and the mainland, using local and regional groundwater models. The study results indicate: 1) the coastal boundary condition is more reasonably described by the first-type boundary condition than by the second-type boundary condition; (2) tides will significantly affect both unconfined and confined aquifers in terms of tidal efficiency factor (or hydraulic head fluctuations); (3) with a 1-meter sea level rise and the expected water pumping rate in the year 2100, salt water will potentially intrude into the confined aquifers as much as 200 to 300 meters, while the intrusion is only about 40 to 60 meters for the unconfined aquifers; (4) the short-term increases in salinity due to storm surge would return to normal after some moderate period of time, but the salinity changes caused by SLR would be permanent. The study results indicate that for the case of 2.0 m SLR, most of the island groundwater would be affected; (5) this is a generic issue for low-lying coastal installations; (6) these changes in groundwater quality due to SLR are potentially quite significant.

5.6 Modeling Morphologic Change

The primary goal has been to develop an efficient numerical model that represents the dynamic adjustments of a complex and interacting set of coastal morphological features to a range of potential future accelerated rates of sea level rise. This has been accomplished. The model represents both the slow and continuous time-averaged changes and the net effect of the sudden morphological changes produced by major storms as two linked and interacting regimes. It is a multi-line model with the morphodynamical algorithms formulated to represent the appropriate large temporal and spatial scales. Individual portions of this model are calibrated in different ways because of the fundamental problem related to obtaining adequately long and sufficiently detailed data sets. Where appropriate, cross-scale modeling is used for the calibrations. In other cases parameter values appropriate to the large scales being represented are evaluated in an iterative procedure to 'walk-in' the model results to match detailed measurements of long-term shoreline and morphological changes.

The model has been shown to produce realistic results when compared to changes documented with measurements from long past time intervals. This lends credibility to projection of future long-term shoreline and morphological changes that are predicted by the model for scenarios representing the required range of possible sea-level rise rates over the next hundred years.

As explained in the previous section of this report, the model study results are significant in advancing the scientific understanding of how complex coastal systems adjust to different rates of future sea level rise. The results are also useful in the practical sense for guiding planning and management decisions regarding the siting, construction and protecting of coastal military base infrastructure.

The results from the morphological change modeling and the related analyses of the role of uncertainty in the projections have been presented at a number of scientific meetings and publications. An additional series of manuscripts are in preparation and will be published after the completion of the funded portion of this study. The MoCCS model is a major part of a dissertation being developed by one of the project graduate assistants. We are seeking additional funding to further the application of this model but such additional work will continue whether or not these efforts are successful because of the intense interest of the investigators and graduate students.

The MoCCS model code has been written in both Fortran and Matlab with considerable annotation and commenting so that it can be provided to users outside of the project team. We plan on some continued development and testing of the model in the process of completing some of the ongoing research and publications. The model will be entered into the Community Surface Dynamics Modeling System collection that is maintained at the University of Colorado. We will also seek opportunities to make the use of this model better known to military personnel.

Uncertainties associated with the coastal modeling are categorized into parametric uncertainty and scenario uncertainty. Parametric uncertainty resides in the number of storms, storm magnitudes, and storm tracks; scenario uncertainty is about occurrence of the five different sea level rise scenarios. A hierarchical method is used to quantify propagation of the uncertainties through the coastal models (morphological and groundwater). First, the analysis of parametric uncertainty is conducted under each individual sea-level rise scenario using the MC method;

subsequently, parametric and scenario uncertainties are jointly quantified using the scenario averaging method. This hierarchical way of uncertainty quantification is general and expected to be applicable to any coastal systems.

While the predictive uncertainty due to parametric uncertainty in general increases with time, mean trends and percentiles of model predictions are significantly different at different locations since the storm effects are different and their distinct initial values. Dunes are more likely to grow with lower initial heights. Backshore also tends to increase at narrower parts of the island. The dunes are more likely to be eroded and the backshore is easier to retreat with higher sea-level rise. There may be more sources of parametric uncertainty, but they can be addressed and quantified in the manner described in the report when more data and information are available for the assessment.

Scenario uncertainty has a more significant effect on predictive uncertainty, as the parametric uncertainty is significantly different under different scenarios. Among the five sea level rise scenarios, the parametric uncertainty is the largest for the scenario of the largest sea level rise.

The results of different scenarios show that with increasing time, scenario uncertainty becomes more and more important. After considering the scenario uncertainty, as shown in Section 4, the probability density functions obtained after scenario averaging always lie between the density functions of the scenarios with the smallest and largest sea-level rise. In other words, decisions based on scenario-averaging are less conservative than that of the worst-case scenario. However, if the worst-case scenario has only a small likelihood of occurrence, decisions may be made for the most likely scenario in order to effectively use limited resources. There is a trade-off between conservative decision-making (for maximum protection) and effective decision-making (for effective use of limited resources). It is suggested that decision-makers should consider multiple scenarios, estimate the likelihood of individual scenarios, and evaluate the corresponding risk to make science-based decisions.

6. Literature Cited

Ataie-Ashtiani, B., Volker, R.E., and Lockington, D.A. (1999). Tidal effects on sea water intrusion in unconfined aquifers. Journal of Hydrology 216:17-31.

Ataie-Ashtiani, B., Volker, R.E., and Lockington, D.A. (1999). Tidal effects on sea water intrusion in unconfined aquifers. Journal of Hydrology 216:17-31.

Balsillie, J.H., Donoghue, J.F., Butler, K.M., Koch, J.L. (2002). Plotting equation for Gaussian percentiles and a spreadsheet program for generating probability plots. Journal of Sedimentary Research 72, 929-933.

Barnett, M.R. (2006). Hurricane Dennis and Hurricane Katrina: Final Report on 2005 Hurricane Season Impacts to Northwest Florida. Report April 2006, Florida Department of Environmental Protection, Division of Water Resource Management, Bureau of Beaches and Coastal Systems, 70 pp.

Biasutti, M., Sobel, A.H., Camargo, S.J., and Creyts, T.T. (2012). Projected changes in the physical climate of the Gulf Coast and Caribbean: Climatic Change, v. 112, p. 819-845, DOI 10.1007/s10584-011-0254-y.

Bouwer, L.M., W.J.W. Botzen, (2011). How sensitive are US hurricane damages to climate? Comment on a paper by W. D. Nordhaus. Climate Change Economics, 2, 1-7.

Browder, A.E., and Dean, R.G. (1999). Pensacola Pass, Florida, inlet management study: Coastal and Oceanographic Engineering Department, University of Florida, UFL/COEL-99-002, 117 p.

Bruun, P., (1988). The Bruun Rule of Erosion by sea-level rise: a discussion on large- scale two- and three-dimensional usages. *Journal of Coastal Research*, 4(4), pp. 627-648

Bruun, P., (1962). Sea-level rise as a cause of shore erosion J. Waterways Harbors Div., ASCE, 88 (WW1), pp. 117–130.

Busen, K., and Bartel, R.L.(2012). Regional Water Supply Plan Update for Santa Rosa, Okaloosa, and Walton Counties Water Supply Planning Region II. Northwest Florida Water Management District Water Resource Assessment 2012-01.

Buttolph, A.M.; Reed, C.W.; Kraus, N.C.; Ono, N.; Larson, M.; Camenen, B.; Hanson, H.; Wamsley, T. and Zundel, A.K., (2006). Two-Dimensional Depth-Averaged Circulation Model CMS-M2D: Version 3.0, Report 2, Sediment Transport and Morphology Change. Coastal and Hydraulics Laboratory Technical Report ERDC/CHL-TR-06-7. Vicksburg, MS: US Army Engineer Research and Development Center.

Capobianco, M., DeVriend, H., Nichols, R.J., and M.J. Stive (1999). Coastal Area Impact and Vulnerability Assessments: The Point of View of a Morphodynamic Modeler, J. Coastal Research, 15, 701-716.

Castaneda, I.S., Schouten, S., (2011). A review of molecular organic proxies for examining modern and ancient lacustrine environments. Quaternary Science Reviews 30, 2851-2891.

CBA, (2012). Florida Lakewatch water quality monitoring. Choctawhatchee Basin Alliance (http:www.basinalliance.org).

Cerling, T.E., Harris, J.M., MacFadden, B.J., Leakey, M.G., Quade, J., Eisenmann, V., Ehleringer, J.R. (1997). Global vegetation change through the Miocene-Pliocene boundary. Nature 389, 153-158.

Chang, S.W., and Clement, T.P. (2011). Does sea-level rise have an impact on saltwater intrusion? Advances in Water Resources, 34, 1283-1291.

Chu-Agor, M.L., Muñoz-Carpena, R., Kiker, G., Emanuelsson, A., and Linkov, I. (2010). Global sensitivity and uncertainty analysis of SLAMM for the purpose of habitat vulnerability assessment and decision-making. World Environmental and Water Resources Congress 2010: Challenges of Change, Watershed Council, pp. 4702-4709, doi 10.1061/41114(371)477.

Clark, R.R., and LaGrone, J.W. (2006). Hurricane Dennis and Hurricane Katrina: Final Report on 2005 Hurricane Season Impacts to Northwest Florida, Florida Department of Environmental Protection, Bureau of Beaches and Coastal Systems, 116 p.

Clauset, A., Shalizi, C.M., and Newman, M. (2009). Power-law distributions in empirical data. SIAM Review, **51**, 661-703.

Clough, J.S., Park, R.A., and Fuller, J., (2010). SLAMM Technical Documentation, Release 6.0 beta, Draft January 2010. Warren Pinnacle Consulting, Inc.

Clough, J.S. (2006). Application of SLAMM 4.1 to Nine Sites in Florida. National Wildlife Federation Report.

Cochran, U.A., Berryman, K.R., Middlenhall, D.C., Hayward, B.W., Southall, K., Hollis, C.J., (2005). Towards a record of Holocene tsunami and storms for northern Hawke's Bay, New Zealand. New Zealand Journal of Geology and Geophysics 48, 507–515.

Collins, E.S., Scott, D.B., Gayes, P.T., (1999). Hurricane records on the South Carolina coast: can they be detected in the sediment record? Quaternary International 56, 15–26.

Coor, J.L., Donoghue, J.F., Wallace, T., Wang, Y., Elsner, J.B., in revision. Detecting a storm history signature in coastal lake sediments, northern Gulf of Mexico coast. Quaternary Research.

Corbett, D.R., Vance, D., Letrick, E., Mallinson, D., Culver, S. (2007). Decadal-scale sediment dynamics and environmental change in the Albemarle Estuarine System, North Carolina. Estuarine, Coastal and Shelf Science 71, 717-729.

Corbett, D.R., Dillon, K., and Burnett, W., (2000). Tracing groundwater flow on a barrier island in the north-east Gulf of Mexico. Estuarine, Coastal and Shelf Science 51: 227-242.

Corbosiero, K.L., and Molinari, J. (2003). The relationship between storm motion, vertical wind shear, and convective asymmetries in tropical cyclones. Journal of the Atmospheric Sciences 60:366–376.

Cowell, P.J., Roy, P.S., and Jones, R.A., (1995). Simulation of LSCB using a Morphological Behavior Model. Marine Geology 126, pp. 45-61.

Cowell P.J., De Vriend H.J., Buijsman M.C., Nicholls R.J., Roy P.S., Kaminsky G.M., Cleveringa J., Reed C.W., De Boer P.L., Stive M.J.F., Niedoroda A.W., and Swift D.J.P., (2003a). The Coastal-Tract (Part 2): Applications of aggregated modeling of lower-order coastal change: Journal of Coastal Research, 19, no.4, p. 828-848.

Cowell, P.J., Swift D.J.P., Kaminsky G.M., Capobianco M., Stive M.J.F., Niedoroda A.W., and deVriend H.J. (2003b). The Coastal-Tract (Part 1): A conceptual approach to aggregated modeling of low-order coastal change: Journal of Coastal Research, v. 19, no. 4, p. 812-827.

Czech, B. (2008). Data Report on SLAMM Model Results for Ten National Wildlife Refuges in South Carolina and Georgia: Wassaw NWR, Georgia.

Das, O., Wang, Y., Donoghue, J., Xu, X., Coor, J., Elsner, J., and Xu, Y., submitted, Reconstruction of paleostorms and paleoenvironment using geochemical proxies in sediment cores from two coastal lakes in northwest Florida. Quaternary Science Reviews.

Davis, R.A. (1997). The evolving coast. Scientific American Library, New York.

Dean, R.G. (2002). Beach Nourishment: Thoery and Practice, Advanced Series in Ocean Engineering – Volume 18, World Scientific Publishing Co. Pte, Ltd., 399 pps

Dean, R.G., Cheng, J., and Malakar, S.B. (1998). Characteristics of the shoreline change along the sandy beaches of the state of Florida: An atlas: Florida Sea Grant Report UFL/COEL-98/015.

deVriend, H.J., (2001). Long-term Morphological Prediction, in Seminara, G. Blondeaux, P. [eds.] River, Coastal and Estuarine Morphodynamcis, Springer, Amsterdam, 211 pps.

deVriend, H.J., Capobianco, M., Chesher, T., de Swart, H.E., Latteux, B., and Stive, M.J.F. (1993). Approaches to long-term modeling of coastal morphology: a Review. Coastal Engineering, 21, 225-269.

deVriend, H.J., (1991). Mathematical modeling and large-scale coastal behavior, Journal of Hydraulic Research, v.29, n.6, p.727 – 740.

DeMaria, M., and Kaplan, J.,(1994). Sea-surface temperature and the maximum intensity of Atlantic tropical cyclones. Journal of Climate, 7, 1324--1334.

Deser, C., Phillips, A.S., and Alexander, M.A., (2010). Twentieth century tropical sea surface temperature trends revisited. Geophysical Research Letters, 37, doi:{10.1029/ 2010GL043321}.

Deutsch, C.V., and Journel, A.G. (1997). GSLIB: Geostatistical Software Library and User's Guide. Oxford University Press, USA. ISBN: 0195100158.

Domenico, P.A., and Schwartz, F.W. (1998). Physical and chemical hydrogeology. Wiley, New York.

Donnelly, J., and Woodruff, J., (2007). Intense hurricane activity over the past 5,000 years controlled by El Nino and the West African monsoon. Nature, 447: 465-468.

Donnelly, J. P., Roll, S., Wengren, M., Butler, J., Lederer, R., and Webb III, T. (2001). Sedimentary evidence of intense hurricane strikes from New Jersey: Geology, v. 29, p. 615-618.

Donnelly, J., Roll, S., Wengren, M., Butler, J., Lederer, R., Webb, T. (2001a). Sedimentary evidence of intense hurricane strikes from New Jersey. Geology, 29: 615-618.

Donnelly, J., Bryant, S., Butler, J., Dowling, J., Fan, L., Hausmann, N., Newby, P., Shuman, B., Stern, J., Westover, K., Webb, T. (2001b). 700 yr sedimentary record of intense hurricane landfalls in southern New England. Geological Society of America Bulletin,113: 714-727.

Donnelly, J., Butler, J., Roll, S., Wengren, M., Webb, T. (2004). A backbarrier overwash record of intense storms from Brigantine, New Jersey. Marine Geology, 210: 107-121.

Eglin AFB. (2010). Eglin CE armors island against hurricanes. http://www.eglin.af.mil/news/story.asp?id=123207822 (accessed 7/12/2012).

Eglin AFB. (2005). A History of Hurricanes in the Western Florida Panhandle 1559-1999 Eglin AFB, 46th Weather Squadron, http://www.freerepublic.com/focus/f-news/1473774/posts (accessed 7/12/2012).

Elsner, J.B., and Jagger, T.H., (2010). On the increasing intensity of the strongest Atlantic hurricanes. Hurricanes and Climate Change, volume 2, Elsner JB, Hodges RE, Malmstadt JC, Scheitlin KN, Eds., Springer, New York, chap. 10, doi: 10.1007/978-90-481-9510-7.

Elsner, J.B., Kossin, J., and Jagger, T.H., (2008). The increasing intensity of the strongest tropical cyclones. Nature 455:92–95.

Fagherazzi S., Marani M., and Blum L.K., (2004a). Introduction: The Coupled Evolution of Geomorphological and Ecosystem Structures in Salt Marshes (Chapter 1), The

Ecogeomorphology of Tidal Marshes, American Geophysical Union Coastal and Estuarine Studies, Washington DC, Volume 59, 266 pages.

Fagherazzi S., Howard, A.D. Wiberg, P.L., (2004b). Modeling fluvial erosion and deposition on continental shelves during sea level cycles, J. Geophys. Res., Vol. 109, No. F3, F03010 10.1029/2003JF000091.

FEMA, (2002). Flood Insurance Study, Okaloosa County, Florida and incorporated areas, Flood Insurance Study Number 12091CV000A.

Florida Lakewatch (2008). A Management Plan for Walton County's Coastal Dune Lakes: University of Florida, http://www.basinalliance.org/CDL/learnCDL.htm, 31 p.

Florida Lakewatch (2008). A Management Plan for Walton County's Coastal Dune Lakes: University of Florida, http://www.basinalliance.org/page.cfm?articleID=47

Fujii, T., and Raffaelli, D., (2008). Sea-level rise, expected environmental changes, and responses of intertidal benthic macrofauna in Humber estuary, UK. Mar. Ecol. Prog. Ser. 371, 23e35.

Gauld, G., (1780). A chart of the bay and harbour of Pensacola in the province of West Florida. London: The Atlantic Neptune. J.F. Des Barres, publisher. Scale 1:32,500

Grinsted, A., Moore, J.C., and Jevrejeva, S. (2010). Reconstructing sea level from paleo and projected temperatures 200 to 2100 AD: Climate Dynamics v. 34, no. 4 (March 2010) DOI 10.1007/s00382-008-0507-2.

Guo, W., and Bennett, G.D., (1998). Simulation of saline/fresh water flows using MODFLOW, p. 267-274, in Poeter, E., et al., Proceedings of the MODFLOW '98 Conference, v. 1, Golden, Colorado.

Guo, W., and Langevin, C.D. (2002). User's guide to SEAWAT: A computer program for simulation of three-dimensional variable-density ground-water flow. U.S. Geological Survey Techniques of Water-Resources Investigations, Book 6, chapter A7, 77 p.

Guo, W., and Langevin, C.D. (2000). User's Guide to SEAWAT: A Computer Program for Simulation of Three-Dimensional Variable-Density Ground-Water Flow.

Hamid, S., Kibria, B.G., Gulati, S., Powell, M., Annanne, B., Cocke, S., et al., (2010). Predicting losses of residential structures in the state of Florida by the public hurricane loss evaluation model. Statistical Methodology, 7(5), 552-573.

Hanson, H., Larson, M., and Kraus, N.C., (2010). Calculation of beach change under interacting cross-shore and longshore processes, Coastal Engineering, 57: 610–619.

Hapke, C.J. and Christiano, M., (2007). Long-term and Storm-related Shoreline Change Trends in the Florida Gulf Islands National Seashore: U.S. Geological Survey Open-file Report 2007-1392, 18p.

Harbaugh, A.W., E.R. Banta, M.C. Hill, and M.G. McDonald., (2000). MODFLOW–2000, the U.S. Geological Survey modular ground water model—User guide to modularization concepts and the ground water flow process. U.S. Geological Survey Open-File Report 00–92.

Hartig, E.K., Gornitz, V., Kolker, A., Mushacke, F., and Fallon, D., (2002). Anthropogenic and climate-change impacts on salt marshes of Jamaica Bay, New York City, Wetlands, 22, 71-89.

Hayes, L.R., D.E. Barr. (1983). Hydrology of the Sand-and-Gravel Aquifer, Southern Okaloosa and Walton Counties, Northwest Florida. USGS Water Resources Investigations Report 82-4110.

Heffernan, T. 2011, comments by Thomas Heffernan, Range Environmental Planner, 46th Test Wing, EAFB, at SERDP Knowledge Transfer Meeting, Eglin AFB, October 4, 2011.

Hendricks, W., R. Koenker, (1991). Hierarchical spline models for conditional quantiles and the demand for electricity. J. Amer. Stat. Assoc., 87, 58-68.

Hilbe, J. M. (2009). Logistic Regression Models. Chapman and Hall/CRC Press, Boca Raton, FL, 656 p.

Hill, M.C. (1992). A computer program (MODFLOWP) for estimating parameters of a transient, three dimensional, groundwater flow model using non-linear regression. U.S. Geological Survey Open File Report 91-484.

Hinkel, J. and R. Klein, (2003). DINAS-Coast: Developing a method and a tool for dynamic and interactive vulnerability assessment, IGBP-LOICZ Newsletter, June 2003.

Hinkel, J. (2005). DIVA: an iterative method for building modular integrated models, Advances in Geosciences, 4, 454-50.

Hippensteel, S.P., Martin, R.E., (1999). Foraminifera as an indicator of overwash deposits, barrier island sediment supply, and barrier island evolution, Folly Island, South Carolina. Palaeogeography, Palaeocli- matology, Palaeoecology 149, 115–125.

Hippensteel, S.P., Martin, R.E., (2000). Foraminifera of storm-generated washover fans: implications for determining storm frequency in relation to sediment supply and barrier island evolution, Folly Island, South Carolina, 351–369. In: Martin, R.E. (Ed.), Environmental Micropaleontology. Kluwer Academic/Plenum Publishers, New York, p. 481.

Hodell, D. A., J. H. Curtis, G. A. Jones, A. Higuera- Gundy, M. Brenner, M. W. Binford, and K. T. Dorsey, 1991. Reconstruction of Caribbean climate change over the past 10,500 years, Nature,352, 790 – 793.

Horton, R., C. Herweijer, C., Rosenzweig, C., Liu, J., Gornitz, V., and Ruane, A.C. (2008). Sea level rise projections for current generation CGCMs based on the semi-empirical method, Geophys. Res. Lett., 35, L02715, doi:10.1029/2007GL032486.

Horton, B., Rossi, V., and Hawkes, A., 2009. The sedimentary record of the 2005 hurricane season from the Mississippi and Alabama coastlines. Quaternary International 195 (2009) 15–30.

Houser, C., Hobbs, C., and Saari, B. (2008). Post-hurricane airflow and sediment transport over a recovering dune, Journal of Coastal Research, 24: 944-953.

Houston, S.H., Shaffer, W.A., Powell, M.D., Chen, J. (1999). Comparisons of HRD and SLOSH surface wind fields in hurricanes: Implications for storm surge modeling. Weather and Forecasting, 14, pp. 671-686.

Howard, R.A., J.E. Matheson, D.W. North, (1972). The decision to seed hurricanes. Science, 176, 1191-1202 (1972).

Hubbert, M.K. (1940). The theory of groundwater motion. Journal of Geology 48, 785–944.

IPCC, (2007). Climate Change 2007: The Physical Science Basis. Contribution of Working Group I to the Fourth Assessment Report of the Intergovernmental Panel on Climate Change [Solomon, S., D. Qin, M. Manning, Z. Chen, M. Marquis, K.B. Averyt, M. Tignor and H.L. Miller (eds.)]. Cambridge University Press, Cambridge, United Kingdom and New York, NY, USA, 996 pp.

Jagger, T., and Elsner, J., (2006). Climatology models for extreme hurricane winds in the United States. Journal of Climate 19:3220–3236.

Jagger, T.H., and Elsner, J.B. (2012). Hurricane clusters in the vicinity of Florida. J. Applied Meteor. Climat., in press, (2012).

Jagger, T.H., Elsner, J.B., and K. Burch, Climate and solar signals in property damage losses from hurricanes affecting the United States, Natural Hazards, **58**, 541-557 (2011).

Jarvinen, B.R., Lawrence, M.B., (1985). An evaluation of the SLOSH storm-surge model. Bulletin of the American Meteorological Society, 66,1408-1411.

Jelesnianski, C.P., Chen, J. and Shaffer, W.A.. (1992). SLOSH: Sea, Lake and Overland Surges From Hurricanes, NOAA Technical Report NWS 48, NOAA, Washington, DC.

Jevrejeva, S., Moore, J.C., and Grinsted, A. (2010). How will sea level respond to changes in natural and anthropogenic forcings by 2100? Geophys. Res. Lett., v. 37, L07703, doi: 10.1029/2010GL042947.

Keim, B.D., Muller, R.A., and Stone, G.W., (2007). Spatiotemporal patterns and return periods of tropical storm and hurricane strikes from Texas to Maine. Journal of Climate 20:3498–3509.

Khain, A., Lynn, B., and Dudhia, J. (2010). Aerosol effects on intensity of landfalling hurricanes as seen from simulations with the WRF model with spectral bin microphysics. Journal of the Atmospheric Sciences, 67: 365–384, doi:10.1175/2009JAS3210.1.

Kirwan, M.L., and Guntenspergen, G.R., (2009). Accelerated sea-level rise e a response to Craft et al., (2009). Front. Ecol. Environ. 7 (2), 126-127.

Kirwan, M.L., Murray, A.B., and Boyd, W.S., (2008). Temporary vegetation disturbance as an explanation for permanent loss of tidal wetlands. Geophysical Research Letters, v. 35, L05403.

Knutson, T.R., and Tuleya, R.E., (2004). Impact of CO2-induced warming on simulated hurricane intensity and precipitation: Sensitivity to the choice of climate model and convective parameterization. Journal of Climate, 17, 3477–3495.

Koenker, R. and G. Bassett, (1978). Regression quantiles. Econometrica, 46, 33-50 (1978).

Kruse, S.E. and Schneider, J.C. (2001). Investigation of the freshwater resources and potential impacts of groundwater pumping on Dog Island, Florida. Report prepared for the barrier island trust.

LaSalle, M.W., and A.A. de la Cruz, (1985). Species profiles: life histories and environmental requirements of coastal fishes and invertebrates (Gulf of Mexico) -- common rangia. U.S. Fish Wildl. Serv. Biol. Rep. 82(11.31). U.S. Army Corps of Engineers, TR EL-82-4. 16 pp.

Lamb, A.L., Wilson, G.P., Leng, M.J., (2006). A review of coastal paleoclimate and relative sea-level reconstructions using $\delta^{13}C$ and C/N ratios in organic materials. Earth Science Review, v. 75, p. 29-57.

Lambert, W.J., Aharon, P., and Rodriguez, A.B. (2008). Catastrophic hurricane history revealed by organic geochemical proxies in coastal lake sediments: a case study of Lake Shelby, Alabama (USA): Journal of Paleolimnology, v. 39, p. 117-131.

Lambert, W.J., (2003). An investigation of organic-rich sediment in Lake Shelby, Alabama, for markers of severe storm impacts. MS Thesis, University of Alabama, Tuscaloosa, AL, 162 p.

Landsea, C.W., G.A. Vecchi, L. Bengtsson, and T.R. Knutson, (2010). Impact of duration thresholds on Atlantic tropical cyclone counts, J. Climate, 23, 2508-2519, doi:10.1175/2009JCLI3034.1.

Lane, P., Donnelly, J.P., Woodruff, J.D., Hawkes, A.D. (2011). A decadally-resolved paleohurricane record archived in the late Holocene sediments of a Florida sinkhole. Marine Geology doi: 10.1016/j.margeo.2011.07.001.

Lane, P., Donnelly, J., Woodruff, J., and Hawkes, A., 2010. A 4500-year record of hurricane frequency in the Gulf of Mexico archived in a North Florida sinkhole: American Meteorological Society, 29th Conference on Hurricanes and Tropical Meteorology, Presentation 2A.7.

Langevin, C.D., (2001). Simulation of ground water discharge to Biscayne Bay, southeastern Florida. U.S. Geological Survey Water-Resources Investigations Report 00–4251.

LaRow, T.E., Lim, Y.K., Shin, D.W., Chassignet E. and Cocke, (2008). South Atlantic basin seasonal hurricane simulations. J. Clim. v 21,p. 3191-3206.

Larson, M., Kraus, N.C., and Connell, K.J., (2006). Modeling sediment storage and transfer for simulation regional coastal evolution, Proceedings 30th Coastal Engineering Conf., ASCE., p.1 -13.

Lavoie, D.M., Baerwald, R.J., Hulbert, M.H., Bennett, R.H., (1996). A drinking-straw mini-corer for sediments. Journal of Sedimentary Research 66, 1030.

Leadon, M.E. et al., (2004). Hurricane Ivan: Beach and Dune Erosion and Structural Damage Assessment and Post-storm Recovery Plan for the Panhandle Coast of Florida, Florida Department of Environmental Protection, Bureau of Beaches and Coastal Systems, 64 p.

Leadon, M.E., Nguyen, N.T., and Clark, R.R. (1998). Hurricane Opal: Beach and Dune Erosion and Structural Damage along the Panhandle Coast of Florida, Florida Department of Environmental Protection, Report No. BCS-98-01.

Li, X., Hu, B.X., and Burnett, W.C. (2009). Submarine Ground Water Discharge Driven by Tidal Pumping in a Heterogeneous Aquifer: Groundwater, v. 47, no. 4, p. 558-568.

Lin, L.; Demirbilek, Z.; Wu., F.; Jackson, J.T. and Shak, A.T., 2006. Coastal numerical modeling of Peninsula Beach, California. Proceedings 10th Estuarine and Coastal Modeling Conference, Newport, RI. USA, 163-185.

Liu, K.B., (2004). Paleotempestology: geographic solution to hurricane hazard assessment and risk prediction. In: Janelle, D., Warf, B., Hansen, K (Eds), World Minds: Geographical Perspectives on 100 Problems. Kluwer Academic Publishers, Dordrecht, pp. 443-448.

Liu, K.B., and Fearn, M.L. (2000a). Reconstruction of prehistoric landfall frequencies of catastrophic hurricanes in northwestern Florida from lake sediment records: Quaternary Research, v. 54, p. 238-245.

Liu, K.B., and Fearn, M., (2000b). Holocene history of catastrophic hurricane landfalls along the Gulf of Mexico coast reconstructed from coastal lake and marsh sediments. In: Ning, Z. H., Abdollahi, K. K. (eds.), Current stresses and potential vulnerabilities: Implications of global change for the Gulf Coast Region of the United States. Franklin Press, Baton Rouge, pp. 38-47.

Liu, K.B., and Fearn, M.L. (1993). Lake-sediment record of late Holocene hurricane activities from coastal Alabama: Geology,v. 21, p. 793-796.

Liu., K., Lu, H., Shen, C. (2008). A 1200-year record of hurricanes and fires from the Gulf of Mexico coast: Testing the hypothesis of hurricane-fire interactions. Quaternary Research, 69: 29-41.

Macko, S.A., Entzeroth, L., and Parker, P.L., (1984). Regional differences in nitrogen and carbon isotopes on the continental shelf of the Gulf of Mexico. Naturwissenschaften, v. 71, p. 374-375.

Maloney, M. T., Richards,C. J. and Pratt, T. R., (1998). Potentiometric Surface of the Floridan Aquifer System in Northwest Florida.

Mander, L., Cutts, N.D., Allen, J., and Mazik, K., (2007). Assessing the development of newly created habitat for wintering estuarine birds. Estuar. Coast. Shelf. Sci. 75,163e174.

Mann, M., Woodruff, J., Donnelly, J., and Zhang, Z., (2009). Atlantic hurricanes and climate over the past 1500 years. Nature, 460: 880-883.

Mertz, L., Hart, M., and Jaeger, J., (2003). Preservation potential of paleocyclone deposits in Gulf of Mexica coastal sediments. GCAGS/GCSSEPM Transactions, vol. 53: 537-547.

Meyer, M. Ye, M.L., Rockhold, S.P., Neuman, K.J., Cantrell, (2007). Combined Estimation of Hydrogeologic Conceptual Model, Parameter, and Scenario Uncertainty, NUREG/CR-6940, PNNL-16396, U.S. Nuclear Regulatory Commission, Office of Nuclear Regulatory Research.

Meyers, P. A., (1997). Organic geochemical proxies of paleoceanographic, paleolimnologic, and paleoclimatic processes. Organic Geochemistry 27, 213-250.

Meyers, P.A., (1994). Preservation of elemental and isotopic source identification in sedimentary organic matter. Chemical Geology, v. 114, p. 289-302.

Middleburg, J.J., Nieuwenhuize, J., (1998). Nitrogen isotope tracing of dissolved inorganic nitrogen behaviour in tidal estuaries. Estuaring, Coastal and Shelf Science 53, 385-391.

Monaghan, A.J., David H. Bromwich, Ryan L. Fogt, Sheng-Hung Wang, Paul A. Mayewski, Daniel A. Dixon, Alexey Ekaykin, Massimo Frezzotti, Ian Goodwin, Elisabeth Isaksson, Susan D. Kaspari, Vin I. Morgan, Hans Oerter, Tas D. Van Ommen, Cornelius J. Van der Veen, Jiahong Wen (2006). Insignificant Change in Antarctic Snowfall Since the International Geophysical Year, Science 2006 313: 827-831.

Moody, D.W. (1964). “Coastal Morphology and Processes in Relation to the Development of Submarine Sand Ridges off Bethany Beach, Delaware,” Ph.D. Dissert., John Hopkins Univ., 167 pps.

Morang, A., (1992). Inlet Migration and Hydraulic Processes at East Pass, Florida: Journal of Coastal Research, v. 8, p. 457-481.

Morris, J.T., Sundareshwar, P.V., Nietch, C.T., Kjerfve, B., and Cahoon, D.R. (2002). Responses of coastal wetlands to rising sea level: Ecology, v. 83, pp. 2869–2877

Morton, R.A., and Montgomery, M.C., (2010). Geomorphology and depositional sub environments of Gulf Islands National Seashore, Perdido Key and Santa Rosa Island, Florida: U.S. Geological Survey Open-File Report 2010-1330 (available online only at http://pubs.usgs.gov/of/2010/1330/).

Morton, R.A., Miller, T.L., and Moore, Laura J., (2004). National assessment of shoreline change: Part 1: Historical shoreline changes and associated coastal land loss along the U.S. Gulf of Mexico: U.S. Geological Survey Open-file Report 2004-1043, 45p.

Morton, R.A., Paine, J.G., and Giberaut, J.C., (1994). Stages and durations of post-storm beach recovery, southeastern Texas coast, Journal of Coastal Research, 10: 884-908.

Mousavi, M.E., Irish J.L., Frey, A.E., Olivera, F., Edge, B.L., (2010). Global warming and hurricanes: the potential impact of hurricane intensification and sea level rise on coastal flooding. Climatic Change, doi:10.1007/s10584-009-9790-0.

Mudd, S.M., Fagherazzi S., Morris, J.T., and Furbish, D.J., (2004). Flow, Sedimentation, and Biomass Production on a Vegetated Salt Marsh in South Carolina: Toward a Predictive Model of Marsh Morphologic and Ecologic Evolution (Chapter 9), The Ecogeomorphology of Tidal Marshes, American Geophysical Union Coastal and Estuarine Studies, Washington DC, Volume 59, 266 pages.

National Research Council, (1987). Responding to Changes in Sea Level: Engineering Implications. Committee on Engineering Implications of Changes in Relative Mean Sea Level, Marine Board, National Research Council: National Academy Press: Washington, D.C., 160 p.

Nicholls, R.J., Dennis, K.C., Volonte, C.R, and Leatherman, S.P., (1993). Methods and Problems in Assessing the Impacts of Accelerated Sea Level Rise. *The World at Risk: Natural Hazards and Climate Change*, AIP Conf. Proc. #277, American Institute of Physics, New York, pp.193-20.

Niedoroda, A.W., Dai, H., Ye, M., Saha, B., Kish, S., and Donoghue, J.F. (2011). Barrier island responses to potential future rates of sea level rise. The Proceedings of the Coastal Sediments 2011: pp. 202-215.

Niedoroda, A.W., Reed, C.W., Das, H., Koch, J., Donoghue., J.F., Wang, Z.B., and Stive, M.J.F., (2003). Modeling large-scale morphodynamics of complex coastal systems: Proceedings, Coastal Sediments 2003, Fifth International Symposium on Coastal Engineering and Science of Coastal Sediment Processes, St. Petersburg, FL.

Niedoroda, A.W., Reed, C.W., Stive, M., and Cowell, P. (2001). "Numerical Simulations of Coastal-tract Morphodynamics." Coastal Dynamics 2001, ASCE 4th Conference on Coastal Dynamics (2001): 403-412.

Niedoroda, A.W., Reed, C.W., Swift, D.J.P., Arato, A., and Hoyanagi, K., (1995a). Modeling shore-normal large scale coastal Evolution. *Marine Geology* 126, (1–4), 181-199.

NOAA, (2012a). National Oceanic and Atmospheric Administration. Historical Hurricane Tracks. http://csc.noaa.gov/hurricanes/#.

NOAA, (2012b). Best track data (HURDAT): National Hurricane Center, National Weather Service, National Oceanic and Atmospheric Administration. http://www.nhc.noaa.gov/pastall.shtml.

NWFWMD (Northwest Florida Water Management District), (2012). Regional Water Supply Plan Update for Santa Rosa, Okaloosa and Walton Counties 2012, Water Resources Assessment 2012-01.

NWFWMD (Northwest Florida Water Management District), (2000). Modeling of ground water flow in Walton, Okaloosa and Santa Rosa counties, Florida.

NWFWMD (Northwest Florida Water Management District). (1999). Potentiometric elevation, recharge and pumping rate electronic data transfer.

NWFWMD (Northwest Florida Water Management District). (2005). Saltwater Intrusion in the Floridan Aquifer in Walton, Okaloosa and Santa Rosa Counties, Florida: Western Model Domain.

Nordhaus, W.D., (2010). The economics of hurricanes and implications of global warming. Climate Change Economics, **1**, 1-20.

Nott, J., (2004). Palaeotempestology: the study of prehistoric tropical cyclones - a review and implications for hazard assessment. Environment International 30, 433-447.

O'Leary, M.H., (1988). Carbon isotopes in photosynthesis. BioScience 38, 328-336.

Otvos, E., 1999. Quaternary coastal history, basin geometry and assumed evidence for hurricane activity, northeastern Gulf of Mexico coastal plain. J. Coast Res., 15: 438-443.

Otvos, E., (2002). Discussion of "Prehistorical landfall frequencies of catastrophic hurricanes…" (Liu and Fearn, 2000). Quaternary Research, 57: 425-428.

Page, M.J., Trustrum, N.A., Orpin, A.R., Carter, L., Gomez, B., Cochran, U.A., Mildenhall, D.C., Rogers, K.M., Brackley, H.L., Palmer, A.S., Northcote, L., (2009). Storm frequency and magnitude in response to Holocene climate variability, Lake Tutira, North-Eastern New Zealand. Marine Geology doi:10.1016/j.margeo.2009.1010.1019.

Parker, A.G., Goudie, A.S., Stokes, S., White, K., Hodson, M.J., Manning, M., Kennet, D., (2006). A record of Holocene climate change from lake geochemical analyses in southeastern Arabia. Quaternary Research 66, 465-476.

Parker, J. C., (1966). Bottom fauna study -- distribution and relative abundance of *Rangia cuneata*. U.S. Fish Wildlife Service Circular 246, 35-36.

Parsons, M.L., (1998). Salt marsh sedimentary record of the landfall of hurrican Andrew on the Louisiana Coat: diatoms and other paleoindicators. Journal of Coastal Research 14, 939–950.

Pfeffer, W.T., Harper, J.T., and O'Neel, S. (2008). Kinematic Constraints on Glacier Contributions to 21st-Century Sea-Level Rise: Science, v. 321, p. 1340-1343.

Pielke, Jr., R.A., Gratz, J., Landsea, C.W., Collins, D., Saunders, M.A., and Musulin, R., (2008). Normalized hurricane damage in the United States: 1900–2005. Natural Hazards Review 9:29–42.

Poore, R.Z., Dowsett, H.J., Verardo, S. and Quinn, T.M., (2003). Millennial- to century-scale variability in Gulf of Mexico Holocene climate records. Paleoceanography, 18, 26-18: 10.1029/2002PA000868.

Pratt, T. R., (2001). Results of Floridan Aquifer Drilling Program in Santa Rosa, Okaloosa and Walton Counties, Florida NWFWMD Technical File Report 01-1.

Pratt, T.R., Richards, C.J., Milla, K.A., Wagner, J.R., Johnson J. L. and Curry, R.J., (1996). Hydrogeology of the Northwest Florida Water Management District . Water Resources Special Report 96-4.

Puckett, T.M., (1992). Distribution and ecology of foraminifera from Mobile Bay, Mississippi Sound, and coastal Alabama. Geological Survey of Alabama Circular 166, 35 p.

Rahmstorf, S. (2007). A semi-empirical approach to predicting future sea-level rise: Science, v. 315, p. 368-370.

Rappaport, E.N., Franklin, J.L., Schumacher, A.B., DeMaria, M., Shay, L.K., and Gibney, E.J. (2010). Tropical cyclone intensity change before U.S. Gulf Coast landfall. Weather and Forecasting, 25:1380–1396, doi:{10.1175/2010WAF2222369.1}.

Rayner, N.A., Brohan, P., Parker, D.E., Folland,C.K., Kennedy, J.J.,Vanicek, M., Ansell, T.J., and Tett, S.F.B., (2003): Improved analyses of changes and uncertainties in sea surface temperature measured in situ since the mid-nineteenth century: The HadSST2 dataset, Journal of Climate, 19, 446-469.

Redfield, A.C., (1972). Development of a New England salt marsh. Ecological Monographs 42:201–237.

Reed, C.W., Brown, M.E., Sanchez, A., Wu, W., and Buttolph, A.M. (2011). The Coastal

Modeling System Flow Model (CMS-Flow): Past and Present. Journal of Coastal Research, Special Issue No. 59, pp 1-6.

Richards, C.J., (1993). Preliminary Hydraulic Assessment of the Walton/Okaloosa/Santa Rosa Regional Utility Authority's Western Sub-Regional Wellfield. NWFWMD Water Resources Special Report 93-1.

Rijn, L.C. van. Principles of Sediment Transport in Rivers, Estuaries and Coastal Areas. Amsterdam: Aqua Publications. 1989.

Robinson, C., Li, L., and Barry, D.A. (2007). Effect of tidal forcing on a subterranean estuary. Advances in Water Resources 30, No. 4: 851–865.

Rosati, J.D., (2009). "Barrier Island Migration over a Consolidating Substrate," Ph.D. Dissert., Louisiana State University and Agricultural and Mechanical College, 230 pps.

Rosati, J.D., (2005). Coastal inlet navigation channel shoaling with deepening and widening. Coastal and Hydraulics Engineering Technical Note ERDC/CHL CHETN-IV-64, Vicksburg, Mississippi: U.S. Army Engineer Research and Development Center, 11 p.

Sackett, W.M., (1964). The depositional history and isotopic organic carbon composition of marine sediments. Marine Geology 2, 173-185.

Sallenger, A.H., Krabill, W., Swift, R., Brock, J., List, J., Hansen, M., Holman, R.A., Manizade, S., Sontag, J., Meredith, A., Morgan, K., Yunkel, J.K., Frederick, E. and Stockdon, H., (2003). Evaluation of airborne scanning lidar for coastal change applications: Journal of Coastal Research, v.19, p. 125-133.

Schneider, J.C., and Kruse, S.E. (2005). Assessing selected natural and anthropogenic impacts on freshwater lens morphology on small barrier Islands: Dog Island and St. George Island, Florida, USA Hydrogeology Journal (2005) 14: 131–145.

Schneider, P., and Berman, E. (2010). HAZUS-MH MR4. Technical Manual, Department of Homeland Security, Federal Emergency Management Agency, Mitigation Division, 600 pp.

Scileppi, E., and Donnelly, J.P., (2007). Sedimentary evidence of hurricane strikes in western Long Island, New York. Geochemistry, Geophysics, Geosystems 8 Q06011, doi:06010.01029/02006GC001463.

Scott, D.B., Collins, E.S., Gayes, P.T., Wright, E., (2003). Records of prehistoric hurricanes on the South Carolina coast based on micropaleontological and sedimentological evidence, with comparison to other Atlantic Coast records. GSA Bulletin 115, 1027–1039.

Sharp, Z., (2007). Principles of Stable Isotope Geochemistry. Pearson Prentice Hall. 344.

Shoemaker, W. Barclay and Edwards, K. M. (2003). Potential for Saltwater Intrusion into the Lower Tamiami Aquifer near Bonita Springs, Southwestern Florida: U.S. Geological Survey Water-Resources Investigations Report 03-4262, 74 p.

Shultz, D.J., Calder, J.A., (1976). Organic carbon $^{13}C/^{12}C$ variations in estuarine sediments. Geochimica et Cosmochimica Acta 40, 381-385.

Siddall, M., Thomas, F., Stocker, T.F., and Clark, P.U. (2009). Constraints on future sea-level rise from past sea-level change: Nature Geoscience 2, p. 571 – 575.

Simmons, C.T., K.A. Narayan, J.A. Woods, and A.L. Herczeg, (2002). Ground water flow and solute transport at the Mourquong saline-water disposal basin, Murray Basin, southeastern Australia. Hydrogeology Journal 10, 278-295.

Simmons, C.T., J.M. Sharp Jr., and N.I. Robinson, (1999). Density-driven free convection in zones of inverted salinity through fractured low permeability units in the Gulf of Mexico Basin, Texas, USA. In Proceedings of the Water 99 Joint Congress, July 6-8, Brisbane, Queensland, Australia.

Stapor, F.W. (1975). Shoreline changes between Phillips Inlet and Pensacola Inlet, northwest Florida coast, Transactions. Gulf Coast Association of Geological Societies, v. 25, p. 373–378.

Stive, M.J.F., and Wang, Z.B., (2003). Morphodynamic modeling of tidal basins and coastal inlets. C. Lakhan (Ed.), *Elsevier Oceanography Series*, 67 (C), pp. 367-392.

Stive, M.J.F., Wang, Z.B., Capobianco, M., Ruol, P., and Bujsman, M.C. (1998). Morphodynamics of a tidal lagoon and adjacent coast. J. Dronkers, M.B.A.M. Sheffers (Eds.), Physics of Estuaries and Coastal Seas, Balkema, Rotterdam, pp. 397–407.

Stive, M.J.F., and de Vriend, H.J., (1995). Modelling shoreface profile evolution. Marine Geology, 126, 235-248.

Stive, M.J.F., Roelvink, J.A., and de Vriend, H.J., (1990). Large Scale Coastal Evolution Concept. Proc. 22nd ICCE, ASCE, New York, pp. 1962-1974.

Stone, G.W., Liu, B., Pepper, D.A., and Wang, P. (2004). The importance of extratropical and tropical cyclones on the short-term evolution of barrier islands along the northern Gulf of Mexico, USA, Marine Geology, 210: 63-78.

Stone, G.W. and Stapor, F.W., Jr. (1996). A Nearshore Sediment Transport Model for the Northwest Gulf of Mexico Coast, U.S.A.: Journal of Coastal Research, v. 12, p. 786–792.

Stone, G.W., and Penland, S. (1992). Historic shoreline change along the northern Gulf of Mexico: p. 267-279 in Majumadar, S.K., et al., eds., Natural and Technological Disasters: Causes, Effects and Preventive Measures; Philadelphia, Pennsylvania Academy of Science.

Stone, G.W., Stapor, Jr. F.W., May, J.P., and Morgan, J.P. (1992). Multiple sediment sources and a cellular, non-integrated, longshore drift system: Northwest Florida and southeast Alabama coast, USA. Marine Geology, 105 (1-4), pp. 141-154.

Stuvier, M., Reimer, P.J., Reimer, R., (2012). CALIB 6.0., http://calib.qub.ac.uk/calib/calib.html.

Swingle, H.A., Bland, D.G., (1974). Distribution of the estuarine clam *Rangia cuneata* Gray in coastal waters of Alabama. Alabama Marine Resources Bulletin 10, 9-16.

Tarbox, D., and Hutchings, W.C., (2003). Aquifer storage and recovery of irrigation water in shallow fresh water lenses on barrier islands. National Ground Water Associate Meeting, Dec09.

Taylor Engineering, (2007). Okaloosa Island Beach Management Feasibility Study, Okaloosa County, Florida, unpublished consulting report, 109 pps.

Thieler, E.R., Himmelstoss, E.A., Zichichi, J.L., and Ergul, A., (2009). Digital Shoreline Analysis System (DSAS) version 4.3 - An ArcGIS extension for calculating shoreline change: U.S. Geological Survey Open-File Report 2008-1278, 79p.

Thornton, S.F. and McManus, J., (1994). Application of organic carbon and nitrogen stable isotope and C/N ratios as source indicators of organic matter provenance in estuarine systems: evidence from the Tay Estuary, Scotland. Estuarine, Coastal and Shelf Science 38, 219-233.

U.S. Army Corps of Engineers, (2009). Water Resource Policies and Authorities Incorporating Sea-Level Change Considerations in Civil Works Programs, CECW-CE Circular No. 1165-2-21.

U.S. Army Corps of Engineers, (1984). Shore Protection Manual, 4th ed.: U.S. Army Corps of Engineers, Coastal Engineering Research Center (2 vol.).

Vacher, H.L., (1988a). Dupuit–Ghyben–Herzberg analysis of strip island lenses. Geological Society of America Bulletin 100,580–591.

Valero-Garces, B.L., Laird, K.R., Fritz, S.C., Kelts, K., Ito, E., Grimm, E.C., (1997). Holocene Climate in the Northern Great Plains Inferred from Sediment Stratigraphy, Stable Isotopes, Carbonate Geochemistry, Diatoms, and Pollen at Moon Lake, North Dakota. Quaternary Research 48, 359-369.

van der Meij, J.L, and B. Minnema. (1999). Modelling of the effect of a sea-level rise and land subsidence on the evolution of the groundwater density in the subsoil of the northern part of the Netherlands. Journal of Hydrology, 226, 152-166.

van Goor, M.A., Stive, M.J.F., Wang, Z.B., and Zitman, T.J., (2001). The influence of relative sea level rise on coastal inlets and tidal basins, Proc. Coastal Dynamics 2001.

Vecchi, G.A., and T.R. Knutson, (2008). On estimates of historical North Atlantic tropical cyclone activity, J. Climate, 21, 3580-3600, doi:10.1175/2008JCLI2178.1.

Vecchi, G.A., and B.J. Soden (2007). Increased tropical Atlantic wind shear in model projections of global warming. Geophys. Res. Lett., 34, L08702, doi:10.1029/2006GL028905.

Vermeer, M. and Rahmstorf, S., (2009). Global sea level linked to global temperature, Proceedings of the National Academy of Sciences 106:51:21527-21532 doi:101073/pnas0907765106.

Vickery, P.J., Lin, J, Skerlj, P.F., Twisdale, L.A., and Huang, K. (2006a). HAZUS-MH hurricane model methodology. I: Hurricane hazard, terrain, and wind load modeling. Natural Hazards Review, 7, 82–93, doi:{10.1061/(ASCE)1527-6988(2006)7:2(82)}.

Vickery, P.J. Lin, J, Skerlj, P.F., Twisdale, L.A., and Huang, K. (2006b). HAZUS-MH Hurricane Model Methodology. II: Damage and Loss Estimation. Natural Hazards Review, **7**, 94-103.

Voss, C.I., and J. Andersson. (1993). Regional flow in the Baltic Shield during Holocene coastal regression. Ground Water, 31(6), 989-1006.

Voss, C.I., and W.W. Wood. (1993). Synthesis of geochemical, isotopic, and ground water modeling analysis to explain regional flow in a coastal aquifer of southern Oahu, Hawaii. In Proceedings of the International Atomic Energy Agency Final Research Coordination Meeting, June 1-4, Vienna, Austria. 147–178.

Voss, C.I. (1999). USGS SUTRA code, history, practical use, and application in Hawaii. In J. Bear et al.(eds.) Seawater Intrusion in Coastal Aquifers, Kluwer Academic Publ., Dordrecht, pp. 249-313.

Wallace, D.J., and Anderson, J.B., (2010). Evidence of similar probability of intense hurricane strikes for the Gulf of Mexico over the late Holocene. Geology 38, 511-514.

Wang, Z.B., Karssen, B., Fokkink, R.J., and Langerak, A. (1998). A dynamic-empirical model for estuarine morphology. Physics of Estuaries and Coastal Seas,, pp. 279-286.

Wang, Z.B., Louters, T., and de Vriend H.J., (1995). Morphodynamic modelling for a tidal inlet in the Wadden Sea. *Marine Geology*, 126 (1-4), pp. 289-300.

Warren Pinnacle Consulting, Inc., (2011a). Application of the sea-level affecting marshes model (SLAMM 6) to Saint Andrew and Choctawhatchee Bays : http://warrenpinnacle.com/prof/SLAMM/TNC/SLAMM_SAC_Florida_Final.pdf.

Warren Pinnacle Consulting, Inc., (2011b). SLAMM Analysis of Grand Bay NERR and Environs: http://warrenpinnacle.com/prof/SLAMM/TNC/SLAMM_MS_Grand_Bay_Report_4-22-2011.pdf

Warren Pinnacle Consulting, Inc., (2011c). Application of the Sea-Level Affecting Marshes Model (SLAMM 6) to Galveston Bay: http://warrenpinnacle.com/prof/SLAMM/TNC/Galveston_Report_6_30_2011.pdf.

Westerink, J.J., R.A. Luettich, Jr., J.C. Feyen, J.H. Atkinson, C. Dawson, M.D. Powell, J.P. Dunion, H.J. Roberts, E.J. Kubatko, H. Pourtaheri. (2008), "A Basin to Channel Scale Unstructured Grid Hurricane Storm Surge Model as Implemented for Southern Louisiana", Monthly Weather Review, Volume 136, 833-864.

Woodruff, J., Donnelly, J., David, M., and Wayne, G., (2008). Reconstructing relative flooding intensities responsible for hurricane-induced deposits from Laguna Playa Grande, Vieques, Puerto Rico. Geology, v. 36, no. 5, p. 391-394.

Zhao, M., Held, I.M., Lin, S.-J. and Vecchi, G.A., (2009). Simulations of global hurricane climatology, interannual variability, and response to global warming using a 50-km resolution GCM. Jour. Clim., v. 22, p. 6653--6678.

Zheng, C. and P.P. Wang, (1999). MT3DMS: A Modular Three-Dimensional Multispecies Transport Model for Simulation of Advection, Dispersion and Chemical Reactions of Contaminants in Groundwater Systems; Documentation and User's Guide, Contract Report SERDP-99-1, U.S. Army Engineer Research and Development Center, Vicksburg, MS.

List of Scientific/Technical Publications Produced

Articles in Peer-Reviewed Journals

Convertino, M, Elsner, J. B., Munoz-Carpena, R., Kiker, G. A., Martinez, C. J., Fisher, R. A., and Linkov, I., 2011. Do shoreline birds like tropical cyclones? Biogeoclimatology of Snowy Plovers in Florida: *PLoS ONE*, 6(1): e15683. doi:10.1371/journal.pone.0015683.

Convertino, M., Donoghue, J.F., Chu-Agor, M.L., Kiker, G.A., Muñoz-Carpena, R., Fischer, R.A., and Linkov, I., 2011. Anthropogenic renourishment feedback on shorebirds: a multispecies Bayesian perspective: *Ecological Engineering*, v. 37, no. 8, p. 1184-1194.

Coor, J.L., Donoghue, J.F., Wallace, T., Wang, Y., and Elsner, J.B., in revision, Detecting a storm history signature in coastal lake sediments, northern Gulf of Mexico coast: *Quaternary Research*.

Coor, J.L., Donoghue, J.F., Das, O., Wang, Y., and Elsner, J.B., submitted, A paleostorm record for the northwest Florida coast. *Marine Geology*.

Das, O., Wang, Y., Donoghue, J., Xu, X., Coor, J., Elsner, J., Xu, Y., in review. Reconstruction of paleostorms and paleoenvironment using geochemical proxies in sediment cores from two coastal lakes in northwest Florida, *Quaternary Science Reviews*.

Donoghue, J.F., 2011. Sea-level history of the northern Gulf of Mexico and sea-level rise scenarios for the near future: *Climatic Change*, v. 107, no. 1, p. 17-33. (DOI 10.1007/s10584-001-0077-x)

Elsner, J.B., Hodges, R. E., and Jagger, T. H., in press, Spatial grids for hurricane climate research: *Climate Dynamics*.

Elsner, J.B., Lewers, S. W., Malmstadt, J. C., and Jagger, T. H., 2011. Estimating contemporary and future wind-damage losses from hurricanes affecting Eglin Air Force Base, Florida: *Journal of Applied Meteorology and Climatology*. Volume 50, Issue 7 (July 2011) pp. 1514-1526. doi: 10.1175/2011JAMC2658.1

Hodges, R.E., J.B. Elsner, and T.H. Jagger, 2012: Predictive models for time-to-acceptance: An example using `hurricane' articles in AMS journals, *Bulletin of the American Meteorological Society*, Accepted for publication.

Jagger, T.H. and Elsner, J.B. Hurricane clusters in the vicinity of Florida, *Journal of Applied Meteorology and Climatology*. In review.

Kish, S.A., and Donoghue, J.F., in press, Coastal response to storms and sea-level rise: Santa Rosa Island, Northwest Florida, USA: *Journal of Coastal Research*.

Malmstadt, J. C., Elsner, J. B., and Jagger, T. H., 2010: The risk of strong hurricane winds to Florida cities. *Journal of Applied Meteorology & Climatology*, 49, 2121-2132.

Malmstadt, J.C., H. Needham, J.B. Elsner, and T.H. Jagger, in review, A statistical model of return periods for combined wind and surge hazards from hurricanes, *The Professional Geographer*.

Malmstadt, J.C., Scheitlin, K.N., and Elsner, J.B., 2009: Florida hurricanes and damage costs. *The Southeastern Geographer*, 49:108–131.

Scheitlin, K.N., Elsner, J.B., Malmstadt, J.C., Hodges, R.E., and Jagger, T.H. (2010). Toward increased utilization of historical hurricane chronologies. *Journal of Geophysical Research* 115, DOI 10.1029/ 2009JD012424.

Scheitlin, K. N., Elsner, J. B., Lewers, S.W., Malmstadt, J.C., and Jagger, T. H., in press: Risk assessment of hurricane winds for Eglin Air Force Base, *Theoretical and Applied Climatology*.

Scheitlin, K.N., Mesev, V., Elsner, J.B., submitted, Polyline average using distance surfaces: A spatial hurricane climatology. *International Journal of GIScience.*

Conference or Symposium Proceedings

Niedoroda, A.W., Dai, H., Ye, M., Saha, B., Kish, S., and Donoghue, J.F., 2011. Barrier island responses to potential future rates of sea-level rise, p. 202-215, *in* Wang, P., Rosati, J.D., and Roberts, T.M., *eds.*, Proceedings, Coastal Sediments 2011. *Seventh International Symposium on Coastal Engineering and Science of Coastal Sediment Processes*, Miami, FL May 2-6, 2011. Amer. Soc. Civil Engineers, World Scientific, v. 1.

Conference or Symposium Abstracts

Convertino, M., Elsner, J.B., Kiker, G.A., Munoz-Carpena, R., Donoghue, J.F., Fischer, R.A., and Linkov, I., 2011. Bayesian inference for assessing feedbacks among species, anthropogenic and climate forcings: shorebirds in Florida: *Abstracts, Ecological Society of America Annual Meeting*, Austin, TX, Aug. 7-12, 2011.

Coor, J.L., Donoghue, J.F., Wang, Y., Das, O., Kish, S.A., Elsner, J.B., Hu, X., Niedoroda, A.W., and Ye, M., 2009. Development of a long-term storm history for the northwest Florida coast using multiple proxies: *Eos, Transactions, Amer. Geophys. Union, v. 90 (52),* Fall Meet. Suppl., Abstract NH11A-1109.

Coor, J.L., Donoghue, J.F., Yang, W., Das, O., Wallace, T., 2011. Using Multiple Proxies to Develop a Mid- to Late Holocene Chronology of Major Storms for the Northwest Florida Coast for use in Risk Modeling: *Geological Society of America , Abstracts with Programs*, v. 43, no. 2, p. 77.

Coor, J.L., Donoghue, J.F., Wang, Y., Das, O., Kish, S.A., Elsner, J.B., Hu, X., Niedoroda, A.W., and Ye, M., 2009. Development of a long-term storm history for the northwest

Florida coast using multiple proxies: *Eos, Transactions, Amer. Geophys. Union, v. 90 (52),* Fall Meet. Suppl., Abstract NH11A-1109.

Dai, H., Ye, M., Niedoroda, A.W., Saha, B., and Donoghue, J.F., 2010. Uncertainty Assessment for Numerical Modeling of Dune and Backshore Evolution Under Sea-Level Rise Scenarios: *Eos, Transactions, Amer. Geophys. Union, v. 91 (51),* Fall Meet. Suppl., Abstract EP33B-0766

Dai, H., A.W. Niedoroda, M. Ye, B. Saha, J.F. Donoghue, and S. Kish (2011). Modeling coastal zone reponse to sea-level rise using MoCCS: A model of complex coastal system: *Eos, Transactions, Amer. Geophys. Union, v. __ (__),* Fall Meet. Suppl.

Das, O., Wang, Y., Donoghue, J.F., Coor, J.L., Kish,S.A., Elsner,J.B., Hu,X., Niedoroda, A.W.,Ye, M., and Xu, Y., 2009. Reconstruction of paleostorm history using geochemical proxies in sediment cores from Eastern Lake, Florida: *Eos, Transactions, Amer. Geophys. Union, v. 90 (52),* Fall Meet. Suppl., Abstract NH11A-1105.

Das, O., Wang, Y., Donoghue, J.F., and Coor, J.L., 2011. Reconstruction of paleostorm history using geochemical proxies in sediment cores from coastal lakes in NW Florida: *Geological Society of America, Abstracts with Programs,* Vol. 43, No. 2, p. 77.

Das, O., Wang, Y., Donoghue, J., Xu, X., Coor, J., Elsner, J., Xu, Y., 2012. Reconstruction of paleostorms and paleoenvironment using geochemical proxies in sediment cores from two coastal lakes in northwest Florida, *Geological Society of America Annual Meeting, Abstracts with Programs.*

Donoghue, J.F., Elsner, J.B., Hu, B., Kish, S.A., Niedoroda, A.N., Wang, Y., and Ye, M., 2011. Effects of Near-Term Sea-Level Rise on Coastal Infrastructure: Invited presentation, Eglin Air Force Base (AFB) Strategic Environmental Research Development Program (SERDP) Knowledge Transfer Meeting, October 4, 2011, Niceville, FL

Donoghue, J.F., 2011. Sea-level rise, climate change and effects on coastal military installations: Implications for other coastal uses: Invited presentation, *Capitol Hill Ocean Week 2011 Conference*, National Marine Sanctuary Foundation, Washington, DC, June 7-9, 2011.

Donoghue, J.F., 2010. Sea-level history of Florida and sea-level rise scenarios for the near future: invited paper, *Workshop on Surviving the Challenges of Sea-Level Rise in Florida,* Lake Placid, FL, Jan 18-20, 2010.

Donoghue, J.F., 2010. Sea-Level Change in the Gulf of Mexico: Past and Future: Invited presentation, *EPA Gulf of Mexico Alliance (GOMA) Sea Level Modeling Workshop*, St. Petersburg, FL, Nov. 3-4, 2010.

Donoghue, J. F., Elsner, James B., Hu, B. X., Kish, S. A., Niedoroda, A. W., Wang, Y., Ye, M., Coor, J. L., Das, O., and Wallace, T., 2011. Modeling near-future response to sea level and climate change on the northwest Florida coast: *Geological Society of America , Abstracts with Programs*, v. 43, no. 2, p. 79.

Donoghue, J.F., Elsner, J.B., Hu, B. X., Kish, S.A., Niedoroda, A., Wang, Y., Ming Ye, M., Jagger, T.H., Coor, J., Dai, H., Das, O., Lewers, S., Malmstedt, J., Scheitlin, K., and Zhang, X., 2010. Modeling the Risk to Military Infrastructure from Future Coastal Sea-Level Change: *Abstracts, SERDP-ESTCP Technical Symposium*, Washington, DC, Nov. 30 – Dec. 2, 2010.

Donoghue, J.F., Elsner, J.B., Hu, B. X., Kish, S.A., Niedoroda, A., Wang, Y., Ming Ye, M., Jagger, T.H., Coor, J., Dai, H., Das, O., Lewers, S., Malmstedt, J., Scheitlin, K., and Zhang, X., 2010. Modeling the Risks of Near-Term Climate Change on Coastal Military Installations: *Abstracts, SERDP-ESTCP Technical Symposium*, Washington, DC, Nov. 30 – Dec. 2, 2010.

Donoghue, J.F., Elsner, J.B., Hu, B.X., Kish, S.A., Niedoroda, A.W., Wang, Y., Ye, M., Bryan, J., Coor, J., Das, O., Lewers, S., Malmstedt, J., Scheitlin, K., Zhang, X., 2010. Effects of sea-level rise and climate change over the next century on the Choctawhatchee basin and Eglin AFB region: *Choctawhatchee Basin Watershed Conference*, Niceville, FL, April 30, 2010.

Donoghue, J.F., Coor, J.L., Wang, Y., Das, O., Kish, S.A., Elsner, J.B., Hu, X., Niedoroda, A.W., and Ye, M., 2009. Coastal lake record of Holocene paleo-storms from northwest Florida: *Eos, Transactions, Amer. Geophys. Union, v. 90 (52),* Fall Meet. Suppl., Abstract NH11A-1110.

Donoghue, J.F., Elsner, J.B., Hu, B. X., Kish, S.A., Niedoroda, A., Wang, Y., Ming Ye, M., Jennifer Coor, J., Das, O., Lewers, S., and Scheitlin, K., 2009. Effects of near-term sea-level rise on coastal infrastructure : *Abstracts, SERDP-ESTCP Technical Symposium and Workshop*, Washington, DC, Dec. 1-3, 2009.

Elsner, J. 2011. On the increasing intensity of Atlantic hurricanes, invited presentation, University of South Florida, January 24, 2011.

Elsner, J. 2011. On the increasing intensity of Atlantic hurricanes, Rhodes Greece, June 28, 2011.

Elsner, J.B., Lewers, S. W., Malmstadt, J.C., Jagger, T.J: 2011. Estimating Future Hurricane Wind Losses: A Case Study at Eglin Air Force Base. *World Climate Research Program, Open Science Conference,* October 24-28, 2011, Denver, CO.

Elsner, J., 2010, Anticipating future hurricanes: Bermuda Institute for Ocean Sciences, Hamilton, October 12, 2010. *Proceedings, Risk Prediction Initiative Annual Research Workshop.*

Elsner, J. and Jagger, T., 2010. On the increasing intensity of Atlantic hurricanes: *Eos, Transactions, Amer. Geophys. Union, v. 91 (51),* Fall Meet. Suppl., Abstract GC51K-08

Kish, S.K., and Donoghue, J.F., 2012. The influence of storm frequency on shoreline stability, Santa Rosa Island, Florida: *Geological Society of America Abstracts with Programs* Vol. 44, No. 4.

Kish, Stephen A., Niedoroda, A., Donoghue, J. F., Elsner, J.B., Hu, W., Wang, Y., and Ye, M., 2010. Long-term and storm-related changes of shorelines and dunes on Santa Rosa Island, Florida: a baseline for studying the effects of climate change and seal level rise on a low-lying barrier island: G*eological Society of America, Abstracts with Programs*, v. 42, p. 246.

Malmstadt, J., Elsner, J, and Jagger, T., 2010. The risk of strong hurricane winds to Florida cities: *Amer. Meteor. Soc. Hurricanes & Tropical Meteorology Conference*, Tucson, AZ, May 1-6, 2010.

Niedoroda, A. W., Dai, H., Ye, M., Saha, B., Kish, S., and Donoghue, J.F., 2011. Barrier island responses to potential future rates of sea-level rise: Abstracts, Coastal Sediments 2011, *Seventh International Symposium on Coastal Engineering and Science of Coastal Sediment Processes*, Miami, FL, May 2-6, 2011.

Niedoroda, A. W., 2010. Response of complex coastal systems to sea-level rise: Invited presentation, *EPA Gulf of Mexico Alliance (GOMA) Sea Level Modeling Workshop*, St. Petersburg, FL, Nov. 3-4, 2010.

Niedoroda, A., Dai, H., Ye, M., Saha, B., Kish, J., and Donoghue, J., 2010. Morphodynamic modeling of coastal barrier response to sea-level rise scenarios: *Eos, Transactions, Amer. Geophys. Union, v. 90 (52),* Fall Meet. Suppl., Abstract *NH13B-04*

Niedoroda, A.W., Donoghue, J.F., Elsner, J.B., Hu, X., Kish, S.A., Wang, Y., and Ye, M., 2010. Modeling the Impact of Sea-Level Change on Complex Coastal Systems and Infrastructure, Northeastern Gulf of Mexico: *Gulf of Mexico Alliance Symposium on Sea-level Rise in the Gulf of Mexico*, Corpus Christi, TX, March 1-3, 2010.

Niedoroda, A.W., M. Ye; B. Saha; J. F. Donoghue; and C. W. Reed, 2009. Simulations of sea level rise effects on complex coastal systems: *Eos, Transactions, Amer. Geophys. Union, v. 90 (52),* Fall Meet. Suppl., Abstract NH13B-04.

Scheitlin, K., and Elsner, J., 2009. A track-relative climatology of hurricanes affecting Eglin Air Force Base: *Eos, Transactions, Amer. Geophys. Union, v. 90 (52),* Fall Meet. Suppl., Abstract NH11A-1103.

Ye, M. and Donoghue,J.F., 2011. Numerical modeling and uncertainty analysis for the effects of near-term sea-level rise on barrier islands: Invited presentation, Florida Climate Institute, Oct. 30, 2011, Tallahassee, FL.

Ye, M., Dai, H., Niedoroda, A.N., Feng, D., Kish, S., and Donoghue, J.F., 2011. Coastal zone responses to sea-level Rise: numerical modeling and uncertainty analysis: Florida Climate Institute annual meeting, Nov. 14, 2011, Gainesville, FL.

Textbooks or Book Chapters

Scheitlin, K. N., and Elsner, J. B., 2010: A track-relative climatology of Eglin Air Force Base hurricanes in a variable climate: p. 217-230, in Elsner, J.B, et al., (eds.), *Hurricanes and Climate Change: Volume 2.* Springer Publ.